

BERGISCHE
UNIVERSITÄT
WUPPERTAL

Numerical Investigation and Development of Design Guidelines for Slender FRP-RC Columns

Dissertation

for the acquisition

of the academic title “Dr.-Ing.”

submitted to the

Faculty of Architecture and Civil Engineering

Bergische Universität Wuppertal

by

Ahmed Usama Syed

from Delhi, India

Wuppertal 2026



BERGISCHE
UNIVERSITÄT
WUPPERTAL

Numerical Investigation and Development of Design Guidelines for Slender FRP-RC Columns

Dissertation

zur Erlangung eines Doktorgrades

(Dr.-Ing.)

in der

Fakultät für Architektur und Bauingenieurwesen

der

Bergische Universität Wuppertal

vorgelegt von

Ahmed Usama Syed

aus Delhi, Indien

Wuppertal 2026

Veröffentlicht als Heft 35 in der Schriftenreihe des
Instituts für Konstruktiven Ingenieurbau
Fakultät für Architektur und Bauingenieurwesen
Bergische Universität Wuppertal

Herausgeber

Der Geschäftsführende Direktor
Institut für Konstruktiven Ingenieurbau
Bergische Universität Wuppertal

Fachgebiet

Tragkonstruktionen Baustatik und Baudynamik
Univ.-Prof. Dr.-Ing. Arndt Goldack
Fakultät für Architektur und Bauingenieurwesen
Bergische Universität Wuppertal

Organisation und Verwaltung

Institut für Konstruktiven Ingenieurbau
Bergische Universität Wuppertal
Pauluskirchstraße 11
42285 Wuppertal
Telefon: (0202) 439-4039

© Dr.-Ing. Ahmed Usama Syed

ISBN 978-3-940795-34-2

Alle Rechte, insbesondere das der Übersetzung in fremde Sprachen, vorbehalten. Mit Genehmigung des Autors ist es gestattet, dieses Heft ganz oder teilweise auf fotomechanischem Wege (Fotokopie, Mikrokopie) zu vervielfältigen.

Foreword

This thesis has been carried out at the Institute of Statics and Dynamics of Structures at the University of Wuppertal under the supervision of Prof. Dr.-Ing. Arndt Goldack. The work was made possible with the support of a scholarship from the German Academic Exchange Service (DAAD).

This thesis has been accepted by the University of Wuppertal in fulfilment of the requirements for the degree of Doctor of Engineering (Dr.-Ing.).

Date of submission:	21 January 2026
Date of oral examination:	19 May 2026
Examination Committee:	Prof. Dr.-Ing. Arndt Goldack
	Prof. Dr.-Ing. Marcus Ricker
	Prof. Dr.-Ing. Steffen Anders
Chair of the Examination Committee:	Prof. Dr.-Ing. Bernd Naujoks

Acknowledgements

I would like to express my sincere gratitude to the Deutscher Akademischer Austauschdienst (DAAD) for funding my PhD studies at the University of Wuppertal. I would also like to extend my profound gratitude to my PhD supervisor, Prof. Dr.-Ing. Arndt Goldack, for his invaluable guidance, continuous support, and motivation throughout my PhD research, both academically and personally. Every meeting with him was a positive source of encouragement that consistently motivated me to further advance my research work.

I am very grateful to all my colleagues at the Chair of Statics and Dynamics of Structures at the University of Wuppertal for their support and assistance throughout my stay in Wuppertal. A special mention goes to Mr. Javad Mohseni and Mrs. Claudia Stein for their help not only at the university but also with personal matters related to German bureaucracy. I would also like to convey my deepest gratitude and sincere thanks to Mr. Richard Köhler for his collaboration and support during the later stages of my work.

I am immensely thankful to my father, Syed Khalique Ahmed, and my mother, Fatima Tanveer, for their unwavering support, motivation, and prayers throughout my PhD journey I would like to express my heartfelt and deepest thanks to my wife, Zuniyarah Irfan Siddiqui, for her constant encouragement, patience, sacrifices, and unconditional support during all phases of my PhD. which made it possible for me to pursue my PhD successfully. Her understanding, strength, and belief in me played a vital role in helping me successfully complete this journey. Special thanks are due to my son, Ibraheem Ashar Syed, and my daughter, Maryam Haniya Syed, who have always been a great source of motivation for me.

Abstract

Due to the distinct material properties of the fiber-reinforced polymer (FRP) bars, they have emerged as an attractive alternative to conventional steel reinforcement. FRP bars are corrosion-resistant, electromagnetically neutral, have low life cycle costs and potentially have low environmental impact. However, they generally have a low modulus of elasticity and a linear stress-strain curve without any plastic deformation in comparison to steel bars. This raises the need to evaluate their performance as a structural reinforcement and the effect of their material properties on the existing design guidelines for reinforced concrete (RC) members. In this study, the behavior of FRP-reinforced concrete (FRP-RC) columns is studied in detail and compared to steel-reinforced concrete (steel-RC) columns. The primary objective of this study was to develop design guidelines and methods, within the framework of Eurocode 2, for slender FRP-RC columns. The detailed objectives of this study are outlined as: (1) To investigate the slenderness limit for FRP-RC columns and to develop an equation for slenderness limit as a design recommendation; (2) To assess the behavior of slender FRP-RC columns, evaluate their nominal curvature and to develop nominal curvature method for simplified second-order analysis of FRP-RC columns and (3) To examine the behavior of slender FRP-RC columns subjected to unequal end moments and to develop an equivalent moment factor expression as a design recommendation.

In order to achieve the objectives of this study, a numerical method for the second-order analysis of slender reinforced columns was developed and successfully implemented as the Direct Curvature Method (DCM). This method is based on the estimation of the column curvature while accounting for the end eccentricities. A second method, the Column Deflection Curve method (CDM), in which curvature is integrated numerically, was also implemented. Both methods were successfully validated using experimental results available from the literature.

It was found in this study that FRP-RC columns are more susceptible to slenderness as compared to steel-RC columns. They exhibited a lower slenderness limit, distinct nominal curvature behavior and required a revised expression for equivalent moment factor compared to steel-RC columns. Equations to estimate the slenderness limit of FRP-RC columns are proposed. A nominal curvature method for

simplified second-order analysis of FRP-RC columns is developed with the required equations derived based on a parametric study on 26,880 columns. Furthermore, an equation to estimate the equivalent moment factor is proposed based on a detailed parametric study of columns subjected to unequal end moments. Finally, normalized load-moment interaction diagrams, applicable to all types of FRP bars, are presented for the design of short and slender FRP-RC columns using the proposed equations. Hence, this study provides a comprehensive approach in the framework of Eurocode 2 for the design and analysis of short and slender FRP-RC columns.

Kurzfassung

Aufgrund der besonderen Materialeigenschaften von faserverstärkten Polymerstäben (FRP) Stäben haben sich diese als attraktive Alternative zur konventionellen Stahlbewehrung etabliert. FRP-Stäbe sind korrosionsbeständig, elektromagnetisch neutral, weisen geringe Lebenszykluskosten auf und besitzen potenziell eine geringe Umweltbelastung. Im Vergleich zu Stahlstäben weisen sie jedoch in der Regel einen niedrigen Elastizitätsmodul sowie ein lineares Spannungs-Dehnungs-Verhalten ohne plastische Verformung auf. Daraus ergibt sich die Notwendigkeit, ihre Leistungsfähigkeit als tragende Bewehrung sowie den Einfluss ihrer Materialeigenschaften auf bestehende Bemessungsrichtlinien für Stahlbetonbauteile zu bewerten.

In dieser Studie wird das Tragverhalten von FRP-bewehrten Betonstützen (FRP-Betonstützen) detailliert untersucht und mit dem von stahlbewehrte Betonstützen (Stahlbetonstützen) verglichen. Das Hauptziel der Arbeit besteht in der Entwicklung von Bemessungsrichtlinien und -methoden für schlanke FRP-Betonstützen im Rahmen des Eurocode 2. Die detaillierten Ziele dieser Studie sind: (1) Untersuchung der Schlankheitsgrenze von FRP-Betonstützen und Entwicklung einer Gleichung zur Bestimmung der Schlankheitsgrenze für die Bemessung; (2) Bewertung des Tragverhaltens schlanker FRP-Betonstützen, Ermittlung ihrer Nennkrümmung sowie Entwicklung einer Nennkrümmungsmethode zur vereinfachten Bemessung; (3) Untersuchung des Tragverhaltens schlanker FRP-Betonstützen mit ungleichen Endmomenten und Entwicklung einer Formulierung für den äquivalenten Momentenbeiwert für die Bemessung.

Zur Erreichung dieser Ziele wurde ein numerisches Verfahren zur Berechnung schlanker Stützen nach Theorie 2. Ordnung entwickelt und erfolgreich als Direkte-Krümmungs-Methode (Direct Curvature Method, DCM) implementiert. Diese Methode basiert auf der Abschätzung der Stützenkrümmung unter Berücksichtigung der Endexzentrizitäten. Darüber hinaus wurde die Stützenverformungskurven-Methode (Column Deflection Curve Method, CDM), bei der die Krümmung numerisch integriert wird, implementiert. Beide Methoden wurden erfolgreich anhand experimenteller Ergebnisse aus der Literatur validiert.

Es wurde festgestellt, dass die Schlankheit bei FRP-Betonstützen einen größeren Einfluss auf das Tragverhalten hat, als bei Stahlbetonstützen. Sie besitzen daher eine geringere Schlankheitsgrenze, ein charakteristisches Nennkrümmungsverhalten und erfordern einen überarbeiteten Ausdruck für den äquivalenten Momentenbeiwert im Eurocode 2. Es werden Gleichungen zur Abschätzung der Schlankheitsgrenze von FRP-Betonstützen vorgeschlagen. Auf Grundlage einer parametrischen Untersuchung von 26.880 FRP-Betonstützen wurde eine Nennkrümmungsmethode für die vereinfachte Berücksichtigung der Theorie 2. Ordnung entwickelt. Darüber hinaus wird eine Gleichung zur Bestimmung des äquivalenten Momentenbeiwerts auf Basis einer detaillierten Untersuchung von Stützen unter ungleichen Endmomenten vorgeschlagen. Schließlich werden normalisierte Last-Momenten-Interaktionsdiagramme präsentiert, die auf alle Arten von FRP-Stäben anwendbar sind und die Bemessung von kurzen und schlanken FRP-Betonstützen mithilfe der vorgeschlagenen Gleichungen ermöglichen. Damit liefert diese Studie einen umfassenden Ansatz für die Analyse und Bemessung von kurzen und schlanken FRP-Betonstützen im Rahmen des Eurocode 2.

Table of Contents

Acknowledgements I

Abstract II

Kurzfassung IV

Table of Contents VI

List of Figures XI

List of Tables XVI

1 Introduction 1

1.1 Fiber-reinforced polymer bars as a reinforcement 1

1.2 FRP-RC columns 2

1.3 Preliminary research 4

1.4 Objectives of the study 9

1.5 Organization of the Thesis 9

1.6 References 14

2 Slenderness Limit for GFRP Reinforced Concrete Columns Based on Axial Force Ratio 18

Abstract 19

2.1 Introduction 20

2.2 Slenderness limit 22

2.2.1 Second-order effects 22

2.2.2 Slenderness limit criteria 23

2.3 Numerical method for second-order analysis of reinforced concrete columns 26

2.3.1 Material properties 27

2.3.1.1 Concrete 27

2.3.1.2 FRP 28

2.3.2 Cross-section resistance 29
2.3.3 Curvature assumption 30
2.3.4 Steps of second-order analysis 32
2.3.5 Validation of the method 33
2.4 Sensitivity analysis 35
2.4.1 General 35
2.4.2 Results and discussions 39
2.4.2.1 Effect of compressive strength of concrete 39
2.4.2.2 Effect of modulus of elasticity of GFRP bars and reinforcement ratio 40
2.4.2.3 Effect of axial force ratio 42
2.5 Definition of slenderness limit for GFRC-RC columns 44
2.6 Conclusions 49
2.7 Acknowledgements 50
2.8 References 51
3 Simplified Second-Order Analysis of Slender FRP-Reinforced Concrete Columns Using Nominal Curvature Method 56
Abstract 57
3.1 Introduction 58
3.2 Second-order analysis using nominal curvature 60
3.3 Total curvature distribution factor 64
3.4 Numerical analysis of reinforced concrete columns 66
3.4.1 Methodology 66
3.4.2 Geometric nonlinearity 67
3.4.3 Material nonlinearity 68
3.4.4 Validation 69
3.4.5 Cross-section 70

3.5 Nominal Curvature 70
3.5.1 Overview of nominal curvature for Steel-RC columns 70
3.5.2 Nominal curvature for FRP-RC columns 74
3.6 Estimation of the nominal curvature for FRP-RC columns 76
3.6.1 Parametric Study 76
3.6.2 Proposed nominal curvature for FRP-RC column 80
3.7 Conclusions 85
3.8 Appendix I 86
3.8.1 Case 1: ρ = 1 % 87
3.8.2 Case 2: ρ = 4 % 89
3.9 Appendix II 91
3.10 Data availability statement 92
3.11 Acknowledgements 93
3.12 Notations 93
3.13 References 96
4 Analysis of Slender FRP-Reinforced Concrete Columns Subjected to Unequal End Moments 100
Abstract 101
4.1 Introduction 102
4.2 Numerical analysis of reinforced concrete columns subjected to unequal end moments 106
4.2.1 General 106
4.2.2 Direct curvature method (DCM) 106
4.2.3 Column deflection curve method (CDM) 108
4.2.4 Material properties 110
4.2.5 Validation and comparison 112
4.3 Equivalent moment factor for simplified second-order analysis 117

4.3.1 General 117
4.3.2 Equivalent moment factor (C_m) for FRP-RC columns 118
4.4 Parametric study 123
4.4.1 General 123
4.4.2 Regression analysis 124
4.5 Conclusions 131
4.6 Acknowledgements 132
4.7 References 133
5 Design of FRP-RC Columns with Nominal Curvature Method and Universal Interaction Diagrams Applicable to Various FRP Bar Types 137
Abstract 138
5.1 Introduction 139
5.2 Design of FRP-RC columns in the framework of Eurocode 2 140
5.3 Universal interaction curves 143
5.4 General discussion on the universal interaction diagram 144
5.5 Universal interaction diagrams for the design of slender columns 148
5.6 Examples 152
5.6.1 Example I: Short column design using universal interaction curves with ε_{tud} = 10 mm/m 154
5.6.2 Example II: Short column design using universal interaction curves with ε_{tud} = 5 mm/m 157
5.6.3 Example III: Slender column design using universal interaction curves with ε_{tud} = 10 mm/m 162
5.6.3.1 Application of the nominal curvature method and the universal interaction diagram for cross-section design 162
5.6.3.2 Application of universal interaction diagrams for slender FRP-RC column 165

5.7 Conclusions 166
5.8 Data availability statement 167
5.9 Acknowledgements 167
5.10 Notation 167
5.11 References 169
6 Summary and Outlook 171
6.1 Summary 171
6.2 Major results and conclusions 172
6.3 Outlook 174
7 Annexure 175
Abstract 176
7.1 Introduction 177
7.2 Non-linear analysis of reinforced concrete columns 177
7.3 Material Properties 179
7.4 Design of FRP-reinforced concrete column 180
7.5 Load-moment interaction 181
7.6 Capacity reduction for slender columns 184
7.7 Conclusions 187
7.8 Acknowledgements 188
7.9 References 189
Curriculum Vitae 192

List of Figures

Fig. 1.1	Effect of increase in slenderness on the (a) load capacity and (b) moment capacity of FRP-RC and steel-RC column [24]	4
Fig. 1.2	Effect of modulus of elasticity of FRP bar on the (a) load capacity, (b) moment capacity and (c) second-order moment of FRP-RC and steel-RC columns [24]	6
Fig. 1.3	Load-moment capacity interaction curve for (a) FRP-RC and (b) Steel-RC column cross-section	7
Fig. 1.4	Effect of material propertied and reinforcement ratio on the balance point of FRP-RC columns	8
Fig. 2.1	(a) Simply supported column with uniform first-order eccentricity; and (b) Illustration of the failure of eccentrically loaded column due to slenderness	23
Fig. 2.2	Slenderness limit criteria (Load Capacity vs Moment Capacity)	26
Fig. 2.3	(a) Cross-section details and (b) Illustration for Concrete stress-strain curve	28
Fig. 2.4	Transformed area of concrete and FRP bars	29
Fig. 2.5	(a) Column in undeformed state and (b) Deformed column with sinusoidal variation of total eccentricity	31
Fig. 2.6	Validation of numerical method with experimental results from (a) Othman and Mohammad [34]; (b) Xue et al. [35]	34
Fig. 2.7	Flowchart for calculating slenderness limit as per (a) Criterion 1 and (b) Criterion 2	38
Fig. 2.8	Effect of concrete strength on the mean and five percentile slenderness limit values for the cases considered in the sensitivity analysis	40
Fig. 2.9	Effect of modulus of elasticity of GFRP bar on mean and five percentile slenderness limit values for cases considered in sensitivity analysis	41
Fig. 2.10	Effect of Reinforcement Ratio on mean and five percentile slenderness limit values for cases considered in sensitivity analysis	42

Fig. 2.11 Effect of axial force ratio on the mean and five-percentile slenderness limit values for all the cases considered in the sensitivity analysis 43

Fig. 2.12 Variation of slenderness limit values for steel-RC and GFRP-RC columns with different reinforcement ratios for $E_{FRP} = 40$ GPa, $f_c = 30$ MPa and $f_y = 500$ MPa. 45

Fig. 2.13 Variation for five percentiles value of slenderness limit for different values of the: (a) concrete compressive strength; (b) Modulus of elasticity of GFRP; and (c) Reinforcement ratio 47

Fig. 2.14 Variation of slenderness limit with axial force ratio for all the cases of sensitivity analysis and performance of proposed equations: (a) when both the criteria are considered simultaneously; and (b) when only criterion 1 is considered 48

Fig. 3.1 Simply supported column bent in single curvature 61

Fig. 3.2 Nominal curvature method 62

Fig. 3.3 Sinusoidal variation of total eccentricity 67

Fig. 3.4 Validation of the numerical method for detailed second-order analysis of FRP-RC columns 69

Fig. 3.5 Rectangular column cross-section with corner reinforcement with b = h = 300 mm 70

Fig. 3.6 Steel-RC Column: (a) Load-moment capacity curve for different slenderness ratios and (b) Load capacity-nominal curvature 71

Fig. 3.7 Load-moment capacity curve of steel-RC column for cross-section analysis with different reinforcement ratios (ρ) 72

Fig. 3.8 FRP-RC column: (a); (c) Load-moment capacity curve for different slenderness ratios; (b); and (d) Load capacity-nominal curvature 75

Fig. 3.9 Performance of the Eq. (19) to estimate the total curvature distribution factor 78

Fig. 3.10 Effect of concrete compressive strength on the nominal curvature of FRP-RC column 79

Fig. 3.11 Effect of modulus of elasticity on the nominal curvature of FRP-RC column 79

Fig. 3.12 Effect of reinforcement ratio on the nominal curvature of FRP-RC column 80

Fig. 3.13 Effect of mechanical reinforcement ratio (ω') on the nominal curvature of FRP-RC column 82

Fig. 3.14 Performance of the proposed nominal curvature equation (Eq. (43) along with Eq. (47)) to predict the moment capacity of the FRP-RC column 83

Fig. 3.15 Load-moment capacity curve of FRP-RC column for cross-section analysis with $d'/h = 0.1\overline{3}$ 87

Fig. 3.16 Rectangular parabolic stress-strain diagram for concrete cross-section without axial force 90

Fig. 3.17 Typical load-moment capacity curves of FRP-RC columns for cross-section analysis with different mechanical reinforcement ratios 92

Fig. 4.1 Equivalent first-order moment transformation for simply supported column under unequal first-order moment bent in (a) double curvature; and (b) single curvature 103

Fig. 4.2 Variation of total eccentricity of a simply supported column bent in (a) single curvature; and (b) double curvature 107

Fig. 4.3 Column deflection curve 108

Fig. 4.4 Numerical integration of the column deflection curve 109

Fig. 4.5 Concrete column cross-section 118

Fig. 4.6 Load-moment capacity interaction curve for FRP-RC column with different first-order end moment ratios 118

Fig. 4.7 Equivalent moment factor (C_m)-load ratio (N_r) of FRP-RC column and steel-RC columns for slenderness ratio of 60 120

Fig. 4.8 Equivalent moment factor (C_m)-load ratio (N_r) of FRP-RC column and steel-RC column with the variation in slenderness ratio 121

Fig. 4.9 Effect of variation in ρ, E_{FRP}, and f_c on the equivalent moment factor (C_m) of FRP-RC column 122

Fig. 4.10 Equivalent moment factor (C_m) - load ratio (N_r) (a) for all the columns considered in the parametric study; and (b) excluding the column data points having no second-order effects 124

Fig. 4.11 Performance of different C_m equations for FRP-RC columns in comparison to the data points considered for regression 127

Fig. 4.12 Equivalent moment factor (C_m) vs load ratio data points considered for regression for first-order end moment ratio of $M_{01}/M_{02} = -0.75$ 128

Fig. 4.13 Cumulative distribution frequency of $C_{m(Eq)}/C_{m(num)}$ calculated using Eq. (40), Eq. (41) and Eq. (42) for FRP-RC columns 129

Fig. 5.1 Universal interaction diagram for cross-section with the normalized mechanical reinforcement ratio ω' (strains in mm/m) 144

Fig. 5.2 Universal interaction curve and capacity curve for tensile failure with ω' = 0.2 145

Fig. 5.3 Typical lines and regions in the universal interaction diagram 146

Fig. 5.4 Universal interaction diagram based on nominal curvature method for $\lambda = 40$ (strains in mm/m) 150

Fig. 5.5 Universal interaction diagram based on nominal curvature method for $\lambda = 60$ (strains in mm/m) 151

Fig. 5.6 Universal interaction diagram based on nominal curvature method for $\lambda = 80$ (strains in mm/m) 152

Fig. 5.7 Column details: (a) system (b) cross-section with reinforcement 153

Fig. 5.8 Universal interaction curve for ω' = 0.14 and ε_{tud} = 10 mm/m (Example I) 156

Fig. 5.9 Universal interaction curve for ω' = 0.14 and ε_{tud} = 5 mm/m (Example II) 158

Fig. 5.10 Universal interaction curve and capacity curve for tension failure for ω' = 0.14 and ε_{tud} = 5 mm/m using the universal interaction curve of $\omega' = 0$ (Example II) 159

Fig. 5.11 Shifting of design load and moment capacity in the permitted design region OCD while (a) $n < n_{bal}$ (b) $n > n_{bal}$ (Example II) for $\varepsilon_{tud} = 5$ mm/m 160

Fig. 7.1 Column cross-section for transformed area and deflection when bent in single curvature 178

Fig. 7.2 Load-moment interaction curves for (a) FRP-RC and (b) steel-RC columns with λ = 0 (no second-order effects) 180

Fig. 7.3 Load-moment interaction curves of CFRP-RC columns for ε_{TFRP}= 0.005 with λ=0 181

Fig. 7.4 Load-moment interaction curves of FRP-RC columns with a varying modulus of elasticity of FRP bar at λ=0 182

Fig. 7.5 Load-moment capacity interaction curves of FRP-RC and steel-RC columns with a varying λ at ρ = 1% 183

Fig. 7.6 Load-moment capacity interaction curves of FRP-RC column with a varying λ at ρ = 2% 184

Fig. 7.7 Reduction in (a) load capacity and (b) moment capacity due to an increase in λ for FRP-RC and steel-RC columns 185

Fig. 7.8 Increase in second-order moment with the increase of λ for FRP-RC and steel-RC columns for n = 0.2, 0.4 and 0.6 186

Fig. 7.9 (a) Load capacity reduction, (b) moment capacity reduction and (c) increase in M_{II}/M_I due to an increase in λ for varying modulus of elasticity of FRP bar 187

List of Tables

Table 1.1	Properties of FRP bars	1
Table 2.1	Mechanical properties of different FRP bars	22
Table 2.2	Verification of the numerical method	34
Table 2.3	Variables of sensitivity analysis	36
Table 3.1	Variables for the parametric study	77
Table 4.1	Validation of the numerical methods	114
Table 4.2	Parametric study variables	124
Table 5.1	Maximum compressive concrete strains ε_{c2} and strains ε_t of FRP reinforcement for different normalized mechanical reinforcements ω' and load moments μ_{Ed} for $N_{Ed} =$ -500 kN using INCA2 [10]	147
Table 5.2	Details of the input parameters for the examples	153
Table 5.3	Calculation of the parameters for Example I	154
Table 7.1	Properties of FRP bars reported in the literature	178

1. Introduction

1.1 Fiber-reinforced polymer bars as a reinforcement

In recent years, Fiber-reinforced Polymer (FRP) bars have received significant consideration as a durable and sustainable alternative to steel bars as a reinforcement for reinforced concrete (RC) structures. Corrosion of steel reinforcement is a concern for reinforced concrete structures, resulting in significant repair and rehabilitation costs [1,2]. FRP bars are corrosion-resistant, electromagnetically neutral, non-conductive, and have a high strength-to-weight ratio. This makes them suitable for corrosive environments, hospitals, and defense infrastructure. In addition, FRP bars can have low life-cycle costs and potentially low environmental impact [3,4]. However, FRP bars have a linear elastic stress-strain behavior with a brittle tension failure. Although they have a high tensile strength, their modulus of elasticity is less than steel. Therefore, replacing steel bars with FRP bars as reinforcement requires a thorough experimental and numerical investigation. The properties of different type of FRP bars are shown in Table 1.1. The existing design methods and guidelines in codes for steel reinforced concrete (steel-RC) structures need to be re-evaluated for FRP bars reinforced concrete (FRP-RC) structures.

Table 1.1. Properties of FRP bars

Type of FRP bar	Source	Ultimate tensile strain (ε_{TFRP} in %)	Tensile modulus of elasticity (GPa)
Glass-FRP (GFRP)	Choo et al.[5]	1.40	45
	fib bulletin 40 [6]	1.20-3.70	35-60
	Afifi et al.[7]	1.56-1.90	53-55
	Maranan et al.[8]	1.89-2.11	62.6-65.1
	Guérin et al.[9]	2.10-2.60	51.3-53.3
	Abdelazim et al.[10]	2.35-2.51	51-62
	Alnajmi and Abed[11]	1.90	45

	Elchalakani et al.[12]	1.60	59
	Elmesalami et al.[13]	1.75	45
	Almomani et al.[14]	2.40	64
Carbon-FRP (CFRP)	Choo et al.[5]	1.60	147
	fib bulletin 40[6]	0.50-1.70	100-580
	Mohamed et al.[15]	1.20-1.33	120-140
	Hadhood et al.[16]	1.19-1.20	130-141
	Othman et al.[17]	1.32-1.38	145-151
	Zhao et al.[18]	1.61	143
Aramid-FRP (AFRP)	Choo et al.[5]	2.40	87
	fib bulletin 40 [6]	1.90-4.40	40-125
Basalt-FRP (BFRP)	Fan et al.[19]	2.76-2.79	42.51-50.32
	Alnajmi et al.[11].	2.10	49.3
	Elmesalami et al.[20]	2.02-2.55	45.9-49.3
	Bakouregui et al.[21]	2.67	64.8

1.2 FRP-RC columns

Compression members, such as columns, are subjected to a combined action of axial force and bending moment and thus shall be designed to resist such combined action. Due to the space efficiency and aesthetics, frequent use of slender columns is observed. In addition to material failure, slender columns also fail due to the instability of the structure. Moreover, the low stiffness of FRP bars makes FRP-RC columns more prone to capacity reduction due to an increase in slenderness [22–24]. Several research studies have been conducted to evaluate the flexural and shear behavior of FRP RC members [8,25,26]. However, the studies to assess the behavior of FRP-RC columns especially in eccentric loading are limited. Elmessalami et al. [27] reported that 90% of the experimental results available in the literature

for FRP-RC columns are for short columns. The majority of these experiments belong to concentrically loaded columns.

In order to simplify the analysis of reinforced concrete columns, design codes provide a slenderness limit, defined as the slenderness ratio below which second-order effects due to geometry can be neglected and columns can be considered as short. Mirimiran et al. [22] suggested a reduced slenderness limit of 17 for GFRP-RC columns compared to 22 for steel-RC columns. They utilized the ACI 318-99 [28] criteria of 5 % strength reduction at an eccentricity ratio of 20 % and reinforcement ratio of 1 % to calculate the slenderness limit. Zadeh and Nanni [29] proposed a slenderness limit of 14 and 17 for GFRP-RC and CFRP-RC columns. Abdelazim et al. [10,30] proposed slenderness limit of 18 for GFRP-RC columns. ACI 440.11-22 [31] provides a slenderness limit of 17 for GFRP-RC columns. However, no literature was found to provide a comprehensive equation for the slenderness limit of FRP-RC columns.

For slender columns, a rigorous numerical analysis that considers second-order effects including geometrical and numerical nonlinearity shall be accomplished for an effective design. To avoid a comprehensive second-order analysis, design codes provide simplified second-order analysis methods. Eurocode 2 provides two simplified methods, namely, the nominal stiffness and nominal curvature method given for steel-RC columns. ACI 318-19 [32] provide a simplified method for second-order analysis of steel-RC columns based on effective stiffness. Mirmiran et al. [22], Xue et al. [33], and Abdelazim et al. [34] provided equations to estimate the effective stiffness of GFRP-RC columns. They found a reduced value of nominal stiffness for FRP-RC columns as compared to steel-RC columns. Moreover, no work in the literature was found on the nominal curvature method for FRP-RC columns. Some national annexures to Eurocode 2 such as German national annexure, permit only the nominal curvature method for the simplified second-order analysis of steel-RC columns, explicitly excluding the nominal stiffness method.

Furthermore, for the simplified second order analysis of the columns subjected to unequal end moments, equivalent moment factor is provided in the design codes for steel-RC columns. However, no research is available in the literature on the equivalent moment factor of FRP-RC columns.

The available works in the literature regarding the design of FRP-RC columns are majorly focused on the design philosophy of North American codes. However, no literature was found based on Eurocode 2 design philosophy. Consequently, preliminary work was conducted on the analysis and design of FRP-RC columns based on the Eurocode 2 design philosophy.

1.3 Preliminary research

As a preliminary research work, the behavior of short and slender FRP-RC columns was studied [24]. Furthermore, the effect of slenderness ratio on the capacity of FRP-RC columns was investigated in detail. Due to the increase in slenderness ratio (λ), the reduction in the load capacity of long column (P_{long}) and moment capacity of long column (M_{long}) in comparison to load capacity (P_{short}) and moment capacity of short column (M_{short}) was assessed for a given eccentricity ratio (e) and given axial force ratio (n) as shown in Fig. 1.1 with a modulus of elasticity of FRP bar (E_{FRP}) of 40 GPa and yield strength of steel (f_y) of 500 MPa. Here, long columns are defined as columns for which the load and moment capacity is calculated considering the effect of slenderness while short columns are the columns for which the load and moment capacity is calculated without considering the effect of slenderness.

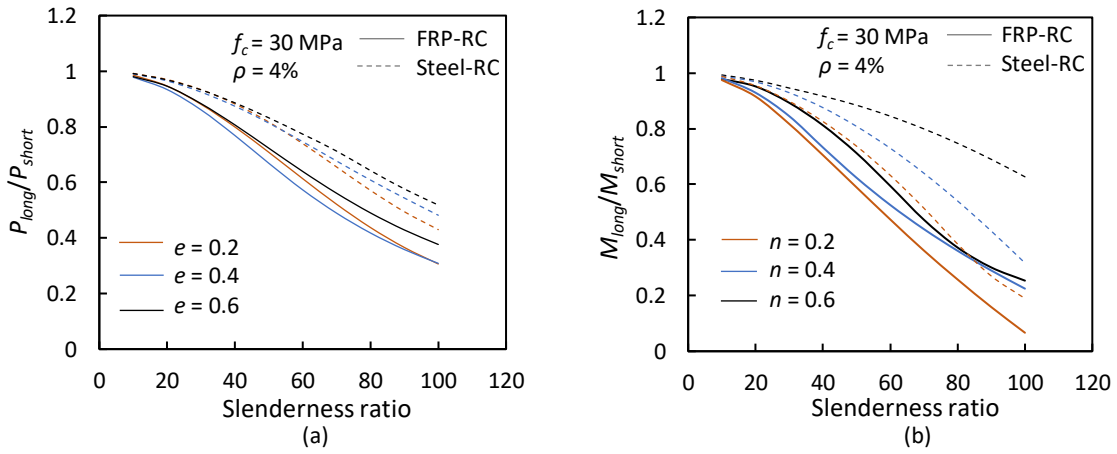


Fig. 1.1. Effect of increase in slenderness on the (a) load capacity and (b) moment capacity of FRP-RC and steel-RC column [24]

Here, f_c is the concrete compressive strength and ρ is the reinforcement ratio expressed as

$$\rho = \frac{A_r}{A_c} 100 \tag{1.1}$$

where, A_r is the area of reinforcement and A_c is the area of concrete. n is expressed as

$$n = \frac{P}{A_c f_c} \tag{1.2}$$

$$e = \frac{e_1}{h} \tag{1.3}$$

where, P is the axial force in the column, e_1 is the first-order column eccentricity and h is the depth of the column cross-section.

It was observed with the increase in the slenderness ratio at a constant value of eccentricity, the load capacity (P_{long}) of long FRP-RC columns decreased more rapidly than steel-RC columns. Similarly, the moment capacity of long FRP-RC columns exhibited a faster decline compared to steel-RC columns at a constant axial force ratio. Furthermore, the load capacity of long columns for FRP-RC column show a steepest decline with the increase of slenderness ratio for the eccentricity ratio of $e = 0.4$ compared to eccentricity ratio of 0.2 and 0.6 considered in this study. However, this is not the same for steel-RC columns where the steepest decline is observed for $e = 0.2$.

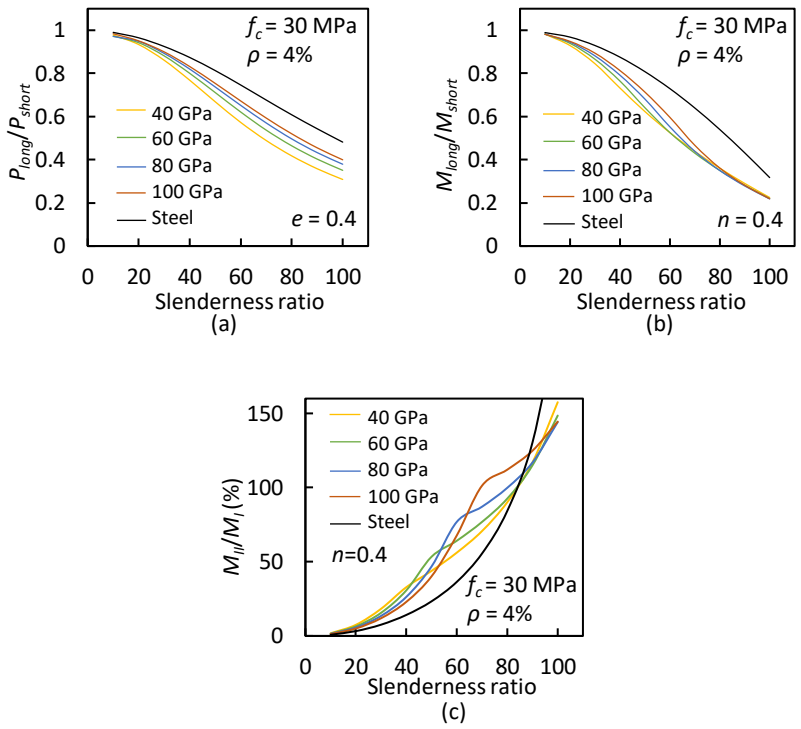


Fig. 1.2. Effect of modulus of elasticity of FRP bar on the (a) load capacity, (b) moment capacity and (c) second-order moment of FRP-RC and steel-RC columns [24]

Additionally, the effect of the change in the modulus of elasticity of FRP bars (E_{FRP}) on the load capacity reduction and moment capacity reduction with increasing slenderness ratio was also investigated as shown in Fig. 1.2. It was observed that with the increase of modulus of elasticity of FRP bars (E_{FRP}) at constant eccentricity ratio, the decrease in load capacity of long FRP-RC columns reduces as the modulus of elasticity is increased. Moreover, at a constant axial force ratio with the increase of modulus of elasticity of FRP bars (E_{FRP}), the decrease in moment capacity of long FRP-RC columns reduces as the modulus of elasticity is increased up to certain slenderness ratio, such as 80 for the values considered for Fig. 1.2(b). However, for slenderness ratio more than 80, no effect of modulus of elasticity of FRP bars is observed on the reduction of the moment capacity of the FRP-RC columns.

Furthermore, the load-moment capacity interaction curves for cross-section of the columns are essential for the simplified second-order analysis. Fig. 1.3 presents a comparison between the load-moment capacity interaction curve of FRP-RC columns and steel-RC columns. Here, ε_{TFRP} represents the ultimate tensile strain of the FRP bar.

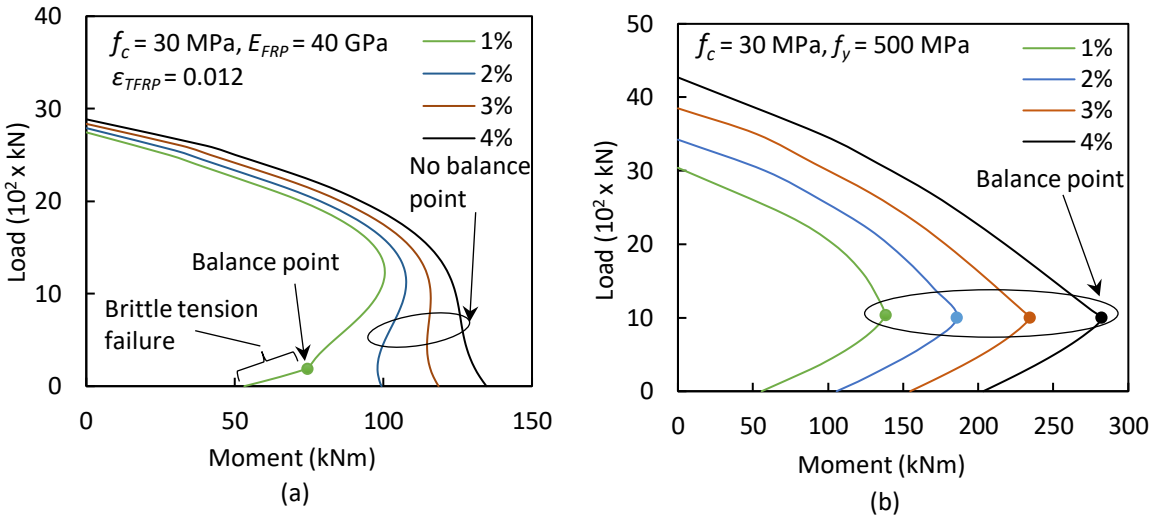


Fig. 1.3. Load-moment capacity interaction curve for (a) FRP-RC and (b) Steel-RC column cross-section [24]

It was observed that while FRP-RC columns exhibit the typical "knee-shaped" load-moment interaction curve, however the characteristics of the curve differ significantly compared to steel-RC columns. The balance point where the maximum ultimate concrete compressive strain and ultimate tensile strain are attained simultaneously for FRP-RC columns is observed at a very low value of axial force and it is not observed for all value of reinforcement ratio. Furthermore, the appearance of balance point for FRP-RC columns is dependent on the modulus of elasticity of FRP bars as shown in Fig. 1.4. Here, E_c represents the modulus of elasticity of the concrete. As the modulus of elasticity of FRP bar is increased, the balance point shifts down in the load-moment capacity interaction curve. Moreover, the appearance of balance point is also dependent on the reinforcement ratio and concrete compressive strength and it is not solely dependent on the ratio of stiffness of FRP bar and concrete ($\frac{E_{FRP}}{E_c}$).

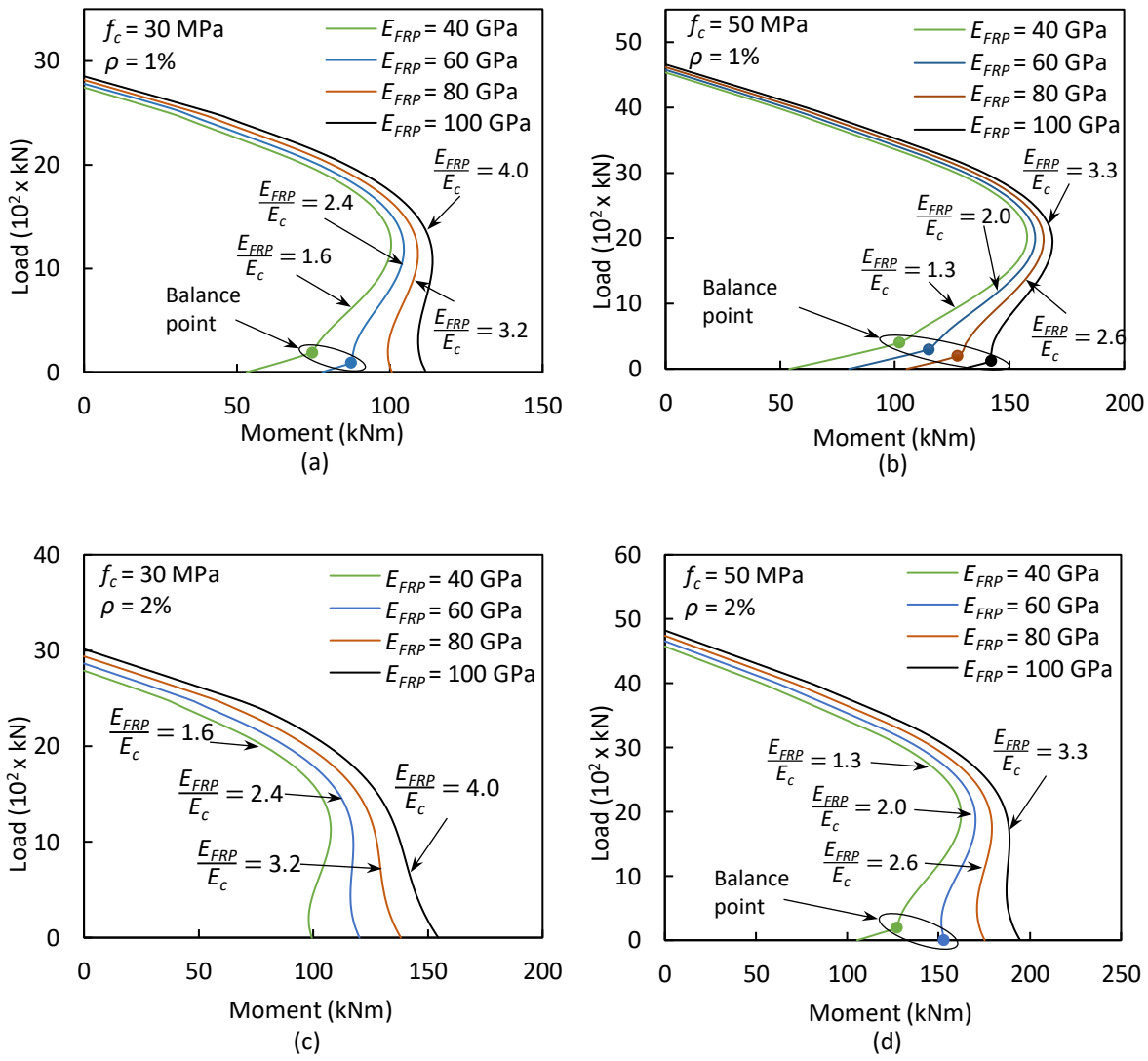


Fig. 1.4. Effect of material propertied and reinforcement ratio on the balance point of FRP-RC columns [24]

However, the balance point for steel-RC columns where steel yields and concrete reach the maximum ultimate compressive strain simultaneously appears at the knee bend of the curve and is independent of the reinforcement ratio as seen in Fig. 1.3(b). The position of balance point for columns is also importance to classify the type of failure of column and for the simplified second-order analysis procedures such as nominal curvature method.

Based on the findings of the preliminary study presented above, the difference observed in the behavior of the load and moment capacity with respect to slenderness ratio, eccentricity ratio and axial force ratio suggests that the application of the available methods to perform the simplified second-order analysis

of steel-RC columns shall require reassessment for FRP-RC columns. Moreover, the equations to estimate the nominal curvature and nominal stiffness may need to be revised upon detailed investigation and study of FRP-RC columns.

1.4 Objectives of the study

The overall objective of this study was to study the behavior of slender FRP-RC columns and to develop design methods and guidelines for their analysis and design. The guidelines and equations were to be developed in the framework of Eurocode 2 such that they can be easily adopted by relevant European standards and guidelines. The specific objectives and sub-objectives were identified as:

1. **To develop the basis to identify short and slender FRP-RC columns**.

   To investigate the effect of slenderness on the increase of second-order moments and to develop slenderness limit equation for FRP-RC columns.
2. **To develop a simplified second-order analysis method for FRP-RC columns**.

   To assess the behavior of the nominal curvature of slender FRP-RC columns and to develop nominal curvature method and related equations for FRP-RC columns.
3. **To expand the applicability of the simplified second-order analysis method for columns subjected to unequal end-moments.**

   To investigate the equivalent moment factor for simplified analysis of FRP-RC columns.
4. **To develop the design tools for the successful implementation of the simplified second-order analysis of FRP-RC columns.**

   To develop generalized load-moment interaction diagrams for FRP-RC columns valid to various type of FRP bars.

1.5 Organization of the Thesis

This thesis is structured into five logically arranged chapters that collectively fulfill all the objectives of the study. The thesis consists of three published journal papers (Chapter 2-4) and one submitted journal paper (Chapter 5). Introductory chapter (Chapter 1) is based on the published conference paper

(Annexure 1). At a few locations, a superscript asterisk (*) has been used to indicate corrections of typographical errors relative to the published versions of the papers.

Brief details of the chapters are presented as follows:

Chapter 1 presents a brief background about the use of FRP bars and their material properties. This chapter also reviews the available research and guidelines for FRP-RC columns. Furthermore, results and discussions from a preliminary research study published as a conference paper (Annexure 1) are briefly presented. The observations from the preliminary research leads to formulate the objectives of this study. The publication details of the conference paper [24] are detailed as follows:

Syed AU, Goldack A. Effect of Slenderness on the Design of FRP Reinforced Concrete Columns. In: IABSE Congress New-Delhi 2023, p. 574–82. https://doi.org/10.2749/newdelhi.2023.0574

Credit authorship contribution statement:

Ahmed Usama Syed: Writing – original draft, Visualization, Validation, Software, Methodology, Investigation, Funding acquisition, Formal analysis, Data curation, Conceptualization. **Arndt Goldack:** Writing – review & editing, Supervision, Resources, Project administration, Methodology, Funding acquisition, Conceptualization.

Chapter 2 presents a detailed study on the slender GFRP-RC columns performed to assess the increase of second-order moments in GFRP-RC columns on increasing the slenderness ratio. The slenderness limit is identified based on two criteria which are adopted by design codes. As a result of the detailed parametric study, slenderness limit equations for GFRP-RC columns are proposed. Hence, this chapter provides basis to identify short and slender FRP-RC columns. Numerical method developed in this study to perform the second-order analysis of reinforced concrete columns is also presented in detail. This part of the study was published as a journal paper [35] detailed as follows:

Syed AU, Goldack A. Slenderness limit for GFRP reinforced concrete columns based on axial force ratio. Engineering Structures 2024;298:117026.

https://doi.org/10.1016/j.engstruct.2023.117026

Credit authorship contribution statement:

Ahmed Usama Syed: Writing – original draft, Visualization, Validation, Software, Methodology, Investigation, Funding acquisition, Formal analysis, Data curation, Conceptualization. **Arndt Goldack:** Writing – review & editing, Supervision, Resources, Project administration, Methodology, Funding acquisition, Conceptualization.

Chapter 3 investigates the behavior of the nominal curvature of FRP-RC column in comparison to steel-RC columns. The application of nominal curvature method for the simplified second-order analysis of slender FRP-RC columns is explored in detail. The equations to estimate the nominal curvature of FRP-RC columns are developed based on an extensive parametric study. Furthermore, equation to estimate the total curvature distribution factor is also proposed. Hence, this chapter provides a complete simplified method of second-order analysis of FRP-RC columns. This part of the study was published as a journal paper [36] detailed as follows:

Syed AU, Goldack A. Simplified Second-Order Analysis of Slender FRP-Reinforced Concrete Columns Using the Nominal Curvature Method. J. Compos. Constr. 2025;29(2):4025007. https://doi.org/10.1061/JCCOF2.CCENG-4944

Credit authorship contribution statement:

Ahmed Usama Syed: Writing – original draft, Visualization, Validation, Software, Methodology, Investigation, Funding acquisition, Formal analysis, Data curation, Conceptualization. **Arndt Goldack:** Writing – review & editing, Supervision, Resources, Project administration, Methodology, Funding acquisition, Conceptualization.

Chapter 4 examines the applicability of the equivalent moment factor adopted in design codes of steel-RC columns for FRP-RC columns in detail. A detailed parametric study is performed to establish a suitable expression for FRP-RC columns. Numerical method to perform second-order analysis of reinforced concrete columns subjected to unequal moments is also presented. This part of the study was published as a journal paper [37] detailed as follows:

Syed AU, Goldack A. Analysis of slender FRP-reinforced concrete columns subjected to unequal end moments. Engineering Structures 2025;340:120768.

https://doi.org/10.1016/j.engstruct.2025.120768

Credit authorship contribution statement:

Ahmed Usama Syed: Writing – original draft, Visualization, Validation, Software, Methodology, Investigation, Funding acquisition, Formal analysis, Data curation, Conceptualization. **Arndt Goldack:** Writing – review & editing, Supervision, Resources, Project administration, Methodology, Funding acquisition, Conceptualization.

Chapter 5 presents the development of universal load-moment interaction diagrams applicable to various kinds of FRP bars. Universal load-moment interaction diagrams for cross-sectional analysis are provided for successful implementation of nominal curvature method presented in this study. Furthermore, based on the nominal curvature method developed for FRP-RC columns in this study, universal load-moment interaction diagrams for slender FRP-RC columns are also presented. Moreover, complete worked examples are presented as a reference. This part of the study is submitted as a manuscript for publication as a journal paper [38] with detail as follows:

Syed AU, Goldack A, Koehler R. Forthcoming. Design of FRP-RC columns with nominal curvature method and universal interaction diagrams applicable to various FRP bar types. Journal of Structural Design and Construction Practice.

https://doi.org/10.1061/JSDCCC/SCENG-2290

Credit authorship contribution statement:

Ahmed Usama Syed: Writing – original draft, Writing – review & editing, Visualization, Validation, Methodology, Investigation, Formal analysis, Data curation, Software, Funding acquisition, Conceptualization. **Arndt Goldack**: Writing – original draft, Writing – review & editing, Formal analysis, Supervision, Resources, Project administration, Methodology, Funding acquisition, Conceptualization. **Richard Koehler:** Writing – review & editing, Software, Validation, Formal analysis, Investigation, Data curation, Visualization

1.6 References

[1] Sheikh MN, Légeron F. Performance based seismic assessment of bridges designed according to Canadian Highway Bridge Design Code. Can. J. Civ. Eng. 2014;41(9):777–87.

[2] Yue L, Tankred L, Arndt G, Mike S. Study on the flexural behaviour of CFRP-grid reinforced concrete one-way slabs. In: 4th Asia-Pacific Conference on FRP in Structures (APFIS 2013).

[3] Cadenazzi T, Dotelli G, Rossini M, Nolan S, Nanni A. Life-Cycle Cost and Life-Cycle Assessment Analysis at the Design Stage of a Fiber-Reinforced Polymer-Reinforced Concrete Bridge in Florida. Adv. Civ. Eng. Matls. 2019;8(2):20180113.

[4] Pavlović A, Donchev T, Petkova D, Staletović N. Sustainability of alternative reinforcement for concrete structures: Life cycle assessment of basalt FRP bars. Construction and Building Materials 2022;334:127424.

[5] Choo C.C., Harik I.E. and Gesund H. Strength of Rectangular Concrete Columns Reinforced with Fiber-Reinforced Polymer Bars. ACI Structural Journal 2006;103(3):452-459.

[6] Fib Bulletin 40. FRP reinforcement in RC structures. Stuttgart: The International Federation for Structural Concrete; 2007.

[7] Afifi MZ, Mohamed HM, Benmokrane B. Axial Capacity of Circular Concrete Columns Reinforced with GFRP Bars and Spirals. J Compos Constr 2014;18(1):4013017.

[8] Maranan GB, Manalo AC, Benmokrane B, Karunasena W, Mendis P. Behavior of concentrically loaded geopolymer-concrete circular columns reinforced longitudinally and transversely with GFRP bars. Engineering Structures 2016;117:422–36.

[9] Guérin M, Mohamed HM, Benmokrane B, Nanni A, Shield CK. Eccentric Behavior of Full-Scale Reinforced Concrete Columns with Glass Fiber-Reinforced Polymer Bars and Ties. ACI Structural Journal 2018;115(2):489–99.

[10] Abdelazim W, Mohamed HM, Benmokrane B. Inelastic Second-Order Analysis for Slender GFRP-Reinforced Concrete Columns: Experimental Investigations and Theoretical Study. J Compos Constr 2020;24(3).

[11] AlNajmi L, Abed F. Evaluation of FRP Bars under Compression and Their Performance in RC Columns. Materials 2020;13(20).

[12] Elchalakani M, Dong M, Karrech A, Mohamed Ali MS, Huo J-S. Circular Concrete Columns and Beams Reinforced with GFRP Bars and Spirals under Axial, Eccentric, and Flexural Loading. J. Compos. Constr. 2020;24(3).

[13] Elmesalami N, Abed F, Refai AE. Concrete Columns Reinforced with GFRP and BFRP Bars under Concentric and Eccentric Loads: Experimental Testing and Analytical Investigation. J. Compos. Constr. 2021;25(2).

[14] Almomani M, Mahmoud K, El-Salakawy EF. Experimental Investigation of Large-Scale Eccentrically Loaded GFRP-Reinforced High-Strength Concrete Columns. J. Compos. Constr. 2022;26(2).

[15] Mohamed HM, Afifi MZ, Benmokrane B. Performance Evaluation of Concrete Columns Reinforced Longitudinally with FRP Bars and Confined with FRP Hoops and Spirals under Axial Load. J. Bridge Eng. 2014;19(7).

[16] Hadhood A, Mohamed HM, Benmokrane B. Flexural Stiffness of GFRP- and CFRP-RC Circular Members under Eccentric Loads Based on Experimental and Curvature Analysis. ACI Structural Journal 2018;115(4):1185–98.

[17] Othman ZS, Mohammad AH. Behaviour of Eccentric Concrete Columns Reinforced with Carbon Fibre-Reinforced Polymer Bars. Advances in Civil Engineering 2019;2019:1–13.

[18] Zhao J, Chenzhe S, Wenbo R, Xiangcheng Z, Yuping S. Experimental and numerical studies on seismic performance of rectangular concrete columns reinforced by CFRP bars with different ratios and positions. Structures 2021;32:237–53.

[19] Fan X, Xu T, Zhou Z, Zhou X. Experimental Study on Basic Mechanical Properties of BFRP Bars. IOP Conf. Ser.: Mater. Sci. Eng; 2017.

[20] Elmesalami N, Abed F, Refai AE. Concrete Columns Reinforced with GFRP and BFRP Bars under Concentric and Eccentric Loads: Experimental Testing and Analytical Investigation. J. Compos. Constr. 2021;25(2).

[21] Bakouregui AS, Mohamed HM, Yahia A, Benmokrane B. Axial load–moment interaction diagram of full-scale circular LWSCC columns reinforced with BFRP and GFRP bars and spirals: Experimental and theoretical investigations. Engineering Structures 2021;242:112538.

[22] Mirmiran A, Yuan W, Chen X. Design for Slenderness in Concrete Columns Internally Reinforced with Fiber-Reinforced Polymer bars. ACI Struct J 2001;98(1):116–25.

[23] Hamid FL, Yousif AR. Behavior of Short and Slender RC Columns with BFRP Bars under Axial and Flexural Loads: Experimental and Analytical Investigation. J. Compos. Constr. 2024;28(1).

[24] Syed AU, Goldack A. Effect of Slenderness on the Design of FRP Reinforced Concrete Columns. In: IABSE Congress New-Delhi 2023, p. 574–82.

[25] Sun L, Wei M, Zhang N. Experimental study on the behavior of GFRP reinforced concrete columns under eccentric axial load. Construction and Building Materials 2017;152:214–25.

[26] Hadhood A, Mohamed HM, Benmokrane B. Experimental Study of Circular High-Strength Concrete Columns Reinforced with GFRP Bars and Spirals under Concentric and Eccentric Loading. J. Compos. Constr. 2017;21(2).

[27] Elmessalami N, El Refai A, Abed F. Fiber-reinforced polymers bars for compression reinforcement: A promising alternative to steel bars. Construction and Building Materials 2019;209:725–37.

[28] ACI 318-99. Building Code Requirements for Structural Concrete & Commentary. Farmington Hills, MI: American Concrete Institute; 1999.

[29] Zadeh HJ, Nanni A. Flexural Stiffness and Second-Order Effects in FRP-RC Frames. ACI Struct J 2017;114(2):533–44.

[30] Abdelazim W, Mohamed HM, Afifi MZ, Benmokrane B. Proposed Slenderness Limit for Glass Fiber-Reinforced Polymer-Reinforced Concrete Columns Based on Experiments and Buckling Analysis. ACI Structural Journal 2020;117(1).

[31] ACI. Building Code Requirements for Structural Concrete Reinforced with Glass Fiber-Reinforced Polymer (GFRP) Bars-Code and Commentary.(ACI CODE-440.11-22). Farmington Hills, MI: American Concrete Institute; 2022.

[32] ACI. Building Code Requirements for Structural Concrete and Commentary(ACI CODE 318-19). Farmington Hills, MI: American Concrete Institute; 2019.

[33] Xue W, Peng F, Fang Z. Behavior and Design of Slender Rectangular Concrete Columns Longitudinally Reinforced with Fiber-Reinforced Polymer Bars. ACI Structural Journal 2018;115(2).

[34] Abdelazim W, Mohamed HM, Benmokrane B. Proposed Flexural Stiffness of Slender Concrete Columns Reinforced with Glass Fiber-Reinforced Polymer Bars. ACI Structural Journal 2021;118(1):227–40.

[35] Syed AU, Goldack A. Slenderness limit for GFRP reinforced concrete columns based on axial force ratio. Engineering Structures 2024;298:117026.

[36] Syed AU, Goldack A. Simplified Second-Order Analysis of Slender FRP-Reinforced Concrete Columns Using the Nominal Curvature Method. J. Compos. Constr. 2025;29(2):4025007.

[37] Syed AU, Goldack A. Analysis of slender FRP-reinforced concrete columns subjected to unequal end moments. Engineering Structures 2025;340:120768.

[38] Syed AU, Goldack A, Koehler R. Forthcoming. Design of FRP-RC columns with nominal curvature method and universal interaction diagrams applicable to various FRP bar types. Journal of Structural Design and Construction Practice.

2. Slenderness Limit for GFRP Reinforced Concrete Columns Based on Axial Force Ratio

Ahmed Usama Syed[1], Arndt Goldack[2]

[1 2] University of Wuppertal, Chair of Statics and Dynamics of Structures, Pauluskichstraße 7, 42285 Wuppertal, Germany.

Published in

Engineering Structures (2024) 298:117026 (DOI: https://doi.org/10.1016/j.engstruct.2023.117026)

ABSTRACT

Concrete columns reinforced with fiber-reinforced polymer (FRP) bars have been of great interest in recent years. The distinct properties of FRP bars, such as linear stress-strain behavior and low modulus of elasticity in comparison to steel bars, make the study of FRP reinforced concrete (FRP-RC) columns of importance, especially with regard to the effect of slenderness. This work presents a numerical method for second-order analysis and examines the slenderness limit of glass FRP bars reinforced concrete (GFRP-RC) columns based on two criteria: a reduction in moment capacity at constant load and a reduction in load capacity at constant eccentricity. In the literature, only limited contributions have been made on the slenderness limit of FRP-RC columns, usually based on the latter criterion, whereas there is a lack of literature regarding the slenderness limit of FRP-RC columns based on the former criterion, which is also the slenderness limit criterion of Eurocode 2 (EC2-04) for steel-reinforced concrete (steel-RC) columns. This work may assist in the development of Eurocode provisions, national annexures and guidelines for the design of GFRP-RC concrete columns. A detailed sensitivity analysis was conducted with parameters including the modulus of elasticity of the GFRP bar, percentage of reinforcement, compressive strength of concrete and axial force ratio to examine the variation of slenderness limit for GFRP-RC columns. The axial force ratio is observed to be an important parameter to estimate the slenderness limit from the sensitivity analysis. Variation of slenderness limit for GFRP-RC columns with axial force ratio is observed to be different and the value of slenderness limit is lower compared to the steel-RC columns. Two equations, which take into account the variation due to the axial force ratio, are proposed to estimate the slenderness limit for GFRP-RC columns.

Keywords: fiber-reinforced polymer bars; GFRP bars reinforced concrete column; second-order analysis; short column; slenderness limit

2.1 Introduction

Fiber-reinforced polymers (FRP) bars have emerged as an innovative solution for reinforcing structural concrete. The properties of FRPs such as non-corrosiveness, high strength-to-weight ratio and non-magnetic properties, make them an attractive alternative to steel as a reinforcement for concrete structures. Compared to steel reinforcement, FRPs have a linear elastic stress-strain behavior and high tensile strength. There have been various research studies investigating the use of glass-FRP (GFRP), carbon-FRP (CFRP) and aramid-FRP (AFRP) as a reinforcement. In recent years, the practical application of GFRP as reinforcement has gained significant interest due to its low cost compared to other FRP types [1]. Despite having high tensile strength, GFRP bars have a low modulus of elasticity as shown in Table 2.1 [2]. Structural members such as columns and frames are typically subjected to eccentric compressive loads. Consequently, the influence of geometric nonlinearities known as second-order effects must be taken into consideration. However, the amount of the second-order effects depends on the flexibility and deformation of the structural member. In such a scenario, the low modulus of elasticity might be a cause of concern for the design of GFRP-reinforced concrete (GFRP-RC) members. To simplify the design of reinforced concrete for second-order effects, design codes for steel-RC allow the second-order effects to be ignored if the slenderness ratio (λ) does not exceed a specific value defined as the slenderness limit (λ_{lim}). Here, slenderness ratio (λ) is defined as:

$$\lambda = kL/r \tag{2.1}$$

where k is the effective length factor; L is the unsupported length of the column, and r is the radius of gyration of the cross-section.

Design codes and guidelines such as ACI 440.11-22 [3], CSA S806-12 [4] and ACI 440.1R-15 [5] provide regulations for the design of FRP reinforced concrete (FRP-RC) structural members, including the slenderness limit. However, such provisions for FRP-RC structures are lacking in Eurocode.

Based on a parametric study, Mirmiran et al. [6] suggested a slenderness limit of 17 for FRP-RC columns. They proposed the slenderness limit based on a 1% reinforcement ratio and 20 % eccentricity ratio considering the basis of ACI 318-99 [7] criterion for steel RC columns. Zadeh and Nanni [8] proposed a slenderness limit of 14 and 17 for glass FRP (GFRP) and carbon FRP (CFRP) reinforced concrete columns respectively based on estimating the column's effective stiffness and neglecting the

tensile force in reinforcement. Abdelazim et al. [9,10] proposed a slenderness limit of 18 for GFRP-RC columns considering a 1% reinforcement ratio. They utilized Euler-Johnson's failure envelope [9] and a numerical model for second-order analysis [10]. All the studies mentioned above followed the slenderness limit criterion similar to the criterion in ACI 318-19 [11].

ACI 440.11-22 [3] states a slenderness limit of 17 for GFRP-RC columns not braced against sidesway. It also provides an equation incorporating first-order end moment ratio for estimating the slendeness limit of columns braced against sidesway, expressed as:

$$\frac{kL}{r} \leq 29 + 12(M_1/M_2) \leq 35 \tag{2.2}$$

where M_1 is the smaller factored end moment and M_2 is the larger factored end moments. M_2 is always considered positive. M_1/M_2 is negative when bent in single curvature.

Relying on the slenderness limit for steel-RC columns as per ACI 318 [9,11], CSA S806-12 [4] gives a slenderness limit value of 22 for FRP-RC columns not braced against sidesway and an equation for columns braced against sidesway, expressed as:

$$\frac{kL}{r} \leq 34 - 12(M_1/M_2) \leq 40 \tag{2.3}$$

Here, M_1/M_2 is considered positive when bent in single curvature.

However, to the best of the authors' knowledge, to date, no literature is available for the slenderness limit of FRP-RC columns based on the slenderness limit criterion of EC2-04 [12]. Furthermore, the existing literature lacks slenderness limit equations for FRP-RC columns that incorporates the factors such as concrete compressive strength, reinforcement ratio and relative normal force or axial force ratio, such as the equation available for steel-RC columns in EC2-04 [12].

This work aims to provide a valuable contribution to the development of Eurocode provisions and national annexures for FRP-RC structures considering the safety and design concept of Eurocode 2 (EC2-04) [12]. Furthermore, it may also assist in the further development of DAfStb (2023) guidelines for FRP-RC structures.

This paper discusses the following points specifically for GFRP-RC columns:

- Second-order analysis of reinforced concrete columns.

- Different criteria to estimate slenderness limit.
- The effect of axial force ratio, concrete strength, reinforcement ratio, and modulus of elasticity of GFRP bar on the slenderness limit value of GFRP-RC columns.
- Equation to estimate the slenderness limit of GFRP-RC columns.

Table 2.1. Mechanical properties of different FRP bars

Property	Steel	GFRP	CFRP	AFRP
Modulus of Elasticity (GPa)	200	35 to 60	100 to 580	40 to 125
Ultimate tensile strength (GPa)	450 to 700	450 to 1600	600 to 3500	1000 to 2500
Ultimate tensile strain (%)	5 to 20	1.2 to 3.7	0.5 to 1.7	1.9 to 4.4

Note: Typical values for the fiber volume fraction (V_f) of 0.5 to 0.75. V_f is defined as the ratio of the volume of fibers to the volume of the matrix material.

2.2 Slenderness limit

2.2.1 Second-order effects

Second-order effects are additional effects caused by the structural deformation of structures upon loading. For compression members like columns, these additional effects are observed in the form of second-order moments. These moments arise from the lateral deflection of the column. The relationship between first-order and second-order moments can be stated as:

$$M_t = M_I + M_{II} \tag{2.4}$$

where M_t is the total moment obtained from the second-order analysis at a particular column section, M_I is the moment due to first-order load eccentricity and M_{II} is the second-order moment due to the lateral deflection at this column section.

The failure of the column is determined by the failure of the column section with the maximum total moment and load. As shown in Fig. 2.1(a), the maximum total moment occurs at the mid-height of the column for a simply supported column with axial load *P* and uniform first-order load eccentricity *e*. For the section at the mid-height of this column, M_I is the first-order moment due to load eccentricity *e* and M_{II} is the second-order moment due to the lateral deflection *w*.

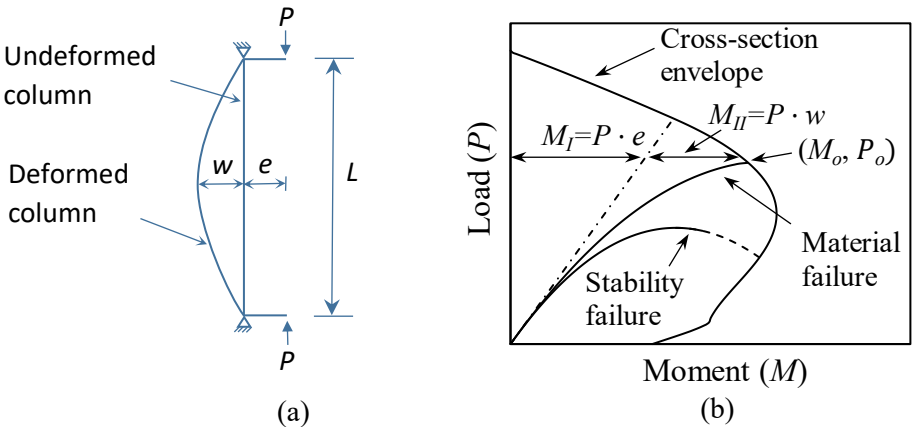


Fig. 2.1. (a) Simply supported column with uniform first-order eccentricity; and (b) Illustration of the failure of eccentrically loaded column due to slenderness

Using the material stress-strain curves, equilibrium of forces and compatibility of strains in the cross-section, the maximum value of the resisting moment for a given value of axial load can be calculated as the cross-sectional moment capacity (M_o). For different values of axial load, an envelope of load vs moment capacity can be obtained as shown in Fig. 2.1(b).

In the case of material failure, the total moment from the second-order analysis (M_t) is equal to the cross-sectional moment capacity (M_o) at failure. Whereas in the case of stability failure, the total moment (M_t) from the second-order analysis may be lower than the cross-sectional moment capacity (M_o) at failure [13].

2.2.2 Slenderness limit criteria

Quantifying the second-order effects, in terms of slenderness ratio, on the behavior of columns leads to the classification of columns into short and long columns. The second-order effects have negligible influence on the ultimate capacity of short columns, therefore they can be ignored for this category of columns. However, for long columns, second-order effects become significant and cannot be neglected in design. The slenderness ratio that corresponds to the limit value of capacity reduction is stated as the slenderness limit (λ_{lim}). Columns with a slenderness ratio not exceeding the slenderness limit are classified as short columns, while others are classified as long columns. The failure of short columns is

due to material failure, whereas stability failure may be a cause of failure in long columns.

Generally, design codes and guidelines use two different criteria to limit the capacity reduction of columns, to determine the slenderness limit. Criterion 1 can be stated as a reduction in moment capacity at constant load. While criterion 2 can be stated as a reduction in load capacity at constant eccentricity. Furthermore, different design codes use varying levels of limiting percentages to determine the slenderness limit criteria, such as 5% or 10% capacity reduction.

Eurocode 2 (EC2-04**)** [12] allows to ignore the second-order effects for steel-reinforced concrete columns if they are less than 10% of the corresponding first-order effects. Based on commentary to Eurocode 2 [14] and literature [15], EC2-04 [12] criteria for slenderness limit corresponds to criterion 1, which is a 10% increase in moments due to second-order effects at constant load. EC2-04 [12] provides an equation to calculate the slenderness limit (denoted as λ_{limEC2}) for steel-reinforced columns based on the mechanical reinforcement ratio (ω), end moment ratio (r_m), axial force ratio at design value (n_d) and effective creep ratio (φ_{ef}). It is expressed as:

$$\lambda_{limEC2} = 20 \cdot A \cdot B \cdot \frac{C}{\sqrt{n_d}} \geq \frac{kL}{r} \tag{2.5}$$

where

$$A = 1/\left(1 + 0.2\varphi_{ef}\right) \tag{2.6}$$

$$B = \sqrt{1 + 2\omega} \tag{2.7}$$

$$C = 1.7 - r_m \tag{2.8}$$

$$\omega = A_s f_{yd}/\left(A_c f_{cd}\right) \tag{2.9}$$

$$n_d = N_{Ed}/A_c f_{cd} \tag{2.10}$$

$$r_m = M_{01}/M_{02} \tag{2.11}$$

M_{01} and M_{02} are the first order end moments (including imperfections) such that $|M_{01}| \leq^* |M_{02}|$, N_{Ed} is the design value of axial force, A_c is the net cross-sectional area of concrete, f_{cd} is the design value of concrete compressive strength, A_s is the total area of longitudinal reinforcement and f_{yd} is the design yield strength of reinforcement. r_m is taken positive when bent in single curvature.

Slenderness limit of steel-RC columns as per the national annexure to Eurocode 2 for Germany (DIN

EN 1992-1-1/NA-13) [16] is denoted here as λ_{limDIN} and is expressed as:

$$\lambda_{limDIN} = \begin{cases} 25 & n_d \geq 0.41 \\ 16/\sqrt{n_d} & n_d < 0.41 \end{cases} \geq \frac{kL}{r} \tag{2.12}$$

(n_d is denoted as n in EC2-04 [12] and DIN EN 1992-1-1/NA-13 [16]).

The ACI 318-19 [11] allows a 5 % increase in moments due to slenderness and provides expressions to calculate slenderness limit of columns in braced and unbraced frames. As presented by Macgregor et al. [13], these expressions are derived considering 5% reduction in load capacity. When considered collectively, a 5% increase in moments and a reduction of about 5% in load capacity, corresponds to criterion 2, which is a decrease of about 5% in load capacity due to second-order effects at constant eccentricity. ACI 318-19 [11] does not explicitly state whether its criteria of a 5% increase in moments is at a constant eccentricity or not. However, Mirmiran et al. [6] mentions that slenderness limit for ACI 318-99 [7] were based on 20% eccentricity ratio.

Considering the limiting percentage of 10% similar to EC2-04 [12], Fig. 2.2 illustrates both the slenderness criteria on the load capacity vs moment capacity plot.

For criterion 1, the second-order moment corresponding to a limit of 10% of the first-order moment can be stated as:

$$M_{II} = 0.1M_I \tag{2.13}$$

The increase in moments due to the second-order effect causes a consequent reduction in the moment capacity of the columns. Typically, for short columns, stability effects are insignificant and the failure is due to material failure. As mentioned previously for material failure, the total moment from the second-order analysis (M_t) is equal to cross-sectional moment capacity (M_o). Therefore, considering M_t equal to M_o at the slenderness limit as per criterion 1, there is a reduction in the moment capacity of about 9 % due to second-order effects [15]. This can be expressed as:

$$M_o = 1.1M_I \tag{2.14}$$

$$M_I = 0.909M_o \tag{2.15}$$

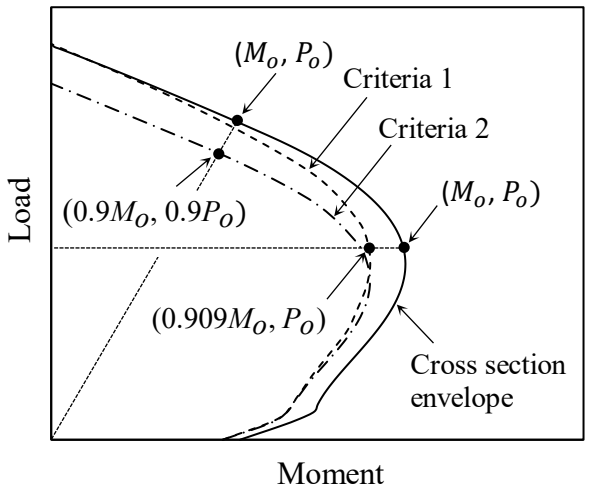


Fig. 2.2. Slenderness limit criteria (Load Capacity vs Moment Capacity)

For criterion 2, if the load capacity reduces by 10 % at a constant eccentricity, a reduction of 10% in the moment capacity is obtained. This can be expressed as:

$$M_I = 0.9M_o \tag{2.16}$$

$$P_{II} = 0.9P_o \tag{2.17}$$

where P_o is the load capacity of the column determined by cross-sectional analysis and P_{II} is the load capacity of the column determined by second-order analysis, both obtained at a constant eccentricity.

2.3 Numerical method for second-order analysis of reinforced concrete columns

A numerical method was implemented in Matlab [17] to perform the analysis of FRP-RC columns incorporating the second-order effects. The analysis is set up as a displacement control procedure, whereby the lateral deflection of the column is increased in an incremental manner. Assuming the column curvature to be sinusoidal, the column curvature is calculated at the column section where the lateral deflection is introduced. Using this value of curvature, the stress-strain state of the column section is determined upon implementing the equilibrium of forces based on the material properties and strain compatibility. Chuang and Kong [18] presented a transformed area method for slender columns with sinusoidal curvature assumption for second-order effects. In this study, the sinusoidal assumption of the curvature also accounts for end eccentricity for the determination of curvature, which is a modification in comparison to the Chuang and Kong [18] method. Najmi and Tayem [19] presented a

transformed area method for inelastic section analysis of short concrete columns. They transformed the area of concrete and steel into an equivalent area with linearly elastic and homogenous material. To account for the non-linear material properties of the section when implementing the equilibrium of forces and strain compatibility, the method in this study is based on the concept of transformation of the area, whereby the area of FRP bars and concrete is transformed into a linearly elastic material with a uniform modulus of elasticity throughout the cross-section.

2.3.1 Material properties

2.3.1.1 Concrete

The concrete inside the lateral ties is considered partially confined while concrete outside lateral ties is considered unconfined [20] as shown in Fig. 2.3. For unconfined concrete, the concrete stress-strain relationship presented by Popovics [21] was used. At the strain value of ε in concrete, for the unconfined concrete the compressive stress $\sigma_c(\varepsilon)$ can be expressed as:

$$\sigma_c(\varepsilon) = f_c\left(\frac{n'(\varepsilon/\varepsilon_o)}{n' - 1 + (\varepsilon/\varepsilon_o)^{n'}}\right) \tag{2.18}$$

where the curve fitting factor is given as $n' = 0.8 + f_c/17$, $\varepsilon_o = f_c n'/E_c(n'-1)$, f_c is the compressive strength of concrete and E_c is the tangent modulus of elasticity of concrete at $\varepsilon = 0$. In this study, E_c is calculated considering it as the secant modulus of elasticity between $\sigma_c = 0$ and $\sigma_c = 0.4f_c$ using Eq. (2.19) as presented by Carrasquillo et al. [22]. E_c is also used as the uniform basis for the transformation of concrete and FRP areas.

$$E_c = 3200\sqrt{f_c} + 6900 \tag{2.19}$$

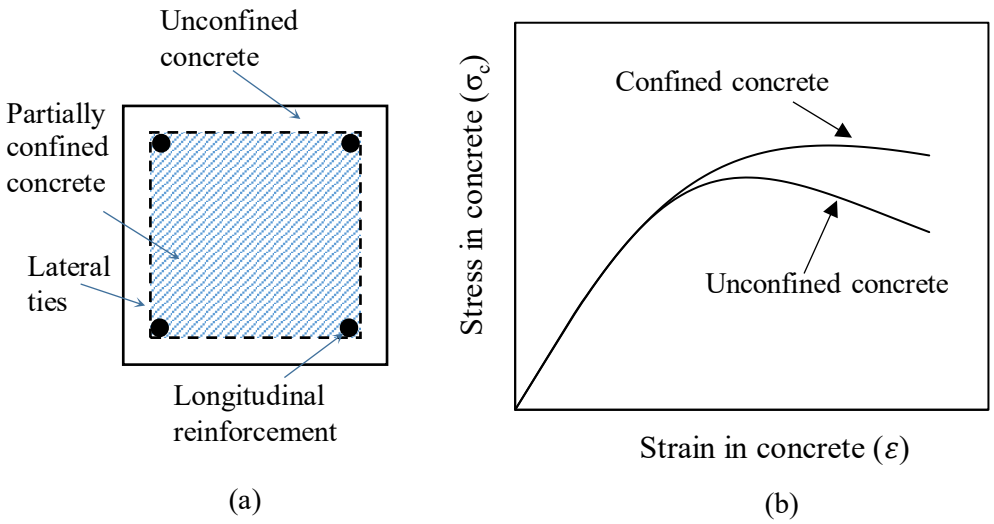


Fig. 2.3. (a) Cross-section details and (b) Illustration for Concrete stress-strain curve

The effect of confinement from lateral ties was considered using the model by Mander et al. [23]. The maximum compressive strain of concrete (ε_c) was assumed to be 0.0035. A perfect bond was assumed to exist between the concrete and FRP bars. The tensile strength of concrete, tension stiffening effect, creep and shrinkage of concrete and creep of FRP bar were neglected.

2.3.1.2 FRP

Stress-strain behavior of FRP bars was considered to be linearly elastic up to failure. The compressive modulus of elasticity was considered the same as in tension in this study [24,25]. ACI 440.1R-15 [5] and CSA S806-12 [4] suggest ignoring the contribution of FRP bars in compression. Likewise, *fib* Bulletin 40 [2] also recommends ignoring the contribution of FRP bars in compression as their contribution is lower as compared to steel bars in compression. ACI 440.11-22 [3] for GFRP-RC suggests considering the same stiffness and strength as the surrounding concrete for the area of GFRP reinforcement in compression. However, there have been multiple research studies in the past years to assess the use of FRP reinforcement in reinforced concrete columns both for axially loaded as well as eccentrically loaded columns, which depicts that ignoring the compressive strength of FRP bars, is a conservative approach. For concentrically loaded reinforced concrete columns, the load capacity contribution of GFRP bars as the reinforcement was reported to be from 3-10% whereas, for the same

amount of steel reinforcement it is about 12-16% [26–29]. For eccentrically loaded columns, a 3-27% increase in load capacity was reported while considering GFRP bars in compression [25,30,31]. Hence, the contribution of FRP bars in compression was considered in this study.

2.3.2 Cross-section resistance

To account for the inelastic behavior of concrete, the width of the transformed concrete area (B_x) across the cross-section as shown in Fig. 2.4, is calculated as:

$$B_x = \frac{\sigma_c(\varepsilon_x)b}{\varepsilon_x E_c} \tag{2.20}$$

where b is the width of the cross-section, ε_x is the strain in the cross-section at a distance x from the neutral axis and $\sigma_c(\varepsilon_x)$ is the stress in the concrete at the strain of ε_x.

The transformed area of concrete (A_{tc}) is calculated as:

$$A_{tc} = \frac{b}{\varphi E_c}\int_{\varepsilon_c'}^{\varepsilon_c} \frac{\sigma_c(\varepsilon_x)}{\varepsilon_x} d\varepsilon_x \tag{2.21}$$

where φ is the curvature of the cross-section, ε_c and ε_c' are the maximum and minimum compressive strain of concrete, respectively and expressed as:

$$\varepsilon_c = \varphi c \tag{2.22}$$

$$\varepsilon_c^{'} = 0;\ c \le h;\ \varepsilon_c^{'} = \varphi\,(c\text{-}h);\ c > h \tag{2.23}$$

where c represents the neutral axis depth from the top of the cross-section and h is the depth of the cross-section. c_c and c_t refer to the distance of the transformed area of concrete and the total transformed area from the neutral axis, respectively.

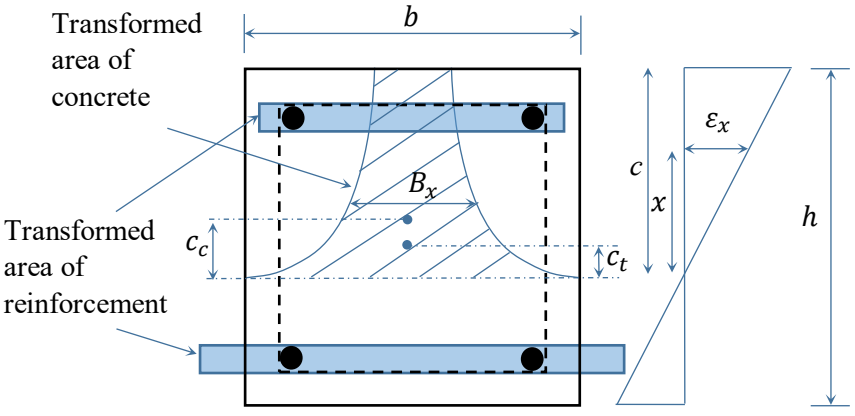


Fig. 2.4. Transformed area of concrete and FRP bars

For each row of reinforcement parallel to the axis of bending in the cross-section, the transformed area of FRP bars (A_{tFRP}) in a particular row is calculated as:

$$A_{tFRP} = \frac{A_{FRP}(E_{FRP}\text{-}E_{dt})}{E_c} \tag{2.24}$$

where A_{FRP} is the total area of the FRP bar in that row and E_{FRP} is the modulus of elasticity of the FRP bars. While calculating A_{tc}, the area of reinforcement was not subtracted from the cross-section. However, the same is compensated in Eq. (24) using E_{dt} which is expressed as:

$$E_{dt} = \frac{\sigma_c(\varepsilon_{FRP})}{\varepsilon_{FRP}};\ \varepsilon_{FRP} > 0 \tag{2.25}$$

$$E_{dt} = 0;\ \varepsilon_{FRP} \leq 0 \tag{2.26}$$

where ε_{FRP} is the strain in FRP bars in that row and $\sigma_c(\varepsilon_{FRP})$ is the stress in concrete at the strain of ε_{FRP}.

With a known value of curvature of the cross-section (φ) and considering the stress at the neutral axis to be zero, it can be expressed as:

$$P\left(\frac{1}{A_t} - \frac{e_t\, c_t}{I_t}\right) = 0 \tag{2.27}$$

where e_t is the load eccentricity from the centroid of the total transformed area, A_t is the total transformed area obtained upon the summation of A_{tc} and A_{tFRP} of all the rows of reinforcement, I_t is the moment of inertia of the total transformed area about its centroid.

Eq (27) can be simplified as:

$$I_t - A_t\, e_t\, c_t = 0 \tag{2.28}$$

The neutral axis of the cross-section (c) can be determined iteratively from Eq. (2.28) using numerical techniques such as Newton*-Raphson iterations.

2.3.3 Curvature assumption

The curvature is assumed to be sinusoidal in this study. However, it is modified to account for the end eccentricities. This modification is based on the sinusoidal eccentricity method presented by Robinson

et al. [32] and later presented by Hellesland et al. [15]. The sinusoidal eccentricity method is considered to be a better approach also when end eccentricities are different [33].

With the assumption of sinusoidal variation of total eccentricity for the column in Fig. 2.5(a), the half wavelength for the curvature distribution is shown in Fig. 2.5(b). Choosing the point of maximum total eccentricity as the origin, the total eccentricity $e_{tot}(x)$ at a distance x from the origin shall be expressed as:

$$e_{tot}(x)=e_0(x)+w(x)=e_{max}\cos\frac{\pi x}{a} \tag{2.29}$$

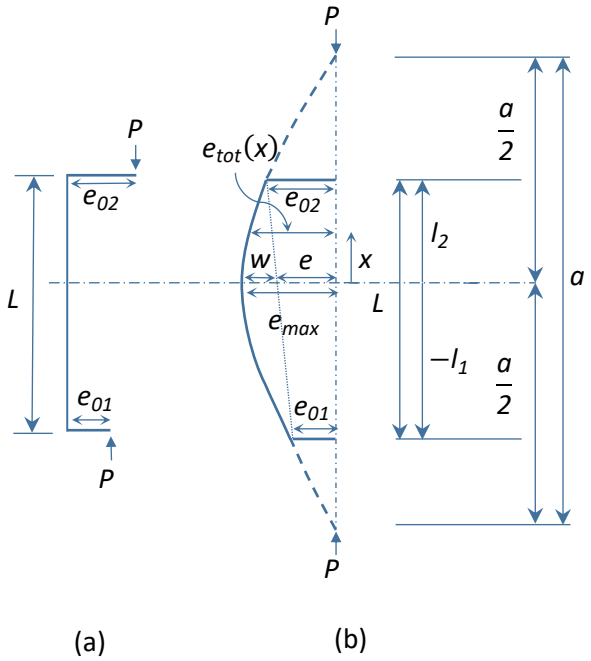


Fig. 2.5. (a) Column in undeformed state and (b) Deformed column with sinusoidal variation of total eccentricity

where $e_0(x)$ and $w(x)$ are the first-order eccentricity and the total lateral deflection at a distance x from the origin, respectively. e_{max} is the maximum total eccentricity i.e., the eccentricity at the origin with $x = 0$. l_1 and l_2 in Fig. 2.5(b) can be expressed as

$$l_1=-\frac{a}{\pi}\cos^{-1}\frac{e_{01}}{e_{max}} \tag{2.30}$$

$$l_2=\frac{a}{\pi}\cos^{-1}\frac{e_{02}}{e_{max}} \tag{2.31}$$

substituting, $l_2 - l_1 = L$, a can be expressed as:

$$a = \frac{\pi L}{cos^{-1}\frac{e_{02}}{e_{max}} + cos^{-1}\frac{e_{01}}{e_{max}}} \tag{2.32}$$

The curvature of the column at the origin with maximum total eccentricity can be expressed as:

$$\varphi = -e_{tot}(x)'' \tag{2.33}$$

$$\varphi = \frac{e_{max}}{L^2}\left(cos^{-1}\frac{e_{02}}{e_{max}} + cos^{-1}\frac{e_{01}}{e_{max}}\right)^2 \tag{2.34}$$

2.3.4 Steps of second-order analysis

The second-order analysis runs in an iterative manner with an assumption of total lateral deflection (w) at the origin (see Fig. 2.5) for each iteration and increasing it in further iterations. The steps for each iteration can be stated as:

1.) The maximum total eccentricity is calculated as:

$$e_{max} = e + w \tag{2.35}$$

where e is the first-order eccentricity at the location of maximum total eccentricity and for columns bent in single curvature it can be calculated as:

$$e = e_{01} - \left(\frac{e_{02} - e_{01}}{L}\right) \cdot l_1 \tag{2.36}$$

Substituting Eq. (2.36) in Eq. (2.35) and using Eq. (2.30), the value of e_{max} is calculated numerically.

2.) The curvature of the section with the maximum value of total eccentricity is calculated using Eq. (2.34)

3.) Using this value of the curvature, the neutral axis is calculated numerically using Eq. (2.28) and taking e_t as:

$$e_t = e_{max} - c_t + c - \frac{h}{2} \tag{2.37}$$

First-order eccentricity (e) and total lateral deflection (w) were taken from the geometric centroid of the cross-section, which is at $h/2$ from the top of the section. As a result, Eq. (2.37) is used to get eccentricities with respect to the centroid of the transformed section.

4.) Based on the curvature value and obtained value of the neutral axis for each value of total lateral deflection (w), the axial load capacity of the section is calculated as:

$$P = \frac{E_c \varepsilon_c}{\frac{1}{A_t} + \frac{e_t\,(c - c_t)}{I_t}} \tag{2.38}$$

5.) Increasing the value of total lateral deflection w in further iterations and repeating the above procedure leads to the development of a load-deflection response.

6.) The load capacity of the column is determined as the peak load value of this response. However, when the maximum compressive concrete strain in the section reaches the value of 0.0035 before the peak load value, the axial load capacity of the section is then determined by the load value at which the concrete strain of 0.0035 is achieved.

2.3.5 Validation of the method

The numerical method was validated by experimental results for FRP-RC columns available in the literature. The ratio of experimental load capacity (P_{test}) and the load capacity from the numerical method (P_{num}), the ratio of the experimental total moment (M_{test}) and the total moment from the numerical method (M_{num}), the percentage absolute error between experimental and numerical values of the total moment (ϵ_m) are presented in Table 2.2. The results obtained from numerical analysis are in good agreement with the experimental results. Fig. 2.6 represents the comparison of load-deflection response obtained from numerical analysis and available experimental results.

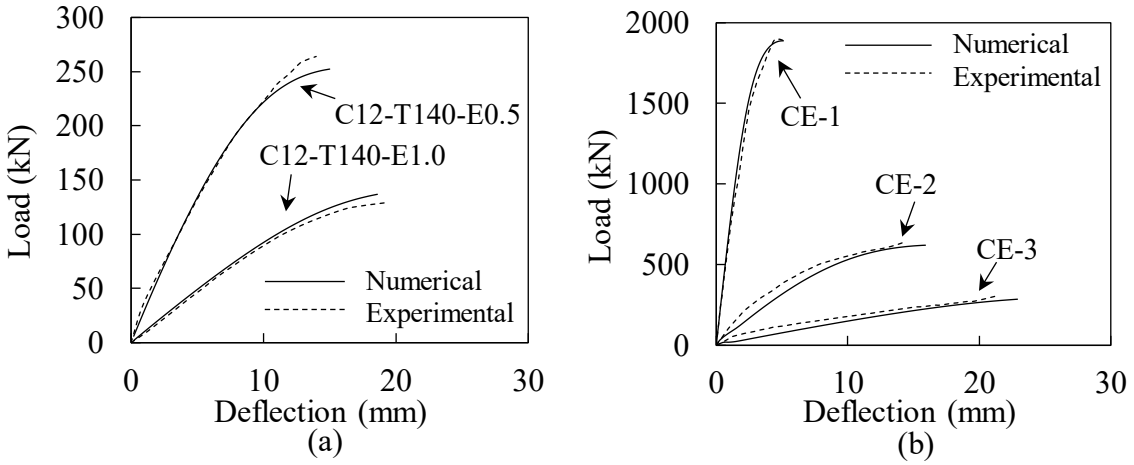


Fig. 2.6. Validation of numerical method with experimental results from (a) Othman and Mohammad [34]; (b) Xue et al. [35]

Table 2.2. Verification of the numerical method

Literature reference	Specimen No.	λ	Numerical Results		$\frac{P_{test}}{P_{num}}$	$\frac{M_{test}}{M_{num}}$	ϵ_m (%) = $\frac{M_{test}-M_{num}}{M_{test}}$
			P_{num} (kN)	M_{num} (kNm)			
Xue et al. [35]	CE-1	20.8	1888.10	122.92	1.01	1.00	0.34
	CE-2	20.8	620.95	103.02	1.04	1.03	3.27
	CE-3	20.8	286.43	92.51	1.07	1.06	5.89
	CE-4	27.7	1801.40	123.76	0.94	0.98	2.28
	CE-5	34.6	1741.20	127.28	0.96	0.99	1.10
	CE-6	41.6	1604.70	125.01	1.02	1.05	5.01
	CE-7	41.6	435.88	96.68	1.15	1.08	7.57
	CE-8	41.6	234.77	93.02	1.28	1.29	22.29
	CE-9	41.6	1587.40	123.18	0.99	1.03	2.62
	CE-10	41.6	1651.70	129.82	1.10	1.09	8.64
	CE-11	41.6	1211.40	93.40	0.85	0.92	9.24
	CE-12	41.6	2094.60	166.10	1.05	0.94	6.00
Guérin et al. [30]	CGA40	17.11	5175.10	228.22	0.92	0.92	8.23
	CGA80	17.11	3805.60	323.48	0.88	0.88	13.73

	CGA160	17.11	1745.70	297.99	1.11	1.10	9.36
	CGA320	17.11	743.91	251.96	1.00	1.01	1.02
	CGB40	17.11	5162.80	227.16	0.86	0.85	17.69
	CGB80	17.11	3794.40	322.33	0.84	0.85	17.67
	CGB160	17.11	1721.30	294.00	0.92	0.92	8.90
	CGB320	17.11	725.42	245.99	0.89	0.89	12.20
Othman and Mohammad [34]	C10-T90-E0.5	34.64	225.80	20.59	1.14	1.16	14.14
	C10-T90-E1.0	34.64	120.64	20.56	0.99	1.01	0.54
	C12-T90-E0.5	34.64	251.43	22.63	1.04	1.08	7.13
	C12-T90-E1.0	34.64	136.19	22.95	0.93	0.92	8.35
	C16-T90-E0.5	34.64	308.60	27.25	0.94	0.99	0.67
	C16-T90-E1.0	34.64	171.14	28.39	0.80	0.82	21.46
	C12-T140-E0.5	34.64	252.36	22.71	1.05	1.03	3.31
	C12-T140-E1.0	34.64	136.86	23.07	0.94	0.95	5.74
	C12-T40-E0.5	34.64	253.35	22.80	0.94	0.96	4.01
	C12-T40-E1.0	34.64	136.92	23.08	0.83	0.83	20.87
Salaheldin et al. [36]	Ge80	17.32	5862.30	499.47	0.87	0.87	15.35
	Ge120	17.32	3947.00	502.45	0.92	0.91	10.30
	Ge160	17.32	2589.20	443.79	0.95	0.96	4.17
	Ge240	17.32	1475.30	379.45	0.93	0.94	6.88
		Mean			0.97	0.98	8.41
		Coefficient of variation			10.78	10.30	

2.4 Sensitivity analysis

2.4.1 General

The analytical model developed in this study is used to perform a sensitivity analysis to evaluate the variation of the slenderness limit of GFRP-RC columns. The sensitivity analysis is performed for

columns of 300 x 300 mm rectangular section with corner reinforcement and 25 mm concrete clear cover, as shown in Fig. 2.3(a). The columns are considered to be simply supported and bent in single curvature with constant first-order eccentricity. The parameters considered for the sensitivity analysis are presented in Table 2.3. In this study, the axial force ratio (n) is calculated based on the concrete compressive strength (f_c) and applied axial force (P). It is expressed as:

$$n = P / A_c f_c \tag{2.39}$$

Further, reinforcement ratio (ρ) is expressed as:

$$\rho = 100 \cdot \frac{A_s}{A_g}\% \tag{2.40}$$

where A_g is the gross area of the cross-section and A_s is the total area of the longitudinal reinforcement

Table 2.3. Variables of sensitivity analysis

Parameters	Values
Concrete Compressive strength (f_c)	30, 50 and 70 MPa
Modulus of elasticity of FRP bar (E_{FRP})	40, 50 and 60 GPa
Reinforcement ratio (ρ)	1, 2, 3 and 4 %
Axial force ratio (n)	0.1, 0.2, 0.3, 0.4, 0.5, 0.6, 0.7, 0.8, 0.9 and 1.0

Ties in the column are important for the stability of longitudinal bars and prevent them from local buckling. Additionally, they provide confinement to concrete compression zone. It is also desired to exploit the ductility offered by the confinement of concrete in FRP-RC sections [2]. To prevent local buckling of GFRP longitudinal bars, tie spacing of $12d_l$ to $14d_l$ (where d_l is the diameter longitudinal FRP bar) is suggested, which is lower than the requirement for steel longitudinal bars [37,38]. Moreover, higher spacing of ties is not recommended in GFRP-RC columns to ensure that a minimum level of confinement can be developed for the concrete core [37,38]. De Luca et al. [39] suggested to half the requirement of $48d$ (where d is the diameter of the tie) in ACI 318 for steel-RC columns to $24d$ for GFRP-RC columns. Also, decreasing the spacing of ties in GFRP-RC columns may result in a slight increase in peak capacities [26–29,40]. In this analysis, tie spacing of 150 mm was selected

conservatively for steel ties with a diameter of 8 mm and yield strength of 500 MPa. The values of tensile modulus of elasticity considered for FRP bars in the sensitivity analysis correspond to GFRP bars. It is seen from the literature that basalt FRP (BFRP) bars also exhibit the value of tensile modulus of elasticity and ultimate tensile strain in the same range as GFRP [41]. AlNajmi and Abed [42] observed similar behavior in compression for GFRP and BFRP bars reinforced concrete columns in terms of load capacity and displacement. Consequently, the results of this sensitivity analysis can also be extended to FRP bar types with the modulus of elasticity and ultimate strain values similar to the ones considered here. The slenderness limit values in this analysis were studied for two criteria, which can be stated as

a) *Criterion 1*: 10% increase in moments due to second-order effects at constant load. For a constant value of the eccentric axial load, the length and the initial eccentricity are adjusted to reach the limit where the increase in total moment is 10% of the corresponding first-order moment.
b) *Criterion 2*: 10% decrease in load capacity due to second-order effects at constant eccentricity. For a constant value of the load eccentricity, the length is adjusted to reach the limit where the reduction in load capacity due to second-order effects is 10% of the corresponding load capacity obtained from the cross-sectional analysis.

The details of the procedure for both criteria are presented as a flowchart in Fig. 2.7.

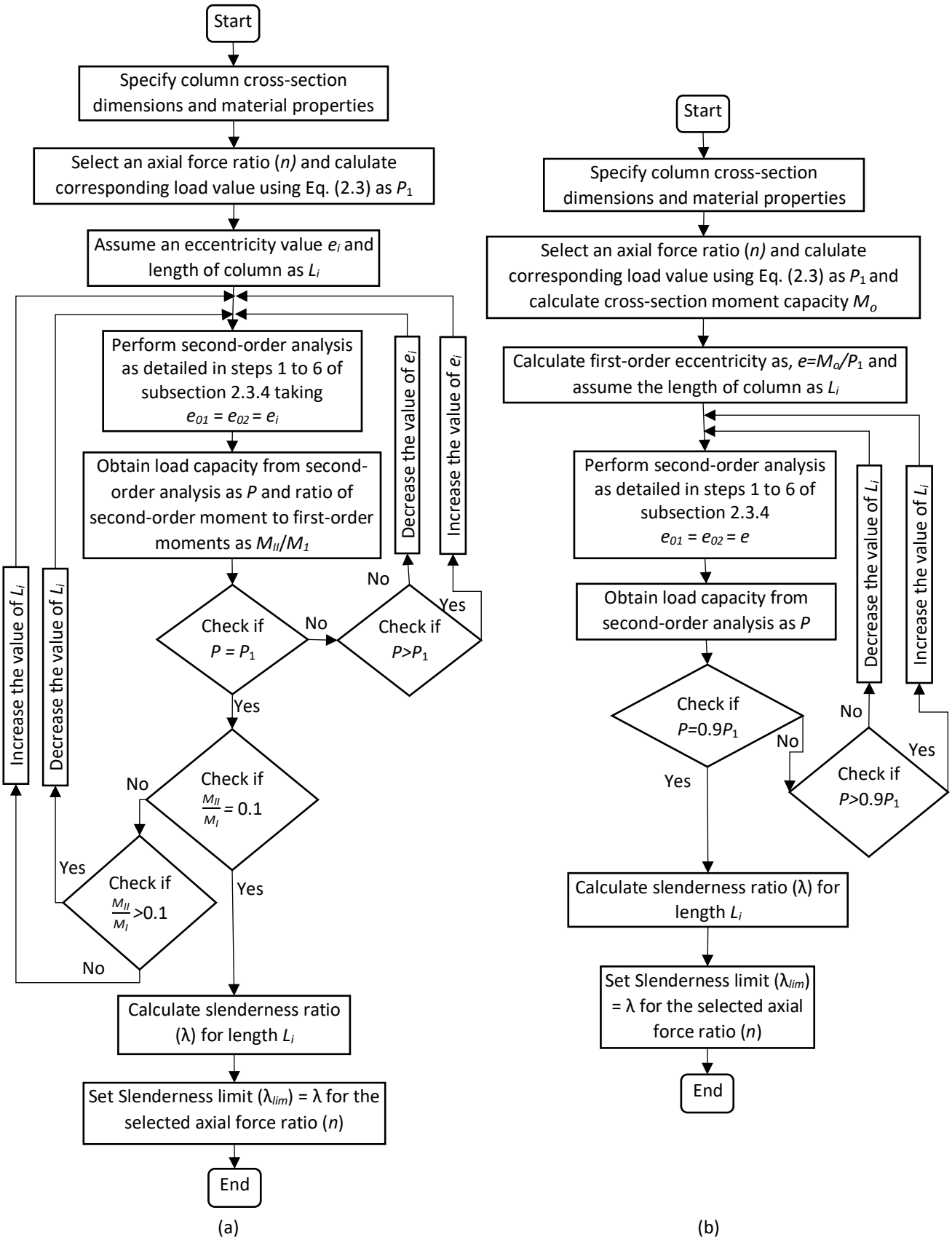


Fig. 2.7. Flowchart for calculating slenderness limit as per (a) Criterion 1 and (b) Criterion 2

2.4.2 Results and discussions

The results of the sensitivity analysis for the slenderness limit are discussed in terms of mean values and five percentile values of the slenderness limit. All the possible columns with the combination of parameters shown in Table 2.3 were considered and evaluated for slenderness limit using both criteria, creating a set of data for slenderness limit values. This data set is used to calculate the mean and five percentile values of the slenderness limit for each axial force ratio to assess the effect of a particular parameter on the slenderness limit value. As an example, to evaluate the effect of concrete strength, the slenderness limit of all the possible columns with the combination of parameters other than concrete strength, as shown in Table 2.3, is calculated for a given value of concrete strength. These values of the slenderness limit are used to evaluate the mean and five-percentile values at each axial force ratio for that given value of concrete strength.

2.4.2.1 Effect of compressive strength of concrete

The variation of the mean and five-percentile values of the slenderness limit with axial force ratio for each value of concrete strength is presented in Fig. 2.8. At a low axial force ratio, a significant reduction is observed on the slenderness limit values as the compressive strength of concrete increases for both the criteria. The consequent decrease of the slenderness limit values corresponding to the increase in concrete strength is less for higher values of concrete strength. However, the variation in slenderness limit values converges for both criteria around the axial force ratio of 0.5 for mean values. The mean value of slenderness limit at an axial force ratio of 0.5 is 22.2 and 24.7 for criteria 1 and 2 respectively.

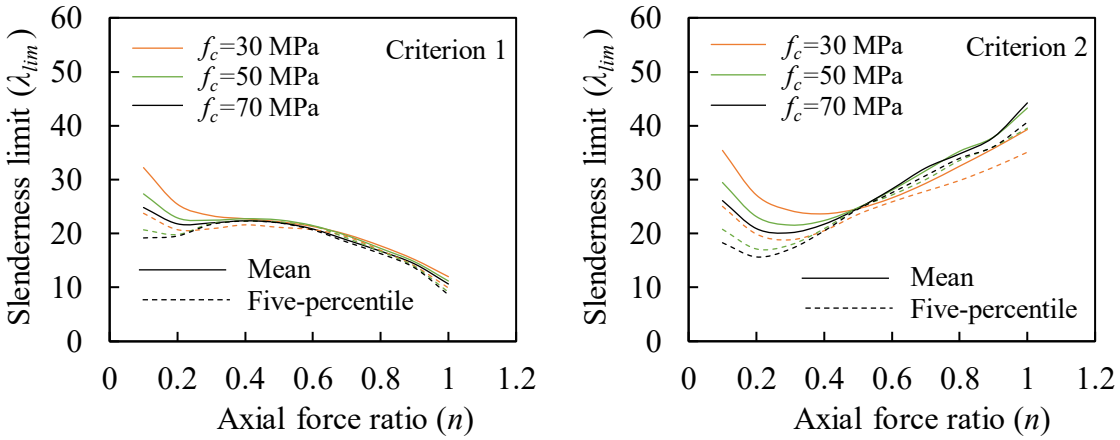


Fig. 2.8. Effect of concrete strength on the mean and five percentile slenderness limit values for the cases considered in the sensitivity analysis

Whereas the slenderness limit for five-percentile values converges at axial force ratios of 0.3 and 0.4 with values of 21.5 and 20.6 for criteria 1 and 2 respectively. The effect of concrete strength on the slenderness limit value is insignificant for both the criteria beyond the axial force ratio of 0.5 and 0.3 for mean and five-percentile values respectively. For criterion 2 at a high axial force ratio slenderness limit value increase as the concrete strength increases, however, this variation is not evident for higher values of concrete strength.

2.4.2.2 Effect of modulus of elasticity of GFRP bars and reinforcement ratio

The variation of mean and five-percentile values of slenderness limit with axial force ratio for each value of modulus of elasticity is presented in Fig. 2.9. As the value of modulus of elasticity of GFRP bar increases, an appreciable amount of increase in slenderness limit value is observed for low axial force ratio. However, this variation of slenderness limit values based on criterion 2 converges at axial force ratios of 0.6 and 0.5 with values of 27.6 and 23.8 for mean and five-percentile values respectively. Whereas for criterion 1, slenderness limit values converge at axial force ratios of 0.5 and 0.3 with the value of 22.2 and 22. Essentially, for criterion 1, no effect of the modulus of elasticity of GFRP on the slenderness limit value is observed beyond the value of the axial force ratio at which the slenderness

limit value converges. However, a slight variation in the slenderness limit due to a change in the modulus of elasticity is observed at a higher axial force ratio for criterion 2.

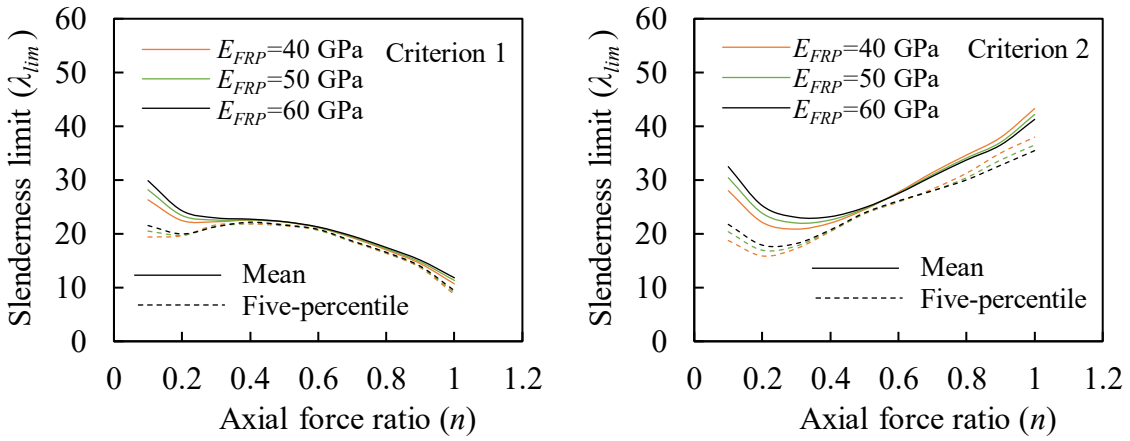


Fig. 2.9. Effect of modulus of elasticity of GFRP bar on mean and five percentile slenderness limit values for cases considered in sensitivity analysis

Four reinforcement ratios of 1% to 4% were studied with different combinations of parameters as shown in Table 2.3. The effect of the reinforcement ratio on the slenderness limit values is presented in Fig. 2.10. As the reinforcement ratio increases, the slenderness limit for low axial force ratios increases. However, the consequent increase in slenderness value corresponding to the increase in reinforcement ratio is reduced at higher values reinforcement ratio. It is also observed that the variation between mean values and the five-percentile values is less than the other parameters in this study. Based on criterion 2, the slenderness limit value converged at an axial force ratio of 0.5, corresponding to the slenderness limit value of 24.7 and 24 for mean and five-percentile values respectively. Beyond this value of axial force ratio, as the reinforcement ratio increases the slenderness limit value decreases. Based on criterion 1, the slenderness limit value converged at an axial force ratio of 0.5 with corresponding slenderness limit values of 22.2 and 21.6 for mean and five-percentile values respectively; beyond this value of axial force ratio, reasonable effect of reinforcement ratio is not observed.

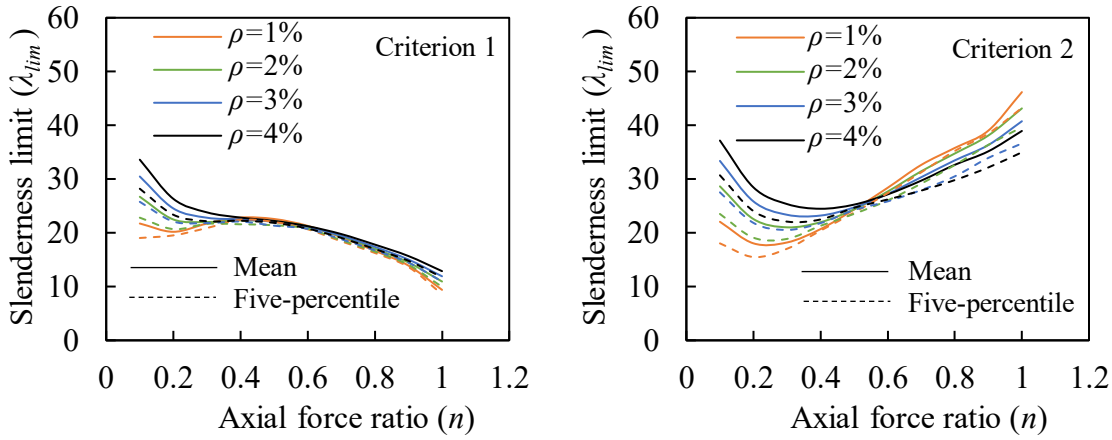


Fig. 2.10. Effect of Reinforcement Ratio on mean and five percentile slenderness limit values for cases considered in sensitivity analysis

2.4.2.3 Effect of axial force ratio

A significant extent of variation in slenderness limit value is observed with the change in axial force ratio as seen in Fig. 2.11. It is observed from Fig. 2.11 that both the criteria show a fairly similar variation of slenderness limit values from an axial force ratio of 0.1 to around 0.4 and 0.3 for mean and five-percentile values respectively. The values of the slenderness limit are also quite similar for both criteria in this range of axial force ratio. However, criterion 2 gives the lowest value of the slenderness limit in this range, which is 22 and 16.4 for the axial force ratio value of around 0.3 and 0.2 for the mean and five-percentile values, respectively. Beyond this range of axial force ratio for criterion 1, slenderness limit value decrease as the axial force ratio increases. While for criterion 2, the slenderness limit value increase as the axial force ratio increases. This illustrates that criterion 1 is more conservative than criterion 2 at high axial force ratios. For criterion 1, the lowest value of the slenderness limit is observed for the axial force ratio of 1.0, which is 8.9 and 11.3 for the mean and five-percentile values respectively. Taking into account the effect of factors evaluated in the sensitivity analysis, it is observed that as the proportion of load carried by the concrete increases or by the reinforcement decreases, the column becomes more unstable and the slenderness limit value decreases. This is observed when the concrete strength is increased or the modulus of elasticity is decreased or the reinforcement ratio is

decreased. Such behavior has also been observed for steel-reinforced columns by Broms and Viest [43] and for GFRP-reinforced columns by Mirmiran et al. [6].

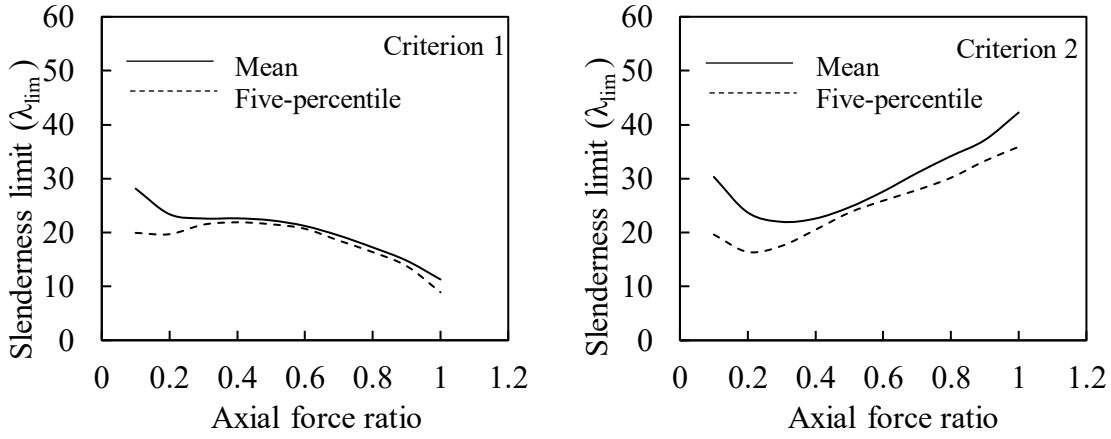


Fig. 2.11. Effect of axial force ratio on the mean and five-percentile slenderness limit values for all the cases considered in the sensitivity analysis

The tensile strain of the GFRP was found to be generally less than 0.012, which is the lowest value of ultimate tensile strain for GFRP bars as seen in Table 2.1. However, in a few cases with a low reinforcement ratio and a low modulus of elasticity of GFRP at an axial force ratio of 0.1, tensile strains exceeded this limit and attained the failure value of 0.0035 for the outermost concrete compressive strain. This behavior is more evident at an axial force ratio of 0.1 as concrete strength increases. However, for GFRP reinforced concrete, it is desirable to avoid section failure due to tensile rupture of GFRP bars. This is to account for the brittle properties of the GFRP bar and to take advantage of the ductility offered by confined concrete [2]. Hence, a minimum reinforcement limit shall be of importance to design such sections. The lowest reinforcement ratio of 1% is found to be satisfactory in the literature [38] to avoid tension rupture of GFRP bars. Also in this study, nearly 99% of the column did not fail due to tensile failure of GFRP bars with a reinforcement ratio equal to or greater than 1%. However, a better alternative would be to estimate the minimum reinforcement ratio considering the concrete strength, axial force ratio and modulus of elasticity to avoid tensile failure of GFRP bars.

2.5 Definition of slenderness limit for GFRC-RC columns

The effect of axial force ratio on slenderness limit for steel and GFRP-RC columns is presented in Fig. 2.12 for a column of 300 x 300 mm rectangular cross-section having corner reinforcement as shown in Fig. 2.3(a). It is observed that the variation of GFRP-RC slenderness limit values with respect to axial force ratio is generally not similar to steel-RC columns. For steel-RC columns, criterion 1 is liberal at low axial force ratios while it is conservative at higher axial force ratios compared to criterion 2, which is conservative at low axial force ratios and liberal at high axial force ratios [15]. However, for GFRP-RC columns, as already seen in subsection 2.4.2.3 and also presented in Fig. 2.12, criteria 1 and 2 have similar behavior at a low axial force ratio, while criterion 1 is conservative compared to criterion 2 at a high axial force ratio.

Reinforcement ratio has a considerable effect on the slenderness limit of steel-RC columns, as observed from Fig. 2.12 and in the literature [14,15]. However, as seen in subsection 2.4.2.2 and seen in Fig. 2.12, for GFRP-RC columns, the reinforcement ratio has little effect of on the slenderness limit. As the proportion of the load carried by the reinforcement increases, the columns become more stable and the slenderness limit increases [6,43]. However, due to the lower modulus of elasticity of GFRP bars compared to steel bars, the amount of increase in the axial load carried by the reinforcement with the increase in the reinforcement ratio is less for GFRP-RC columns than for steel-RC columns. This could be a possible explanation for the effect of the reinforcement ratio on the slenderness limit of GFRP-RC columns.

As observed in Fig. 2.12, the value of the slenderness limit and its extent of variation is not the same for GFRP-RC and steel-RC. Furthermore, the equations available in existing codes for steel-RC columns, such as EC2-04 [12] and its respective national annexures like DIN EN 1992-1-1/NA-13 [16], may be inappropriate to estimate the slenderness limit for GFRP-RC columns.

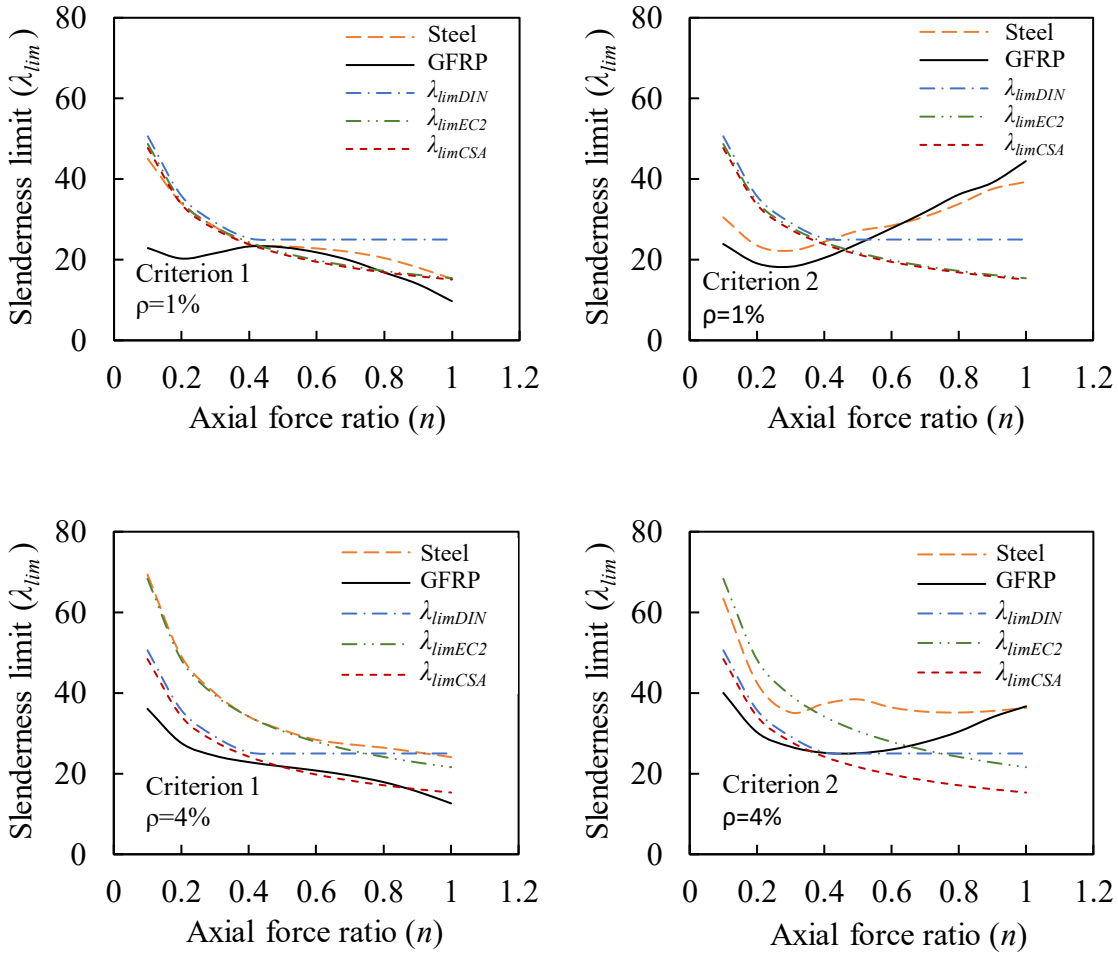


Fig. 2.12. Variation of slenderness limit values for steel-RC and GFRP-RC columns with different reinforcement ratios for $E_{FRP} = 40$ GPa, $f_c = 30$ MPa and $f_y = 500$ MPa.

It can also be noticed from Fig. 2.12 that Eq.(5), Eq.(12), and Eq.(41) to determine the slenderness limit of steel-RC columns from EC2-04 [12], DIN EN 1992-1-1/NA-13 [16], and CSA A23.3-19 [4,44] closely align with the slenderness limit variation as per criterion 1. Here, EC2-04 [12] and CSA A23.3-19 [4,44] slenderness limit equation are presented for columns with uniform first order bending, i.e. bent in single curvature with identical end moments. Also, EC2-04 [12] slenderness limit equation is presented here without considering the effect of creep. Specified values of concrete compressive strength, reinforcement yield strength and axial load are used here for comparison rather than design or factored values for calculating the slenderness limit based on EC2-04 [12], DIN EN 1992-1-1/NA-13 [16] and CSA A23.3-19 [4,44].

The slenderness limit for steel-RC as per CSA A23.3-19 [44] (λ_{limCSA}) for non-sway frames is expressed as:

$$\lambda_{limCSA} = \frac{25 - 10(M_1/M_2)}{\sqrt{P_f/(f_c A_g)}} \geq \frac{kL}{r} \tag{2.41}$$

where P_f is the factored axial load. Here, M_1/M_2 is taken as positive when bent in single curvature and it is not taken less than -0.5.

As presented earlier, criterion 1 corresponds to the criterion stated in EC2-04 [12] for the slenderness limit. However, the commentary to Eurocode 2 [14] mentions that it is believed by some that criterion 2 may also have been used for ENV rules which were the predecessor to EC2-04 [12]. This may be reasonable because criterion 1 is liberal for low axial force ratios, so criterion 2 would have been a better choice in that range. Therefore, in this study to determine the slenderness limit for GFRP-RC columns, Eq. (2.42) is proposed considering both criteria 1 and 2 simultaneously and Eq. (2.43) is proposed considering only criterion 1. These equations are developed using the curve fitting approach and based on the 720 columns evaluated in the sensitivity analysis.

When both the slenderness limit criteria are considered simultaneously, for a given axial force ratio, the lowest value of the slenderness limit can be selected from the two values obtained using the two limit criteria for a given column. The variation of five-percentile values of the slenderness limit for each parameter, such as concrete compressive strength, reinforcement ratio and GFRP modulus of elasticity, when both the criteria are considered simultaneously is presented in Fig. 2.13. It is observed that these parameters have their effect on the slenderness limit in the range of low to moderate axial force ratio up to around 0.5. Beyond that, however, they do not have any substantial effect and the axial force ratio is the only significant parameter. In addition, even when criterion 1 is considered separately, the axial force ratio is a significant parameter affecting the slenderness limit, as observed in the sensitivity analysis. Hence, the axial force ratio is considered as the predicting variable for the slenderness limit to develop Eq. (2.42) and Eq. (2.43). These equations are limited to $f_c \leq 70$ MPa, $E_{FRP} \geq 40$ GPa and $\rho \geq 1\%$ owing to the range of parameters considered in this study.

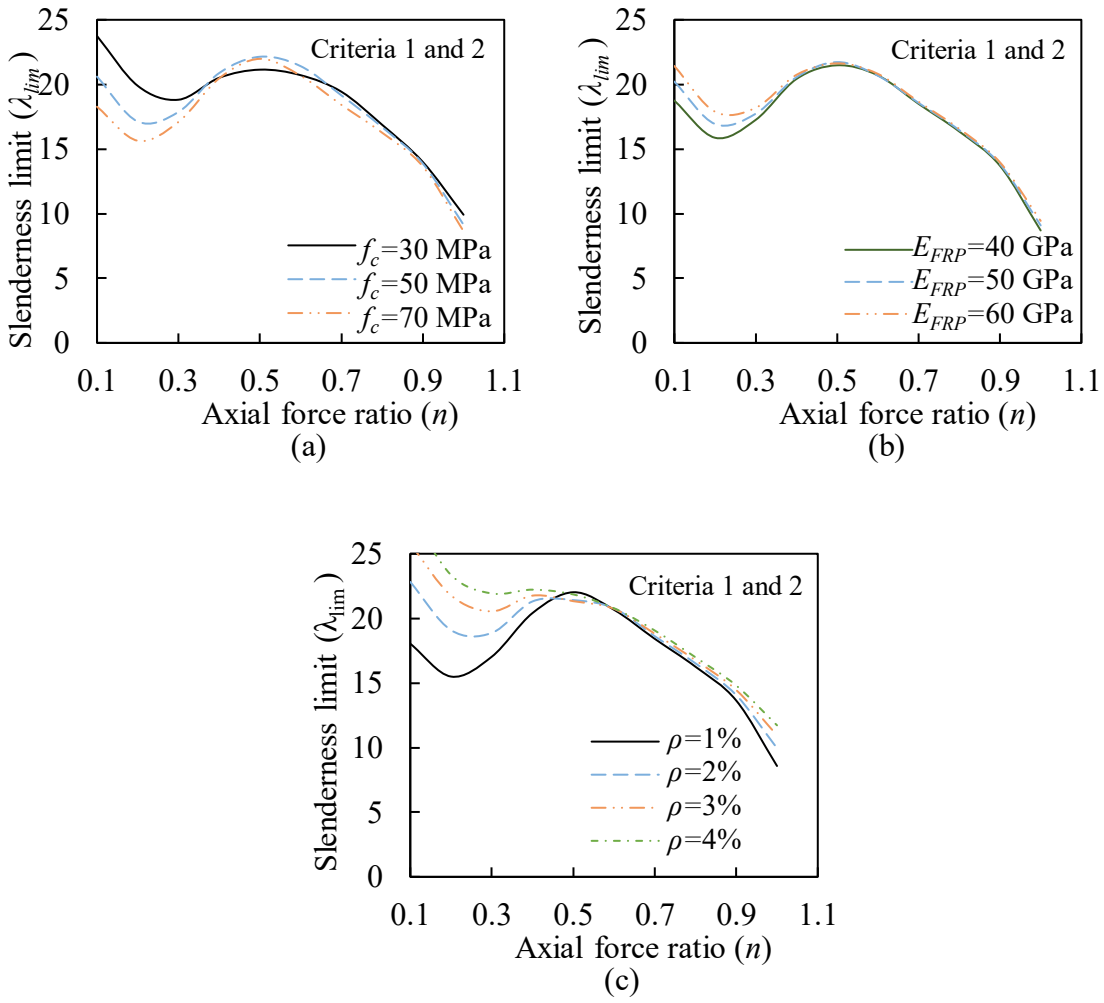


Fig. 2.13. Variation for five percentiles value of slenderness limit for different values of the: (a) concrete compressive strength; (b) Modulus of elasticity of GFRP; and (c) Reinforcement ratio

The slenderness limit of steel-RC columns was found to be significantly influenced by factors such as the first-order end moment ratio (r_m) and the end restraints of the column [14,15]. For a column with uniform first-order bending ($r_m = 1.0$), the effect of end restraints could fairly be taken into account by including effective length factors [45]. However, this is not true for non-uniform bending as r_m decreases from 1.0 to -1.0. The slenderness limit increases as the value of r_m decreases, being lowest for $r_m = 1.0$ and highest for $r_m = -1.0$, both for steel-RC columns [45] and for FRP-RC columns [6]. In this paper, slenderness limit equations for GFRP-RC columns are developed for a simply supported column with uniform first-order bending. The slenderness limit equations for GFRP-RC columns developed in this paper for $r_m = 1.0$, would be conservative for other moment ratios. In the preliminary

calculations performed by the authors, it is observed that the use of the effective length factor can reasonably reflect the effect of different end restraints with $r_m = 1.0$ for GFRP-RC columns, like steel-RC columns. However, a detailed analysis, which is beyond the scope of this paper, would be of further interest to precisely determine the effect of different end restraints for all the values of first-order end moment ratio on the slenderness limit of GFRP-RC columns.

$$\lambda_{lim} = \begin{cases} 10.5/\sqrt[4]{n} & n \leq 0.2 \\ 80n^3 + 15 & 0.2 < n \leq 0.42 \\ 22 - 13n^4 & n > 0.42 \end{cases} \tag{2.42}$$

$$\lambda_{lim} = \begin{cases} 17n^2 + 19 & n \leq 0.4 \\ 22 - 13n^4 & n > 0.4 \end{cases} \tag{2.43}$$

On the conservative side, to account for the variation of slenderness limit values obtained from the sensitivity analysis, the five-percentile and one-percentile values of slenderness limit are considered to propose the equation. For each value of axial force ratio, the five-percentile and one-percentile values of slenderness limit for all the cases considered in the sensitivity analysis are presented in Fig. 2.14. Both the equations perform quite well for both five-percentile and one-percentile values of the slenderness limit obtained from the sensitivity analysis. The correlation factor (R^2) value for Eq. (2.42) and Eq. (2.43) based on five-percentile values is 0.97 and 0.99, respectively.

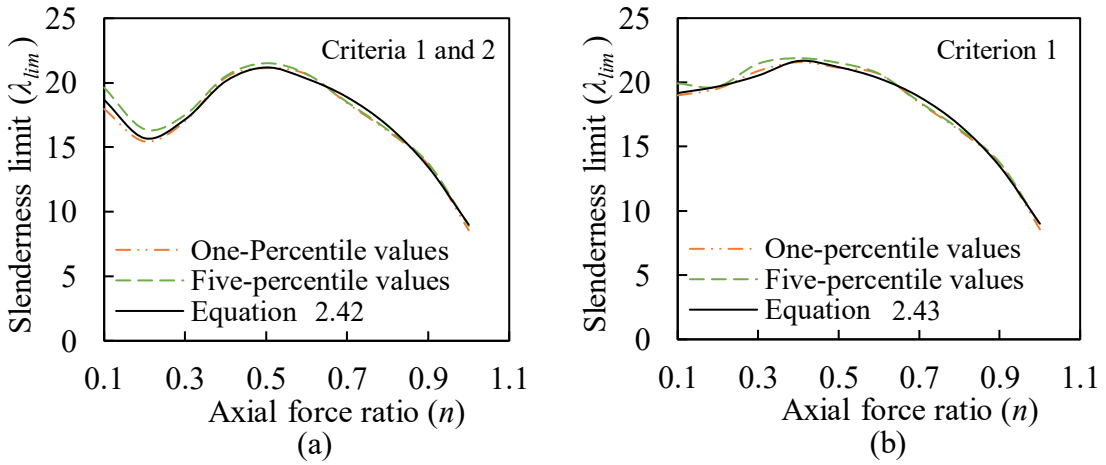


Fig. 2.14. Variation of slenderness limit with axial force ratio for all the cases of sensitivity analysis and performance of proposed equations: (a) when both the criteria are considered simultaneously; and (b) when only criterion 1 is considered

2.6 Conclusions

The slenderness limit for GFRP-RC columns was studied through a validated numerical method. Sensitivity analysis performed on a total of 720 columns based on the two slenderness limit criteria led to the proposal of equations to estimate the slenderness limit for GFRP-RC columns with axial force ratio as the determining parameter. The following conclusions can be drawn from this research:

1. The numerical method for second-order analysis of the reinforced concrete columns based on the curvature assumption incorporating the first-order eccentricity accurately estimated the load and moment capacity of FRP-RC columns. Further, it has been effectively validated with experimental results available in the literature.
2. The concrete compressive strength, modulus of elasticity of GFRP and reinforcement ratio have an appreciable effect on the slenderness limit based on both the criteria discussed in this study, up to the axial force ratio of about 0.5. In addition, around this value of axial force ratio, the slenderness limit values for both criteria converge for all the parameters mentioned. Beyond the axial force ratio of 0.5, there is a slight variation in slenderness limit values for criterion 2, but the variation is insignificant for criterion 1.
3. The consequent change in slenderness limit value is reduced corresponding to the change in concrete compressive strength, modulus of elasticity of GFRP bars and reinforcement ratio at higher values of these parameters. The same is observed when changing concrete strength from 50 to 70 MPa, modulus of elasticity of GFRP bars from 50 to 60 GPa and reinforcement ratio from 3 to 4%.
4. The variation in slenderness limit value due to the change in axial force ratio is considerable and it is found to be a significant factor to estimate the slenderness limit. The lowest value of the slenderness limit occurs for the axial force ratio ranging from 0.2 to 0.4 for criterion 2, while for criterion 1 lowest value slenderness limit occurs for 1.0, which is the highest value of the axial force ratio considered in this study.
5. Slenderness limit variation with axial force ratio for GFRP-RC columns is typically not similar to that of steel-RC columns. In addition, the value of the slenderness limit and its extent of variation with axial force ratio are lower for GFRP-RC columns than for steel-RC columns.

Existing equations for steel RC columns may not be able to effectively estimate the slenderness limit for GFRP-RC columns.

6. Two equations are proposed to estimate the slenderness limit of GFRP-RC columns based on the axial force ratio. The first equation (Eq. 42) is proposed considering both slenderness limit criteria in tandem. The second equation (Eq. 43) is proposed considering only criterion 1, which is the criterion in EC2-04 [12] for steel-RC columns.

2.7 Acknowledgements

The authors would like to gratefully acknowledge the funding support provided by German Academic Exchange Service (DAAD) to pursue this research work.

2.8 References

[1] Xue W, Peng F, Zheng Q. Design Equations for Flexural Capacity of Concrete Beams Reinforced with Glass Fiber–Reinforced Polymer Bars. J. Compos. Constr. 2016;20(3).

[2] Fib Bulletin 40. FRP reinforcement in RC structures. Stuttgart: The International Federation for Structural Concrete; 2007.

[3] ACI. Building Code Requirements for Structural Concrete Reinforced with Glass Fiber-Reinforced Polymer (GFRP) Bars-Code and Commentary.(ACI CODE-440.11-22). Farmington Hills, MI: American Concrete Institute; 2022.

[4] CAN/CSA S806-12. Design and construction of building structures with Design and construction of building structures with fibre-reinforced polymers(CSA S806-12): Canadian Standards Association; 2012.

[5] ACI 440.1R. Guide for the design and construction of structural concrete reinforced fiber-reinforced polymer (FRP) bars.(ACI 440.1R-15). Farmington Hills, MI: American Concrete Institute; 2015.

[6] Mirmiran A, Yuan W, Chen X. Design for Slenderness in Concrete Columns Internally Reinforced with Fiber-Reinforced Polymer bars. ACI Struct J 2001;98(1):116–25.

[7] ACI 318-99. Building Code Requirements for Structural Concrete & Commentary. Farmington Hills, MI: American Concrete Institute; 1999.

[8] Zadeh HJ, Nanni A. Flexural Stiffness and Second-Order Effects in FRP-RC Frames. ACI Struct J 2017;114(2):533–44.

[9] Abdelazim W, Mohamed HM, Afifi MZ, Benmokrane B. Proposed Slenderness Limit for Glass Fiber-Reinforced Polymer-Reinforced Concrete Columns Based on Experiments and Buckling Analysis. ACI Structural Journal 2020;117(1).

[10] Abdelazim W, Mohamed HM, Benmokrane B. Inelastic Second-Order Analysis for Slender GFRP-Reinforced Concrete Columns: Experimental Investigations and Theoretical Study. J Compos Constr 2020;24(3).

[11] ACI. Building Code Requirements for Structural Concrete and Commentary(ACI CODE 318-19). Farmington Hills, MI: American Concrete Institute; 2019.

[12] EN 1992-1-1. Eurocode 2: Design of concrete structures - Part 1-1:General rules and rules for buildings: EN 1992-1-1: Eurocode 2: Design of concrete structures - Part 1-1: General rules and rules for buildings(EN 1992-1-1:2004). Brussels: European Committee for Standardisation.

[13] MacGregor JG, Breen JE, Pfrang OE. Design of Slender Concrete Columns. ACI Journal Proceedings 1970;67(1):6–28.

[14] European Concrete Platform ASBL. Eurocode 2 Commentary: European Concrete Platform ASBL; 2008.

[15] Hellesland J, Challamel N, Casandjian C, Lanos C. Reinforced concrete beams, columns and frames: section and slender member analysis. Surrey: John Wiley & Sons; 2013.

[16] DIN EN 1992-1-1/NA. Nationaler Anhang -National festgelegte Parameter -Eurocode 2: Bemessung und Konstruktion von Stahlbeton- und Spannbetontragwerken -Teil 1-1: Allgemeine Bemessungsregeln und Regeln für den Hochbau: Deutsches Institut für Normung; 2013.

[17] MATLAB version: 9.13.0 (R2022b). Natick, Massachusetts: The MathWorks Inc; 2022.

[18] Chuang P-H, Kong S-K. Strength of Slender Reinforced Concrete Columns. J. Struct. Eng. 1998;124(9):992–8.

[19] Najmi A, Tayem A. Uniaxial Bending of Columns. J. Struct. Eng. 1993;119(4):1206–21.

[20] Tikka TK, Mirza SA. Nonlinear EI Equation for Slender Reinforced Concrete Columns. ACI Struct J 2005;102(6):839–48.

[21] Popovics S. A numerical approach to the complete stress-strain curve of concrete. Cement and concrete research 1973;3:583–99.

[22] Carrasquillo RL, Nilson AH, Slate FO. Properties of High Strength Concrete Subject to Short-Term Loads. ACI Journal 1981;78(3):171–8.

[23] Mander JB, Priestly JN, Park, R. Theoretical Stress-Strain Model for Confined Concrete. J. Struct. Eng. 1988;114(8):1804–26.

[24] Deitz DH, Harik IE, Gesund H. Physical Properties of Glass Fiber Reinforced Polymer Rebars in Compression. J Compos Constr 2003;7(4):363–6.

[25] Khorramian K, Sadeghian P. Experimental and analytical behavior of short concrete columns reinforced with GFRP bars under eccentric loading. Engineering Structures 2017;151:761–73.

[26] De Luca A, Matta F, Nanni A. Behavior of Full-Scale Glass Fiber-Reinforced Polymer Reinforced Concrete Columns under Axial Load. ACI Struct J 2010;107(5):589–96.

[27] Tobbi H, Farghaly SA, Benmokrane B. Concrete Columns Reinforced Longitudinally and Transversally with Glass Fiber-Reinforced Polymer Bars. ACI Struct J 2012;109(4):551–8.

[28] Afifi MZ, Mohamed HM, Benmokrane B. Axial Capacity of Circular Concrete Columns Reinforced with GFRP Bars and Spirals. J Compos Constr 2014;18(1):4013017.

[29] Elchalakani M, Ma G. Tests of glass fibre reinforced polymer rectangular concrete columns subjected to concentric and eccentric axial loading. Engineering Structures 2017;151:93–104.

[30] Guérin M, Mohamed HM, Benmokrane B, Nanni A, Shield CK. Eccentric Behavior of Full-Scale Reinforced Concrete Columns with Glass Fiber-Reinforced Polymer Bars and Ties. ACI Structural Journal 2018;115(2):489–99.

[31] Hadhood A, Mohamed HM, Ghrib F, Benmokrane B. Efficiency of glass-fiber reinforced-polymer (GFRP) discrete hoops and bars in concrete columns under combined axial and flexural loads. Composites Part B: Engineering 2017;114(1):223–36.

[32] Robinson J, Fouré F, Bourghli M. Le flambement des poteaux en béton armé chargés avec des excentricités différentes à leurs extrémités. Annales de l'ITBTP 1975;333:46–74.

[33] Corres H, Moran F. Design of slender reinforced concrete columns. IABSE Proceedings P-59/83 1983;7:37–50.

[34] Othman ZS, Mohammad AH. Behaviour of Eccentric Concrete Columns Reinforced with Carbon Fibre-Reinforced Polymer Bars. Advances in Civil Engineering 2019;2019:1–13.

[35] Xue W, Peng F, Fang Z. Behavior and Design of Slender Rectangular Concrete Columns Longitudinally Reinforced with Fiber-Reinforced Polymer Bars. ACI Structural Journal 2018;115(2).

[36] Salah-Eldin A, Mohamed HM, Benmokrane B. Structural performance of high-strength-concrete columns reinforced with GFRP bars and ties subjected to eccentric loads. Engineering Structures 2019;185:286–300.

[37] Zadeh HJ, Nanni A. Design of RC Columns Using Glass FRP Reinforcement. J Compos Constr 2013;17(3):294–304.

[38] Hadhood A, Mohamed HM, Benmokrane B, Nanni A, Shield CK. Assessment of Design Guidelines of Concrete Columns Reinforced with Glass Fiber-Reinforced Polymer Bars. ACI Structural Journal 2019;116(4):193–207.

[39] De Luca A, Matta F, Nanni A. Structural response of full-scale reinforced concrete columns with internal FRP reinforcement under compressive load. In: 9th International Symposium on Fiber Reinforced Polymer Reinforcement for Concrete Structures (FRPRCS-9), Sydney, Australia; 2009.

[40] Almomani M, Mahmoud K, El-Salakawy EF. Experimental Investigation of Large-Scale Eccentrically Loaded GFRP-Reinforced High-Strength Concrete Columns. J. Compos. Constr. 2022;26(2).

[41] Fan X, Xu T, Zhou Z, Zhou X. Experimental Study on Basic Mechanical Properties of BFRP Bars. IOP Conf. Ser.: Mater. Sci. Eng; 2017.

[42] AlNajmi L, Abed F. Evaluation of FRP Bars under Compression and Their Performance in RC Columns. Materials 2020;13(20).

[43] Broms B, Viest IM. Long Columns: Ultimate Strength of Hinged Columns. Transactions ASCE 1961;126(2):309–39.

[44] CSA A23. 3-19. Design of concrete structures: Canadian Standards Association; 2019.

[45] Hellesland J. Mechanics and Slenderness Limits of Sway-Restricted Reinforced Concrete Columns. J. Struct. Eng. 2008;134(8):1300–9.

3. Simplified Second-Order Analysis of Slender FRP-Reinforced Concrete Columns Using Nominal Curvature Method

Ahmed Usama Syed[1], Arndt Goldack[2]

[1 2] University of Wuppertal, Chair of Statics and Dynamics of Structures, Pauluskichstraße 7, 42285 Wuppertal, Germany.

Published in

Journal of Composites for Construction (2025) 29(2):04025007 (DOI: https://doi.org/10.1061/JCCOF2.CCENG-4944)

ABSTRACT

The nominal curvature method is one of the simplified methods for the second-order analysis of steel-reinforced concrete columns (steel-RC) in design codes such as Eurocode 2. The two parameters that are important in the application of this method are the total curvature distribution factor and the nominal curvature. Generally, for steel-RC columns, nominal curvature can be reasonably estimated from the curvature of the cross-section for a balanced failure and linear interpolation is performed for load values other than the balanced failure load. However, when fiber-reinforced polymer (FRP) bars are used as a reinforcement for concrete columns, the balance point may not appear in the load-moment capacity curve or it may appear at a very low load value and not at the "knee bend" of the load-moment capacity curve. Due to such behavior of FRP bars reinforced concrete (FRP-RC) columns, the estimation of nominal curvature is complex. This work examines the application of the nominal curvature method for the second-order analysis of FRP-RC columns and presents an equation based on a parametric study to estimate the nominal curvature of FRP-RC columns. In addition, when applying the nominal curvature method, the total curvature distribution factor is normally assumed as 10, which may be unconservative in some cases. In this work, an equation is presented to reasonably estimate the total curvature distribution factor, both for steel-RC and FRP-RC columns. Furthermore, a worked-out example and load-moment capacity curves for cross-sectional analysis are presented for FRP-RC columns. The outcomes would be of benefit for developing the design standards for FRP-reinforced concrete structures and the simplified second-order analysis of reinforced concrete columns.

Keywords: Slender columns; Fiber-reinforced polymer (FRP) bars; FRP bars reinforced concrete; Second-order analysis; Nominal curvature; Stability

3.1 Introduction

Second-order analysis of reinforced-concrete columns is complex owing to the nonlinear material properties and the second-order moments due to the geometric nonlinearity. In short columns, second-order moments are less significant and they are allowed to be neglected by the design codes. However, for slender columns, second-order moments are quite significant and need to be considered to assess the design capacity. The second-order moment adds to the total moment in the column and effectually reduces the first-order moment capacity of slender columns compared to short columns. Second-order analysis is necessary to calculate the second-order moments. The detailed second-order analysis of reinforced concrete columns requires advanced numerical iterative procedures such that the deformations induced in the column upon loading are considered to satisfy the equilibrium along with the nonlinear material properties. Due to the complexity involved in the detailed second-order analysis, design codes provide simplified methods for second-order analysis.

Two simplified approaches for the second-order analysis of reinforced concrete columns generally considered in the current design codes can be classified as the additional moment approach and the moment magnifier approach. In the case of the additional moment approach, the additional second-order moment is estimated based on the nominal curvature. In the case of the moment magnifier approach, the first-order moment is magnified with a factor based on a nominal stiffness to estimate the second-order moment. The efficiency of both simplified approaches depends on the accuracy of the estimation of nominal curvature and nominal stiffness. Generally, for steel bars reinforced concrete (steel-RC) columns, nominal stiffness is estimated by reducing the bending stiffness of the cross-section based on the prescribed factors in the design codes. The efficiency of the estimation of nominal stiffness is associated with the reduction factors and it could be too conservative. Eurocode 2 [1] adopts both additional moment and moment magnifier approaches as nominal curvature and nominal stiffness methods, respectively. However, the national annexure to Eurocode 2 [2] for Germany, does not allow the use of the nominal stiffness method. Araújo [3] compared the nominal stiffness and nominal curvature methods of Eurocode 2. He found the nominal curvature method to be more accurate. The additional moment approach based on nominal curvature is also recommended by CEB-FIB model code 1990 [4] and FIB model code 2010 [5]. The moment magnifier approach has been adopted by ACI

CODE 318-19 [6] for steel-RC columns and by ACI CODE-440.11-22 [7] for columns with glass fiber-reinforced plastic (GFRP) bars.

In general, fiber-reinforced plastic (FRP) bars have a linear stress-strain curve and generally a lower modulus of elasticity as compared to steel bars. FRP bars reinforced concrete (FRP-RC) columns are more prone to load and moment capacity reduction with the increase of slenderness as compared to steel-RC columns [8]. Therefore, for a successful application of the simplified second-order analysis methods for FRP-RC columns, parameters such as nominal stiffness and nominal curvature need to be appropriately determined.

Previously, Jiang and Teng [9,10] performed comprehensive studies to estimate the slenderness limit and nominal curvature of FRP-confined circular reinforced concrete columns. Recently, Syed and Goldack [11] conducted a detailed study on the slenderness limit of GFRP bars reinforced concrete (GFRP-RC) columns. Few attempts have been made to estimate the nominal stiffness of FRP-RC columns in the recent past [12–14]. ACI CODE 440.11-22 [7] provides an equation to estimate the effective stiffness or nominal stiffness of glass FRP-RC columns. However, no attempt has been made to estimate the nominal curvature of the FRP-RC columns and to use the nominal curvature method for the second-order analysis of FRP-RC columns. The existing design standards and manuals of FRP-RC lack guidelines for simplified second-order analysis of columns using the nominal curvature method. This work presents a novel approach to estimating the nominal curvature and the total curvature distribution factor for the simplified second-order analysis of the FRP-RC column using the nominal curvature method. The results of this study would contribute greatly towards the development of guidelines in this area. In addition, the proposed equation for calculating the total curvature distribution factor would also be beneficial for steel-RC columns.

The paper is organized as follows: First, the basis of the nominal curvature as a simplified method of second-order analysis is discussed briefly. Further, an equation is presented to effectively calculate the total curvature distribution factor. This is followed by the development of load-moment capacity curves of the reinforced concrete columns to assess the estimation of the nominal curvature of FRP-RC columns and compare it with the present methodology to estimate the nominal curvature of steel-RC columns. Furthermore, based on the detailed parametric study of slender FRP-RC columns, an equation

is proposed to estimate the nominal curvature for FRP-RC columns. Finally, the effectiveness of the proposed equations for the total curvature distribution factor and nominal curvature are assessed using the results from the detailed numerical analysis and the experimental data from the literature. In the Appendix, a worked-out example along with load-moment capacity curves for cross-section analysis of the FRP-RC column are presented for further applications.

3.2 Second-order analysis using nominal curvature

The maximum total moment (M_{tot}) in a column shown in Fig. 3.1 can be expressed as

$$M_{tot} = M_I + M_{II} \tag{3.1}$$

$$M_I = Ne_0 \tag{3.2}$$

$$M_{II} = Ne_2 \tag{3.3}$$

where M_I = maximum first-order moment; and M_{II} = maximum second-order moment, e_0 = first-order eccentricity, e_2 = maximum total deflection and N = load capacity. The section where the maximum total moment in the column occurs is considered the critical column section. As shown in Fig. 3.1, for a simply supported column with equal end moments and bent in single curvature, the critical column section occurs at mid-height where the total deflection is the maximum total deflection (e_2). In addition, this is the point where the maximum first-order moment and maximum second-order moment occur. Therefore, the consideration of M_I as the maximum first-order moment and M_{II} as the maximum second-order moment in the application of Eq. (3.1) is valid.

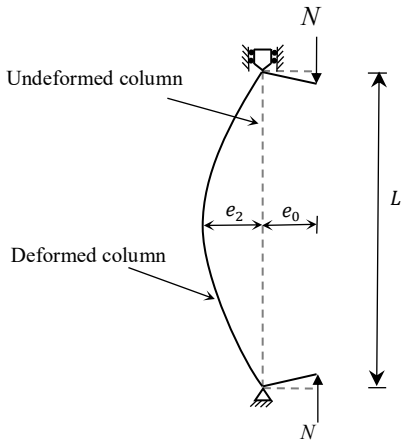


Fig. 3.1. Simply supported column bent in single curvature

In the case of columns under unequal end moments without transverse loading, the maximum first-order moment and maximum second-order moments do not occur at the same location. Consequently, the maximum first-order moment is replaced by an equivalent first-order moment [1,4,15] to use Eq. (3.1) and it is expressed as

$$M_I = M_{eqI} = 0.6M_{02} + 0.4M_{01} \geq 0.4M_{02} \tag{3.4}$$

where M_{01} = smaller end moment; and M_{02} = larger end moment, such that $|M_{02}| \geq |M_{01}|$.

In the case of columns with transverse loading, Eq. (3.1) can be used if M_I and M_{II} occur at the same location. In other cases, adding M_I and M_{II} using Eq. (3.1) to obtain the maximum total moment may be conservative.

The maximum second-order moment (M_{II}) in Eq. (3.1) can be expressed in terms of the curvature of the critical column section ($1/r$) at constant load N using the second derivative of the total deflection. For the case of the axially loaded column where the first-order eccentricity (e_0) is zero, based on Euler's buckling formulation, the total deflection follows a sinusoidal distribution for the length equal to the effective length (L). Further, the relationship between M_{II} and $1/r$ can be expressed as

$$M_{II} = N \cdot e_2 = N \cdot \frac{1}{r} \cdot \frac{L^2}{\pi^2} \tag{3.5}$$

In the case of eccentrically loaded columns, as shown in Fig. 3.1, the total deflection may not have a purely sinusoidal distribution over the effective length (L) [16]. However, regardless of the distribution function of the total deflection over the effective length (L), according to geometric nonlinear beam theory, the relationship between the total deflection and the curvature can be approximated to be linear [17]. Considering the linear relationship between the total deflection and curvature, Eurocode 2 [1] adopts a formulation based on the total curvature distribution factor (c) similar to Eq. (3.5) to calculate the maximum second-order moment (M_{II}) for eccentrically loaded columns, which is expressed as [16,18]

$$M_{II} = N \cdot e_2 = N \cdot \frac{1}{r} \cdot \frac{L^2}{c} \tag{3.6}$$

where N = load capacity; e_2 = maximum total deflection; $1/r$ = curvature of the critical column section at constant load N; L = effective length of the column; and c = total curvature distribution factor.

A schematic diagram in terms of maximum total moment and curvature at a constant value of load equal to the load capacity (N) is presented in Fig. 3.2 for the critical column section of the column in Fig. 3.1 to represent the basis of the nominal curvature method.

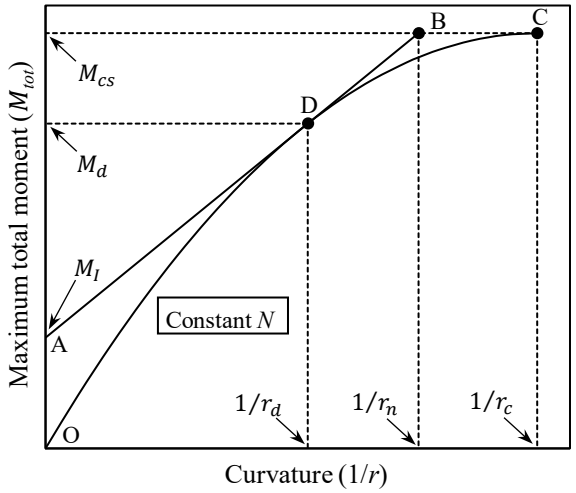


Fig. 3.2. Nominal curvature method

The inclined straight-line AB in Fig. 3.2 refers to the external moment due to geometric nonlinearity and it follows Eq. (3.1) and Eq. (3.6) at a constant load equal to the load capacity (N), for an eccentric

column with a given first-order eccentricity (e_0) and effective length (L). The line AB starts at the given external moment M_I, where the curvature due to geometric nonlinearity is zero. While the moment-curvature curve ODC for the critical column section is plotted based on the cross-sectional analysis using the nonlinear material properties and strain compatibility at a constant load equal to the load capacity (N). This curve represents the internal moment or the moment of resistance offered by the critical column section, where point C represents the cross-section failure. The line AB basically shows that when a constant load equal to the load capacity of the given eccentric column is applied, the external moment at the critical column section is related linearly with the curvature. The external moment can be resisted by the cross-section at the point where the line AB meets the cross-sectional moment-curvature curve which represents the resistance provided by the cross-section due to its material strength. At the load level equal to the load capacity (N) of the eccentric column, the line AB is a tangent to the cross-sectional moment-curvature curve as depicted in Fig. 3.2. Slope of the line AB is now the tangential stiffness of the cross-section at the tangent point D where the external moment line AB touches the internal moment curve ODC. Compatibility and equilibrium are fulfilled. Point D represents the maximum total moment (M_{tot}) which can be applied to this critical column section considering the second-order effects. For slender columns, the tangent point D may be considerably lower than the cross-sectional moment capacity (M_{cs}) at point C and this represents that the failure is due to stability rather than a material failure.

It is much more straightforward to work with cross-sectional moment capacity (M_{cs}) than the maximum total moment at stability failure (M_d), therefore for the purpose of analysis, point B is considered as the point of equivalent stability failure [16]. This enables us to identify the maximum total moment (M_{tot}) equal to the cross-sectional moment capacity (M_{cs}) in Eq. (3.1). M_{cs} at a particular value of load capacity (N) is determined from the load-moment capacity curve of ~~RC~~ reinforced concrete cross-section based on cross-sectional analysis which is readily available in design manuals and guidelines. Some examples of the load-moment capacity curve of FRP-RC columns are presented in Appendix II.

The curvature corresponding to point B is termed the nominal curvature ($1/r_n$), however, this is a hypothetical curvature and not the actual curvature ($1/r_d$) which exists for the critical column section

at failure. Therefore, it is termed as the nominal curvature. Using Eq. (3.6), the maximum second-order moment (M_{II}) corresponding to the nominal curvature can be written as

$$M_{II} = N \cdot e_2 = N \cdot \frac{1}{r_n} \cdot \frac{L^2}{c} \tag{3.7}$$

The maximum first-order moment (M_I) that can be resisted by the critical column section is the moment capacity and it is represented by the moment at point *A*. Further, to determine the maximum first-order moment (M_I) using Eq. (3.1) for a column of a given effective length at a required load capacity (N) using the nominal curvature method, it is important to estimate the maximum second-order moment (M_{II}). M_{tot} is known as M_{cs} from the cross-sectional load-moment capacity curve as seen earlier. To determine the M_{II} using Eq. (3.7), the unknowns are nominal curvature and total curvature distribution factor. In the further sections, the nominal curvature and curvature distribution factor are determined.

3.3 Total curvature distribution factor

Considering, $1/r_n = M_{tot}/EI_n$ and using Eq. (3.7), the maximum total deflection (e_2) can be written as

$$e_2 = \frac{M_{tot}}{EI_n} \cdot \frac{L^2}{c} \tag{3.8}$$

The bending stiffness of a reinforced concrete cross-section (EI) is not constant, but changes as the moment of resistance and the curvature change. As seen in Fig. 3.2 for the nominal curvature method, point B is considered as the point of equivalent stability failure where the maximum total moment (M_{tot}) is taken equal to the cross-sectional moment capacity (M_{cs}). Therefore, in Eq. (3.8) EI_n is the bending stiffness corresponding to the nominal curvature and the maximum total moment (M_{tot}) equal to M_{cs}. This is termed as the nominal stiffness (EI_n).

Further, the maximum total deflection (e_2) can be split into first-order deflection (δ_1) and second-order deflection (δ_2) given as

$$e_2 = \delta_1 + \delta_2 \tag{3.9}$$

In a similar form, as the maximum total deflection is expressed in Eq. (3.8), δ_1 and δ_2 can be expressed as [16]

$$\delta_1 = \frac{M_I}{EI_n} \cdot \frac{L^2}{c_I} \tag{3.10}$$

$$\delta_2 = \frac{M_{II}}{EI_n} \cdot \frac{L^2}{c_{II}} \tag{3.11}$$

where, c_I = first-order curvature distribution factor; and c_{II} = second-order curvature distribution factor. c_I can be determined from the curvature distribution due to the first-order moment. For the column in Fig. 3.1 considering a constant bending stiffness of EI_n, δ_1 can be expressed as

$$\delta_1 = \frac{M_I}{EI_n} \cdot \frac{L^2}{8} \tag{3.12}$$

Comparing Eq. (3.10) and Eq. (3.12) gives $c_I = 8$ for a simply supported column with equal end moment and bent in single curvature. $c_{II} = \pi^2 \approx 10$ can normally be approximated for a column with constant cross-section and axial load [1]

Further, M_{II} can be expressed as

$$M_{II} = N \cdot e_2 = N \cdot (\delta_1 + \delta_2) \tag{3.13}$$

Using Eq. (3.10), Eq. (3.11), Eq. (3.13) and $c_{II} = \pi^2$

$$M_{II} = M_I \left(\frac{(\pi^2/c_I) \cdot \alpha}{1 - \alpha} \right) \tag{3.14}$$

where $\alpha = N/N_B$; and $N_B = \pi^2 EI_n/L^2$

Comparing Eq. (3.1) and Eq. (3.14), M_{tot} can be written as

$$M_{tot} = M_I \left(1 + \frac{(\pi^2/c_I) \cdot \alpha}{1 - \alpha} \right) \tag{3.15}$$

Using Eq. (3.1), Eq. (3.7), and Eq. (3.8), M_{tot} can also be expressed as

$$M_{tot} = M_I \left(\frac{1}{1 - (\alpha \cdot \pi^2/c)} \right) \tag{3.16}$$

Comparing Eq. (3.15) and Eq. (3.16), the total curvature distribution factor (c) can be expressed as

$$c = c_I + \alpha(\pi^2 - c_I) \tag{3.17}$$

For multiple first-order effects, Eq. (3.17) can be expressed as

$$c = \frac{\sum_{i=1}^{n'} M_i}{\sum_{i=1}^{n'} \frac{M_i}{c_i}} + \alpha \left(\pi^2 - \frac{\sum_{i=1}^{n'} M_i}{\sum_{i=1}^{n'} \frac{M_i}{c_i}} \right) \tag{3.18}$$

where M_i = first-order moment due to the ith first-order load; c_i = first-order curvature distribution factor for the ith first-order load and n' = number of first-order loads.

Eq. (3.18) is similar to the equation provided in the FIB model code 2010 [5] for the total curvature distribution factor (c). However, when using the nominal curvature method, it is more convenient to work with nominal curvature ($1/r_n$) as it is known rather than α as it is dependent on EI_n. Hence, Eq. (3.17) can be written as

$$c = c_I + \frac{1}{r_n} \cdot \frac{L^2}{\pi^2} \cdot \frac{1}{e_{cs}} (\pi^2 - c_I) \tag{3.19}$$

where $e_{cs} = M_{cs}/N$

For multiple first-order effects, Eq. (3.19) can be expressed as

$$c = \frac{\sum_{i=1}^{n'} M_i}{\sum_{i=1}^{n'} \frac{M_i}{c_i}} + \frac{1}{r_n} \cdot \frac{L^2}{\pi^2} \cdot \frac{1}{e_{cs}} \left(\pi^2 - \frac{\sum_{i=1}^{n'} M_i}{\sum_{i=1}^{n'} \frac{M_i}{c_i}} \right) \tag{3.20}$$

Eq. (3.19) and Eq. (3.20) are proposed in this work to be used to estimate the total curvature distribution factor for RC columns while using the nominal curvature method to estimate the second-order moment. The performance of Eq. (3.19) to estimate the total curvature distribution factor is assessed further.

3.4 Numerical analysis of reinforced concrete columns

3.4.1 Methodology

The detailed second-order analysis of reinforced concrete columns requires that the material nonlinearity of concrete be considered along with the geometric nonlinearity during the analysis. In this study, a numerical method presented by Syed and Goldack [11] implemented in *MATLAB* [19] was used. In this numerical method, for a given cross-section, effective length (L) and first-order eccentricity (e_0) the maximum total deflection (e_2) is varied at the critical column section which is at the mid-height for the column shown in Fig. 3.1. To take into account the geometrical nonlinearity, for a particular value of (e_2), the curvature at the critical column section (φ) is calculated using Eq. (3.23) based on the assumed distribution of the curvature. For this value of φ at a particular e_2, the load resisted by the cross-section is calculated by considering the nonlinear material properties to implement the

equilibrium of forces and compatibility of the strain. An envelope of maximum total deflection (e_2)-load ~~(N)~~ is obtained. The maximum load of this envelope is considered as the load capacity (N) of the column. The value of the φ corresponding to the load capacity (N) is considered as the curvature at the cross-section failure ($1/r_d$). The value of the maximum total deflection (e_2) corresponding to the load capacity (N) is used to calculate the maximum total moment for a given value of first-order eccentricity (e_0) and this corresponds to M_d in Fig. 3.2. Using these values of $1/r_d$ and M_d, the point D in Fig. 3.2 is determined from the numerical analysis.

3.4.2 Geometric nonlinearity

The consideration of geometrical nonlinearity in this method is presented as follows. The variation of the total eccentricity (e_t) for the column in Fig. 3.1 is assumed to be sinusoidal over an extended effective length (a) as shown in Fig. 3.3 [16,20].

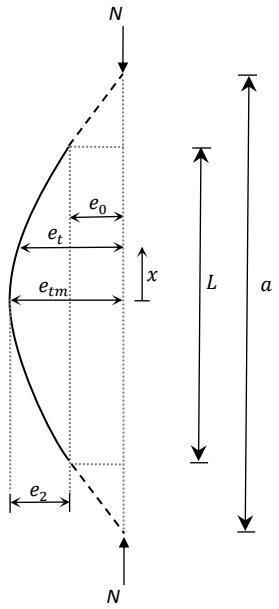


Fig. 3.3. Sinusoidal variation of total eccentricity

Considering the critical column section at mid-height as the origin, the total eccentricity (e_t) at any distance x from the origin for the simply supported column in Fig. 3.1 is expressed as

$$e_t = e_{tm} \cos\frac{\pi x}{a} \tag{3.21}$$

$$a = \frac{\pi L}{2\,cos^{-1}\frac{e_0}{e_{tm}}} \tag{3.22}$$

where $e_{tm} = e_0 + e_2$.

Using the second derivative of the total eccentricity, the value of the curvature at the mid-height can be expressed as

$$\varphi = \frac{e_{tm}}{L^2}\left(2cos^{-1}\frac{e_0}{e_{tm}}\right)^2 \tag{3.23}$$

The slenderness ratio (λ) is considered as

$$\lambda = \frac{L}{r_g} \tag{3.24}$$

where r_g = radius of gyration of the cross-section. The effect of λ is considered by the effective length (L) while assuming the curvature using Eq. (3.23) for the detailed second-order analysis.

3.4.3 Material nonlinearity

The stress-strain relationship for unconfined concrete is considered according to the expression provided by Popovics [21]. For a compressive strain of ε_c, the compressive stress is expressed as

$$\sigma_c(\varepsilon_c) = f_c\left(\frac{n_c\,(\varepsilon_c/\varepsilon_o)}{n_c\,-\,1\,+\,(\varepsilon_c\,/\,\varepsilon_o)^{n_c}}\right) \tag{3.25}$$

where $n_c = 0.8 + f_c/17$ [22]; $\varepsilon_o = f_c n_c/E_c(n_c - 1)$; $E_c = 3200\sqrt{f_c} + 6900$ [23]; f_c is the compressive strength of concrete; and E_c is the tangent modulus of elasticity of concrete. Concrete within lateral ties is considered partially confined and concrete outside lateral ties is considered unconfined. Mander et al. [24] model is used to model the partially confined concrete within the lateral ties. The maximum concrete compressive strain (ε_{cm}) is considered 0.0035 [1]. The cracking of concrete is considered; however, the tensile strength of concrete, creep, shrinkage, and tension stiffening are neglected. Furthermore, the bond between the concrete and FRP bars is assumed to be perfect. The modulus of elasticity of FRP bars in tension and compression is considered to be the same and the contribution of FRP bars in compression is also considered.

Steel reinforcement is modeled considering an ideal elastic-plastic stress-strain behavior while FRP

reinforcement was modeled with a linear elastic stress-strain behavior up to failure. The actual value of the ultimate tensile strain of FRP could lead to undesirably high curvature and deformations in the case of tension failure of the FRP-RC column. Hence, the ultimate tensile strain for design with the GFRP bars is suggested to be limited to 0.01 in the literature [7,25,26]. In this study, the ultimate tensile strain of the FRP bar (ε_{tu}) corresponding to all the values of modulus of elasticity is considered as 0.01. However, a consideration of FRP bars with an ultimate tensile strain less than 0.01 is addressed later.

3.4.4 Validation

The performance of this numerical method is validated by the experimental results, as shown in Fig. 3.4 for eccentrically loaded columns having both rectangular and circular cross-sections and a slenderness ratio ranging from around 20 to 60. N_{test} / N_{num} represents the ratio of load capacity from the experiment to load capacity obtained from numerical analysis. $M_{tot(test)}$ /$M_{tot(num)}$ represents the ratio of the maximum total moment from the experiment and numerical analysis. Eccentricity ratio (e_o/h or e_o/D) is considered as the ratio of first-order eccentricity (e_o) to depth of cross-section (h) for rectangular columns or the ratio of e_o to the diameter (D) of the column for circular columns. The mean values of N_{test} / N_{num} and $M_{tot(test)}$ /$M_{tot(num)}$ for the 46 experimental results presented in Fig. 3.4 are 1.00 and 1.03, respectively. This shows that the numerical and experimental results have a strong correlation.

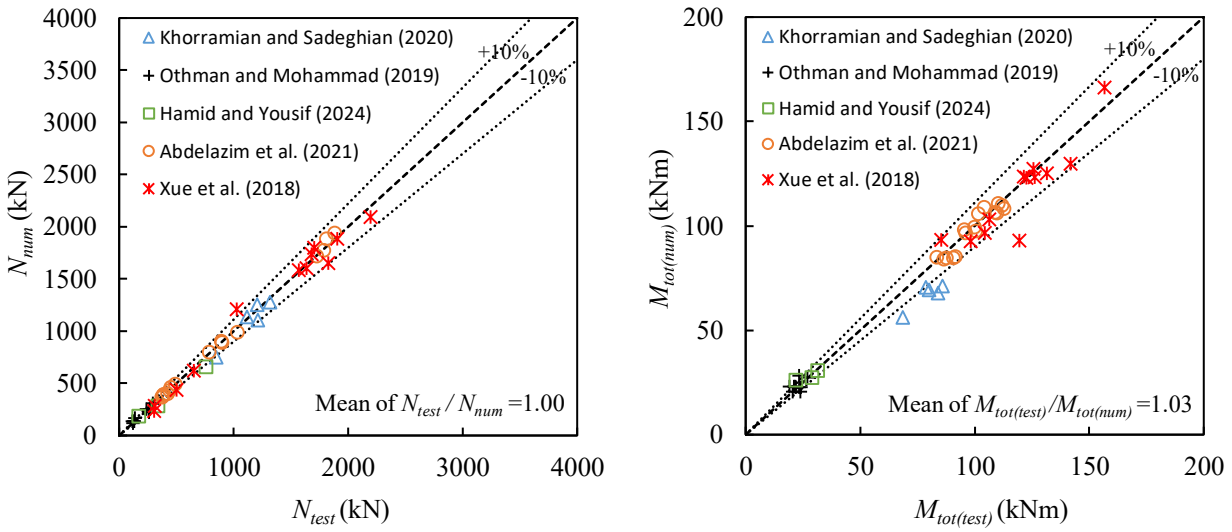


Fig. 3.4. Validation of the numerical method for detailed second-order analysis of FRP-RC columns

3.4.5 Cross-section

A rectangular column cross-section with breadth (b) and height (h) of 300 mm and 300 mm is considered throughout this study as shown in Fig. 3.5.

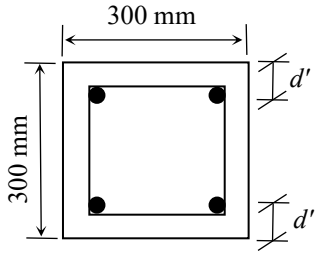


Fig. 3.5. Rectangular column cross-section with corner reinforcement with $b = h = 300$ mm

The ratio of the distance of the center of the reinforcement from the edge of the column (d') to the height of the cross-section is considered as $0.1\overline{3}$. Steel ties of 8 mm diameter with a yield strength of 500 MPa are considered at a spacing of 150 mm for all the steel-RC and FRP-RC columns analyzed in this study. The reinforcement ratio (ρ) considered in this study is defined as

$$\rho = 100 \cdot \frac{A_l}{A_c}\% \tag{3.26}$$

where A_l = total area of the longitudinal reinforcement; and A_c = total area of concrete.

3.5 Nominal curvature

3.5.1 Overview of nominal curvature for steel-RC columns

The equation for line AB in Fig. 3.2 can be expressed as

$$M_{tot} = M_I + \beta \cdot \frac{1}{r} \tag{3.27}$$

where β = constant expressing the slope of the line AB. The maximum first-order moment (M_I); the maximum total moment at point D (M_d); and curvature at point D ($1/r_d$) are known from the detailed second-order analysis and utilized to calculate β as

$$\beta = \frac{M_d - M_I}{1/r_d} \tag{3.28}$$

The total moment at point C (M_{cs}) is known from the cross-sectional load-moment capacity curve. Using the coordinates of line AB at point B, nominal curvature can be calculated as

$$\frac{1}{r_n} = \frac{M_{cs} - M_I}{\beta} \tag{3.29}$$

The load-moment capacity curve of a steel-RC column for different slenderness ratios is shown in Fig. 3.6(a) based on the detailed second-order analysis using the numerical procedure mentioned earlier. Using Eq. (3.29), the corresponding nominal curvature at failure for the critical section at mid-height of the column in Fig. 3.1 is shown as a load capacity-nominal curvature in Fig. 3.6(b). The yield strength of steel (f_y) and the compressive strength of concrete (f_c) were considered to be 500 MPa and 30 MPa, respectively.

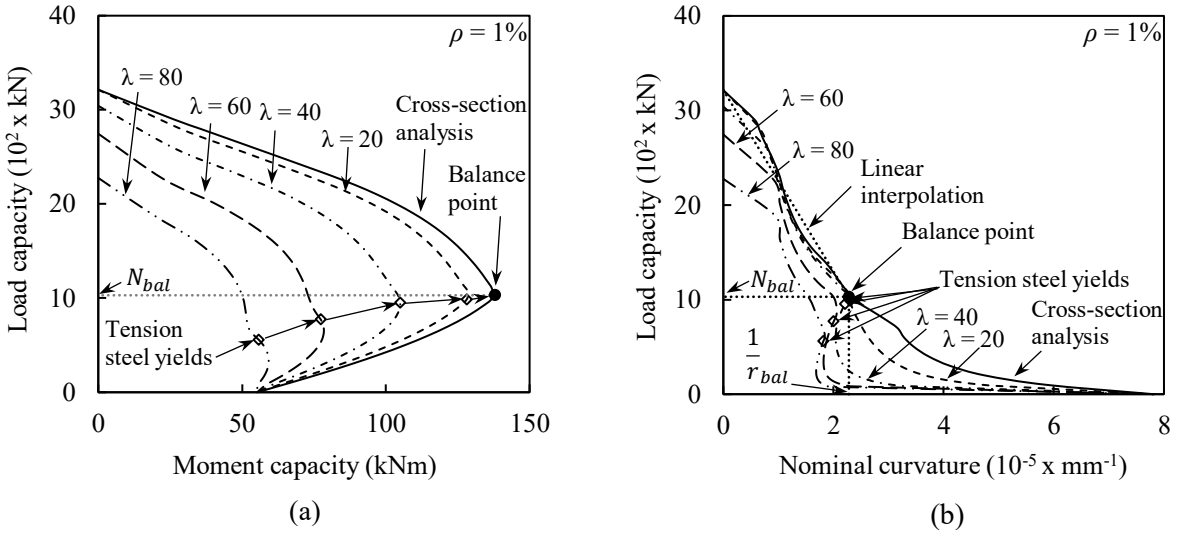


Fig. 3.6. Steel-RC Column: (a) Load-moment capacity curve for different slenderness ratios and (b) Load capacity-nominal curvature

The point on the load-moment capacity curve where the tension steel starts to yield and the concrete compressive strain at the extreme compression fiber is equal to the maximum concrete compressive strain (ε_{cm}) is marked as the balance point. It can be observed in Fig. 3.6(b) that for a low slenderness ratio of around 20 to 40, the nominal curvature ($1/r_n$) and the curvature of cross-section failure ($1/r_c$) are very close for the load higher than the balanced failure load (N_{bal}). Hence, for steel-RC columns with a low slenderness ratio and load higher than the N_{bal}, the nominal curvature can reasonably be estimated using the curvature of cross-section failure ($1/r_c$). However, for columns with a high slenderness ratio, the nominal curvature ($1/r_n$) is less than the curvature of the cross-section failure ($1/r_c$). Hence, a reduction due to the slenderness effect may be required in the value of the curvature

of the cross-section failure ($1/r_c$) to estimate the nominal curvature of steel-RC columns with a high slenderness ratio. Furthermore, the balance point appears at the "knee bend" of the load-moment capacity curve for the cross-sectional analysis of the steel-RC columns as shown in Fig. 3.7. This makes it simple to identify the balance failure load from the load-moment capacity curve for cross-section analysis.

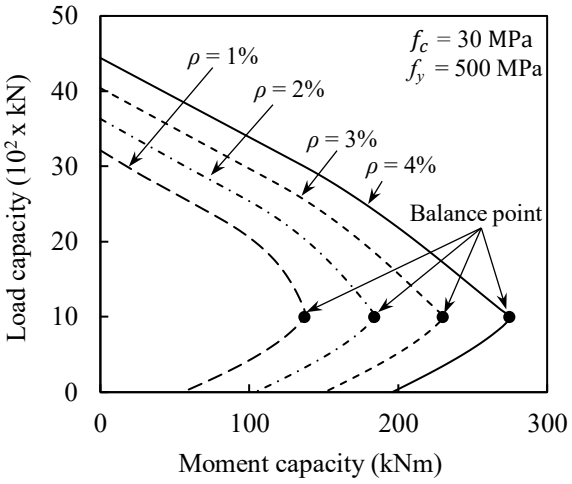


Fig. 3.7. Load-moment capacity curve of steel-RC column for cross-section analysis with different reinforcement ratios (ρ)

The curvature of the cross-section failure at the balanced failure load (N_{bal}) can be determined using the maximum concrete compressive strain (ε_{cm}) and yield strain of steel. Further, the curvature of the cross-section failure ($1/r_c$) for load values higher than N_{bal} can be simply determined using linear interpolation between the maximum load capacity of the column from cross-section analysis (N_u) and N_{bal} as the variation is nearly a straight line (see Fig. 3.6(b)).

The discussion done in the previous paragraphs can be a reasonable explanation for the expression provided by CEB Recommendations [15,27] to calculate the nominal curvature for steel-RC columns and it is stated as follows

$$\left(\frac{1}{r_n}\right)_{CEB} = \frac{\left(0.003 + \frac{f_{yd}}{E_s} - \frac{L}{50000h}\right)}{h} \cdot K_1 \tag{3.30}$$

$$K_1 = \frac{N_{ud} - N_d}{N_{ud} - N_{bald}} \leq 1 \tag{3.31}$$

where f_{yd} = design yield strength of steel; E_s = modulus of elasticity of steel; N_{ud} = maximum axial design load capacity; N_d = design axial load; N_{bald} = design axial load for balanced failure; and h = height of the cross-section.

Eurocode 2 [1] provides the equation for the nominal curvature of steel-RC columns as:

$$\left(\frac{1}{r_n}\right)_{EC2} = \frac{1}{r_0} \cdot K_r \cdot K_\varphi \tag{3.32}$$

where

$$\frac{1}{r_0} = \frac{\varepsilon_{yd}}{0.45d} \tag{3.33}$$

$$\varepsilon_{yd} = \frac{f_{yd}}{E_s} \tag{3.34}$$

$$K_r = \frac{n_u - n}{n_u - n_{bal}} \tag{3.35}$$

$$n = \frac{N_d}{A_c f_{cd}} \tag{3.36}$$

$$n_u = 1 + \omega \tag{3.37}$$

$$\omega = \frac{A_s f_{yd}}{A_c f_{cd}} \tag{3.38}$$

d = effective depth; f_{cd} = design compressive strength of concrete; n_{bal} = value of n at maximum moment resistance (which is at the balance point); A_s = total area of the steel longitudinal reinforcement and K_φ = factor depending on the creep of concrete. Eq. (3.32) from Eurocode 2 is very similar to Eq. (3.30), however some minor differences can be observed. The curvature of the balanced failure [28] in Eq. (3.32) from Eurocode 2 is calculated based on the yield of the reinforcement in tension and compression. Further, the effect of slenderness on the nominal curvature is neglected. These differences in Eq. (3.32) compared to Eq. (3.30) would make Eq. (3.32) simpler to use, however, it may be over-conservative in some cases such as columns with a high slenderness ratio where slenderness effects may reduce the nominal curvature.

Nominal curvature is taken as constant while limiting the value of K_1 and K_r to 1 for load below the

balanced failure load according to both Eq. (3.31) and Eq. (3.35). This can be understood from Fig. 3.6(b). It is observed for the cross-section analysis, that as the load decreases the curvature at cross-section failure ($1/r_c$) increases. However, for slender columns, the nominal curvature ($1/r_n$) at failure increases with the decrease of the load until the tension reinforcement does not yield. After the yielding of the tension reinforcement, nominal curvature starts decreasing with the decrease of the load until a very low load value is reached where nominal curvature increases rapidly. Hence, for load below the balanced failure load (N_{bal}), the nominal curvature is generally equal to or less than the $1/r_{bal}$ (see Fig. 3.6(b)). Therefore, $1/r_{bal}$ can be a reasonable estimate of nominal curvature for load values below the balance load. It can be overconservative for a high slenderness ratio such as λ = 80. For a low slenderness ratio such as λ = 20, this may be unconservative as the nominal curvature increases as the load decreases even after the yielding of steel. However, at such a low slenderness ratio, second-order effects are negligible, such that they can be ignored and the column can be considered as a short column.

3.5.2 Nominal curvature for FRP-RC columns

The load-moment capacity curve and the corresponding nominal curvature using Eq. (3.29) are presented in Fig. 3.8, based on the detailed numerical analysis for an FRP-RC column shown in Fig. 3.1. The modulus of elasticity of FRP bar (E_{FRP}) and the compressive strength of concrete (f_c) is considered as 40 GPa and 30 MPa respectively. The balance point is marked where the tensile strain in the FRP bar (ε_{tFRP}) reaches the ultimate tensile strain of the FRP bar (ε_{tu}) of 0.01 and the concrete compressive strain (ε_c) at the extreme compression fiber is equal to the maximum concrete compressive strain (ε_{cm}). It can be observed for the reinforcement ratio of 1%, the balance point appears at a low value of axial load and it does not appear at the "knee bend" which is the point of the maximum moment capacity for the cross-sectional analysis of FRP-RC columns. Further, the balance point does not necessarily appear for all cases, as seen in Fig. 3.8(c) for the cross-sectional analysis with a reinforcement ratio of 4%.

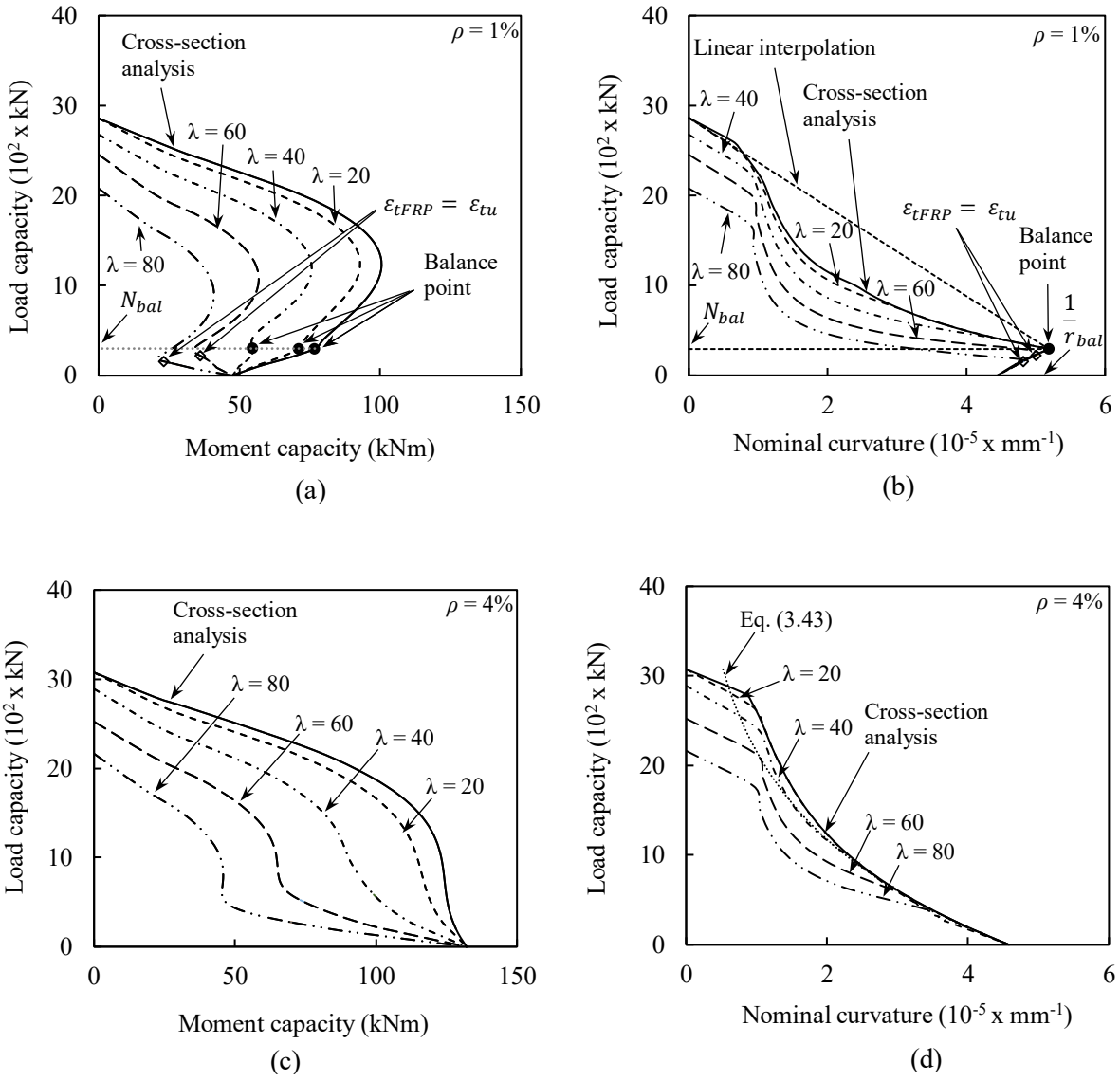


Fig. 3.8. FRP-RC column: (a); (c) Load-moment capacity curve for different slenderness ratios; (b); and (d) Load capacity-nominal curvature

The appearance and the position of the balance point in the cross-section load-moment capacity envelope of FRP-RC columns would depend on the concrete compressive strength, modulus of elasticity of FRP bar, reinforcement ratio, and ultimate tensile strain of FRP bar [8]. This is quite different in comparison to the cross-section analysis of steel-RC columns where the balance point appears at the "knee bend" of the load-moment capacity curve. Hence, the methodology for steel-RC columns to estimate the nominal curvature from the curvature of the section in balanced failure would not be appropriate for FRP-RC columns. In addition, for the case where a balance point appears in the load-moment capacity curve such as in Fig. 3.8(a), the linear interpolation of the curvature for load

values as done for steel-RC columns would be too conservative. This requires the development of an appropriate equation for estimating the nominal curvature of the FRP-RC column.

3.6 Estimation of the nominal curvature for FRP-RC columns

3.6.1 Parametric study

To investigate the behavior of the nominal curvature of the FRP-RC column and the factors affecting it, an extensive parametric study was conducted. The parametric study was carried out by performing the detailed second-order analysis on the FRP-RC column shown in Fig. 3.1 and with the variables presented in Table 3.1. The range of concrete compressive strength considered in the parametric study corresponds to the normal compressive strength of concrete with a compressive strength of 10 to 50 MPa. This range of concrete strength was considered to correspond to the characteristic concrete compressive strength of 12 to 50 MPa with a constant ultimate compressive strain of 0.0035 according to Eurocode 2 [1,18]. A minimum reinforcement ratio of 1% is suggested in the literature [7,26,29,30] to avoid the brittle tension failure of FRP-RC columns. The maximum reinforcement ratio in the column corresponds to the effective compaction of concrete near the reinforcement. Similar to steel-RC columns, ACI CODE-440.11-22 [7] allows an 8% reinforcement ratio for GFRP-RC columns. In this study, the maximum reinforcement ratio is taken as 4% corresponding to the Eurocode 2 [1] limit for steel-RC columns outside lap locations. A wide range of eccentricity ratios are considered to cover maximum points in the load-moment capacity curve of the slender FRP-RC column. The range of modulus of elasticity of FRP bars considered corresponds to different types of FRP bars available in the market, such as glass, basalt, aramid, and carbon FRP bars. A rectangular column cross-section with corner reinforcement as shown in Fig. 3.5 was considered for the parametric study. The ratio of the distance of the center of the reinforcement from the edge of the column (d') to the height of the cross-section (h) was considered $0.1\overline{3}$ for all the cases of the parametric study.

Table 3.1. Variables for the parametric study

Parameters	Values	Number of values
Concrete Compressive strength (f_c)	10; 20; 30; 40 and 50 MPa	5
Modulus of elasticity of FRP bar (E_{FRP})	40; 60; 80 and 100 GPa	4
Slenderness ratio (λ)	20; 30; 40; 50; 60; 70 and 80	7
Reinforcement ratio (ρ)	1; 2; 3 and 4 %	4
Eccentricity ratio (e_o/h)	$1/30$; $2/30$ to $48/30$	48
	Total cases of analysis	26880

From Eq. (3.1) and Eq. (3.7), while considering $M_{tot} = M_{cs}$, M_{cs} can be expressed as

$$M_{cs} = M_I + N \cdot \frac{1}{r_n} \cdot \frac{L^2}{c} \tag{3.39}$$

Using Eq. (3.39) and Eq. (3.19), nominal curvature can also be expressed as

$$\frac{1}{r_n} = \frac{M_{cs}c_I - M_I c_I}{M_I k + NL^{2-} M_{cs}k} \tag{3.40}$$

$$k = \frac{L^2}{\pi^2} \cdot \frac{1}{e_{cs}} (\pi^2 - c_I) \tag{3.41}$$

Using Eq. (3.39) and Eq. (3.29) while considering $M_{tot} = M_{cs}$, the total curvature distribution factor (c) can be expressed as

$$c = \frac{NL^2}{\beta} \tag{3.42}$$

To be consistent with Eq. (3.39), $1/r_n$ from Eq. (3.40) is considered to calculate the total curvature distribution factor (c) using Eq. (3.19). The total curvature distribution factor (c) calculated using Eq. (3.42) is completely based on the detailed second-order analysis. Therefore, the value of c calculated from Eq. (3.42) is considered as the basis to evaluate the performance of Eq. (3.19) to estimate the total curvature distribution factor (c). The comparison of the total curvature distribution factor (c) calculated from Eq. (3.19) and Eq. (3.42) is presented in Fig. 3.9.

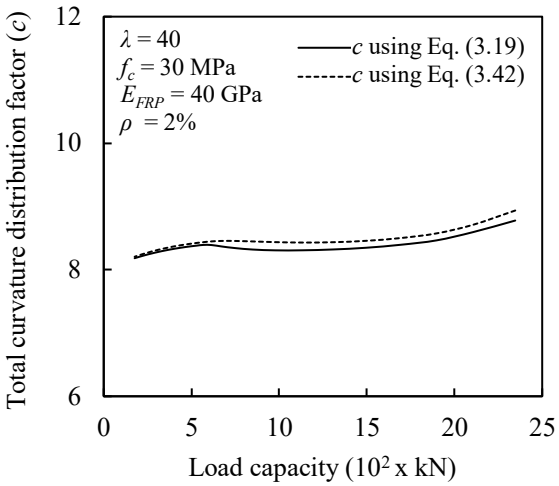


Fig. 3.9. Performance of the Eq. (3.19) to estimate the total curvature distribution factor

For all the cases evaluated in the parametric study, the mean percentage error in calculating c from Eq. (3.19) in comparison to Eq. (3.42) is 0.73%. Hence, Eq. (3.19) can very well estimate the total curvature distribution factor (c). The minor difference between the c value from Eq. (3.19) and Eq. (3.42) can be attributed to the assumption of $c_{II} = \pi^2$ for Eq. (3.19). The nominal curvature of the FRP-RC column in the parametric study is calculated using Eq. (3.40) to be consistent with the proposal of Eq. (3.19) to calculate c. The difference between the nominal curvature calculated using Eq. (3.40) and Eq. (3.29) corresponds to the difference in the c value calculated using Eq. (3.19) and Eq. (3.42), respectively. As this difference between the c values is not significant the difference between the nominal curvature calculated using Eq. (3.40) and Eq. (3.29) is also negligible.

The effect of concrete compressive strength, modulus of elasticity of FRP bar, and reinforcement ratio on the nominal curvature of FRP-RC column based on the parametric study is presented in Fig. 3.10-3.12. It can be observed that as the concrete compressive strength increases the nominal curvature increases. With the increase in modulus of elasticity and reinforcement ratio the nominal curvature increases, however, for low load values it is vice versa.

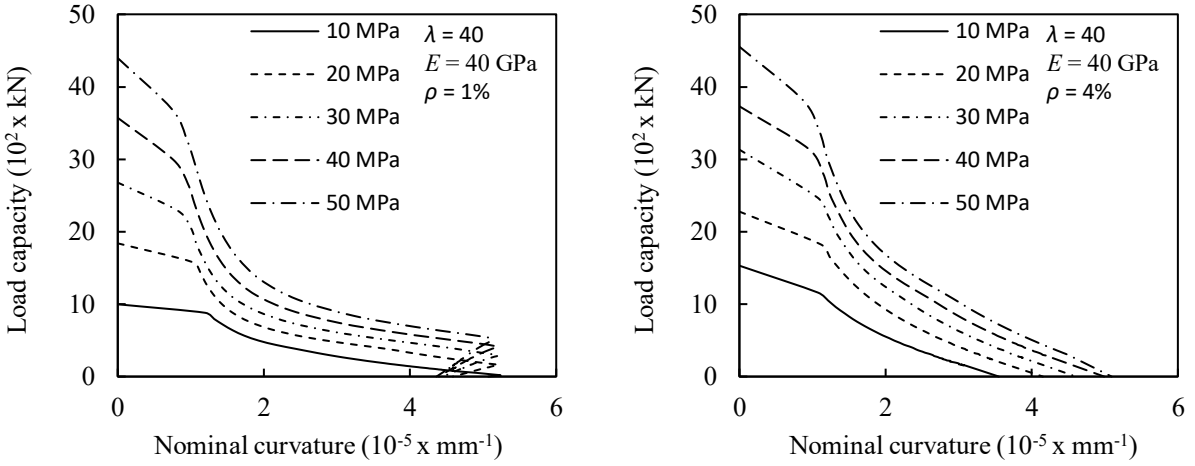


Fig. 3.10. Effect of concrete compressive strength on the nominal curvature of FRP-RC column

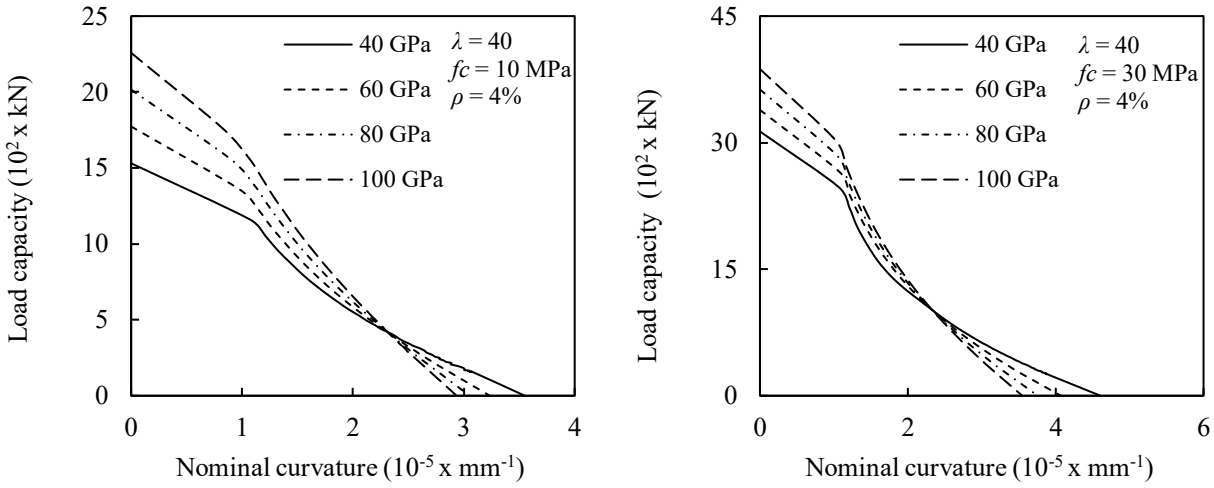


Fig. 3.11. Effect of modulus of elasticity on the nominal curvature of FRP-RC column

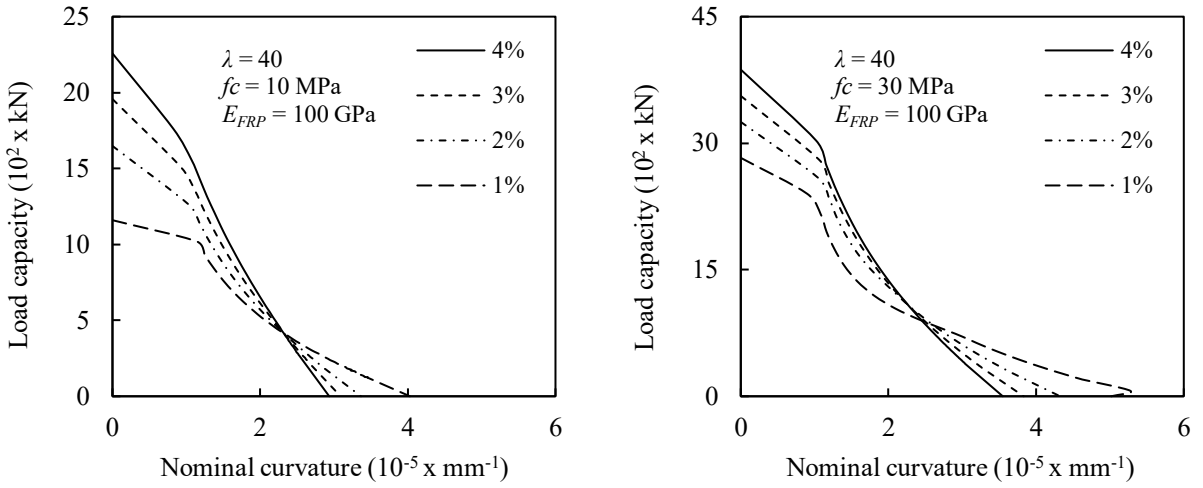


Fig. 3.12. Effect of reinforcement ratio on the nominal curvature of FRP-RC column

The effect of the slenderness ratio on the nominal curvature of the FRP-RC column can be observed in Fig. 3.8(b) and 3.8(d). The low values of the slenderness ratio have less effect on the nominal curvature in comparison to the curvature of cross-section failure, however as the slenderness ratio increases, its effect on the nominal curvature increases. From Fig. 3.6(b) and 3.8(b), it can be observed that the effect of slenderness on the nominal curvature is greater for the FRP-RC column than for the steel-RC column. This can be attributed to the low modulus of elasticity of FRP bars as compared to steel bars.

3.6.2 Proposed nominal curvature for FRP-RC column

Using the curve fitting approach, the form of the equation with an exponential function to estimate the nominal curvature of FRP-RC columns at a particular value of load capacity (N) can be expressed as

$$\left(\frac{1}{r_n}\right)_{FRP} = \frac{1}{r_m} e^{-(A*n_r)} \tag{3.43}$$

$$n_r = (N - N_m)/(N_u - N_m) \geq 0 \tag{3.44}$$

where e = mathematical constant and base of the natural logarithm; $1/r_m$ = maximum curvature of cross-section failure in the load-moment capacity curve for cross-section analysis; N_u = maximum axial load capacity of the column from cross-sectional analysis; and N_m = load capacity of the column for the curvature of $1/r_m$. For the columns where the balance point appears in the load-moment capacity

curve for cross-sectional analysis, $N_m = N_{bal}$ and $1/r_m = 1/r_{bal}$. For the columns where the balance point does not appear in the load-moment capacity curve, $N_m = 0$ and $1/r_m$ can be easily calculated using force equilibrium in the cross-section with no axial load (see Appendix I). It can be seen in Fig. 3.8(b) that for a load value higher than N_{bal}, the behavior of the nominal curvature for the column where the balance point appears in the load-moment capacity curve is quite similar to the nominal curvature of the column in Fig. 3.8(d) where balance does not appear. In addition, to avoid the brittle-tension failure of the column, the region of the load-moment capacity curve below the N_{bal} is undesirable for design. This is the basis to subtract N_m to calculate the normalized load ratio n_r.

A is the variable that would depend on factors such as slenderness ratio, reinforcement ratio, concrete strength, and modulus of elasticity of FRP bar. *A* is expressed as

$$A = P + Q\lambda + R\omega' \tag{3.45}$$

where *P, Q,* and *R* are the regression coefficients. ω' is the mechanical reinforcement ratio for the FRP-RC column which can be expressed as

$$\omega' = \frac{A_{FRP}E_{FRP}\varepsilon_{tu}}{A_c f_c} \tag{3.46}$$

where A_{FRP} = the total area of the FRP longitudinal reinforcement.

It can be observed in Fig. 3.11 and Fig. 3.12 that the effect of the modulus of elasticity and reinforcement ratio on nominal curvature is greater for low values of concrete strength. This indicates that the effect of f_c, E_{FRP}, and ρ on the nominal curvature of the FRP-RC column is interdependent. Therefore, ω' is considered to incorporate the effect of concrete strength, modulus of elasticity of FRP bar, and reinforcement ratio while estimating the nominal curvature of FRP-RC column. The mechanical reinforcement ratio considering ε_{tu} as 0.01 is expressed as $\omega'_{0.01}$. It can be seen in Fig. 3.13 for different values of f_c, E_{FRP}, and ρ, however with the same value of $\omega'_{0.01}$ the variation of nominal curvature with n_r corresponding to the eccentricity ratio considered in the parametric study is quite similar. This shows the strength of ω' to incorporate the effect of f_c, E_{FRP}, and ρ while estimating the nominal curvature of FRP-RC columns.

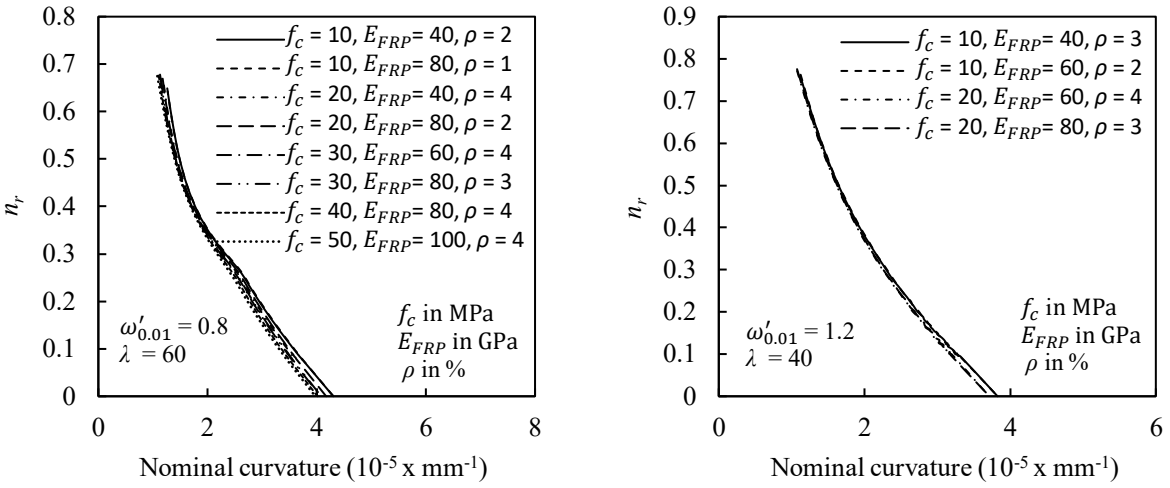


Fig. 3.13. Effect of mechanical reinforcement ratio (ω') on the nominal curvature of FRP-RC column

To develop an expression to estimate the variable A for the nominal curvature of the FRP-RC column, a nonlinear regression using Eq. (3.43) and Eq. (3.45) is implemented in *MATLAB* [19]. Based on the nonlinear regression analysis the equation to estimate A is expressed as

$$A = 2.32 + 0.0064\lambda - 0.511\omega'_{0.01} \tag{3.47}$$

To develop Eq. (3.47), all the cases evaluated in the parametric study were considered for the regression analysis except the cases where the column fails in brittle tension failure and consequently n_r is negative. Therefore, a total of 24963 cases were considered for the regression analysis to estimate Eq. (3.47). The nominal curvature was evaluated using Eq. (3.40) while performing the regression analysis. The coefficient of determination (R^2) and the standard error of the regression are found to be 0.947 and 2.35×10^{-6}, respectively; which represents a good correlation with the numerical results.

The performance of Eq. (3.43) to calculate the nominal curvature of the FRP-RC column while using Eq. (3.47) to calculate the variable A is determined in comparison to the experimental results from the literature in terms of first-order moment capacity as shown in Fig. 3.14. Columns with both rectangular [13,31–33] and circular cross-sections [14,29] have been considered in Fig. 3.14. The mean of the ratio of the first-order moment capacity from the experimental results ($M_{I(test)}$) and the first-order moment capacity obtained using Eq. (3.39) while calculating the nominal curvature from Eq. (3.43) ($M_{I(prop)}$) was found to be 1.10 for the 51 experimental results with slenderness ratios ranging from around 20 to

60. This shows that Eq. (3.43) while using Eq. (3.47) to calculate the variable *A,* can reasonably and conservatively predict the nominal curvature of FRP-RC columns. A limited number of experimental results for slender FRP-RC columns with slenderness ratios ranging from around 50 to 80 were found in the literature. This identifies the need to conduct more experiments in the future on slender FRP-RC columns, especially with a slenderness ratio exceeding 50.

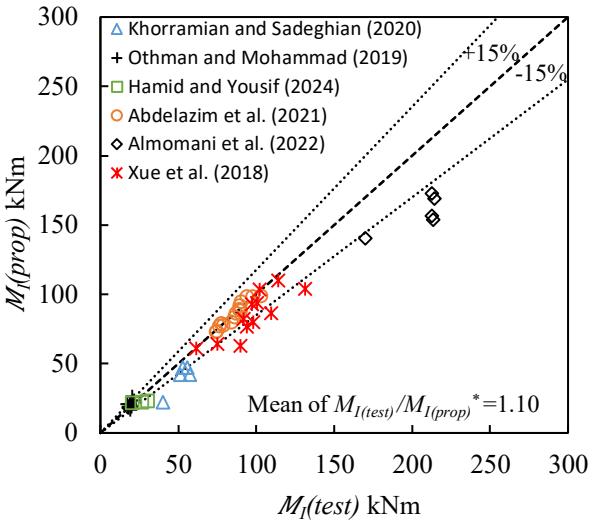


Fig. 3.14. Performance of the proposed nominal curvature equation (Eq. (3.43) along with Eq. (3.47)) to predict the moment capacity of the FRP-RC column

Eq. (3.47) is limited to the slenderness ratio of 20 to 80 considered in the parametric study. It can be seen in Fig. 3.8(b) and 3.8(d) that as the slenderness ratio increases nominal curvature decreases. Nominal curvature calculated using Eq. (3.47) for a slenderness ratio greater than 80 shall be more than the actual value of the nominal curvature. Hence, using Eq. (3.47) for a slenderness ratio greater than 80 will give a higher value of second-order moment (M_{II}) and consequently lower value of (M_I). Therefore, for a slenderness ratio higher than 80, Eq. (3.47) would be too conservative. Although Eq. (3.47) was determined using the parametric study for the column with a rectangular cross-section, it is observed from Fig. 3.14 that the performance of Eq. (3.47) is similar for rectangular and circular cross-sections. Hence, Eq. (3.47) can be utilized for different column cross-sections provided that the cross-sectional load-moment capacity curves are available for the given cross-section. However, Eq. (3.47) is limited to the FRP bars reinforced columns and it does not extend to FRP confined columns. Further investigation is required to determine the application and extension of this method to determine the

nominal curvature of FRP-confined concrete columns. Further, Eq. (3.47) is developed and limited to the concrete compressive strength of 10 to 50 MPa. However, the performance of Eq. (3.47) for FRP-RC columns with high strength concrete can be observed in Fig. 3.14 for the experimental results from Almomani et al. [29]. They used concrete strength of around 60 MPa and the performance of the Eq. (3.47) is good and on the conservative side for their experimental results. Further investigation to develop an expression A for high strength concrete would be of advantage.

For the parametric study, the ultimate tensile strain for the FRP bar (ε_{tu}) of 0.01 is considered. However, for some types of FRP bars, the ultimate tensile strain or the design value of ultimate tensile strain can be less than 0.01. For the cases where ε_{tu} is less than 0.01, $\omega'_{0.01}$ can be replaced in Eq. (3.47) with ω' as

$$\omega' = \frac{\omega'_{0.01}\varepsilon_{tu}}{0.01} \tag{3.48}$$

and A can be further expressed as

$$A = 2.32 + 0.0064\lambda - 0.0051\frac{\omega'}{\varepsilon_{tu}} \tag{3.49}$$

This is because the region of the tensile failure of the load-moment capacity curve below the balanced failure load (N_{bal}) is avoided while developing Eq. (3.43) and Eq. (3.47). The ultimate tensile strain of the FRP bar would not affect the nominal curvature of the FRP-RC column with load higher than the balanced failure load (N_{bal}). N_{bal} would depend on the value of ε_{tu}. However, N_{bal} is identified using the load-moment capacity curve for cross-sectional failure which is based on the specified value of ε_{tu}. Hence, Eq. (3.49) is proposed to determine the variable A while using Eq. (3.43) to calculate the nominal curvature of the FRP-RC column. The range of $\omega'_{0.01}$ considered in the parametric study varies from 0.08 to 4 which corresponds to ω' of $8\varepsilon_{tu}$ to $400\varepsilon_{tu}$. Hence, the proposed equation (Eq. (3.49)) to estimate the variable A is limited to the ω' range of $8\varepsilon_{tu}$ to $400\varepsilon_{tu}$.

An example of the simplified second-order analysis of the FRP-RC column using the equations proposed in this study is given in Appendix I.

3.7 Conclusions

The behavior of the nominal curvature of steel-RC columns was discussed in brief along with the existing equations to estimate the nominal curvature for steel-RC columns. The application of the nominal curvature method for the simplified second-order analysis of FRP-RC columns was assessed and a parametric study on the total of 26880 FRP-RC columns was performed. The following conclusions are made:

1. The load-nominal curvature behavior of FRP-RC columns is not similar to steel-RC columns. The linear interpolation of the nominal curvature about load values using the curvature at balanced failure would be too conservative for FRP-RC columns. In addition, the balance point does not appear in all cases for FRP-RC columns. This requires reworking the equation to estimate the nominal curvature of the FRP-RC column.
2. The effect of the slenderness ratio on the nominal curvature is greater for the FRP-RC column compared to the steel-RC column. Concrete compressive strength, modulus of elasticity of FRP bar, and reinforcement ratio have a reasonable effect on the nominal curvature of the FRP-RC column.
3. Mechanical reinforcement ratio can effectively take into account the effect of concrete compressive strength, modulus of elasticity of FRP bar, and reinforcement ratio to estimate the nominal curvature of FRP-RC column.
4. Based on the extensive parametric study conducted in this study, Eq. (3.43) along with Eq. (3.49) is proposed to estimate the nominal curvature of the FRP-RC column. The proposed nominal curvature equation for the FRP-RC column performed fairly well in comparison to the experimental results. The proposed equation of Eq. (3.49) is limited to the range of mechanical reinforcement ratio, concrete compressive strength and slenderness ratio considered in this study.
5. An equation (Eq. (3.19)) to estimate the total curvature distribution factor utilizing the nominal curvature is proposed. The proposed expression is found to be in good agreement with the numerically calculated value of the total curvature distribution factor with a mean error of 0.73%.

3.8 Appendix I

The moment capacity of a slender FRP-RC column is determined using the nominal curvature method using the equations proposed in this study. The column is simply supported and bent in single curvature as shown in Fig. 3.1.

Input parameters are:

- Column cross-section (b x h): 300 x 300 mm
- Length of the column (L): 3000 mm
- Concrete compressive strength (f_c) = 40 MPa
- Modulus of elasticity of FRP bar (E_{FRP}) = 60 GPa
- Reinforcement ratio (ρ): Case 1: ρ = 1 %; and Case 2: ρ = 4 %
- $d'/h = 0.1\overline{3}$
- Required load capacity (N) = 1800 kN

Steel stirrups with a yield strength of 500 MPa and 8 mm diameter are provided at a spacing of 150 mm throughout the length of the column.

Generally, in practice, a rectangular parabola is used as a design stress-strain curve for concrete. Eurocode 2 [1] provides the equation of concrete stress-strain curve for the design of cross-sections as

$$\sigma_c(\varepsilon_c) = \begin{cases} f_{cd}\left(1-\left(1-\dfrac{\varepsilon_c}{\varepsilon_o}\right)^{n_c}\right) & 0 \le \varepsilon_c \le \varepsilon_o \\ f_{cd} & \varepsilon_o \le \varepsilon_c \le \varepsilon_{cm} \end{cases} \tag{3.50}$$

Where, for normal strength concrete with characteristic cylindrical compressive concrete strength (f_{ck}) of 12 to 50 MPa, ε_o = 0.002, n_c = 2, and ε_{cm} = 0.0035. Compared to the concrete stress-strain curve in Eq. (3.25), Eq. (3.50) would provide slightly higher values of load and moment capacity. However, the proposed equations for nominal curvature can be effectively used as all the required parameters in Eq. (3.43) and Eq. (3.49) are calculated based on the load-moment capacity curves for cross-section analysis using Eq. (3.50).

3.8.1 Case 1: ρ = 1 %

Using Eq. (3.39), M_I is the moment capacity that needs to be calculated. Unknowns are M_{cs}, $1/r_n$, and c. Considering the ultimate tensile strain for the FRP bar (ε_{tu}) as 0.01, $\omega'_{0.01}$ is calculated using Eq. (3.46) as 0.15. Based on the concrete stress-strain curve using Eq. (3.50) while considering $f_{cd} = f_c$, the load-moment capacity curve for cross-section analysis with $\omega'_{0.01}$ = 0.15 is shown in Fig. 3.15. Furthermore, ε_o = 0.002, n' = 2 and ε_{cm} = 0.0035 are considered while taking $f_{ck} = f_c$ for developing the curves in Fig. 3.15. In this example, $\omega'_{0.01}$ is calculated using the given concrete compressive strength (f_c), however, design compressive strength of concrete (f_{cd}) and design ultimate tensile strain of FRP bar shall be used for the purpose of design. The cross-section moment capacity for required load capacity (N) of 1800 kN which corresponds to $N/f_c bh = 0.5$ and $M_{cs}/f_c bh^2 = 0.13$ is calculated as M_{cs} = 140.40 kNm and maximum axial load is calculated as N_u = 3672 kN corresponding to $N_u/f_c bh = 1.02$ from Fig. 3.15.

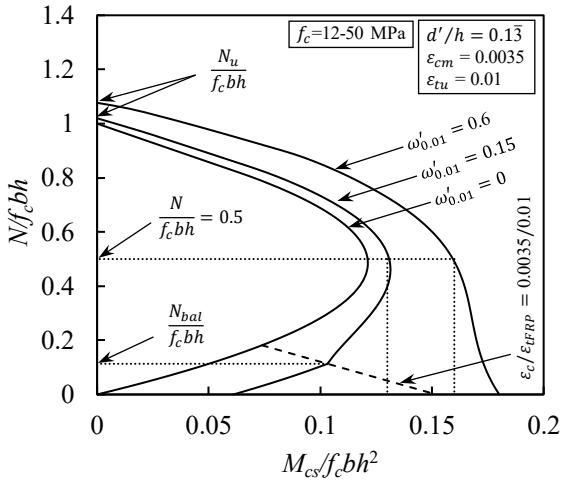


Fig. 3.15. Load-moment capacity curve of FRP-RC column for cross-section analysis with $d'/h = 0.1\overline{3}$

In Fig. 3.15, for $\omega'_{0.01}$ = 0.15 at a low value of the load, a point in the curve can be seen, below which a sharp linear decrease in the moment with the decrease in the load is observed. The compressive strain in the concrete (ε_c) reaches the ultimate concrete compressive strain (ε_{cm}) of 0.0035 and the tensile

strain in the FRP bar (ε_{tFRP}) is 0.01 at this point, hence it is identified as the balance point. In this case, to calculate $1/r_n$ using Eq. (3.43), $N_m = N_{bal}$ and $1/r_m = 1/r_{bal}$ is considered and calculated as

N_{bal} = 396 kN (corresponding to $N_{bal}/f_c bh = 0.11$ from Fig. 3.13)

$$\frac{1}{r_{bal}} = \frac{\varepsilon_{cm} + \varepsilon_{tu}}{h - d'} = \frac{0.0035 + 0.01}{300 - 40} = 5.19 \times 10^{-5}\ \text{mm}^{-1}$$

Slenderness ratio is calculated using Eq. (3.24) as λ = 34.6.

Using Eq. (3.47) and Eq. (3.44)

$$A = 2.32 + (0.0064 \times 34.6) - (0.511 \times 0.15) = 2.46$$

$$n_r = \frac{1800 - 396}{3672 - 396} = 0.43$$

Using Eq. (3.43) nominal curvature is calculated as

$$\left(\frac{1}{r_n}\right)_{FRP} = \left(5.19 \times 10^{-5}\right) \times e^{-(2.46 \times 0.43)} = 1.80 \times 10^{-5}\ \text{mm}^{-1}$$

$$e_{cs} = \frac{M_{cs}}{N} = \frac{140.40}{1800} \times 1000 = 78\ \text{mm}$$

Using Eq. (3.19) while considering c_I = 8 and $1/r_n = (1/r_n)_{FRP}$, the total curvature distribution factor is calculated as

$$c = 8 + \left(1.80 \times 10^{-5}\right)\left(\frac{3000}{\pi}\right)^2 \left(\frac{1}{78}\right)(\pi^2 - 8) = 8.39$$

Using Eq. (3.39), moment capacity and maximum value of first-order eccentricity (e_0) are calculated as

$$M_I = \left(140.40 \times 10^6\right) - \left(1800 \times 10^3\right)\left(1.80 \times 10^{-5}\right)\left(\frac{3000^2}{8.39}\right) = 105.64\ \text{kNm}$$

$$e_0 = \frac{M_I}{N} = \frac{105.64^*}{1800} \times 1000 = 58.68^*\ \text{mm}$$

Conducting a detailed second-order analysis using the numerical method presented earlier and considering the rectangular parabolic concrete stress-strain curve, the moment capacity is found to be 108.28 kNm for the input values considered in this example. This is quite near to the value of $M_I =$ 105.64 kNm predicted using the proposed equation.

3.8.2 Case 2: ρ = 4 %

All the input parameters remain the same as for case 1. However, the reinforcement ratio (ρ) is increased to 4 %. $\omega'_{0.01}$ is calculated using Eq. (3.46) as 0.6. It is observed from Fig. 3.15 that the line of concrete compressive strain (ε_c) and tensile strain in FRP bar (ε_{tFRP}) with ultimate values of 0.0035 and 0.01, respectively, does not pass through the load-moment capacity curve for $\omega'_{0.01}$ = 0.6. Hence, the balance point does not appear in the load-moment capacity curve for $\omega'_{0.01}$ = 0.6. At a required load capacity (N) of 1800 kN, $N/f_c bh = 0.5$ and $M_{cs}/f_c bh^2 = 0.16$ for $\omega'_{0.01}$ = 0.6 in Fig. 3.15. Hence, cross-section moment capacity is identified as M_{cs} = 172.80 kNm and N_u = 3888 kN corresponding to $N_u/f_c bh = 1.08$.

In this case, to calculate $1/r_n$ using Eq. (3.43), $N_m = 0$ and $1/r_m$ is calculated using the rectangular parabolic concrete stress-strain curve with the stress-strain diagram shown in Fig. 3.16 for a cross-section without axial force. Using the force equilibrium, it can be expressed as

$$F_{cc} + F_{fc} = F_{ft} \tag{3.51}$$

where F_{cc} = compressive force in concrete; F_{fc} = compressive force in FRP reinforcement; and F_{ft} = tensile force in FRP reinforcement.

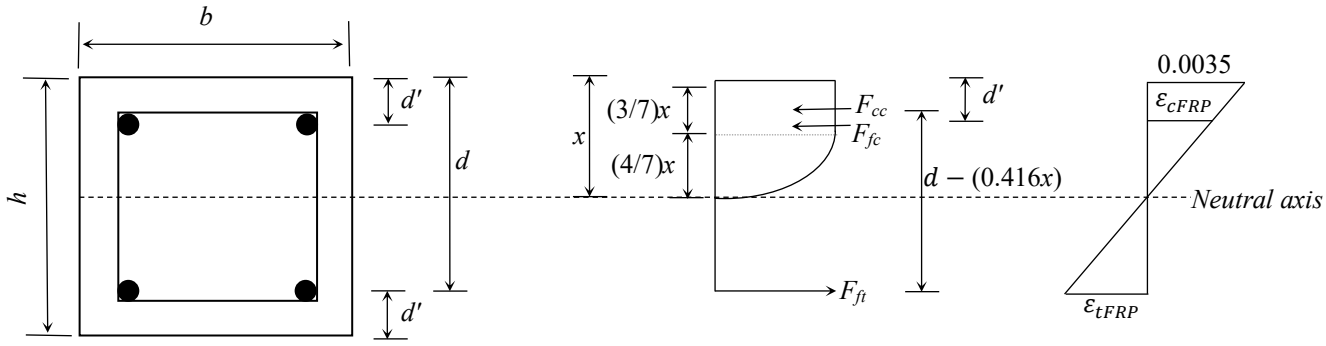


Fig. 3.16. Rectangular parabolic stress-strain diagram for concrete cross-section without axial force

Using the stress-strain diagram in Fig. 3.16, it can be expressed as

$$F_{cc} = 0.81 b f_c x \tag{3.52}$$

$$F_{fc} = 0.0035\, A_{fc} E_{FRP} \left(\frac{x - d'}{x}\right) \tag{3.53}$$

$$F_{ft} = 0.0035\, A_{ft} E_{FRP} \left(\frac{d - x}{x}\right) \tag{3.54}$$

where A_{fc} and A_{ft} are the area of FRP reinforcement in compression and tension. Also, $A_{fc} + A_{ft} = A_{FRP}$. Using Eq. (3.51-54), the distance of the neutral axis from the top of the cross-section (x) is calculated by solving a quadratic equation as

$$(0.81 b f_c)x^2 + (0.0035 E_{FRP} A_{FRP})x - 0.0035 E_{FRP}\left(A_{fc} d' + A_{ft} d\right) = 0 \tag{3.55}$$

Assuming $x <$ d for a column with corner reinforcement as shown in Fig. 3.14, $A_{fc} = A_{ft} = A_{FRP}/2$ is considered and Eq. (3.55) is solved to obtain $x = 75$ mm.

Further, $1/r_m$ is calculated as

$$\frac{1}{r_m} = \frac{\varepsilon_{cm}}{x} = \frac{0.0035}{75} = 4.67 \times 10^{-5}\ \text{mm}^{-1}$$

Using Eq. (3.47) and Eq. (3.44)

$$A = 2.32 + (0.0064 \times 34.6) - (0.511 \times 0.6) = 2.23$$

$$n_r = \frac{1800 - 0}{3888 - 0} = 0.46$$

Using Eq. (3.43) nominal curvature is calculated as

$$\left(\frac{1}{r_n}\right)_{FRP} = \left(4.67 \times 10^{-5}\right) \times e^{-(2.23 \times 0.46)} = 1.67 \times 10^{-5}\ \text{mm}^{-1}$$

$$e_{cs} = \frac{M_{cs}}{N} = \frac{172.80}{1800} \times 1000 = 96\ \text{mm}$$

Using Eq. (3.19) while considering c_I = 8 and $1/r_n = (1/r_n)_{FRP}$, the total curvature distribution factor is calculated as

$$c = 8 + \left(1.67 \times 10^{-5}\right)\left(\frac{3000}{\pi}\right)^2 \left(\frac{1}{96}\right)(\pi^2 - 8) = 8.30$$

Using Eq. (3.39), moment capacity and maximum value of first-order eccentricity are calculated as

$$M_I = \left(172.80 \times 10^6\right) - \left(1800 \times 10^3\right)\left(1.67 \times 10^{-5}\right)\left(\frac{3000^2}{8.30}\right) = 140.20\ \text{kNm}$$

$$e_0 = \frac{M_I}{N} = \frac{140.20^*}{1800} \times 1000 = 77.88^*\ \text{mm}$$

The moment capacity from the detailed second-order analysis using the numerical method presented earlier and considering the rectangular parabolic concrete stress-strain curve is found to be 134.29 kNm for the input values considered in this case. This is pretty close to the value of M_I = 140.20 kNm predicted using the proposed equation.

3.9 Appendix II

Typical load-moment capacity curves for cross-section analysis with different values of mechanical reinforcement ratio are presented in Fig. 3.17 for a rectangular concrete cross-section with corner reinforcement as shown in Fig. 3.16. These curves are based on rectangular parabolic concrete stress-strain curve using Eq. (3.50) while considering $f_{cd} = f_c$. These curves correspond to the f_{ck} of 12 to 50 MPa as ε_o = 0.002, n_c = 2 and ε_{cm} = 0.0035 were considered. For the purpose of design, f_c shall be

replaced with f_{cd} while using these curves and mechanical reinforcement ratio (ω') shall be calculated using f_{cd}. Here, $\omega'_{0.005}$ is the mechanical reinforcement ratio (ω') calculated while considering $\varepsilon_{tu} = 0.005$.

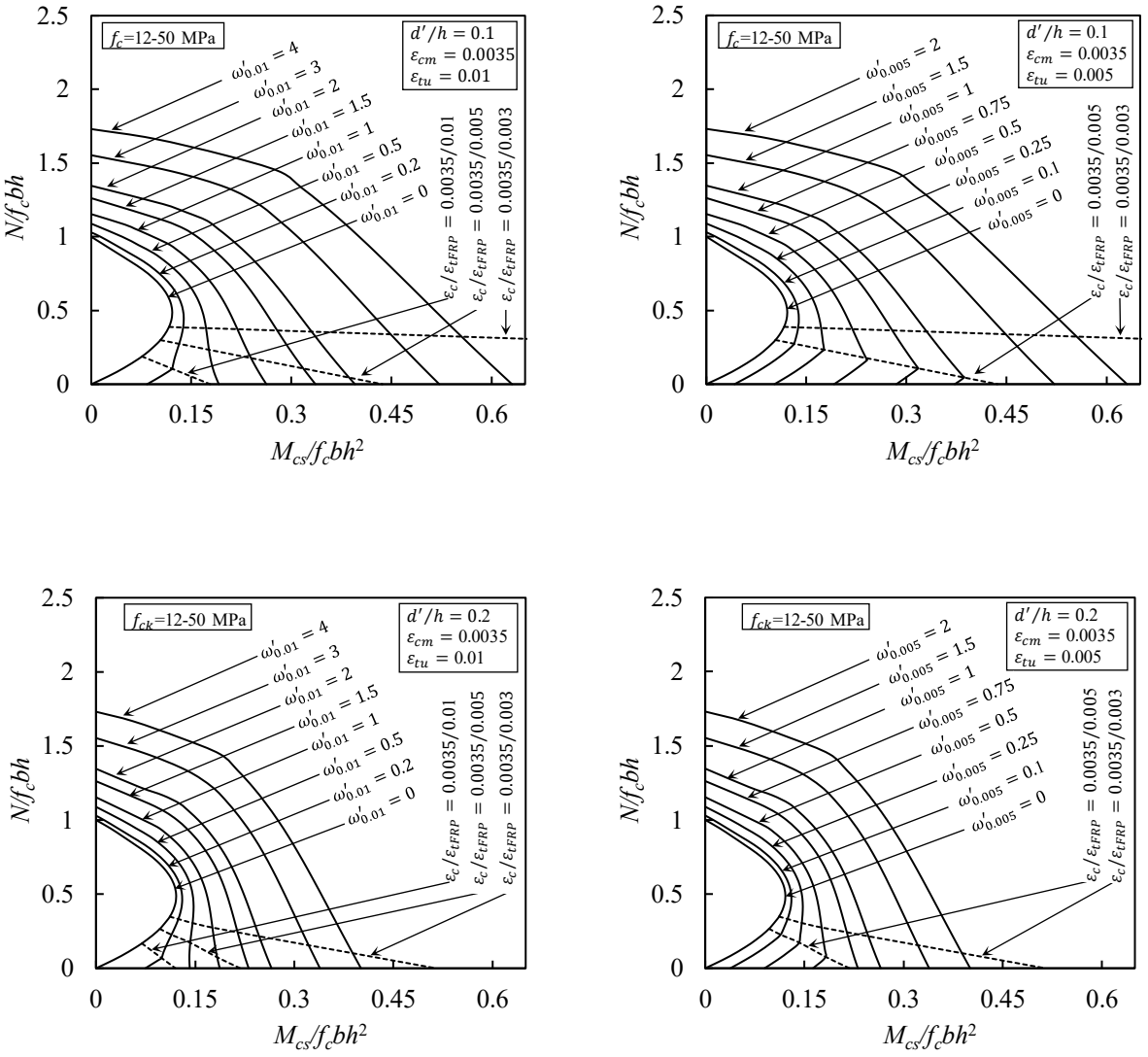


Fig. 3.17. Typical load-moment capacity curves of FRP-RC columns for cross-section analysis with different mechanical reinforcement ratios

3.10 Data availability statement

Some or all data, models, or code that support the findings of this study are available from the corresponding author upon reasonable request.

3.11 Acknowledgements

The authors would like to express their gratitude for the financial support provided by the German Academic Exchange Service (DAAD) to pursue this research.

3.12 Notations

The following symbols are used in this paper:

A_c = total area of concrete

A_{FRP}= total area of the FRP longitudinal reinforcement

A_{fc} = area of FRP reinforcement in compression

A_{ft} = area of FRP reinforcement in tension

A_l= total area of the longitudinal reinforcement

A_s = total area of the steel longitudinal reinforcement

b = cross-section breadth

c = total curvature distribution factor

c_I = first-order curvature distribution factor

c_{II} = second-order curvature distribution factor

c_i = first-order curvature distribution factor for the ith first-order load

D = Diameter of the circular column cross-section

d' = distance of the center of the reinforcement from the edge of the column

E_c = modulus of elasticity of concrete

E_{FRP} = modulus of elasticity of FRP bar

E_s = modulus of elasticity of steel

EI_n = nominal stiffness

e = base of the natural logarithm

e_0 = first-order eccentricity

e_2 = maximum total deflection

F_{cc}= compressive force in concrete

F_{fc}= compressive force in FRP reinforcement

F_{ft}= tensile force in FRP reinforcement

f_c = compressive strength of concrete

f_{cd} = design compressive strength of concrete

f_{ck} = characteristic cylindrical compressive strength of concrete

f_y = yield strength of steel

f_{yd} = design yield strength of steel

h = cross-section height

L = effective length of the column

M_{01} = smaller end moment

M_{02} = larger end moment

M_I = maximum first-order moment

M_{II} = maximum second-order moment

M_{cs} = cross-sectional moment capacity

M_d = total moment at stability failure

M_{eqI} = equivalent first-order moment

M_i = first-order moment due to the ith first-order load

M_{tot} = maximum total moment

$M_{tot(num)}$ = maximum total moment from numerical analysis

$M_{tot(test)}$= maximum total moment from experiment

N = Load capacity

N_{bal} = balanced failure load

N_{bald} = design axial load for balanced failure

N_d = design axial load

N_m = axial load capacity of the column for the curvature of $1/r_m$

N_{num} = load capacity from numerical analysis

N_{test} = load capacity from experiment

N_u = maximum load capacity of the column from cross-section analysis

N_{ud} = maximum axial design load capacity

n' = number of first-order loads

r_g = radius of gyration of the cross-section

β = slope of the external moment line

δ_1 = first-order deflection

δ_2 = second-order deflection

ε_c = compressive strain in concrete

ε_{cm} = maximum concrete compressive strain

ε_{tu} = ultimate tensile strain for the FRP bar

λ = slenderness ratio

ρ = reinforcement ratio

$\sigma_c(\varepsilon_c)$ = compressive stress in concrete at a strain of ε_c

ω' = mechanical reinforcement ratio for the FRP-RC column

$\omega'_{0.01}$ = mechanical reinforcement ratio for the FRP-RC column with ε_{tu} = 0.01

$\omega'_{0.005}$ = mechanical reinforcement ratio for the FRP-RC column with ε_{tu} = 0.005

$1/r$ = curvature of the critical column section at constant load N

$1/r_c$ = curvature of cross-section failure at constant load N

$1/r_d$ = actual curvature at stability failure at constant load N

$1/r_n$ = nominal curvature

$(1/r_n)_{CEB}$ = nominal curvature for steel-RC columns as per CEB Recommendations

$(1/r_n)_{EC2}$ = nominal curvature of steel-RC columns as per Eurocode 2

$(1/r_n)_{FRP}$ = proposed nominal curvature for FRP-RC columns

$1/r_m$ = maximum curvature of cross-section failure in the load-moment capacity curve

3.13 References

[1] EN 1992-1-1. Eurocode 2: Design of concrete structures - Part 1-1:General rules and rules for buildings: EN 1992-1-1: Eurocode 2: Design of concrete structures - Part 1-1: General rules and rules for buildings(EN 1992-1-1:2004). Brussels: European Committee for Standardisation.

[2] DIN EN 1992-1-1/NA. Nationaler Anhang -National festgelegte Parameter -Eurocode 2: Bemessung und Konstruktion von Stahlbeton- und Spannbetontragwerken -Teil 1-1: Allgemeine Bemessungsregeln und Regeln für den Hochbau: Deutsches Institut für Normung; 2013.

[3] Araújo JM de. Comparative study of the simplified methods of Eurocode 2 for second order analysis of slender reinforced concrete columns. Journal of Building Engineering 2017;14:55–60.

[4] CEB. CEB-FIP model code 1990: Design code. Bulletin d'information / Comité Euro-International du Béton;213/214. London: Thomas Telford; 1993.

[5] FIB. FIB Model Code for Concrete Structures 2010. Lausanne, Switzerland: Berlin: Wilhelm Ernst & Sohn; 2013.

[6] ACI. Building Code Requirements for Structural Concrete and Commentary(ACI CODE 318-19). Farmington Hills, MI: American Concrete Institute; 2019.

[7] ACI. Building Code Requirements for Structural Concrete Reinforced with Glass Fiber-Reinforced Polymer (GFRP) Bars-Code and Commentary.(ACI CODE-440.11-22). Farmington Hills, MI: American Concrete Institute; 2022.

[8] Syed AU, Goldack A. Effect of Slenderness on the Design of FRP reinforced Concrete Columns. In: IABSE Congress, New Delhi 2023: Engineering for Sustainable Development, New Delhi, India, 9/20/2023 - 9/22/2023.

[9] Jiang T, Teng JG. Slenderness Limit for Short FRP-Confined Circular RC Columns. J. Compos. Constr. 2012;16(6):650–61.

[10] Jiang T, Teng JG. Behavior and Design of Slender FRP-Confined Circular RC Columns. J. Compos. Constr. 2013;17(4):443–53.

[11] Syed AU, Goldack A. Slenderness limit for GFRP reinforced concrete columns based on axial force ratio. Engineering Structures 2024;298.

[12] Mirmiran A, Yuan W, Chen X. Design for Slenderness in Concrete Columns Internally Reinforced with Fiber-Reinforced Polymer bars. ACI Struct J 2001;98(1):116–25.

[13] Xue W, Peng F, Fang Z. Behavior and Design of Slender Rectangular Concrete Columns Longitudinally Reinforced with Fiber-Reinforced Polymer Bars. ACI Structural Journal 2018;115(2).

[14] Abdelazim W, Mohamed HM, Benmokrane B. Proposed Flexural Stiffness of Slender Concrete Columns Reinforced with Glass Fiber-Reinforced Polymer Bars. ACI Structural Journal 2021;118(1):227–40.

[15] Cranston WB. Analysis and design of reinforced concrete columns; 1972.

[16] Hellesland J, Challamel N, Casandjian C, Lanos C. Reinforced concrete beams, columns and frames: section and slender member analysis. Surrey: John Wiley & Sons; 2013.

[17] Tarantino AM, Lanzoni L, Falope FO. The Bending Theory of Fully Nonlinear Beams. Cham: Springer; 2019.

[18] European Concrete Platform ASBL. Eurocode 2 Commentary: European Concrete Platform ASBL; 2008.

[19] MATLAB version: 9.13.0 (R2022b). Natick, Massachusetts: The MathWorks Inc; 2022.

[20] Broms BB. Ultimate Strength of Long Reinforced Concrete Columns: University of Illinois at Urbana-Champaign; 1956.

[21] Popovics S. A numerical approach to the complete stress-strain curve of concrete. Cement and concrete research 1973;3:583–99.

[22] Collins MP, Mitchell D. Prestressed concrete structures. Canada: Response Publications; 1997.

[23] Carrasquillo RL, Nilson AH, Slate FO. Properties of High Strength Concrete Subject to Short-Term Loads. ACI Journal 1981;78(3):171–8.

[24] Mander JB, Priestly JN, Park, R. Theoretical Stress-Strain Model for Confined Concrete. J. Struct. Eng. 1988;114(8):1804–26.

[25] Hadhood A, Mohamed HM, Benmokrane B, Nanni A, Shield CK. Assessment of Design Guidelines of Concrete Columns Reinforced with Glass Fiber-Reinforced Polymer Bars. ACI Structural Journal 2019;116(4):193–207.

[26] Zadeh HJ, Nanni A. Design of RC Columns Using Glass FRP Reinforcement. J Compos Constr 2013;17(3):294–304.

[27] CEB. CEB-FIP International Recommendations for the Design and Construction of Concrete Structures; 1970.

[28] Beeby AW, Narayanan RS. Designers' guide to EN 1992-2-1 and EN 1992-1-2 Eurocode 2: Design of concrete structures General rules and rules for buildings and structural fire design. London: Thomas Telford Ltd; 2005.

[29] Almomani M, Mahmoud K, El-Salakawy EF. Experimental Investigation of Large-Scale Eccentrically Loaded GFRP-Reinforced High-Strength Concrete Columns. J. Compos. Constr. 2022;26(2).

[30] Hadhood A, Mohamed HM, Benmokrane B. Axial Load–Moment Interaction Diagram of Circular Concrete Columns Reinforced with CFRP Bars and Spirals: Experimental and Theoretical Investigations. J. Compos. Constr. 2017;21(2).

[31] Othman ZS, Mohammad AH. Behaviour of Eccentric Concrete Columns Reinforced with Carbon Fibre-Reinforced Polymer Bars. Advances in Civil Engineering 2019;2019:1–13.

[32] Khorramian K, Sadeghian P. Experimental Investigation of Short and Slender Rectangular Concrete Columns Reinforced with GFRP Bars under Eccentric Axial Loads. J. Compos. Constr. 2020;24(6).

[33] Hamid FL, Yousif AR. Behavior of Short and Slender RC Columns with BFRP Bars under Axial and Flexural Loads: Experimental and Analytical Investigation. J. Compos. Constr. 2024;28(1).

4. Analysis of Slender FRP-Reinforced Concrete Columns Subjected to Unequal End Moments

Ahmed Usama Syed[1], Arndt Goldack[2]

[1 2] University of Wuppertal, Chair of Statics and Dynamics of Structures, Pauluskichstraße 7, 42285 Wuppertal, Germany.

Published in

Engineering Structures (2025) 340:120768 (DOI: https://doi.org/10.1016/j.engstruct.2025.120768)

ABSTRACT

The equivalent moment factor is essential for the simplified second-order analysis of the slender reinforced concrete columns subjected to unequal end moments. Various design codes for steel-reinforced concrete (steel-RC) provide the same well-established equation to estimate the equivalent moment factor. In recent years, fiber-reinforced polymer (FRP) bars have gained popularity as a means of reinforcing concrete. Design codes and guidelines for reinforced concrete are being adapted for FRP reinforcement because of their distinct material properties as compared to conventional steel bars. This paper shows that the existing equivalent moment factor expression for steel-RC columns is not sufficiently conservative to estimate the equivalent moment factor for FRP bars reinforced concrete (FRP-RC) columns. Based on the regression and percentile analysis, an equation is proposed to estimate the equivalent moment factor for FRP-RC columns. A detailed parametric study was conducted to assess the behavior and to regress the equation to estimate the equivalent moment factor for FRP-RC columns. Hence, two numerical methods, the direct curvature method (DCM) and the column deflection curve method (CDM), were implemented and validated with experimental results. Furthermore, the paper shows that the numerical method, DCM for the detailed second-order analysis with curvature distribution estimation can predict the column capacity with sufficient accuracy in comparison to the experimental results. To date, no study is available in the literature on the equivalent moment factor of FRP-RC columns, this study serves as a significant contribution and guidance for the codal committees to form design guidelines for FRP-RC columns.

Keywords: Slender columns; Reinforced concrete; FRP bars; Unequal end moments; Equivalent moment factor; Second-order analysis

4.1 Introduction

The equivalent moment factor (C_m) enables to transform the column subjected to unequal first-order end moments into a column subjected to equal first-order end moments, as shown in Fig. 4.1, to analyze the column while using the simplified methods of second-order analysis such as the nominal curvature and nominal stiffness methods in Eurocode 2 [1]. This eliminates the requirement of detailed calculations to solve the differential equation while performing the second-order analysis of the columns subjected to unequal end moments.

The total moment (M_t) at any column section for a slender reinforced concrete (RC) column comprises the first-order moment and the second-order moment induced due to second-order effects. The location of the maximum total moment (M_{tmax}) (see Fig. 4.1) determines the critical column section. The detailed second-order analysis of slender RC columns is necessary to determine the value of the maximum total moment (M_{tmax}) to be considered for the design. For a simply supported column subjected to equal first-order end moments and bent in single curvature, the location of the maximum total moment (M_{tmax}) can be easily determined as the mid-height. However, for the columns subjected to unequal first-order end moments, the location of the maximum total moment also needs to be determined while conducting the second-order analysis. This makes the second-order analysis of the columns subjected to unequal first-order end moments more complex. To avoid the complexities involved in performing detailed second-order analysis, design codes provide simplified methods for the second-order analysis. For the simplified second-order analysis of steel-reinforced concrete (steel-RC) columns subjected to unequal first-order end moments, the unequal first-order end moments are replaced with an equivalent first-order moment (M_{e1}).

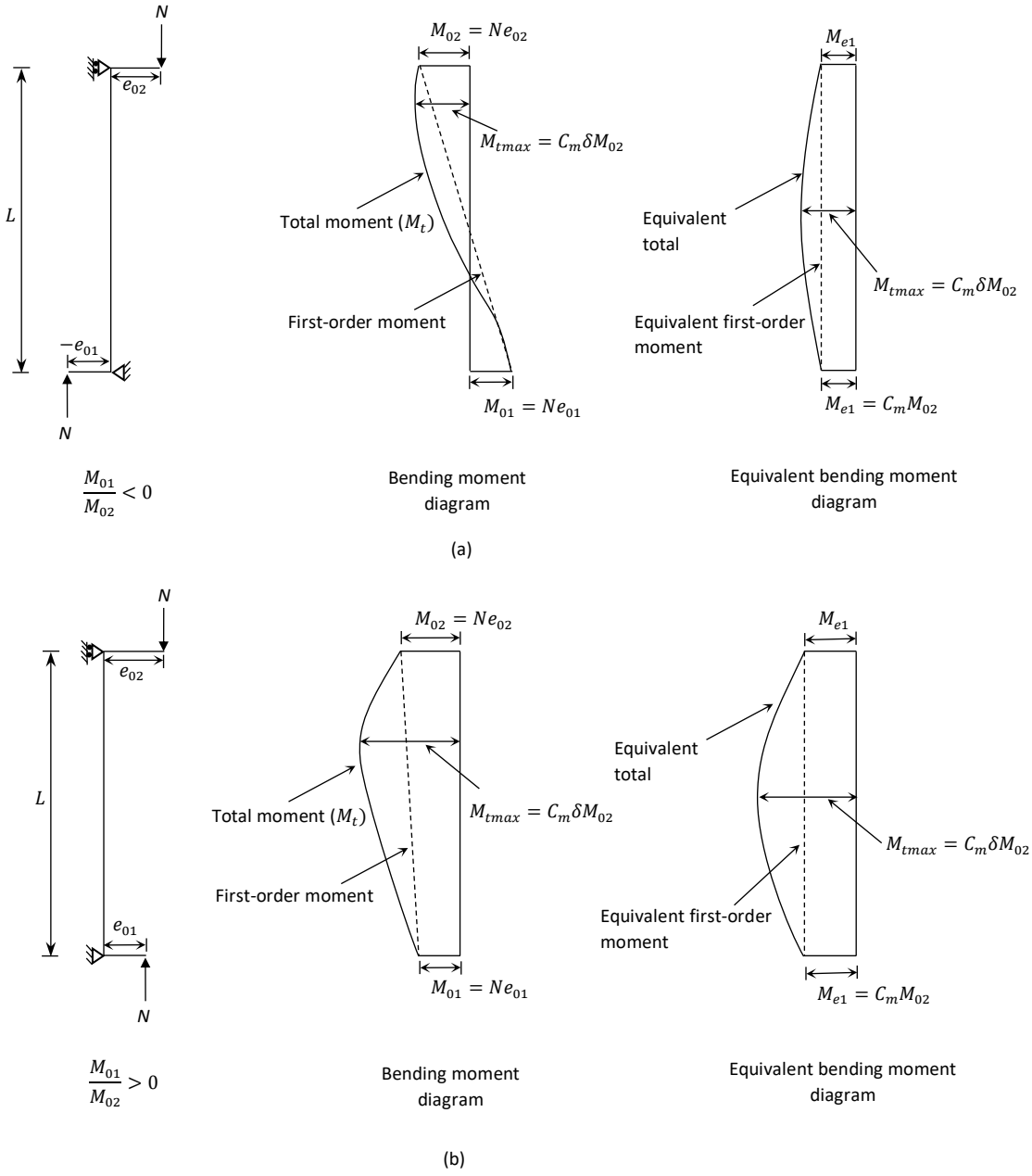


Fig. 4.1. Equivalent first-order moment transformation for simply supported column under unequal first-order moment bent in (a) double curvature; and (b) single curvature

Eurocode 2 [1] provides an expression to calculate the equivalent first-order moment (M_{e1}) for steel-RC columns as:

$$M_{e1}=0.6M_{02} + 0.4M_{01} \geq 0.4M_{02} \quad (4.1)$$

where M_{01} and M_{02} are the first-order end moments and $|M_{02}| \geq |M_{01}|$. M_{01}/M_{02} is positive when bent in single curvature and negative when bent in double curvature. The equivalent moment factor (C_m) can be defined as

$$C_m = \frac{M_{e1}}{M_{02}} \tag{4.2}$$

Eq. (4.1) is similar to the approximation provided by Austin [2] for elastic columns. ACI CODE 318-19 [3] provides an expression for steel-RC columns similar to Eq. (4.1) and Austin's approximation to calculate the equivalent first-order moment using the equivalent moment factor (C_m) as:

$$C_m = 0.6 - 0.4\frac{M_{01}}{M_{02}} \tag{4.3}$$

where M_{01}/M_{02} is negative when bent in single curvature and positive when bent in double curvature. In this study, the sign convention according to Eurocode 2 [1] is used throughout this study, where M_{01}/M_{02} is positive when bent in single curvature and negative when bent in double curvature. Furthermore, columns with unequal end eccentricities are referred to as columns subjected to unequal end moments, such that $M_{01}/M_{02} \neq 1$ and columns with equal end eccentricities are referred to as columns subjected to equal end moments, such that $M_{01}/M_{02} = 1$. M_{01}/M_{02} ranges from -1 for columns bent in double curvature to 1 for columns bent in single curvature.

Reinforced concrete exhibits inelastic material behavior. Hence, Tikka and Mirza [4] performed an extensive parametric study to develop the equivalent moment factor (C_m) for steel-RC columns considering the second-order effects and the inelastic material properties of steel-reinforced concrete. They found that Eq. (4.3) is sufficiently effective for application to steel-RC columns.

Existing codes and guidelines for fiber-reinforced polymer (FRP) bars RC (FRP-RC) columns, such as ACI 440.1R-15 [5], CSA S806-12 [6], *fib* Bulletin 40 [7], DAfStb Heft-660 [8] do not provide any equation or information regarding the equivalent moment factor for FRP-RC columns except ACI CODE-440.11-22 [9]. ACI CODE-440.11-22 [9] adopts the equivalent moment factor (C_m) for glass FRP-reinforced concrete (GFRP-RC) columns the same as for steel-RC columns as presented in Eq. (4.3). However, no study is available in the literature on the equivalent moment factor (C_m) of FRP-RC

columns and to support the adoption of the C_m equation of steel-RC columns for FRP-RC columns. The present study therefore focuses on addressing this research gap.

In comparison to steel reinforcement, FRP bars generally have a relatively low modulus of elasticity and a linear elastic stress-strain curve. In the previous studies, due to the distinct material properties of FRP bars, in comparison to steel-RC columns, FRP-RC columns were found to have different characterstics of load-moment capacity interaction [10], lower slenderness limit [11–14] and different equations to estimate the nominal stiffness [12,13,15–17] and nominal curvature [18,19] for simplified second-order analysis. Therefore, it is important to verify the applicability of the existing C_m equation of steel-RC columns for FRP-RC columns. In this study, the behavior of the equivalent moment factor for FRP-RC columns is compared to steel-RC columns and elastic columns. Further, a detailed parametric study is conducted to ascertain the suitability of the existing C_m equation of elastic columns and steel-RC columns for FRP-RC columns. Based on the data obtained from the parametric study, the equation to estimate the equivalent moment factor for FRP-RC columns is regressed. Moreover, two different numerical methods are considered to perform the detailed second-order analysis of RC columns in this study. The first method, direct curvature method (DCM), is based on the estimation of the curvature distribution of the column, while the second method, column deflection curve method (CDM), does not require any estimation of the curvature.

Presently, various committees for codes and design guidelines such as working committee for DAfStb Heft-660, *fib* Task group 5.1 and Eurocode committees for national annexures have been working swiftly to adapt the guidelines and the upcoming version of Eurocode 2 [20] of steel-reinforced concrete (steel-RC) for FRP bars reinforced concrete (FRP-RC). Furthermore, a few studies [12,15,18,19] have been done in the recent past to adapt the methods to perform simplified second-order analysis of slender FRP-RC columns subjected to equal end moments. However, these simplified methods cannot be extended to FRP-RC columns subjected to unequal end moments without a proper equation for the equivalent moment factor. Therefore, the present study would be a valuable contribution towards framing the codal guidelines for simplified second-order analysis of slender FRP-RC columns subjected to unequal end moments.

4.2 Numerical analysis of reinforced concrete columns subjected to unequal end moments

4.2.1 General

Two numerical methods are considered in this study to perform the detailed second-order analysis of the RC columns incorporating the material and geometric nonlinear effects. The first one is based on the method presented by Syed and Goldack [11], where the curvature distribution of the deflected column is estimated while incorporating the effects of end eccentricity. This method is referred to as the direct curvature method (DCM) in this study. The second method is based on the numerical approach to the column deflection curve (CDC) presented by Chen and Atsuta [21]. No estimation of the deflected shape of the column is required in this method. The column is subdivided into various segments and the deflected shape of the column is integrated numerically using the moment-curvature relationship from cross-sectional analysis. This method is referred to as the column deflection curve method (CDM) in this study.

4.2.2 Direct curvature method (DCM)

In this method for the detailed second-order analysis, the deflected shape of the column of length (L) is assumed to be sinusoidal over a length a as shown in Fig. 4.2 for a simply supported column [22,23]. The total eccentricity (e_{tx}) at a distance x from the origin can be expressed as

$$e_{tx} = e_{tm} \cos \frac{\pi x}{a} \tag{4.4}$$

where e_{tm} is the maximum total eccentricity at $x = 0$. First-order end eccentricities, e_{01} and e_{02}, can be expressed as

$$e_{01} = e_{tm} \cos \frac{\pi(-l_1)}{a} \tag{4.5}$$

$$e_{02} = e_{tm} \cos \frac{\pi(l_2)}{a} \tag{4.6}$$

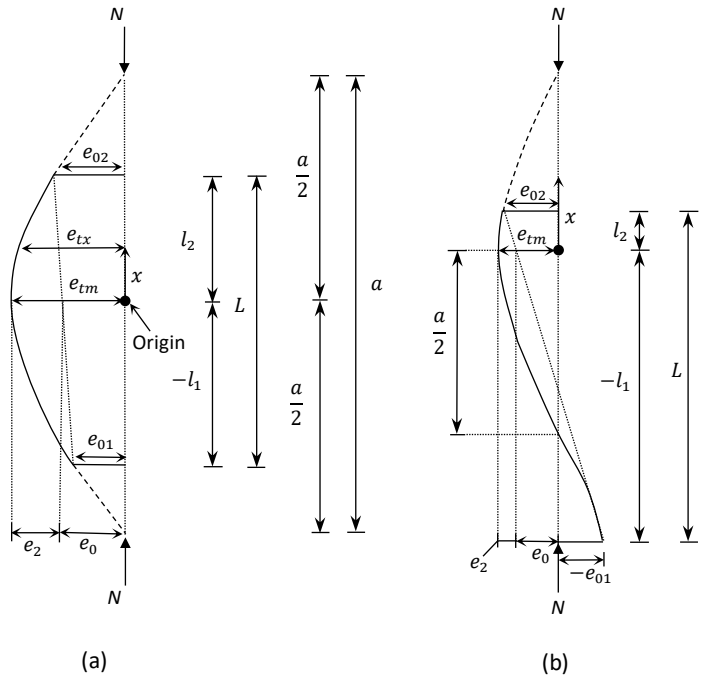


Fig. 4.2. Variation of total eccentricity of a simply supported column bent in (a) single curvature; and (b) double curvature

Further, the lengths l_1, l_2 and a are expressed as

$$l_1 = -\frac{a}{\pi}\arccos\frac{e_{01}}{e_{tm}} \tag{4.7}$$

$$l_2 = \frac{a}{\pi}\arccos\frac{e_{02}}{e_{tm}} \tag{4.8}$$

$$a = \frac{\pi L}{\arccos\frac{e_{02}}{e_{tm}} + \arccos\frac{e_{01}}{e_{tm}}} \tag{4.9}$$

The curvature (φ) of the column at the point of maximum total eccentricity is expressed considering $x = 0$ as

$$\varphi = \frac{e_{tm}}{L^2}\left(\arccos\frac{e_{02}}{e_{tm}} + \arccos\frac{e_{01}}{e_{tm}}\right)^2 \tag{4.10}$$

The first-order eccentricity at $x = 0$ (e_0) is calculated considering a linear variation of first-order eccentricity between the two ends of the column, as shown in Fig. 4.2 and considering the origin at $x = 0$. e_0 is expressed as

$$e_0 = e_{01} - \left(\frac{e_{02} - e_{01}}{L}\right) \cdot l_1 \qquad (4.11)$$

where $e_{02} \geq e_{01}$.

The detailed second-order analysis is performed for a simply supported column with the given first-order end eccentricities and length (L) by assuming the value of the deflection (e_2) at the point of maximum total eccentricity, which is the critical column section.

Further, e_{tm} is calculated as

$$e_{tm} = e_0 + e_2 \qquad (4.12)$$

For a given column and the assumed value of deflection (e_2) at the critical column section, e_{tm}, e_0 and l_1 are determined iteratively using Eq. (4.7), Eq. (4.11) and Eq. (4.12). Further, the curvature (φ) of the critical column section is calculated using Eq. (4.10). Using value of the curvature (φ) at the critical column section, the equilibrium of forces is implemented for the column cross-section considering the compatibility of strain and nonlinear material properties to calculate the axial load resisted by the cross-section at an assumed value of e_2.

Further increasing the value of e_2 and repeating the above-detailed procedure, a load-deflection envelope is obtained. The maximum load value of this envelope is determined as the load capacity of the column for the given first-order end eccentricities and length.

4.2.3 Column deflection curve method (CDM)

In this method, it is considered that the deflected shape of the column with end moments can be represented by the portion of the deflected shape of an equivalent column without any end moments, as shown in Fig. 4.3.

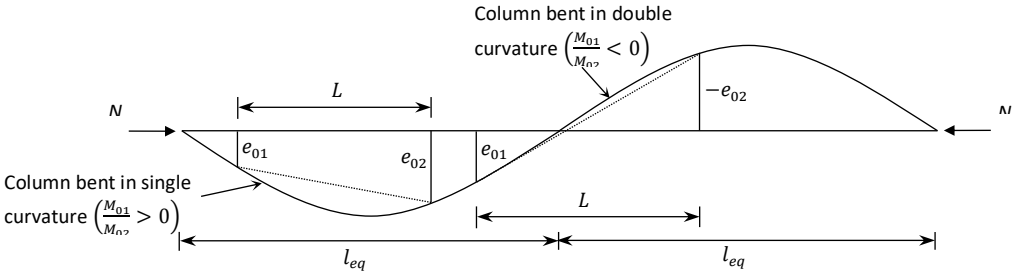


Fig. 4.3. Column deflection curve

This is similar to the direct curvature method. However, the shape of the equivalent column is not assumed in this method; conversely, it is integrated numerically by dividing the equivalent column into several segments as shown in Fig. 4.4.

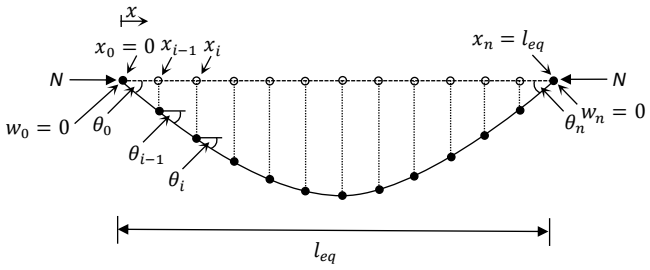


Fig. 4.4. Numerical integration of the column deflection curve

The deflected shape of the equivalent column is termed the column deflection curve (CDC). In Fig. 4.4 for the *i*th node, at a distance x_i from the origin, the rotation, deflection and curvature are represented by θ_i, w_i and φ_i, respectively. The column deflection curve is integrated using the expressions presented by Chen and Atsuta [21] as

$$w_i = w_{i-1} + \theta_{i-1}(x_i - x_{i-1}) - 0.5\varphi_{i-1}(x_i - x_{i-1})^2 \quad (4.13)$$

$$\theta_i = \theta_{i-1} - \varphi_i(x_i - x_{i-1}) \quad (4.14)$$

The moment at the *i*th node (M_i) is calculated as

$$M_i = Nw_i \quad (4.15)$$

For a considered value of axial load (*N*), CDC is computed assuming the value of rotation θ_0 at node x_0. Using $w_0 = 0$, $\varphi_0 = 0$, and θ_0, the lateral deflection at subsequent node x_1 is calculated using Eq. (4.13) as w_1. Further, the moment at node x_1 (M_1) is calculated using Eq. (4.15).

The load-moment-curvature envelopes (*N*-*M*-φ) for the cross-section are pre-developed to calculate the curvature (φ) at any node. These *N*-*M*-φ envelopes are developed using the nonlinear material properties of the reinforced concrete for a given cross-section by implementing the equilibrium of forces and compatibility of the strain in the cross-section.

The curvature at node x_1 (φ_1) is calculated from the *N-M-φ* envelope using *N* and M_1. θ_1 is calculated using Eq. (4.14). Further, using w_1, φ_1 and θ_1, w_2 is calculated using Eq. (4.13). This procedure is repeated for the subsequent nodes until w_n is determined as 0. Summing the length of all the segments, the length of the CDC (l_{eq}) for the considered load *N* and θ_0 is calculated as

$$l_{eq} = \sum_{i=1}^{n} (x_i - x_{i-1}) \tag{4.16}$$

where *n* represents the number of nodes. For the considered value of load (*N*), the value of θ_0 is iteratively changed and the whole procedure is repeated such that the given first-order end eccentricities and the given length *L* of the simply supported column can be satisfied as the portion of the CDC, as shown in Fig. 4.3.

Further, the considered value of load (*N*) is increased. The whole procedure is repeated such that the highest value of the axial load (*N*) is determined as the load capacity of the column for given first-order end eccentricities, length, and cross-sectional material properties. Any increase beyond the load capacity in the considered value of axial load (*N*) would lead to material or stability failure. In the case of material failure, the load, moment, and curvature at the critical node in the column would lie beyond the *N-M-φ* envelope of the cross-section. For the case of stability failure, no such assumption of θ_0 would satisfy the given length *L* for the given first-order end eccentricities.

4.2.4 Material properties

The stress-strain expression for unconfined concrete, as presented by Popovics [24] and used in this study to account for the material nonlinear behavior of concrete, is expressed as

$$\sigma_c(\varepsilon) = f_c \left(\frac{n' (\varepsilon/\varepsilon_o)}{n' - 1 + (\varepsilon / \varepsilon_o)^{n'}} \right) \tag{4.17}$$

$$n' = 0.8 + f_c/17 \tag{4.18}$$

$$\varepsilon_o = f_c n'/E_c(n' - 1) \tag{4.19}$$

$$E_c = 3200\sqrt{f_c} + 6900 \quad (4.20)$$

where f_c is the compressive strength of concrete in MPa, ε is the compressive strain in concrete, $\sigma_c(\varepsilon)$ is the compressive stress in concrete at a strain of ε and E_c is the tangent modulus of elasticity of concrete in MPa. Popovics curve, used for concrete constitutive modeling in the literature [11,13,18,25], provided the load capacity of FRP-RC columns in close comparison to experimental results. Hence, this curve is used in the present study. The concrete inside the lateral ties is considered to be partially confined using the stress-strain relationship by Mander et al. [26] while the concrete outside the lateral ties is considered to be unconfined. The linear stress-strain relationship up to failure is used for FRP reinforcement with the same modulus of elasticity (E_{FRP}) in compression and tension. Steel reinforcement was modeled with a linear stress-strain relationship up to yielding and an ideal plastic behavior after yielding. The reinforcement ratio (ρ) for the cross-section of the RC column is considered as

$$\rho = 100 \cdot \frac{A_r}{A_c}\% \quad (4.21)$$

where A_r is the total area of the longitudinal reinforcement and A_c is the total area of the concrete. The maximum compressive strain in the extreme concrete fiber in bending is considered to be 0.0035. To limit the high curvatures, excessive deformations and cracking, the maximum tensile strain of the FRP bar (ε_{tu}) is proposed to be limited to 0.01 in the literature [9,17,27]. This proposal exhibited good correlation with experimental results [13,28,29]. Hence, the maximum tensile strain of the FRP bar (ε_{tu}) is limited to 0.01 in this study. To take into account the material nonlinearity while implementing the equilibrium of forces and compatibility of strain in the cross-section, the transformed area method [11] was utilized in this study. The area of concrete and reinforcement is transformed into a linear elastic material with a uniform modulus of elasticity. The bond between the reinforcement and concrete was assumed to be perfect. The effects of creep and shrinkage were neglected. Furthermore, the concrete strength in tension and the tension stiffening effect were also neglected.

4.2.5 Validation and comparison

The methods for numerical second-order analysis implemented in this study are validated against the experimental results available from the literature for both FRP-RC and steel-RC columns. Experimental results for the columns bent in single and double curvature are considered. Experimental results for FRP-RC columns subjected to unequal end moments where $M_{01}/M_{02} \neq 1$ are not available in the literature. Hence, experimental results available from the literature for FRP-RC columns and steel-RC columns subjected to equal end moments and for steel-RC columns subjected to unequal end moments are used to validate the numerical methods.

The difference between the implemented numerical methods for second-order analysis of steel-RC and FRP-RC columns subjected to unequal end moments ($M_{01}/M_{02} \neq 1$) lies in the difference between the nonlinear material modeling of the reinforced concrete column cross-section for steel and FRP bars as a reinforcement. The numerical methods are validated against the experimental results for FRP-RC columns subjected to equal end moments and bent in single curvature ($M_{01}/M_{02} = 1$). This also validates the implementation of the nonlinear material modeling of the reinforced concrete column cross-section with FRP bar as a reinforcement for both numerical methods.

Further, the validation of the numerical methods with experimental results for steel-RC columns subjected to unequal end moments also verifies their treatment of the second-order effects for columns subjected to unequal end moments. As the nonlinear material modeling of the reinforced concrete column cross-section with FRP bars and the treatment of second-order effects by numerical methods for columns subjected to unequal end moments are validated, this confirms the correctness of the implemented numerical methods both for FRP-RC columns and steel-RC columns subjected to unequal and equal end moments.

The slenderness ratio (λ) considered in this study is expressed as

$$\lambda = L_e/r \tag{4.22}$$

where L_e is the effective length of the column and r is the radius of gyration of the cross-section. For a simply supported column considered throughout this study, the effective length (L_e) is equal to the given column length (L).

Afefy and Tony [30] tested simply supported steel-RC columns subjected to both equal and unequal end moments with end eccentricity to cross-section depth ratio ranging from 0.1 to 0.5. The columns had the concrete compressive strength of 42.89 MPa, steel yield strength of 418 MPa and a slenderness ratio of 41.57. MacGregor and Barter [31] tested simply supported columns subjected to unequal end eccentricities and bent in double curvature with eccentricity to cross-section depth ratio of 0.2 and 1.5. The columns had a rectangular cross-section with concrete compressive strength ranging from 29 to 33.64 MPa, steel yield strength of 308 MPa and a slenderness ratio of 92.8. The experimental results of FRP-RC columns considered for validation include both glass FRP (GFRP) and carbon FRP (CFRP) bars as a reinforcement. Xue et al. [16] tested simply supported reinforced concrete columns with GFRP bar reinforcement subjected to equal end moments and bent in single curvature. The end eccentricity to cross-section depth ratio varied from 0.2 to 1.0. Furthermore, the columns had a square cross-section with concrete compressive strength ranging from 29.1 to 55.2 MPa, GFRP bar tension modulus of elasticity of 39 GPa and slenderness ratio ranging from 20.8 to 41.6. Othman and Mohammad [32] tested CFRP bar reinforced concrete columns with simply supported end conditions subjected to equal end moments and bent in single curvature. The end eccentricity to cross-section depth ratio varied from 0.5 to 1.0. The columns had a square cross-section with concrete compressive strength of 44.7 MPa, CFRP bar tension modulus of elasticity ranging from 145 to 151 GPa and a slenderness ratio of 34.64. The aforementioned experimental studies were considered for the validation of the numerical methods in this study.

The ratio of the load capacity calculated using the numerical method (N_{num}) and the load capacity obtained from the experiment (N_{test}) for both methods is shown in Table 4.1.

Table 4.1. Validation of the numerical methods

Reference	Specimen	λ	$\frac{M_{01}}{M_{02}}$	DCM $\frac{N_{test}}{N_{num}}$	CDM $\frac{N_{test}}{N_{num}}$	Reinforcement Type
Bent in single curvature						
Xue et al. [16]	CE-1	20.8	1	1.01	1.01	GFRP
	CE-2	20.8	1	1.04	1.04	GFRP
	CE-3	20.8	1	1.07	1.07	GFRP
	CE-4	27.7	1	0.94	0.94	GFRP
	CE-5	34.6	1	0.96	0.95	GFRP
	CE-6	41.6	1	1.02	1.00	GFRP
	CE-7	41.6	1	1.15	1.10	GFRP
	CE-8	41.6	1	1.28	1.27	GFRP
	CE-9	41.6	1	0.99	0.96	GFRP
	CE-10	41.6	1	1.10	1.08	GFRP
	CE-11	41.6	1	0.85	0.83	GFRP
	CE-12	41.6	1	1.05	1.02	GFRP
Othman and Mohammad [32]	C10-T90-E0.5	34.64	1	1.14	1.13	CFRP
	C10-T90-E1.0	34.64	1	0.99	0.98	CFRP
	C12-T90-E0.5	34.64	1	1.04	1.03	CFRP
	C12-T90-E1.0	34.64	1	0.93	0.92	CFRP

	C16-T90-E0.5	34.64	1	0.94	0.94	CFRP
	C16-T90-E1.0	34.64	1	0.80	0.80	CFRP
	C12-T140-E0.5	34.64	1	1.05	1.04	CFRP
	C12-T140-E1.0	34.64	1	0.94	0.94	CFRP
	C12-T40-E0.5	34.64	1	0.94	0.94	CFRP
	C12-T40-E1.0	34.64	1	0.83	0.82	CFRP
Afefy and Tony [30]	S-1-1	41.57	1	0.89	0.89	Steel
	S-3-3	41.57	1	1.06	1.05	Steel
	S-5-5	41.57	1	0.96	0.96	Steel
	S-0-1	41.57	0	0.94	0.93	Steel
	S-1-3	41.57	0.33	1.17	1.15	Steel
	S-1-5	41.57	0.2	1.07	1.07	Steel
	S-0-3	41.57	0	1.20	1.20	Steel
	S-3-5	41.57	0.6	1.02	1.03	Steel
	S-5-0	41.57	0	1.16	1.16	Steel
Bent in double curvature						
MacGregor and Barter [31]	A1	92.8	-1	0.96	0.95	Steel
	A2	92.8	-1	1.02	1.01	Steel
	B1	92.8	-1	1.25	1.25	Steel
	B2	92.8	-1	1.19	1.19	Steel

Mean	1.03	1.02
Coefficient of variation (%)	11.24	11.21

It can be observed from Table 4.1 that both methods predict the load capacity of slender reinforced concrete columns very well. This shows that the model considered for both the methods to estimate the cross-sectional material properties and the second-order effects works reasonably well to estimate the load capacity of the column. Additionally, the implementation of two independent numerical methods (DCM and CDM) yielded analogous results. This finding further serves to substantiate the correctness of the implemented methods. Therefore, both methods can be utilized for the second-order analysis of reinforced concrete columns with sufficient accuracy. Moreover, it can be seen that the DCM with an assumption of the curvature can predict the capacity of the column with comparable accuracy as the CDM, which does not require any assumption of the curvature.

The column deflection curve method (CDM) is computationally more tedious compared to the direct curvature method (DCM) as it requires a set of column deflection curves to be generated at different values of given load and slope at the ends. Furthermore, to generate a column deflection curve, pre-generated load-moment-curvature (N-M-φ) envelopes for cross-sectional analysis are required. Similar to the CDM, second-order analysis of the reinforced concrete columns is computationally demanding using commercial finite element (FE) software. This is because the compatibility and equilibrium need to be fulfilled for every node of each element. However, for the DCM, the compatibility and equilibrium need to be fulfilled only at the critical column section and this makes it computationally more efficient. Consequently, it is simpler to ascertain the type of failure, such as material or stability, while using the DCM compared to CDM and FE software. This exhibits the strength of the DCM as it predicts the load capacity with the same accuracy as the CDM. Hence, further in this study, DCM is used for the detailed second-order analysis of reinforced concrete columns.

4.3 Equivalent moment factor for simplified second-order analysis

4.3.1 General

For a simply supported elastic column with first-order end moments M_{01} and M_{02} such that $|M_{02}| \geq |M_{01}|$, the maximum total moment (M_{tmax}) including the second-order effects can be expressed as [33,34]

$$M_{tmax}=C_m \delta M_{02} \geq M_{02} \tag{4.23}$$

$$C_m=\sqrt{\frac{(M_{01}/M_{02})^2 - 2(M_{01}/M_{02})\cos kL + 1}{2(1-\cos kL)}} \tag{4.24}$$

$$\delta=\sqrt{\frac{2(1-\cos kL)}{\sin^2 kL}} \tag{4.25}$$

with,

$$k=\frac{\pi}{L}\sqrt{\frac{N}{N_B}} \tag{4.26}$$

$$N_B=\frac{\pi^2 EI}{L^2} \tag{4.27}$$

where EI = bending stiffness of the column and δ = moment magnification factor. M_{01}/M_{02} is positive when the column is bent in single curvature and negative when the column is bent in double curvature.

Various approximations have been provided in the literature for the equivalent moment factor (C_m) for elastic columns. Massonnet [35] provided the approximation as

$$C_m = \sqrt{0.3(M_{01}/M_{02})^2 + 0.4(M_{01}/M_{02}) + 0.3} \tag{4.28}$$

Austin [2] provided a simpler approximation for C_m as

$$C_m = 0.6 + 0.4(M_{01}/M_{02}) \geq 0.4 \tag{4.29}$$

Eq. (4.29) for approximating C_m has been widely adopted by various steel-RC design codes as mentioned earlier.

4.3.2 Equivalent moment factor (C_m) for FRP-RC columns

FRP bars have a different material behavior compared to conventional steel bars. They generally have a lower modulus of elasticity than steel bars. Further, they exhibit a linear stress-strain relationship up to failure and no yielding. Hence, the existing expressions of equivalent moment factor (C_m) need to be examined for FRP-RC columns. The rectangular cross-section, as shown in Fig. 4.5, with a breadth (b) of 300 mm and a height (h) of 300 mm, has been considered both for FRP-RC and steel-RC columns further in this study. For steel-RC columns, the yield strength of longitudinal steel reinforcement (f_y) is considered as 500 MPa. Steel ties at 150 mm spacing with 8 mm diameter and 500 MPa yield strength are considered both for FRP-RC and steel-RC columns.

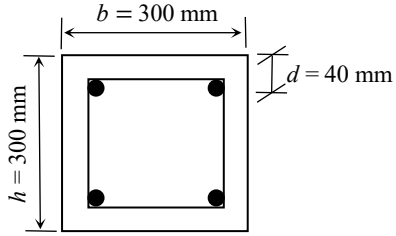


Fig. 4.5. Concrete column cross-section

The load-moment capacity interaction for a simply supported FRP-RC column developed by performing the detailed second-order analysis using the DCM is presented in Fig. 4.6.

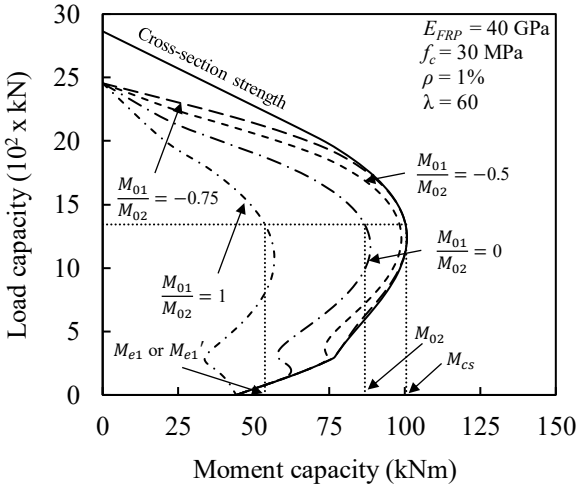


Fig. 4.6. Load-moment capacity interaction curve for FRP-RC column with different first-order end moment ratios

For the purpose of simplified second-order analysis of RC columns, the maximum total moment (M_{tmax}) in Eq. (4.23) is replaced with cross-sectional moment capacity (M_{cs}) at a given axial load (N) [23]. Hence Eq. (4.23) can be written as

$$M_{cs}=C_m\delta M_{02} \geq M_{02} \tag{4.30}$$

when both the first-order end moments are equal and the column is bent in single curvature, using Eq. (4.24), the equivalent moment factor is calculated as $C_m = 1$. Considering the equivalent first-order moment (M_{e1}) when $C_m = 1$ as ${M_{e1}}'$ (see Fig. 4.6) and using Eq. (4.2), ${M_{e1}}' = M_{02}$. Moreover, when $C_m = 1$, Eq. (4.30) can be rewritten as

$$M_{cs}=\delta {M_{e1}}' \tag{4.31}$$

Comparing Eq. (4.30) and Eq. (4.31), the equivalent moment factor (C_m) for a column subjected to unequal first-order end moments is expressed as

$$C_m=\frac{{M_{e1}}'}{M_{02}} \tag{4.32}$$

Eq. (4.32) is used to calculate the theoretical values of the equivalent moment factor of RC columns further in this study. The values of ${M_{e1}}'$ and M_{02} for a given axial load (N) are calculated by performing the detailed second-order analysis using the direct curvature method (DCM). The behavior of the equivalent moment factor (C_m)-load ratio (N_r) for simply supported FRP-RC and steel-RC columns with different values of first-order end moment ratio is presented in Fig. 4.7. Here, load ratio is considered as

$$N_r=\frac{N}{N_B} \tag{4.33}$$

The bending stiffness (EI) of the reinforced concrete column in Eq. (4.27) is calculated using the expression [4,36].

$$EI=\frac{NL^2}{4\left(\arccos\frac{M'_{e1}}{M_{cs}}\right)^2} \tag{4.34}$$

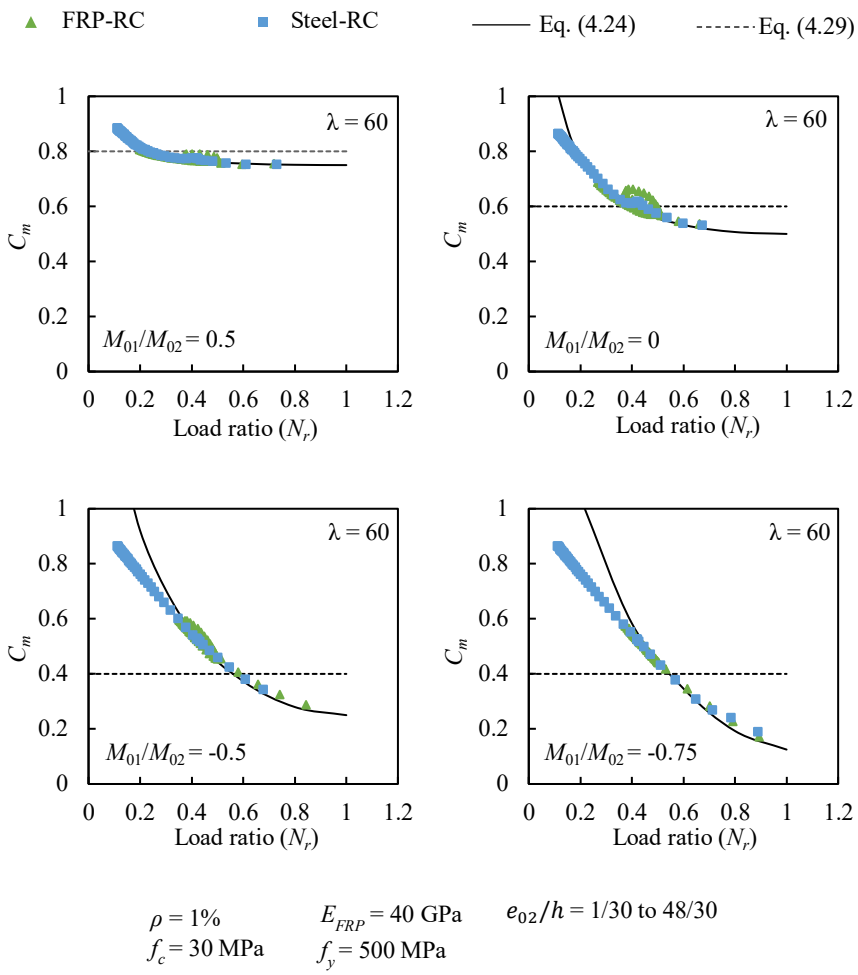


Fig. 4.7. Equivalent moment factor (C_m)-load ratio (N_r) of FRP-RC column and steel-RC columns for slenderness ratio of 60

The equivalent moment factor (C_m) for FRP-RC columns behaves quite similarly to C_m for steel-RC columns as the load ratio changes. In addition, the variation of C_m with load ratio (N_r) for both FRP-RC and steel-RC columns exhibits similar behavior as that of elastic columns, which is represented by Eq. (4.24). However, for the column bent in double curvature with first-order end moment ratio (M_{01}/M_{02}) of -0.5 and -0.75, it can be seen that C_m for steel-RC and FRP-RC columns is lower than the C_m for elastic columns at low values of load ratio. Also, for the range of eccentricity ratio (e_{02}/h) considered in Fig. 4.7, the lowest value of load ratio obtained for FRP-RC columns is around 0.2. However, this is not the same as for steel-RC columns. For first-order end moment ratios (M_{01}/M_{02}) of 0 and -0.5, the C_m for FRP-RC columns is observed to be slightly higher than for steel-RC columns and elastic columns for the load ratio of around 0.3 to 0.6.

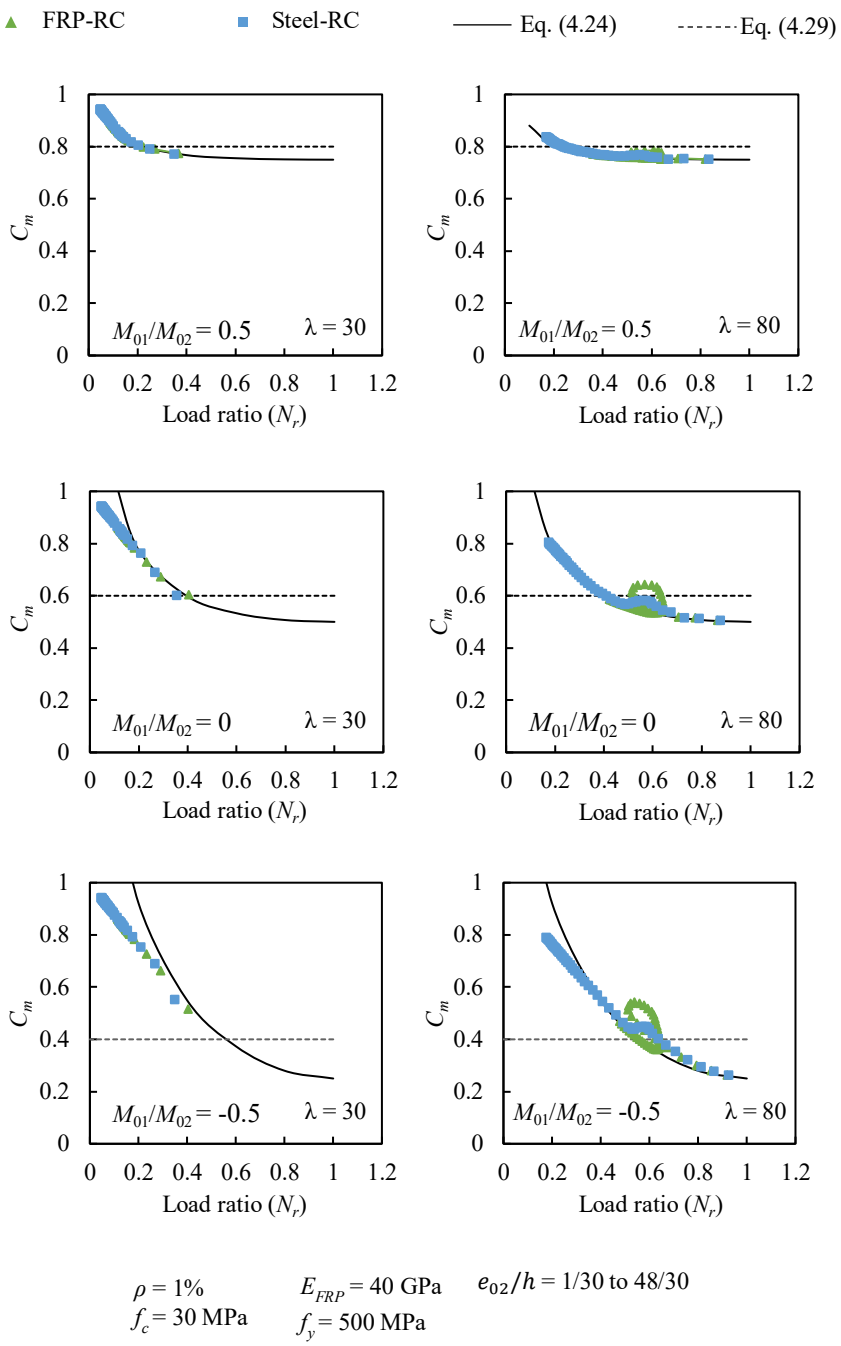


Fig. 4.8. Equivalent moment factor (C_m)-load ratio (N_r) of FRP-RC column and steel-RC column with the variation in slenderness ratio

The effect of the slenderness ratio on C_m is presented in Fig. 4.8, where slenderness ratios of 30 and 80 are considered to calculate C_m at M_{01}/M_{02} values of 0.5, 0 and -0.5 for a simply supported column. The effect of slenderness ratio is only seen in the medium range of load ratio of around 0.3 to 0.6. In this range of load ratio, as the slenderness ratio increases, C_m for FRP-RC columns also increases.

Furthermore, as the slenderness ratio decreases, the behavior of C_m for FRP-RC columns becomes very similar to the behavior of steel-RC columns.

Further, the effect of change in the reinforcement ratio, modulus of elasticity of FRP bar and concrete strength on the equivalent moment factor of FRP-RC column is presented in Fig. 4.9.

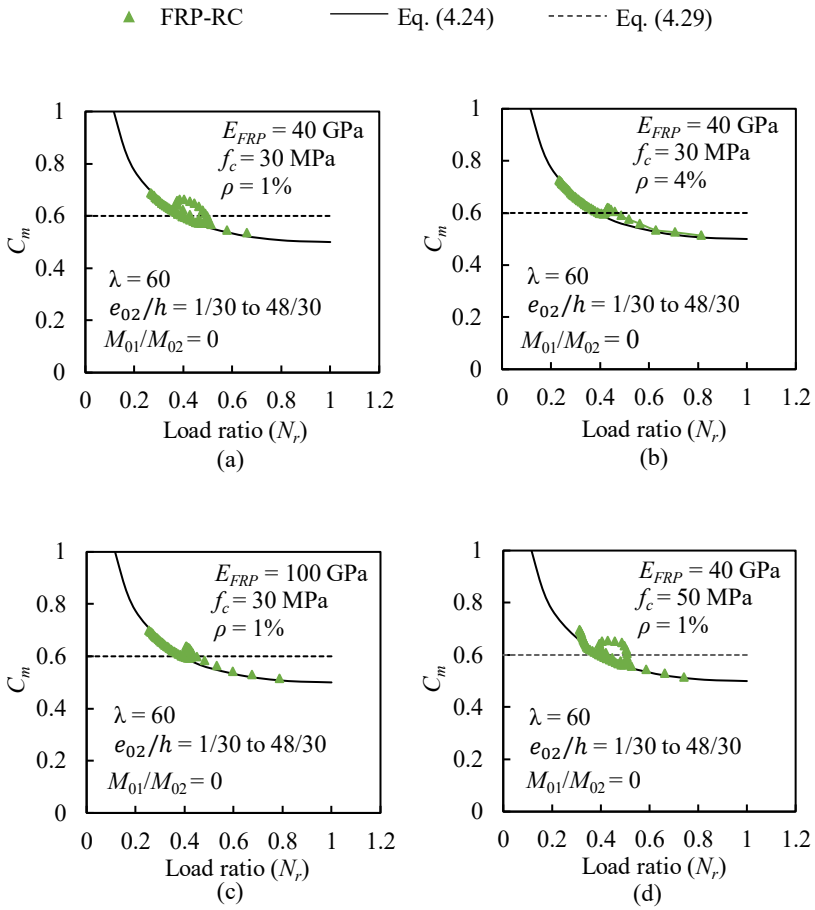


Fig. 4.9. Effect of variation in ρ, E_{FRP}, and f_c on the equivalent moment factor (C_m) of FRP-RC column

The reinforcement ratio, modulus of elasticity of FRP bar and concrete strength have an effect only in the range of medium values of load ratio of around 0.3 to 0.6. Moreover, as the reinforcement ratio increases or the modulus of elasticity of FRP bar increases, the behavior of C_m for FRP-RC columns becomes more similar to the behavior of elastic columns. However, as the concrete strength increases, the increase in the C_m values for FRP-RC columns in comparison to elastic columns at medium values of load ratio becomes more distinct.

Furthermore, it is observed from Fig. 4.8 and 4.9 that the value of C_m is more dependent on the M_{01}/M_{02} and load ratio (N_r). Also, it can be seen from Fig. 4.7 and 4.8 that the effect of N_r on the value of C_m reduces as M_{01}/M_{02} increases. Therefore, M_{01}/M_{02} appears to be the major parameter affecting the equivalent moment factor (C_m) of FRP-RC columns.

4.4 Parametric study

4.4.1 General

A detailed parametric study was conducted to determine the equation to estimate the equivalent moment factor for FRP-RC columns and to verify the suitability of the existing C_m approximation for elastic columns and steel-RC columns for FRP-RC columns. The variables considered for the parametric study are presented in Table 4.2. The range of the concrete strength considered corresponds to the normal strength concrete. The modulus of elasticity of the FRP bar considered in this study corresponds to the commercially available FRP bars such as glass FRP, aramid FRP and basalt FRP bars [7,10]. CFRP bars may have a higher modulus of elasticity, however, the FRP bars with low modulus of elasticity are of major concern for second-order effects. Hence, the range of modulus of elasticity of 40 to 80 GPa is considered in this study. The column cross-section presented in Fig. 4.5 was considered for the parametric study. C_m values were calculated by conducting a detailed second-order analysis using the direct curvature method. The parametric study results for 12288 data points are presented in Fig. 4.10 (a), where n_d represents the number of data points.

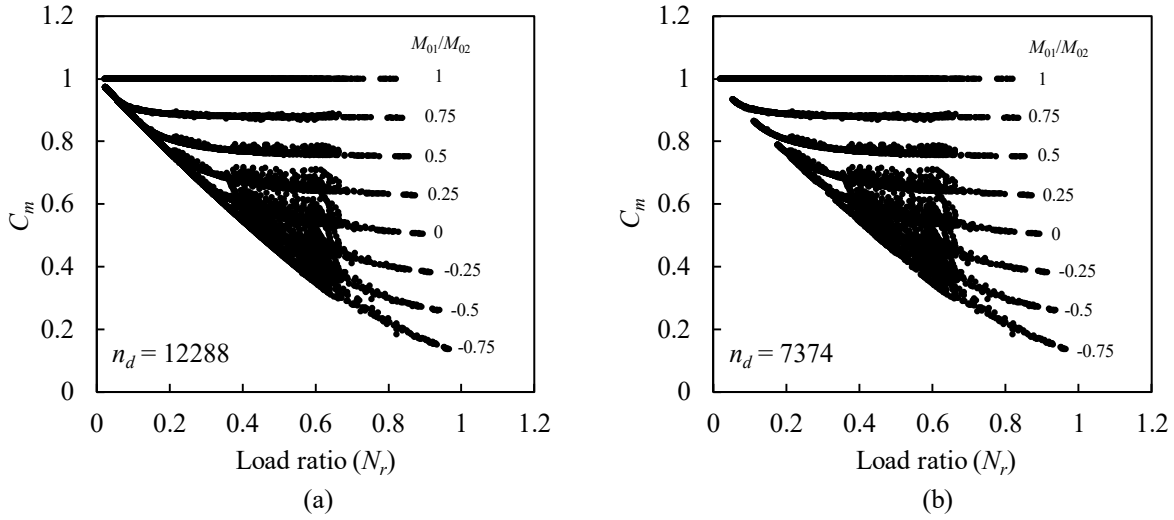


Fig. 4.10. Equivalent moment factor (C_m) - load ratio (N_r) (a) for all the columns considered in the parametric study; and (b) excluding the column data points having no second-order effects

Table 4.2. Parametric study variables

Parameters	Values	Number of values
Concrete compressive strength (f_c)	30 and 50 MPa	2
Modulus of elasticity of FRP bar (E_{FRP})	40 and 80 GPa	2
Slenderness ratio (λ)	20, 40, 60 and 80	4
Reinforcement ratio (ρ)	1 and 4 %	2
Eccentricity ratio (e_{02}/h)	1/30, 2/30 to 48/30	48
First-order end moment ratio (M_{01}/M_{02})	-0.75, -0.5, -0.25, 0, 0.25, 0.5, 0.75 and 1	8
	Total cases	12288

4.4.2 Regression analysis

Based on the C_m values obtained from the parametric study, multiple linear regression was carried out in *Matlab* [37]. The column data points from the parametric study that did not experience any increase

in the total moment due to geometric second-order effects were excluded from the data set considered for the purpose of the regression analysis, as shown in Fig. 4.10(b). The maximum moment occurred at one of the column ends for such columns and the data points for those columns lie on the diagonal in Fig. 4.10(a).

A total of 7374 data points were considered for regression. To estimate the equivalent moment factor (C_m) for the FRP-RC column, two equations were used for regression, which are expressed as

$$C_m = \alpha + \beta(M_{01}/M_{02}) \tag{4.35}$$

$$C_m = \alpha + \beta(M_{01}/M_{02}) + \gamma(N_r) + \delta(\omega') + \vartheta(\lambda) \tag{4.36}$$

where α, β, γ, δ and ϑ are the regression coefficients. ω' represents the mechanical reinforcement ratio for FRP-RC columns and it is expressed as

$$\omega' = \frac{A_r E_{FRP} \varepsilon_{tu}}{A_c f_c} \tag{4.37}$$

The form of Eq. (4.35) is considered to be similar to Eq. (4.29). As observed earlier, M_{01}/M_{02} is seen as the major parameter affecting the C_m value of FRP-RC columns, however, to further verify this, Eq. (4.36) was considered to include load ratio (N_r), mechanical reinforcement ratio (ω') and slenderness ratio (λ) along with M_{01}/M_{02} in determining the C_m of FRP-RC columns. The two equations obtained upon performing the multiple linear regression are

$$C_m = 0.61 + 0.37(M_{01}/M_{02}) \tag{4.38}$$

$$C_m = 0.68 + 0.34(M_{01}/M_{02}) - 0.2(N_r) - 0.018(\omega') + 0.0004(\lambda) \tag{4.39}$$

The coefficient of determination (R^2) and the standard error of the regression for Eq. (4.38) are 0.95 and 0.045 and for Eq. (4.39), they are 0.97 and 0.040. This shows that the effect of including parameters other than M_{01}/M_{02} has a minor impact on determining the C_m values of FRP-RC columns for the range of parameters considered in this study. This is similar to steel-RC columns [4]. Hence, the form of C_m equation for FRP-RC columns is considered further according to Eq. (4.35). The coefficients in Eq. (4.38) are modified to adapt to the condition when $M_{01}/M_{02} = 1$, $C_m = 1$. This corresponds to the

column bent in single curvature with equal first-order end moments. Consequently, two equations adapted for the equivalent moment factor (C_m) of FRP-RC columns are expressed as

$$C_m = 0.7 + 0.3(M_{01}/M_{02}) \quad (4.40)$$

$$C_m = 0.6 + 0.4(M_{01}/M_{02}) \quad (4.41)$$

The coefficient of determination (R^2) for Eq. (4.40) and Eq. (4.41) is obtained as 0.81 and 0.95. The ratio of the equivalent moment factor from the regressed equation to the equivalent moment factor from the detailed second-order analysis is considered as $C_{m(Eq)}/C_{m(num)}$. The average, five-percentile and one-percentile values of $C_{m(Eq)}/C_{m(num)}$ of FRP-RC columns for Eq. (4.40) are 1.12, 1 and 0.96, respectively.

Tikka and Mirza (2004) found the average and one-percentile values of $C_{m(Eq)}/C_{m(num)}$ of steel-RC columns for Eq. (4.41) as 1.08 and 1.00. This shows that Eq. (4.41) was sufficiently conservative for steel-RC columns. The performance of Eq. (4.40) and Eq. (4.41) for FRP-RC columns is shown in Fig. 4.11. The average, five-percentile and one-percentile values of $C_{m(Eq)}/C_{m(num)}$ of FRP-RC columns for Eq. (4.41) are 1, 0.83 and 0.67, respectively. Furthermore, comparing the average and one-percentile values of $C_{m(Eq)}/C_{m(num)}$ for steel-RC and FRP-RC columns while using Eq. (4.41), it is observed that Eq. (4.41) is not sufficiently conservative for FRP-RC columns as it was for steel-RC columns. On the contrary, Eq. (4.40) is a more appropriate and conservative equation for FRP-RC columns in comparison to Eq. (4.41). This can be attributed to the different stress-strain behavior and low modulus of elasticity of FRP bars compared to steel bars. As discussed previously, the inclusion of mechanical reinforcement ratio does not improve the estimation of C_m value for FRP-RC columns. However, the material properties of FRP bars, especially, low modulus of elasticity, affect the overall estimation of C_m value while having M_{01}/M_{02} as the determining variable. Furthermore, design codes such as ACI 440.11-22, where Eq. (4.41) is adopted for the equivalent moment factor of glass FRP-RC columns, may need to reconsider the same, as Eq. (4.41) may lead to unconservative results in a large number of cases.

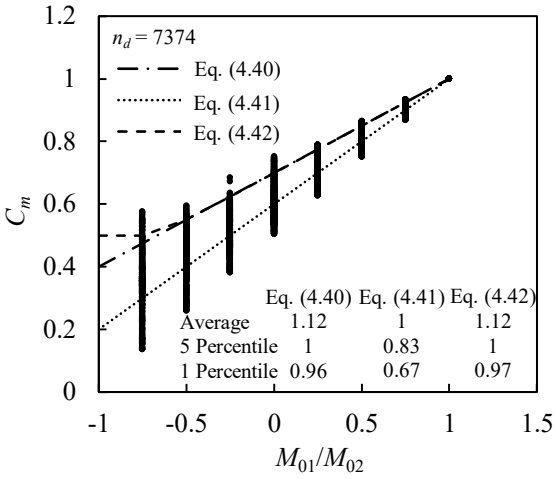


Fig. 4.11 Performance of different C_m equations for FRP-RC columns in comparison to the data points considered for regression

The lower limit of 0.4 for Austin's approximation of C_m for elastic columns (Eq. (4.29)) was derived in relation to the lateral torsional buckling. However, this limit is not required for in-plane bending [23]. Tikka and Mirza [4] proposed a lower limit of 0.3 on the C_m value of steel-RC columns to keep the one-percentile C_m values near 0.9 for M_{01}/M_{02} ranging from 0.75 to -0.75. ACI CODE 318-19 [3] does not have a lower limit on C_m value of steel-RC columns as seen in Eq. (4.3). However, Eurocode 2 [1] adopts a limit of 0.4 for steel-RC columns similar to Austin's approximation. Lai et al. [38] argued that the limit of 0.4 for steel-RC columns would provide more conservativeness for the columns bent in double curvature at high values of axial load when the column suddenly unwinds into the first buckling mode. The average, five-percentile and one-percentile values of $C_{m(Eq)}/C_{m(num)}$ while using Eq. (4.40) for first-order end moment ratio (M_{01}/M_{02}) of -0.75 corresponding to the data set considered for regression in this study is presented in Fig. 4.12. Out of 7374 data points considered for the regression, 368 data points correspond to $M_{01}/M_{02} = -0.75$.

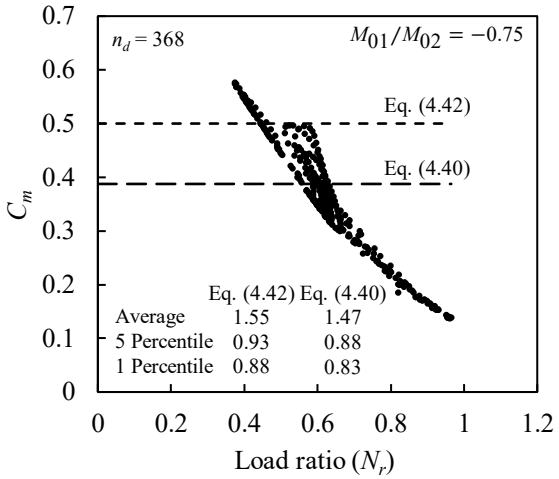


Fig. 4.12. Equivalent moment factor (C_m) vs load ratio data points considered for regression for first-order end moment ratio of $M_{01}/M_{02} = -0.75$

It can be seen in Fig. 4.11 that Eq. (4.40) is a more conservative estimate in comparison to Eq. (4.41). However, for negative values of M_{01}/M_{02}, Eq. (4.40) can also be unconservative for a few cases, as shown for $M_{01}/M_{02} = -0.75$ in Fig. 4.12.

Hence, a lower limit of 0.5 is introduced to Eq. (4.40) to make the five-percentile values of $C_{m(num)}/C_{m(Eq)}$ equal to 0.9 for the individual data sets of each M_{01}/M_{02} ratio considered in this study. Eq. (4.40) with a lower limit of 0.5 is presented as Eq. (4.42) and it is proposed to estimate the equivalent moment factor (C_m) for FRP-RC columns.

$$C_m = 0.7 + 0.3(M_{01}/M_{02}) \geq 0.5 \qquad (4.42)$$

The performance of Eq. (4.42) in relation to Eq. (4.40) and Eq. (4.41) is also shown in Fig. 4.11. The average, five-percentile and one-percentile values of $C_{m(Eq)}/C_{m(num)}$ of FRP-RC columns for Eq. (4.42) are 1.12, 1 and 0.97. Its performance is similar to Eq. (4.40), however, some improvement in the one-percentile value can be observed due to the introduction of the lower limit. Furthermore, a cumulative distribution frequency of the $C_{m(Eq)}/C_{m(num)}$ for the data points considered in the regression analysis is plotted on a normal probability scale in Fig. 4.13. It can be seen that only for 5% of the cases considered, $C_{m(Eq)}$ calculated using Eq. (4.40) and Eq. (4.42) is less than $C_{m(num)}$, which

corresponds to a five-percentile value of 1. However, for 30% of the cases considered, $C_{m(Eq)}$ calculated using Eq. (4.41) is less than $C_{m(num)}$. Hence, Eq. (4.42) is a more appropriate proposal for the equivalent moment factor of FRP-RC columns.

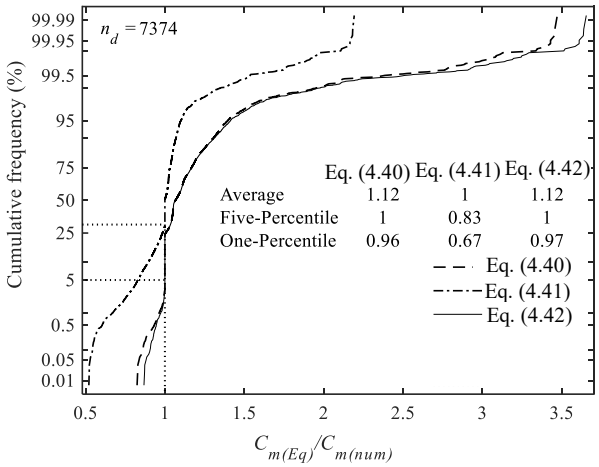


Fig. 4.13. Cumulative distribution frequency of $C_{m(Eq)}/C_{m(num)}$ calculated using Eq. (4.40), Eq. (4.41) and Eq. (4.42) for FRP-RC columns

The proposed equation (Eq. 4.42) is based on the parametric study performed using the numerical method DCM. As shown earlier, DCM exhibited reasonable correlation with the available experimental data. However, more experiments for FRP-RC columns specially subjected to unequal end moments would be of further interest. Moreover, Eq. (4.42) proposed in this study is on the conservative side such that five-percentile values of $C_{m(num)}/C_{m(Eq)}$ is equal to 1 for all the data points considered for regression in this study and five-percentile values of $C_{m(num)}/C_{m(Eq)}$ is equal to 0.9 for individual data sets of each M_{01}/M_{02}. The proposed equation (Eq. 4.42) is limited to the range of parameters considered in this study, specifically for E_{FRP} of 40-80 GPa and normal strength concrete up to 50 MPa. This corresponds to ω' of 0.08 to 1.07. Furthermore, the proposed equation (Eq. 4.42) is conservative compared to the equation available for steel-RC columns and also adopted by ACI 440.11-22 for glass FRP-RC columns.

Two examples are presented to understand the effect of using the C_m equation to calculate the load capacity of the FRP-RC column. The column cross-section is considered as shown in Fig. 4.5. In the

first example, for a column with f_c = 30 MPa, E_{FRP} = 40 GPa, ρ = 1%, $M_{01}/M_{02} = -0.25$, λ = 60, e_{02} = 50 mm, the axial load capacity and C_m calculated numerically using DCM is found as N_{num} = 1645 kN and $C_{m(num)} = 0.51$. For this column with $M_{01}/M_{02} = -0.25$, C_m is calculated using Eq. (4.42) and Eq. (4.41) as $C_{m(Eq.(4.42))} = 0.625$ and $C_{m(Eq.(4.41))} = 0.50$. Further, the column is transformed into a column with equivalent uniform first-order end eccentricity using $C_{m(Eq.(4.42))}$ with $e_{02} = e_{01} = 31.25$ mm. In addition, using $C_{m(Eq.(4.41))}$ with $e_{02} = e_{01} = 25$ mm. The load capacity of these equivalent columns with equivalent uniform first-order end eccentricity is further calculated using DCM while considering M_{01}/M_{02} = 1. The load capacity of the equivalent column transformed using Eq. (4.42) and Eq. (4.41) is found as $N_{(Eq.(4.42))} = 1529.8$ kN and $N_{(Eq.(4.41))} = 1666.4$ kN. $N_{(Eq.(4.42))}/N_{num}$ = 0.93 and $N_{(Eq.(4.41))}/N_{num}$ = 1.01.

In the second example, all the input parameters remain the same as in the first example. However, f_c = 50 MPa and e_{02} = 130 mm is considered. In this case, N_{num} = 776.01 kN and $C_{m(num)} = 0.61$ is calculated numerically using DCM. For this column with $M_{01}/M_{02} = -0.25$, C_m is calculated using Eq. (4.42) and Eq. (4.41) as $C_{m(Eq.(4.42))} = 0.625$ and $C_{m(Eq.(4.41))} = 0.50$. Further, it is transformed into a column with equivalent uniform first-order end eccentricity using $C_{m(Eq.(4.42))}$ with $e_{02} = e_{01} = 81.25$ mm. In addition, using $C_{m(Eq.(4.41))}$ with $e_{02} = e_{01} = 65$ mm. Further, the load capacity of the equivalent column with equivalent uniform first-order end eccentricity transformed using Eq. (4.42) and Eq. (4.41) is found using DCM as $N_{(Eq.(4.42))} = 730.60$ kN and $N_{(Eq.(4.41))} = 1174.3$ kN. $N_{(Eq.(4.42))}/N_{num}$ = 0.94 and $N_{(Eq.(4.41))}/N_{num}$ = 1.51. It can be observed from the two examples that Eq. (4.42) leads to a more conservative prediction of the column load capacity for FRP-RC columns in comparison to Eq. (4.41). Moreover, Eq. (4.41) makes a huge overestimation of the column load capacity for a large number of cases as it passes through the lower portion of the data points as seen in Fig. 4.11. Using Eq. (4.41) can lead to unsafe design for many cases. Hence, Eq. (4.42) is a safe and rational choice for the C_m of FRP-RC columns.

4.5 Conclusions

The equivalent moment factor to transform the FRP-RC column subjected to unequal end moments into a column subjected to equal end moments for simplified second-order analysis was studied in detail in comparison to steel-RC and elastic columns. Further, two numerical methods were successfully implemented to perform the detailed second-order analysis of reinforced concrete columns with unequal end moments bent in single and double curvature. The conclusions from the study are summarized as follows:

1. Existing equations to estimate the equivalent moment factor for steel-RC and elastic columns are found to be not conservative enough for FRP-RC columns owing to the distinct material properties of FRP bars, especially the low modulus of elasticity of FRP bars.
2. A detailed parametric study was conducted and utilized to perform regression to estimate the equivalent moment factor for FRP-RC columns. Eq. (4.42) was proposed to estimate the equivalent moment factor for FRP-RC columns corresponding to the range of material properties considered in the parametric study. A lower limit of 0.5 was proposed for the equivalent moment factor of FRP-RC columns.
3. For the medium range of load ratio (N_r) of around 0.3 to 0.6, with the increase in slenderness ratio of the column, decrease in the reinforcement ratio, decrease in the modulus of elasticity of FRP bar and increase in the concrete compressive strength of concrete, the equivalent moment factor for FRP-RC column was observed to be higher than the steel-RC and elastic columns. However, the first-order end moment ratio (M_{01}/M_{02}) was found to be a major determining parameter for the equivalent moment factor of FRP-RC columns.
4. The direct curvature method (DCM) with an estimation of the deflected shape of the column could effectively predict the capacity of the RC columns with comparable performance as the column deflection curve method (CDM) without any assumption of the deflected shape of the column. Both methods were successfully verified with the experimental results from the literature. No experiments were found in the literature on the FRP-RC columns subjected to unequal end moments, which highlights the need for more experiments.

5. This study provides valuable insights towards framing guidelines for the design codes of FRP-RC columns, particularly the extension of the simplified second-order analysis methods for columns subjected to unequal end moments using equivalent moment factor for FRP-RC columns.

4.6 Acknowledgements

The authors would like to gratefully acknowledge the funding support provided by the German Academic Exchange Service (DAAD) to pursue this research work.

4.7 References

[1] EN 1992-1-1. Eurocode 2: Design of concrete structures - Part 1-1:General rules and rules for buildings: EN 1992-1-1: Eurocode 2: Design of concrete structures - Part 1-1: General rules and rules for buildings(EN 1992-1-1:2004). Brussels: European Committee for Standardisation.

[2] Austin WJ. Strength and Design of Metal Beam-Columns. J. Struct. Div. 1961;87(4):1–34.

[3] ACI. Building Code Requirements for Structural Concrete and Commentary(ACI CODE 318-19). Farmington Hills, MI: American Concrete Institute; 2019.

[4] Timo K. Tikka, S. Ali Mirza. Equivalent Uniform Moment Diagram Factor for Reinforced Concrete Columns. SJ 2004;101(4):521–31.

[5] ACI 440.1R. Guide for the design and construction of structural concrete reinforced fiber-reinforced polymer (FRP) bars.(ACI 440.1R-15). Farmington Hills, MI: American Concrete Institute; 2015.

[6] CAN/CSA S806-12. Design and construction of building structures with Design and construction of building structures with fibre-reinforced polymers(CSA S806-12): Canadian Standards Association; 2012.

[7] Fib Bulletin 40. FRP reinforcement in RC structures. Stuttgart: The International Federation for Structural Concrete; 2007.

[8] DAfStb. Erläuterungen und Beispiele zur DAfStb-Richtlinie Betonbauteile mit nichtmetallischer Bewehrung - 2024-06 - DIN Media(Heft Nr. 660); Available from: https://www.dinmedia.de/en/publication/dafstb-heft-660/379490412.

[9] ACI. Building Code Requirements for Structural Concrete Reinforced with Glass Fiber-Reinforced Polymer (GFRP) Bars-Code and Commentary.(ACI CODE-440.11-22). Farmington Hills, MI: American Concrete Institute; 2022.

[10] Syed AU, Goldack A. Effect of Slenderness on the Design of FRP reinforced Concrete Columns. In: IABSE Congress, New Delhi 2023: Engineering for Sustainable Development, New Delhi, India, 9/20/2023 - 9/22/2023.

[11] Syed AU, Goldack A. Slenderness limit for GFRP reinforced concrete columns based on axial force ratio. Engineering Structures 2024;298.

[12] Mirmiran A, Yuan W, Chen X. Design for Slenderness in Concrete Columns Internally Reinforced with Fiber-Reinforced Polymer bars. ACI Struct J 2001;98(1):116–25.

[13] Abdelazim W, Mohamed HM, Benmokrane B. Inelastic Second-Order Analysis for Slender GFRP-Reinforced Concrete Columns: Experimental Investigations and Theoretical Study. J Compos Constr 2020;24(3).

[14] Abdelazim W, Mohamed HM, Afifi MZ, Benmokrane B. Proposed Slenderness Limit for Glass Fiber-Reinforced Polymer-Reinforced Concrete Columns Based on Experiments and Buckling Analysis. ACI Structural Journal 2020;117(1).

[15] Abdelazim W, Mohamed HM, Benmokrane B. Proposed Flexural Stiffness of Slender Concrete Columns Reinforced with Glass Fiber-Reinforced Polymer Bars. ACI Structural Journal 2021;118(1):227–40.

[16] Xue W, Peng F, Fang Z. Behavior and Design of Slender Rectangular Concrete Columns Longitudinally Reinforced with Fiber-Reinforced Polymer Bars. ACI Structural Journal 2018;115(2).

[17] Zadeh HJ, Nanni A. Design of RC Columns Using Glass FRP Reinforcement. J Compos Constr 2013;17(3):294–304.

[18] Syed AU, Goldack A. Simplified Second-Order Analysis of Slender FRP-Reinforced Concrete Columns Using the Nominal Curvature Method. J. Compos. Constr. 2025;29(2):4025007.

[19] Bujotzek L, Waldmann D. Innovative buckling safety verification method for the determination of second-order effects in slender FRP reinforced columns including effects of FRP creep. Engineering Structures 2025;322:119143.

[20] EN 1992-1-1. Eurocode 2: Design of concrete structures - Part 1-1:General rules and rules for buildings: EN 1992-1-1: Eurocode 2: Design of concrete structures - Part 1-1: General rules and rules for buildings(prEN 1992-1-1:2023). Brussels: European Committee for Standardisation.

[21] Chen W-F, Toshio A. Theory of beam-columns, volume 1: In plane behavior and design: J. Ross Publishing; 1976.

[22] Broms BB. Ultimate Strength of Long Reinforced Concrete Columns: University of Illinois at Urbana-Champaign; 1956.

[23] Hellesland J, Challamel N, Casandjian C, Lanos C. Reinforced concrete beams, columns and frames: section and slender member analysis. Surrey: John Wiley & Sons; 2013.

[24] Popovics S. A numerical approach to the complete stress-strain curve of concrete. Cement and concrete research 1973;3:583–99.

[25] Khorramian K, Sadeghian P. Experimental and analytical behavior of short concrete columns reinforced with GFRP bars under eccentric loading. Engineering Structures 2017;151:761–73.

[26] Mander JB, Priestly JN, Park, R. Theoretical Stress-Strain Model for Confined Concrete. J. Struct. Eng. 1988;114(8):1804–26.

[27] Hadhood A, Mohamed HM, Benmokrane B, Nanni A, Shield CK. Assessment of Design Guidelines of Concrete Columns Reinforced with Glass Fiber-Reinforced Polymer Bars. ACI Structural Journal 2019;116(4):193–207.

[28] Guérin M, Mohamed HM, Benmokrane B, Nanni A, Shield CK. Eccentric Behavior of Full-Scale Reinforced Concrete Columns with Glass Fiber-Reinforced Polymer Bars and Ties. ACI Structural Journal 2018;115(2):489–99.

[29] Hamid FL, Yousif AR. Behavior of Short and Slender RC Columns with BFRP Bars under Axial and Flexural Loads: Experimental and Analytical Investigation. J. Compos. Constr. 2024;28(1).

[30] Afefy HM, El-Tony EM. Simplified Design Procedure for Reinforced Concrete Columns Based on Equivalent Column Concept. Int J Concr Struct Mater 2016;10(3):393–406.

[31] MacGregor JG, Barter SL. Long Eccentrically Loaded Concrete Columns Bent in Double Curvature. SP 1966;13:139–56.

[32] Othman ZS, Mohammad AH. Behaviour of Eccentric Concrete Columns Reinforced with Carbon Fibre-Reinforced Polymer Bars. Advances in Civil Engineering 2019;2019:1–13.

[33] Galambos TV. Structural Members and Frames: Prentice-Hall; 1968.

[34] Chen WF, Lui EM. Structural Stability: Theory and Implementation. New York: Elsevier Science Publishing Co; 1987.

[35] Massonnet C. Stability Considerations in the Design of Steel Columns. J. Struct. Div. 1959;85(7):75–112.

[36] Timoshenko SP. Theory of Elastic Stability: McGraw-Hill Book Company; 1961.

[37] MATLAB version: 9.13.0 (R2022b). Natick, Massachusetts: The MathWorks Inc; 2022.

[38] Lai SMA, MacGregor JG, Hellesland J. Geometric Nonlinearities in Nonsway Frames. J. Struct. Eng. 1983;109(12):2770–85.

5. Design of FRP-RC Rectangular Columns with Nominal Curvature Method and Universal Interaction Diagrams Applicable to Various FRP Bar Types

Ahmed Usama Syed[1], Arndt Goldack[2], Richard Koehler[3]

[1 2 3] University of Wuppertal, Chair of Statics and Dynamics of Structures, Pauluskichstraße 7, 42285 Wuppertal, Germany.

Accepted in

Journal of Structural Design and Construction Practice (DOI: https://10.1061/JSDCCC/SCENG-2290)

ABSTRACT

Design method for slender fiber-reinforced polymer (FRP) reinforced concrete (FRP-RC) rectangular columns based on the nominal curvature are not yet included in the new Eurocode 2 Annexure R. However, a proposal to expand Eurocode 2 in this regard is presently being considered and would also be included in the new DAfStb guideline for non-metallic reinforcement. Additionally, other national codes, such as ACI 440.11-22 and CSA S806-12, also require load–moment capacity curves for the design of FRP reinforced concrete (FRP-RC) column cross-sections. However, distinct load-moment capacity curves are required for each type of FRP bar in FRP-RC columns due to their different modulus of elasticity and ultimate design strain limits. This paper presents a novel concept of universal interaction diagrams, which can be used regardless of the type of FRP reinforcement bar such as Glass, Carbon, Basalt or Aramid FRP. This significantly enhances both its usability and practicality in structural design. These diagrams only depend on concrete strength, reinforcement configuration, and cover-to-depth ratio. This paper introduces provisions to expand Eurocode 2, provides universal interaction diagrams for rectangular cross sections for cross-section design, and provides universal interaction diagrams for slender FRP-RC columns with slenderness ratios of 40, 60, and 80, all of which are based on the nominal curvature method. The universal interaction diagrams for slender columns bypass the iterative solution of the presented equations and therefore have high practical value. Finally, the paper provides three worked examples that illustrate how to analyze and design short and slender FRP-RC columns using the presented diagrams.

Keywords: FRP reinforced concrete columns; Load-moment interaction curves; Nominal curvature method; Short columns, Slender columns

5.1 Introduction

In addition to the proven design methods in codes and guidelines, suitable practical design aids are of significant interest for the design of reinforced concrete using fiber-reinforced polymer (FRP) bars with glass, basalt, or carbon fibers. These include normalized load (*N*)- moment (*M*) interaction diagrams for the design of FRP reinforced concrete (FRP-RC) cross-sections and also for the design of slender FRP-RC columns using the nominal curvature method.

The difficulty with providing such design aids is that the modulus of elasticity and permissible ultimate tensile strains of different types of FRP reinforcement bars vary significantly depending on the fibres and resin used. Based on the recent research studies [1–4], the proposal for the design guidelines in the framework of Eurocode 2 [5] for FRP-RC columns is presented by Goldack et al. [6]. However, robust normalized interaction curves with ν_{Ed} and μ_{Ed}, which are a prerequisite to design columns using such guidelines, suitable for each type of FRP bars, are not available in the literature. Korentz and Czarnecki [7] presented normalized interaction diagrams for FRP-RC columns for different mechanical reinforcement ratios; however, with permissible ultimate tensile strain limited to 10 mm/m. These diagrams cannot be extended to FRP with permissible ultimate tensile strain other than 10 mm/m. Niyazuddin and Basappa [8] presented load (*N*)- moment (*M*) interaction diagrams for a given strength of concrete and ultimate tensile strength of GFRP bar for a fixed reinforcement ratio and four different values of permissible ultimate tensile strain. Hence, these curves are limited to the material properties and reinforcement ratio considered by them and cannot be used for different combinations of material properties and reinforcement ratios. Recently, Hosseini and Sadeghian [9] developed some practical interaction diagrams for glass FRP-RC columns. However, they presented the diagrams for a constant value of permissible ultimate tensile strain for the GFRP bar with a modulus of elasticity of 50 GPa and design tensile strength of 900 MPa.

To avoid the need to create new design *N*-*M* interaction diagrams for each type of FRP reinforcement or for the same type of FRP bar from different manufacturers, this paper introduces the concept of universal diagrams for FRP-RC members. The presented diagrams can be used for the cross-section

design of FRP-RC concrete members subjected to bending with axial load, independent of the type of FRP bars.

To avoid iterating the cross-section capacity when designing FRP-RC columns with the nominal curvature method for cross-section design, this paper presents universal diagrams for a slenderness ratio of 40, 60 and 80, based on the nominal curvature method equations. The required reinforcement ratio for a given cross-section can easily be determined by the acting normal force and the first-order bending moment.

This paper is the result of extensive research on the design of FRP-RC rectangular columns in the framework of Eurocode 2 [5]. For the universal interaction diagram for cross-section design, more than 50,000 rectangular cross-sections with reinforcement distributed on two sides were examined to generate sufficient data points. For rectangular cross-sections with web reinforcement, as an approximation the web reinforcement can be split into adjacent corner reinforcement and the universal interaction diagrams presented in this paper could be used. However, a better alternative would be to develop separate diagrams for such configurations. In this study to develop universal interaction diagrams, the cross-section analysis was performed establishing the equilibrium and compatibility using the nonlinear material properties of the cross-section by transformation of area as described in detail by Syed and Goldack [1]. Universal interaction diagrams for slender FRP-RC columns are based on the nominal curvature method for slender FRP-RC columns developed by Syed and Goldack [2]. They performed detailed second-order analysis on 26,880 columns with different slenderness ratios using the Direct Curvature Method (DCM) [3]. The equations developed by them were successfully presented in the Eurocode 2 framework by Goldack et al. [6] and are utilized in this study. Finally, three worked examples are presented to show the application of these diagrams.

5.2 Design of FRP-RC columns in the framework of Eurocode 2

The first step in designing columns is to determine whether they are short or slender. Short columns are those for which second-order effects have no significant impact on deflection and the bearing capacity

reduction is less than 10%. Syed and Goldack [1] provided a limit for the slenderness ratio (λ) for FRP-reinforced concrete columns as λ_{lim} expressed as:

$$\lambda \leq \lambda_{\text{lim}} = \begin{cases} 17\,n^2 + 19 & n \leq 0.4 \\ 22 - 13n^4 & n > 0.4 \end{cases} \tag{5.1}$$

where $n = |N_{Ed}|/A_c f_{cd}$ is the non-dimensional axial force with the design value of the applied axial load (N_{Ed}), the net cross-section area of concrete without reinforcement (A_c) and the design value of concrete compressive strength (f_{cd}).

Eurocode 2 [5] provides a nominal curvature method for the simplified analysis and design of slender steel-RC columns. Syed and Goldack [2] proposed a nominal curvature method for fiber-reinforced polymer (FRP) reinforced concrete columns, as outlined in the DAfStb guideline for nonmetallic reinforcement.

The maximum total design moment $M_{tot,d}$ is calculated as

$$M_{tot,d} = M_{Ed} + N_{Ed}\left(\frac{L^2}{c}\right)\frac{1}{r} \tag{5.2}$$

where M_{Ed} is the first order design moment and L is the effective length of the column. In addition, the following equations apply:

- for the nominal curvature ($1/r$) of the critical column section at constant load:

$$\frac{1}{r} = k_{\text{r}} \cdot k_{\varphi,\text{FRP}} \cdot \frac{1}{r_0} \tag{5.3}$$

$$k_{\text{r}} = e^{-(C_k \cdot n_r)} \leq 1 \tag{5.4}$$

$$C_k = 2.32 + 0.0064\,\lambda - 0.0051\frac{\omega}{\varepsilon_{tud}} \tag{5.5}$$

$$n_r = \frac{n - n_{bal}}{n_u - n_{bal}} \geq 0 \tag{5.6}$$

$$n = \frac{|N_{Ed}|}{A_c f_{cd}} \tag{5.7}$$

$$n_{bal} = \frac{|N_{bal}|}{A_c f_{cd}} \tag{5.8}$$

$$\omega = \frac{A_{FRP}\, E_{FRP}\, \varepsilon_{tud}}{A_c\, f_{cd}} \tag{5.9}$$

$$n_u = 1 + \omega \frac{\varepsilon_{c2}}{\varepsilon_{tud}} \tag{5.10}$$

- for the total curvature distribution factor (c):

$$c = c_I + \frac{1}{r}\frac{L^2}{\pi^2}\frac{1}{e_{cs}}(\pi^2 - c_I) \tag{5.11}$$

$$e_{cs} = \frac{M_{cs}}{|N_{\mathrm{Ed}}|} \tag{5.12}$$

where k_r is a coefficient depending on the axial force, A_{FRP} is the total area of the longitudinal FRP reinforcement, E_{FRP} is the modulus of elasticity of the longitudinal FRP reinforcement, ε_{tud} is the design value of the ultimate tensile strain of the FRP reinforcement, A_c is the net cross-section area of concrete without reinforcement, ε_{c2} is the compressive strain in the concrete at the peak stress f_c of concrete, ω is the mechanical reinforcement ratio, N_{Ed} is the design value of the applied axial force, n_r is the normalized load ratio, and N_{bal} is the value of the load at the balance point. $N_{bal} = 0$, if the balance point does not appear in the load-moment interaction curve. c_I is the first-order curvature distribution factor. $c_I = 8$ for the simply supported columns bent in single curvature with equal and opposite first-order end moments. M_{cs} is the moment capacity of the cross-section for a load level of N_{Ed}. $k_{\varphi,FRP}$ is the coefficient to account for creep. As creep is not in the scope of work of this study, the coefficient for creep $k_{\varphi,FRP} = 1$. Further information on $k_{\varphi,FRP}$ can be found in Goldack et al. [6] and Bujotzek and Waldmann [4]. Furthermore, if the balance point appears in the universal interaction diagram, $1/r_0$ is calculated as

$$\frac{1}{r_0} = \frac{\varepsilon_{tud} + \varepsilon_{cu}}{d} \tag{5.13}$$

where ε_{cu} is the maximum compressive strain of concrete and d is the effective depth of a cross-section. If the balance point does not appear in the universal interaction diagram, $1/r_0$ is calculated as

$$\frac{1}{r_0} = \frac{\varepsilon_{cu}}{x_c} \tag{5.14}$$

where x_c is the neutral axis depth of the cross-section for the moment equal to the moment capacity in pure bending. x_c can be calculated using force equilibrium in the cross-section [2]. Two worked examples for the application of these equations can be found in Syed and Goldack [2].

5.3 Universal interaction curves

The nominal curvature method requires information about the mechanical properties of the cross-section, such as the value of the load at balance point (N_{bal}) and the moment capacity of the cross-section (M_{cs}) for a load level of N_{Ed}. This can be found in the universal interaction curve for cross-section analysis for the normalized load of ν_{Ed} and the normalized moment of μ_{Ed}. All universal interaction curves for various normalized mechanical reinforcement ratios are summarized in the universal interaction diagram in Fig. 5.1. This diagram is based on the design stress-strain relation for concrete, considering a rectangular parabola according to Eurocode 2 [5]. The compressive concrete strength is considered in the range of C12/15 to C50/60. Furthermore, the net cross-section of concrete A_C without longitudinal reinforcement is used. The ratio of effective concrete cover to the depth is considered as $d_1/h = 0.1$. The mechanical reinforcement ratio in Eq. (5.15) is normalized in Eq. (5.16) by the design value of ultimate tensile strain (ε_{tud}) of the FRP reinforcement and scaled by 1/100 for better representation in the diagram and to generalize the same diagram for different values of ε_{tud}. The strain ε_{c2} in the universal interaction diagram refers to the concrete compressive strain of the outermost concrete in the cross-section.

$$\omega = \frac{E_{FRP}\ \varepsilon_{tud}\ A_{FRP}}{f_{cd}\ A_c} \tag{5.15}$$

$$\omega' = \frac{\omega}{\varepsilon_{tud} 100} \tag{5.16}$$

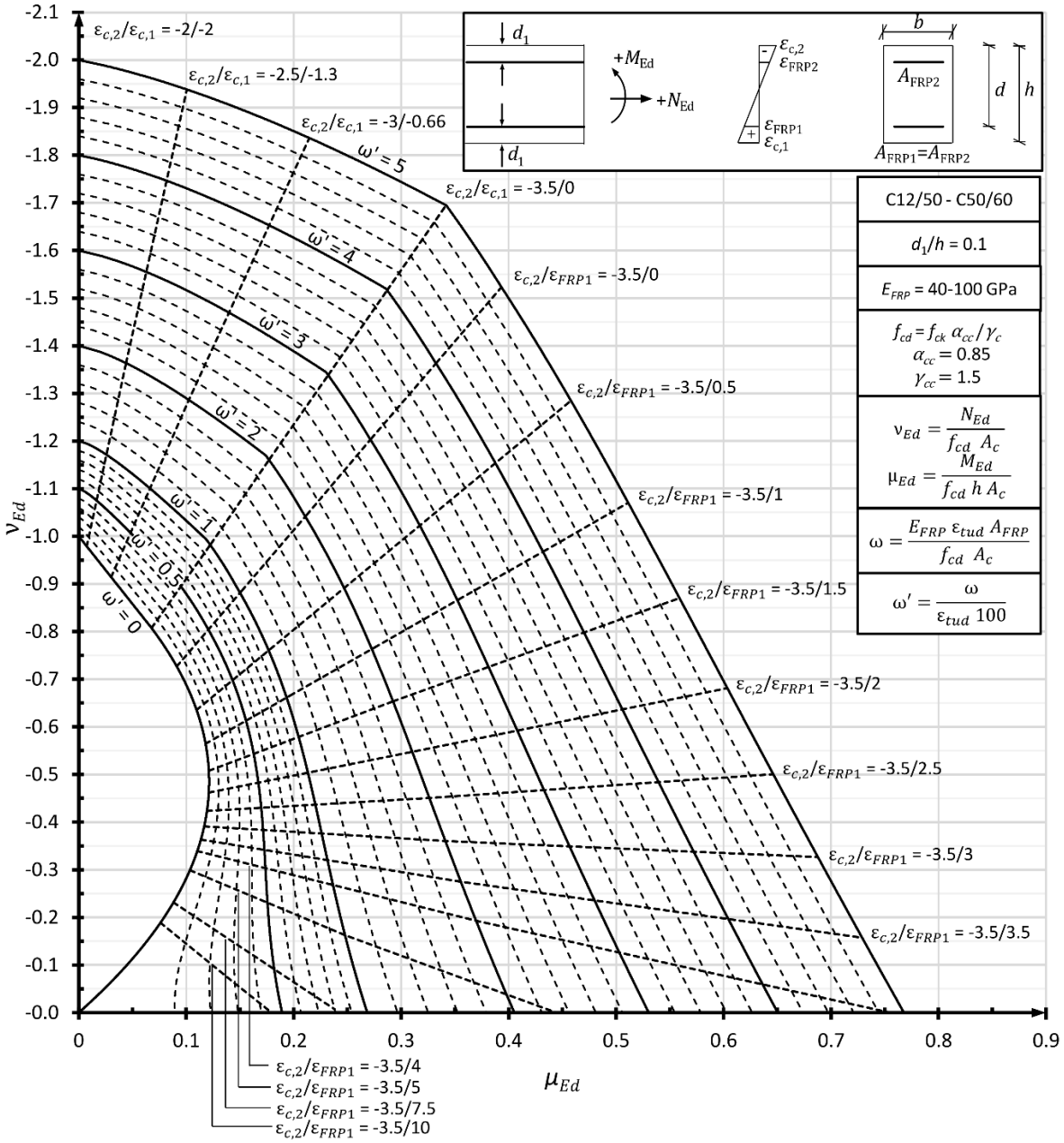


Fig. 5.1. Universal interaction diagram for cross-section with the normalized mechanical reinforcement ratio ω' (strains in mm/m)

5.4 General discussion on the universal interaction diagram

The universal interaction diagram in Fig. 5.1 shows the capacity of the cross-section for unlimited tensile strain of the reinforcement and compression failure of concrete with maximum compressive concrete strain ($\varepsilon_{c,2}$) of -3.5 mm/m in bending. Lines for constant $\varepsilon_{c,2}$ / ε_{FRP1} with the tensile strain of

the FRP reinforcement ε_{FRP1} are provided in the diagram to account for the design ultimate tensile strain (ε_{tud}) of different FRP reinforcements. These lines indicate a region of tensile failure below and a compression failure above for a FRP reinforcement with a given value of $\varepsilon_{FRP1} = \varepsilon_{tud}$. For the purpose of design, the maximum value of ε_{FRP1} permissible is considered equal to ε_{tud} of the FRP bar for cross-section design. ε_{tud} is based on the values provided in codes or in approvals and it is used in the nominal curvature equations.

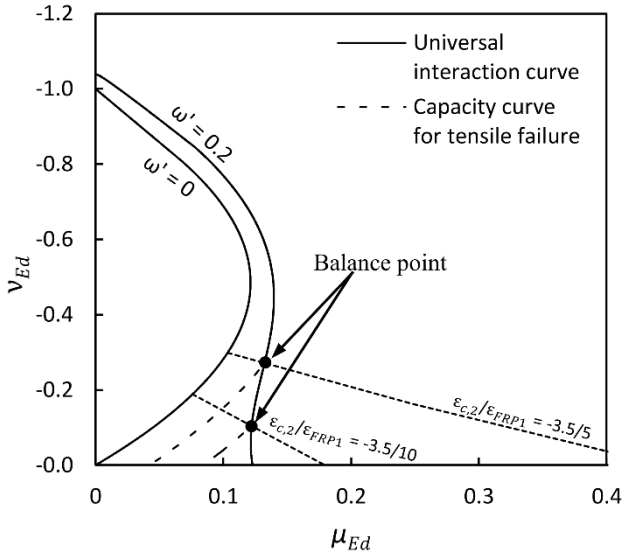


Fig. 5.2. Universal interaction curve and capacity curve for tensile failure with ω' = 0.2

Fig. 5.2 presents the universal interaction curve for ω' = 0.2. For a given design ultimate tensile strain (ε_{tud}) of a FRP bar, the point where $\varepsilon_{FRP1} = \varepsilon_{tud}$ is reached along with outermost concrete compressive strain $\varepsilon_{c,2} = \varepsilon_{cu}$ of -3.5 mm/m is the balance point for this value of ε_{tud}. The normalized load value at the balance point is termed as n_{bal}. For FRP bars with a given ε_{tud}, tensile strain in FRP bar (ε_{FRP1}) shall not be greater than ε_{tud}, hence, for normalized load values lower than n_{bal}, the capacity curve for tensile failure is created using cross-section analysis, considering the design ultimate tensile strain (ε_{tud}) equal to ε_{FRP1} for the FRP bar for all the points below balance point. It can be seen in Fig. 5.2 that the capacity curve for tensile failure is separated from the universal interaction curve with unlimited tensile strain. Furthermore, it can be observed that the capacity curve for tensile failure corresponding to any value of $\varepsilon_{FRP1} = \varepsilon_{tud}$ is parallel to the ω' = 0 interaction curve. This shows that

the universal interaction curve with unlimited ultimate tensile strain can be easily used to develop the capacity curve for tensile failure with a given ω' below the balance point without the need for numerical cross-section analysis. The capacity curve for tensile failure for a given value of ε_{tud}, starts from the balance point on the universal interaction curve corresponding to the given value $\varepsilon_{FRP1} = \varepsilon_{tud}$, and it is parallel to the ω' = 0 interaction curve.

As an example, in Fig. 5.3, the universal interaction curve for the normalized mechanical reinforcement ratio of $\omega' = 0.4$ and a permissible ultimate tensile strain of $\varepsilon_{FRP1} = \varepsilon_{tud} =$ 5 mm/m of the reinforcement is presented and discussed here. The capacity of the cross-section for unlimited tensile strain of the reinforcement and compressive failure of concrete in bending is represented by the DCB line. The balance point C is located at the intersection of the DCB line with the line for $\varepsilon_{c,2}$ / ε_{FRP1} = -3.5/5 at n_{bal} =0.244. Below the line for $\varepsilon_{c,2}$ / ε_{FRP1} = -3.5/5, there is a tension failure region which must be addressed separately, because the universal interaction curve assumes unlimited tensile strain in FRP reinforcement. A capacity curve for tensile failure is added accordingly, parallel to the curve for ω' = 0 below the balance point C, to the diagram as line AC.

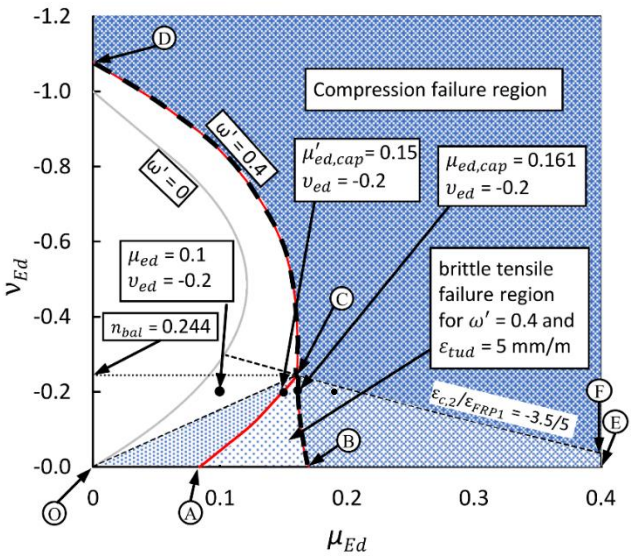


Fig. 5.3. Typical lines and regions in the universal interaction diagram

The region OACD in Fig. 5.3 indicates cross-sections without failure. The strains in Table 5.1 for a design point μ_{Ed} = 0.102, ν_{Ed}= -0.202 in region OACD are below ε_{cu}= -3.5 mm/m and ε_{tud} = 5 mm/m.

An increased moment $\mu'_{Ed,cap}$ = 0.150 has strains $\varepsilon_{c,2}$= -3.0361 mm/m for concrete and ε_{FRP1} = 5 mm/m for the tension FRP reinforcement. At a moment level of $\mu_{Ed,cap}$ = 0.162, the concrete strain reaches the strain limit of concrete with increased tension strains of the reinforcement.

Assuming a load increase and a linear relationship between ν_{Ed} and μ_{Ed} by first-order eccentricity for the design point above the OC line such as for μ_{Ed} = 0.102, ν_{Ed}= -0.202, with second-order effects being negligible, the point will shift along a line from the diagram's origin through itself until it touches the CD line, where concrete compression failure occurs. Here, OC is the line which joins origin with the balance point on the interaction diagram. Points on the line OC for a given design load and moment ratio (ν_{Ed}, μ_{Ed}) will move along this line as the load increases, reaching the balance point. Points in the region OAC will reach tension failure with an increasing design load. The region OAC is possible for design, but increasing loads or moments could lead to brittle tension failure. Points in the ABC region have a tension failure. In region BEFC, there is a mixed failure where the concrete and reinforcement strain exceed the limit. The region above the DCF line designates a compression failure. The tension failure for FRP-RC columns is not desirable for design due to sudden brittle rupture of FRP bars [10]. Hence, for FRP-RC columns to avoid the sudden failure, it is preferable to utilize the ductility available from concrete and its confinement due to stirrups [11]. The compressive failure of concrete for FRP-RC columns was found to be more gradual and less catastrophic in the literature [12]. Therefore, region OCD is recommended for design.

Table 5.1. Maximum compressive concrete strains $\varepsilon_{c,2}$ and strains ε_{FRP1} of FRP reinforcement for different normalized mechanical reinforcement ratio ω' and normalized design moment μ_{Ed} for N_{Ed} = -500 kN using INCA2 [13]

ω' [-]	ρ [%]	ν_{Ed} [-]	M_{Ed} [kNm]	μ_{Ed} [-]	$\varepsilon_{c,2}$ [mm/m]	ε_{FRP1} [mm/m]
0.14	1.00	-0.198	75.734	0.100	-2.3276	4.4414
0.14	1.00	-0.198	78.125	0.103	-2.5438	5.0000
0.14	1.00	-0.198	87.559	0.116	-3.5000	7.2402
0.4	2.83	-0.202	75.734	0.102	-1.5095	1.9334

0.4	2.83	-0.202	111.770	0.150	-3.0361	5.0000
0.4	2.83	-0.202	120.270	0.162	-3.5000	5.7914
0.9	6.37	-0.209	75.734	0.105	-1.1685	1.0518
0.9	6.37	-0.209	165.87	0.231	-3.500	4.6844

5.5 Universal interaction diagrams for the design of slender columns

Several types of diagrams are available to simplify the design of slender steel-reinforced RC columns according to Eurocode 2 [5], such as the normalized load (N)-moment (M) interaction curves for various slenderness ratios based on the nominal curvature equation, nomograms [14], μ-nomograms [15] and e/h diagrams [15]. The presented concept of universal interaction curves can also be used for different slenderness ratios λ using the equations of the nominal curvature method [2] for FRP-RC columns, as shown for different slenderness ratios $\lambda = 40, 60, 80$ in Fig. 5.4, 5.5, 5.6. The strain lines for $\varepsilon_{c,2}$ and ε_{FRP1} are taken from the diagram for the cross-section analysis. These strains belong to the moment capacity M_{cs} of the cross-section for a given N_{Ed}. As the equations for the nominal curvature method [2] for FRP-RC are derived and regressed considering a permissible tensile strain of ε_{FRP1} = 10 mm/m, the area below the $\varepsilon_{c,2} \,/\, \varepsilon_{FRP1} = -3.5 \,/\, 10$ line should not be used for the design. Furthermore, it is recommended to design for compression failure above a given $\varepsilon_{c,2} \,/\, \varepsilon_{FRP1}$ with the $\varepsilon_{FRP1} = \varepsilon_{tud}$. To avoid a stability-prone failure and to design more towards a bending failure, a minimum eccentricity ratio of $e_0 \,/\, h$ = 0.1 is recommended to design slender FRP-RC columns and shaded gray in Fig. 5.4. Here, e_0 is the first-order eccentricity. Furthermore, the nominal curvature equations for FRP-RC columns developed by Syed and Goldack [2] considered an exponential behavior of nominal curvature also for the low $e_0 \,/\, h$ ratios. They observed a very good correlation of the nominal curvature of FRP-RC column with exponential behavior for all values of $e_0 \,/\, h$ ratios except for very low $e_0 \,/\, h$. Bujotzek and Waldmann [4] also observed the exponential behaviour of the curvature of the FRP-RC column at cross-section failure. However, as shown by Syed and Goldack [2], as $e_0 \,/\, h$ decreases, the column behavior shifts from bending to pure compression, the actual nominal curvature also reduces and it is not essentially exponential. Furthermore, they considered a range of $e_0 \,/\, h$ ratio starting from 0.033,

which is the minimum eccentricity ratio required by Eurocode 2 [5]. Hence, their equations are conservative for low e_0 / h ratios. Due to the exponential behavior and the conservativeness of the regressed equation for low e_0 / h ratios, for higher slenderness ratios of λ = 80, where the conservativeness is even higher, a pivot can be observed in Fig. 5.6 where higher ω' curves cross each other in the upper region with low e_0 / h. However, setting a limit of e_0 / h = 0.1 for FRP-RC columns as a minimum eccentricity limit for effective application of nominal curvature equations for simplified analysis presented by Syed and Goldack [2], avoids such pivot regions observed for FRP-RC columns. This limit of e_0 / h = 0.1 is also considered for steel-RC columns for the curves presented in DAfStb-Heft 525 [16], which suggests that for e_0 / h < 0.1, the simplified model column approach with the given steel-RC nominal curvature equations becomes inefficient or too conservative for such values of e_0 / h ratios.

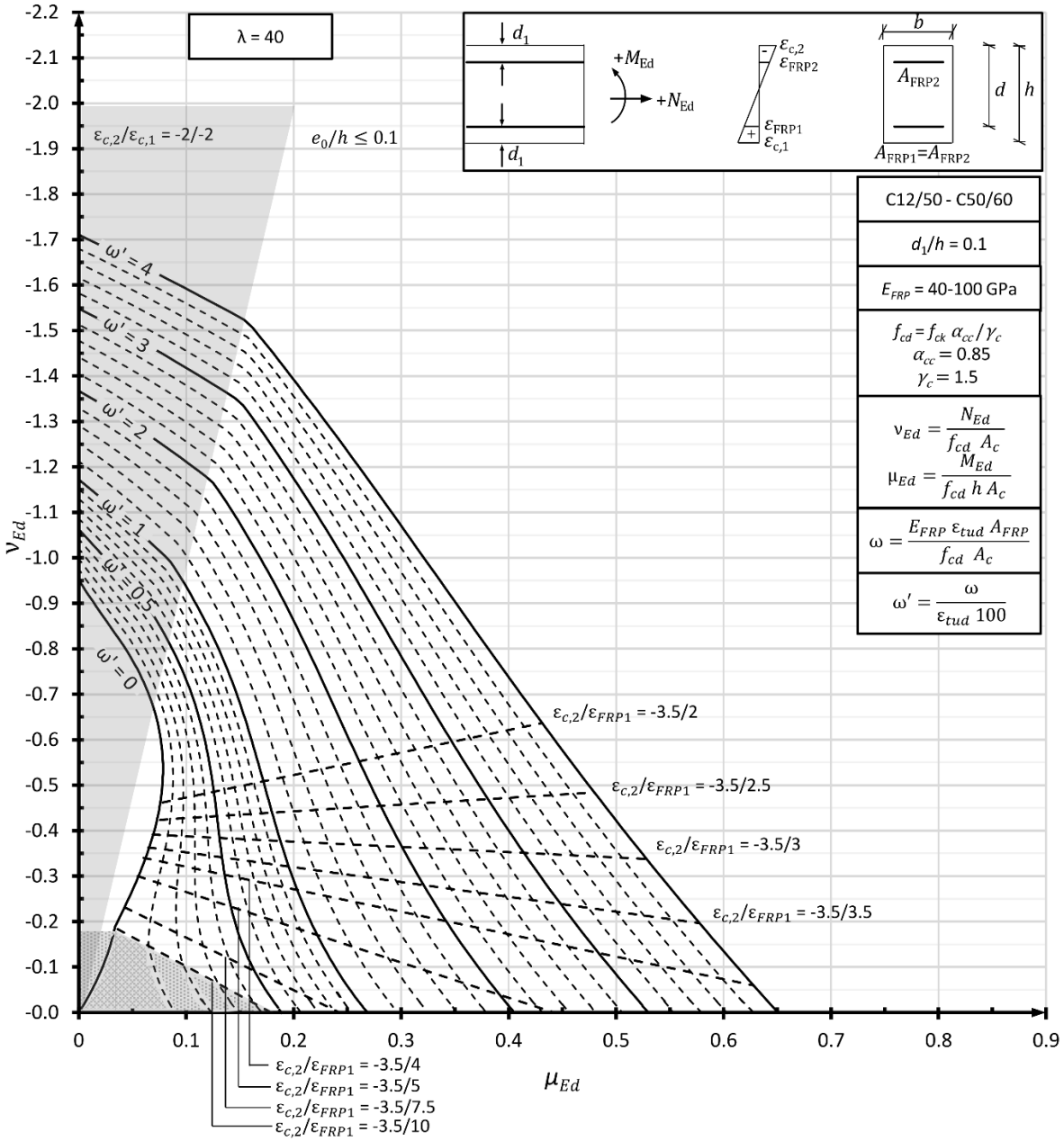


Fig. 5.4. Universal interaction diagram based on nominal curvature method for $\lambda = 40$ (strains in mm/m)

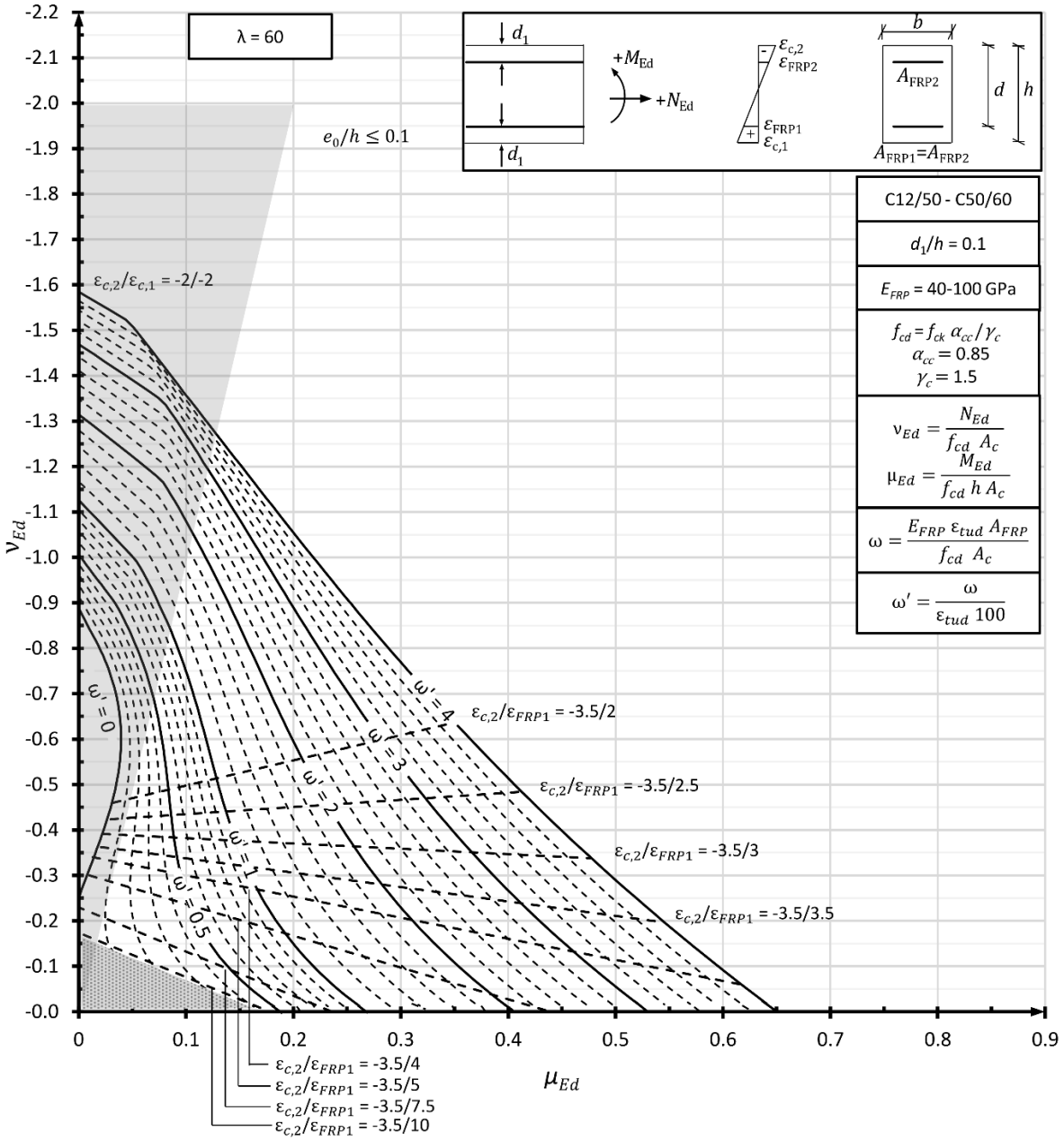


Fig. 5.5. Universal interaction diagram based on nominal curvature method for $\lambda = 60$ (strains in mm/m)

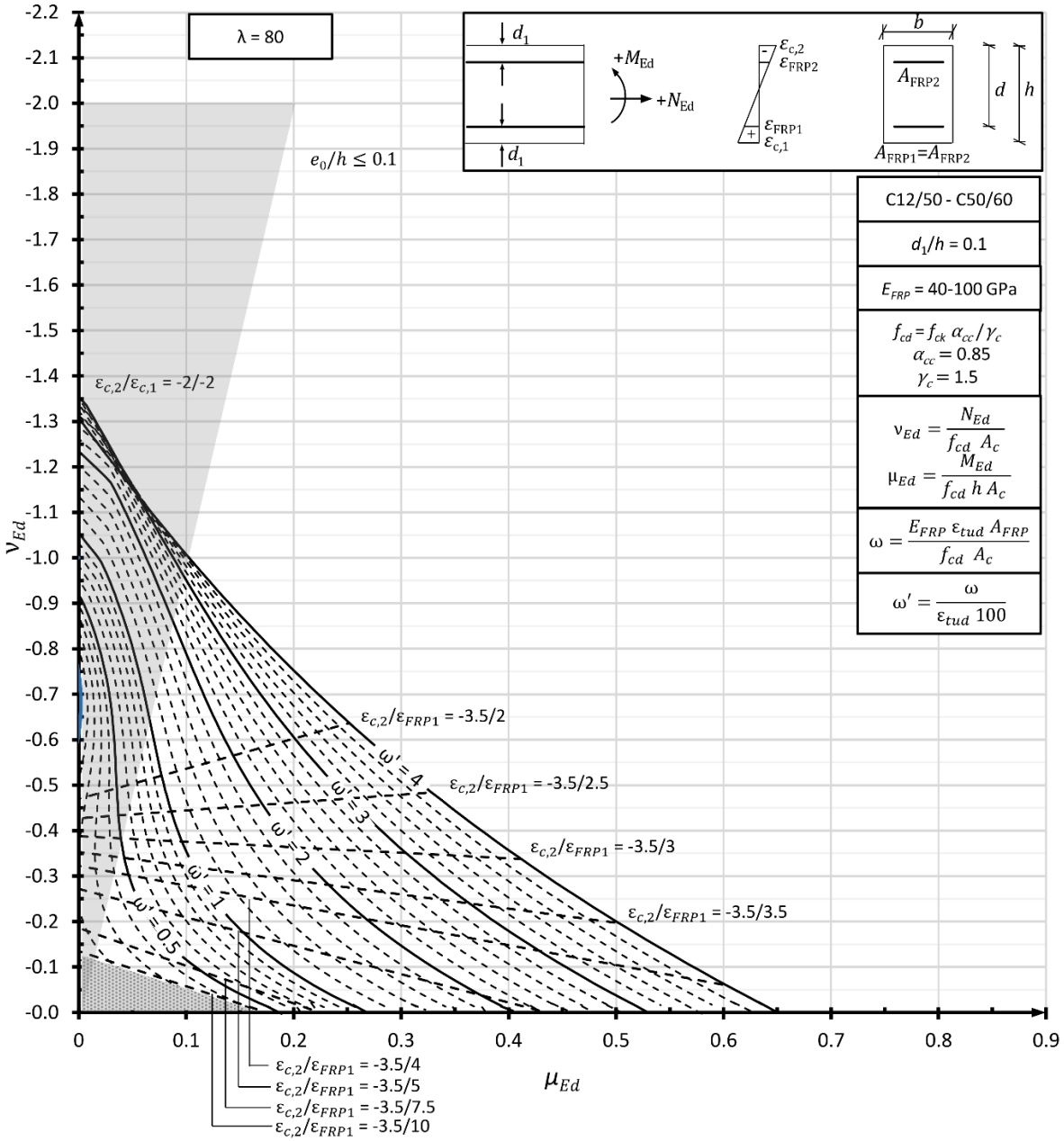


Fig. 5.6. Universal interaction diagram based on nominal curvature method for $\lambda = 80$ (strains in mm/m)

5.6 Examples

This paper presents three examples to illustrate the steps involved in analyzing and designing FRP-RC columns. The first and second examples consider short columns, while the third example considers a slender column. The first and third examples consider an ultimate design strain (ε_{tud}) of 10 mm/m for

the FRP bar, while the second example considers an ultimate tensile strain (ε_{tud}) of 5 mm/m. In all the examples, the columns are considered as simply supported. They are subjected to equal and opposite first-order end moments such that they are bent in single curvature as shown in Fig. 5.7. A rectangular cross-section with corner reinforcements as shown in Fig. 5.7 is considered for all the examples.

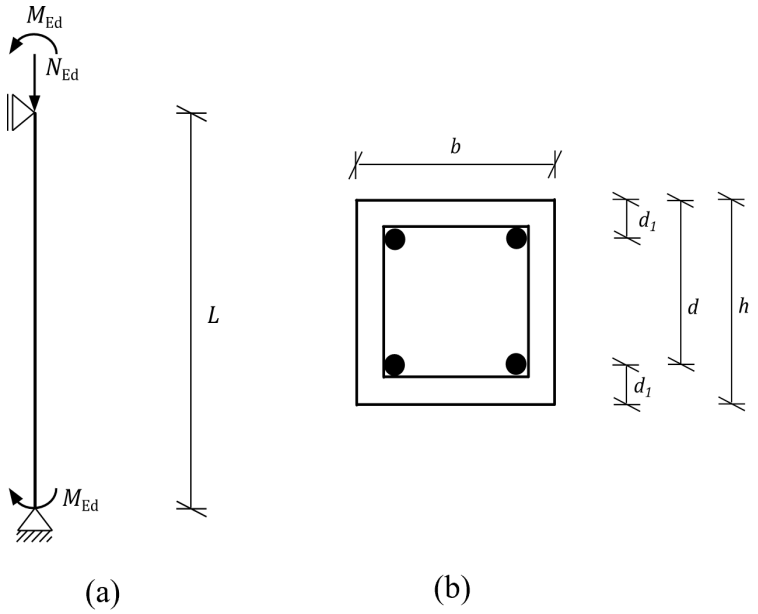


Fig. 5.7. Column details: (a) system (b) cross-section with reinforcement

The general input parameters are detailed in Table 5.2.

Table 5.2. Details of the input parameters for the examples

Details	Values
Width of the column cross-section (b)	= 300 mm
Depth of the column cross-section (h)	= 300 mm
Ratio of effective concrete cover to the depth (d_1/h)	= 0.1
Characteristic concrete compressive strength (f_{ck})	= 50 MPa (C50/60)
Design concrete compressive strength (f_{cd})	= 28.33 MPa
Length of the column (L)	
Example I, II:	= 1000 mm

Example III:	= 3436 mm
Modulus of elasticity of FRP bar (E_{FRP})	= 40 GPa
Ultimate design strain of FRP bar (ε_{tud})	
Example I, III:	= 10 mm/m
Example II:	= 5 mm/m
Design load (N_{Ed})	= - 500 kN
Design moment (M_{Ed})	= 75 kNm

5.6.1 Example I: Short column design using universal interaction curves with ε_{tud} = 10 mm/m

The first step is to identify whether the column is a short column or a slender column using Eq. (5.1). This requires calculating the non-dimensional axial force (n). To calculate (n), the net area of concrete (A_c) is required. It must be noted that the normalized design load (ν_{Ed}) in the universal interaction diagram equals to the design non-dimensional axial force (n) for the slenderness limit and nominal curvature method.

A reinforcement ratio (ρ) of 1% is assumed as the first iteration. Further steps to evaluate the parameters required for analysis using universal interaction diagrams are detailed in Table 5.3.

Table 5.3. Calculation of the parameters for Example I

Details	Formula	Values
Total area of cross-section (A)	= 300 x 300	= 90000 mm^2
Net area of concrete (A_c)	= $A/(\rho/100 + 1)$	= 89108.91 mm^2
Normalized design load (ν_{Ed})	= $N_{Ed}/A_c f_{cd}$	= - 0.20
Normalized design moment (μ_{Ed})	= $M_{Ed}/A_c f_{cd} h$	= 0.10
Slenderness ratio of the column (λ)	= $\sqrt{12}\, L/h$	= 11.54
Slenderness limit using Eq. (5.1) (λ_{lim})	= $17\, n^2 + 19$ $(n \leq 0.4)$	= 19.68

As $\lambda < \lambda_{lim}$, the column is considered as a short column.

Although the net area of concrete (A_c) is used to normalize the load and the moment for the universal interaction diagram, a useful simplification for the practical design is to design for the total cross-section area (A) resulting in ν_{Ed}= -0.196 and μ_{Ed}= 0.0981.

The given design load and moment result in a design point on the universal interaction curve with normalized design load of $\nu_{Ed} = -0.196 \approx -0.20$ and the normalized design moment of $\mu_{Ed} = 0.0981 \approx 0.10$. This point is marked on the uniform interaction diagram in Fig. 5.8. A value for ω' is chosen for the design of the cross-section such that the point lies on the left of the universal interaction curve. In this example, the value of $\omega' = 0.14$ was chosen to achieve a reinforcement ratio of 1% and to ensure comparability with other examples, although ω' is slightly higher than necessary. The reinforcement ratio (ρ) is calculated using the mechanical reinforcement ratio $\omega = \omega' \varepsilon_{tud}\, 100$ with $\omega' = 0.14$ as follows

$$\rho = \frac{f_c}{E_{FRP}\, \varepsilon_{tud}} \omega = 0.01 \tag{5.17}$$

For ω' = 0.14, the given value of the normalized load capacity of ν_{Ed} = -0.2 and the normalized design moment of $\mu_{Ed} = 0.1$, Table 5.1 provides the associated concrete strains and tensile strains of the reinforcement. The design point lies in the compression-controlled region as it is greater than the balanced load ratio (n_{bal}) and is also in the permitted region OCD. Hence, it is not required to add the capacity curve for tension failure and the universal interaction curve can be easily used. The normalized moment capacity $\mu_{Ed,cap} = 0.12$ is read from the universal interaction curve (Fig. 5.8) for the given value of the normalized load capacity (ν_{Ed}) = -0.2. The exact value from the database used to develop Fig. 5.1 is $\mu_{Ed,cap} = 0.116$. The cross-section moment capacity (M_{cs}) at the design load capacity level (N_{ed}) for the given value of reinforcement ratio is calculated with $\mu_{Ed,cap} = 0.116$ to $M_{cs} = \mu_{Ed,cap}\, A_c\, f_c\, h = 87.85$ kNm $\geq M_{ed}$ and the utilization as $M_{Ed}/M_{cs} = 0.85$. For $\mu_{Ed} = 0.12$, the utilization of 0.82 is slightly lower. A cross-section analysis by the free software INCA2 [13] gives a reinforcement strain $\varepsilon_{FRP1} = 7.2402$ mm/m for M_{cs} according to Table 5.1 and confirms that the assumed value of the reinforcement ratio (ρ) of 1% is sufficient for the required capacity. Here, the use

of software INCA2 to develop Table 5.1 also cross-verifies the procedure used in this paper for cross-section analysis based on [1] to develop universal interaction diagrams for the cross-section.

Furthermore, if a normalized mechanical reinforcement ratio of $\omega' = 0.1$ is considered for this example, the reinforcement ratio is $\rho = 0.7$ % and the moment capacity calculates to $M_{cs} = 80.73$ kNm, which is still greater than M_{Ed}, resulting in a utilization of 0.93.

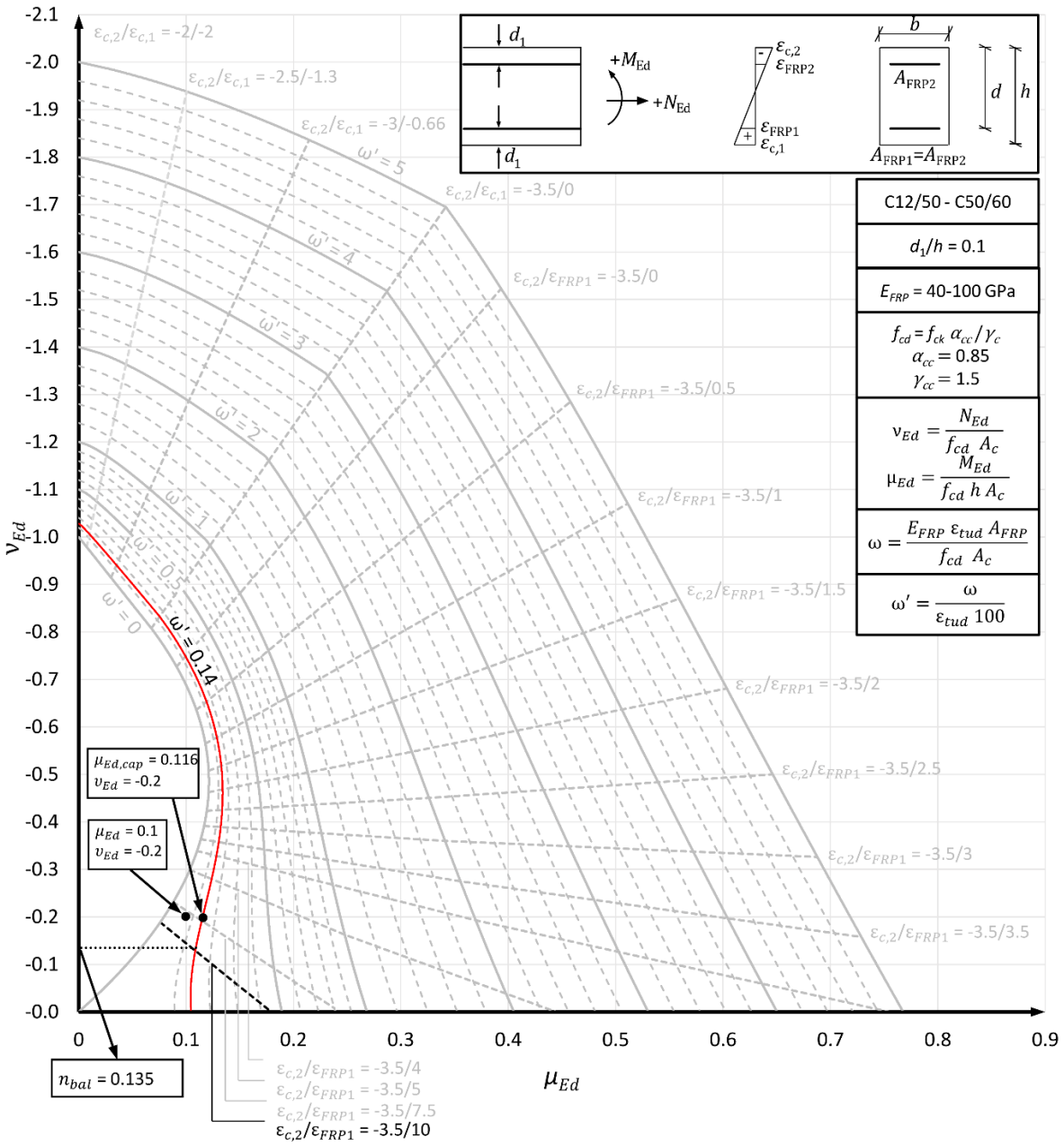


Fig. 5.8. Universal interaction curve for $\omega' = 0.14$ and $\varepsilon_{tud} = 10$ mm/m (Example I)

5.6.2 Example II: Short column design using universal interaction curves with ε_{tud} = 5 mm/m

In Example II, the design value of ultimate tensile strain of the FRP reinforcement is reduced to ε_{tud} = 5 mm/m and marked in Fig. 5.9 with the dashed line for $\varepsilon_{c,2}$ / ε_{FRP1} = -3.5 / 5. The point of normalized design load and moment is marked again at ν_{Ed} = -0.2 and μ_{Ed} = 0.1. The reinforcement ratio of ρ = 1% has the same normalized mechanical reinforcement ratio of ω' = 0.14. For ω' = 0.14, the given value of the normalized load capacity (ν_{Ed}) = -0.2 is smaller than the balanced load ratio (n_{bal}) corresponding to ε_{tud} = 5 mm/m as seen in Fig. 5.9. Furthermore, the point of normalized design load and moment capacity lies in the tension failure region below n_{bal}. Hence, it is important to add the capacity curve for the tensile failure region in the diagram of the universal interaction curve.

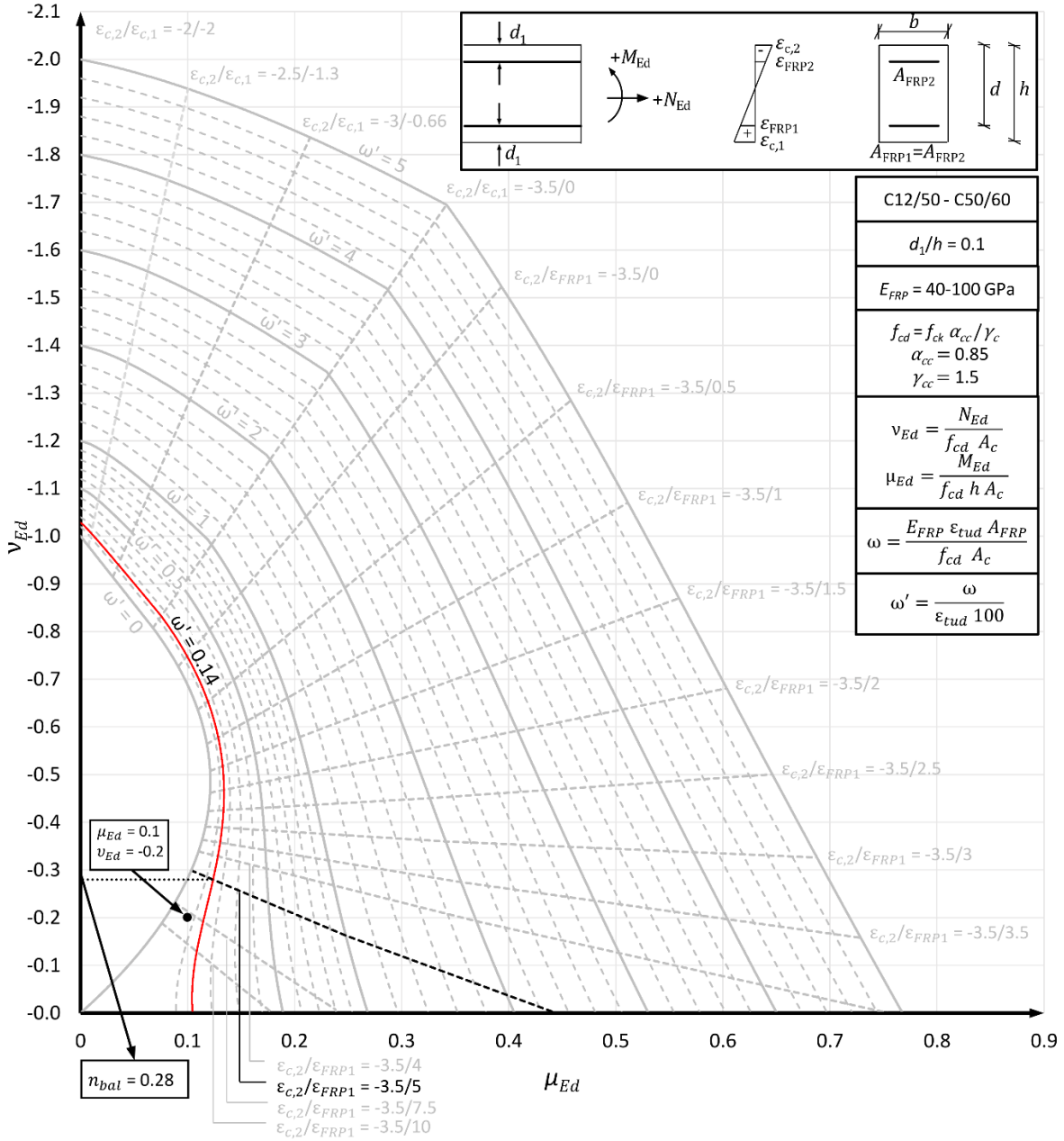


Fig. 5.9. Universal interaction curve for ω' = 0.14 and ε_{tud} = 5 mm/m (Example II)

The capacity curve for the tension failure region for ω' = 0.14 and ε_{tud} = 5 mm/m is drawn parallel to ω' = 0 as discussed earlier and shown in Fig. 5.10.

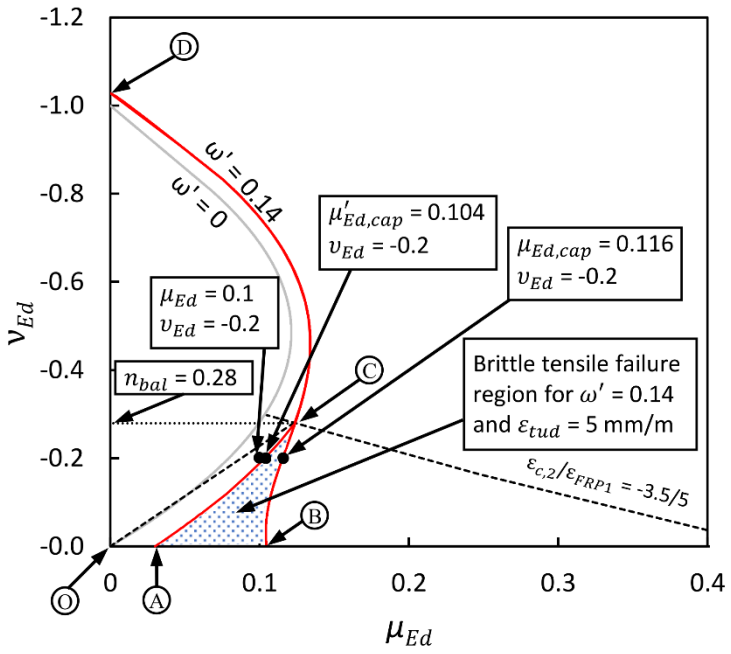


Fig. 5.10. Universal interaction curve and capacity curve for tension failure for ω' = 0.14 and ε_{tud} = 5 mm/m using the universal interaction curve of $\omega' = 0$ (Example II)

For the normalized design load ν_{Ed} = -0.2, three points are marked in Fig. 5.10 and discussed in the following. The accompanying strains are listed in Table 5.1.

The point of normalized design load and moment (ν_{Ed} = -0.2, μ_{Ed} = 0.1) lies left of the capacity curve for tension failure (AC). The normalized moment capacity ($\mu'_{Ed,cap}$) is read from the load-moment capacity curve for the constant value of the normalized design load (ν_{Ed}) = -0.2 as $\mu'_{Ed,cap} = 0.10$, where the exact value from the database used to develop Fig. 5.10 is 0.104. The cross-section moment capacity (M_{cs}) at the design load capacity level for the given value of reinforcement ratio and the exact value of 0.104 is calculated as $M_{cs} = \mu'_{Ed,cap}\, A_c\, f_c\, h = 78.76$ kNm $\geq M_{Ed}$. The design has a utilization of $M_{Ed}\ /\ M_{cs}\ = 0.95$. Hence, the assumed value of the reinforcement ratio (ρ) of 1% is sufficient for the required design load and moment.

A small increase in the design moment at constant load or a linear increase in load and moment would lead to a brittle tension failure, because in the blue dotted region ABC, the failure of the cross-section is caused by exceeding the limit strain of the FRP reinforcement. The point on the universal interaction

curve CB at ν_{Ed} = -0.2 and $\mu_{Ed,cap} = 0.116$ has concrete strain $\varepsilon_{c,2}$ of -3.5 mm/m at the outer edge and FRP reinforcement tension strain ε_{FRP1} of 7.2402 mm/m > ε_{tud}.

Two options to accomplish the design are discussed here, besides changing the concrete cross-section or the concrete strength for higher values of the normalized design load ν_{Ed}. As the first option, the design point is shifted in the permitted design region of OCD, however, below the balanced load ratio (n_{bal}) shown in Fig. 5.11(a) by increasing the normalized mechanical reinforcement from $\omega' = 0.14$ to $\omega' = 0.4$, gaining more safety against tension failure. As the second option, the design point is shifted in the permitted design region of OCD above the balanced load ratio (n_{bal}) with a large increase from $\omega' = 0.14$ to $\omega' = 0.9$ as shown in Fig. 5.11(b).

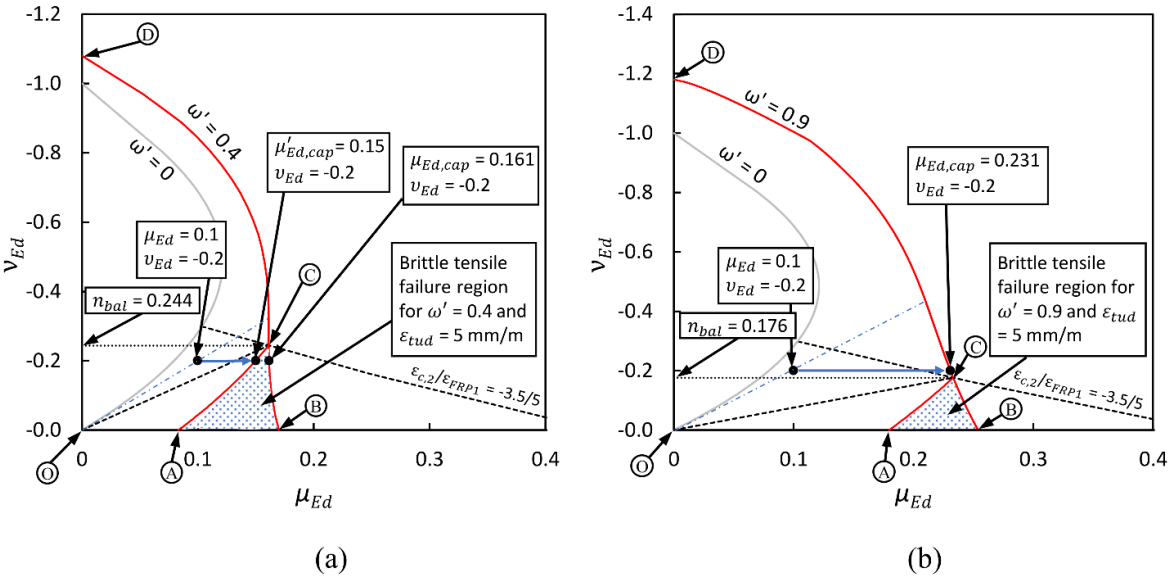


Fig. 5.11. Shifting of design load and moment capacity in the permitted design region OCD while (a) $n < n_{bal}$ (b) $n > n_{bal}$ (Example II) for $\varepsilon_{tud} = 5$ mm/m

For the first option with $\omega' = 0.4$, M_{cs} is calculated as: $\rho = 2.83\ \% < 8\ \%$ (as per Eurocode 2) with $A_c = A/\left((\rho/100) + 1\right) = 87523.1$ mm^2, $\nu_{Ed} = N_{Ed}/A_c f_{cd} = 0.20$ and $M_{cs} = \mu'_{Ed,cap}\, A_c\, f_c\, h = 111.57$ kNm $\geq M_{Ed}$. The utilization of the cross-section is $M_{Ed}\ /\ M_{cs} = 0.67$.

For the second option with ω' = 0.9, M_{cs} is calculated as: ρ = 6.36 % < 8 % (as per Eurocode 2) with $A_c = A/\left((\rho/100)+1\right)$ = 84612.31 mm^2 , $\nu_{Ed} = N_{Ed}/A_c f_{cd}$ = -0.20 and $M_{cs} = \mu_{Ed,cap}\, A_c\, f_c\, h =$ 166.10 kNm $\geq M_{Ed}$. The utilization of the cross-section is $M_{Ed}\ /\ M_{cs}\ = 0.45$.

The first option with ω' = 0.4 is more economical in terms of reinforcement cross-section. However, if the load eccentricity increases, as in the case of moment redistribution in frames, the failure may turn out to be a brittle tension failure. While for the second option with ω' = 0.9, the failure would most likely be a compression failure of concrete, but less economical. The design point for the second option lies in the region above the balance point in the permitted design region, OCD. This region is recommended for design as failure would be compression-controlled in this region also due to an accidental increase of load or moment. Henceforth, the region above the balance point in OCD is referred to as the compression-controlled failure region. The reinforcement ratio is increased for the second option by a factor of around 6.4 in comparison to the reinforcement ratio for the FRP with ε_{tud} = 10 *mm/m* seen in Example I. This shows that to keep the FRP-RC column design within the compression-controlled failure region for low design loads, the reinforcement ratio has to be increased significantly. This requires setting the reinforcement ratio at a high level. Furthermore, when design moment values are low, section moment capacity utilization is also low. For example, the second option utilizes only 45% of the section moment capacity. However, a higher value of reinforcement may also be required to satisfy the requirements of deflection due to service loads. This may be checked separately while performing the serviceability checks.

As an alternative to the two options presented here for changing the reinforcement ratio, reducing the cross-section or concrete strength would increase the normalized design load above the balance point, thereby shifting the design point into the region of compression-controlled failure recommended for design purposes.

5.6.3 Example III: Slender column design using universal interaction curves with ε_{tud} = 10 mm/m

5.6.3.1 Application of the nominal curvature method and the universal interaction diagram for cross-section design

In this example, all the input parameters remain the same as in Example I, except the length of the column (L) = 3436 mm. Similar to Example I, a reinforcement ratio (ρ) of 1% is assumed as the first iteration. Furthermore, for slender columns, the reinforcement ratio influences the amount of the second-order moments. Therefore, the design is iterative.

Slenderness ratio of the column (λ) $= \sqrt{12}\, L/h$ = 40

As $\lambda > \lambda_{lim}$, the column is considered a slender column.

Similar to Example 1, the design starts with an assumption of $\omega = \omega'$ = 0.14 from the universal interaction diagram in Fig. 5.3. The total design moment ($M_{tot,d}$), including second-order effects, is required to design for a slender column. In this example, the total design moment is calculated using the nominal curvature approach for FRP-RC columns presented by Syed and Goldack [2] and further presented as a proposal for Eurocode 2 [6] using the universal interaction diagram in Fig. 5.1.

Iteration 1:

For ω' = 0.14, the given value of the normalized load capacity (ν_{Ed}) = -0.2 lies in the compression-controlled region as it is greater than the balanced load ratio (n_{bal}) point corresponding to ε_{tud} = 10 mm/m. Hence, it is not required to develop the capacity curve for the tension failure and the universal interaction curve can be easily used. The strain line with $\varepsilon_{c,2}$ = -3.5 mm/m and ε_{FRP1} = 10 mm/m intersects the universal interaction curve for ω' = 0.14. Further, in this case with ε_{tud} = 10 mm/m, this point of intersection is the balance point. Hence Eq. (5.13) gives

$$\frac{1}{r_0} = \frac{0.0035 + 0.01}{270} = 5 \times 10^{-5}\ \text{mm}^{-1} \tag{5.18}$$

As shown in Fig. 5.8 for ω' = 0.14, n_{bal} is read from the universal interaction curves as

$n_{bal} = 0.135$. Using Eq. (5.10) while taking ε_{c2} = -2 mm/m for the concrete strain at the peak compressive stress, n_u is calculated as $n_u = 1.028$. Further using Eq. (5.6) and (5.5) with $n = |\nu_{Ed}|$= -0.2 gives

$$n_r = \frac{n - n_{bal}}{n_u - n_{bal}} = \frac{0.2 - 0.135}{1.028 - 0.135} = 0.073 \tag{5.19}$$

$$C_k = 2.32 + 0.0064\,\lambda - 0.0051\frac{\omega}{\varepsilon_{tud}} = 2.32 + 0.256 - 0.071 = 2.505. \tag{5.20}$$

k_{r} is calculated using Eq. (5.4) as,

$$k_{\mathrm{r}} = e^{-(C_k \cdot n_r)} = e^{-(2.505 \times 0.073)} = 0.833. \tag{5.21}$$

Considering $k_{\varphi,\mathrm{FRP}} = 1$, the nominal curvature is calculated using Eq. (5.3) as

$$\frac{1}{r} = k_{\mathrm{r}} \cdot k_{\varphi,\mathrm{FRP}} \cdot \frac{1}{r_0} = 0.833 \times 1 \times 5 \times 10^{-5} = 4.1652 \times 10^{-5}\ \mathrm{mm}^{-1} \tag{5.22}$$

The cross-section moment capacity (M_{cs}) at the design load capacity level is calculated using $\mu_{Ed,cap} = 0.116$ from the universal interaction curve for ω' = 0.14 and $n = |\nu_{Ed}|$= -0.2 as, $M_{cs} = \mu_{Ed,cap}\, A_c\, f_{cd}\, h = 87.86$ kNm. Further e_{cs} is calculated using Eq. (5.12) as,

$$e_{cs} = \frac{M_{cs}}{|N_{\mathrm{Ed}}|} = \frac{87.86 \times 10^3}{500} = 175.72\ \mathrm{mm} \tag{5.23}$$

The first-order curvature distribution factor (c_I) is considered as 8, which corresponds to a uniform moment distribution. The total curvature distribution factor is calculated using Eq. (5.11) as,

$$c = c_I + \frac{1}{r}\frac{L^2}{\pi^2}\frac{1}{e_{cs}}(\pi^2 - c_I) = 8 + (4.2 \times 10^{-5})\left(\frac{3436}{\pi}\right)^2\left(\frac{1}{175.7}\right)(\pi^2 - 8) = 8.53 \tag{5.24}$$

$M_{tot,d}$ is calculated using Eq. (5.2) as,

$$M_{tot,d} = M_{Ed} + N_{Ed}\left(\frac{L^2}{c}\right)\frac{1}{r} = (75 \times 10^6) + (500 \times 10^3)\left(\frac{3436^2}{8.53}\right)(4.1652 \times 10^{-5}) = 103.82\ \mathrm{kNm} \tag{5.25}$$

As $M_{tot,d} > M_{cs}$, the cross-section moment capacity is not sufficient in comparison to the total moment caused due to second-order effects. Further to check the first-order moment capacity (M_I) of the column with $\omega = \omega' = 0.14$ and $n = 0.2$, $M_{tot,d}$ is replaced with M_{cs} and M_{Ed} is replaced with the first-order moment capacity (M_I) of the column at a given design load (N_{Ed}) in Eq. (5.2) and rewritten as,

$$M_{cs} = M_I + N_{Ed}\left(\frac{L^2}{c}\right)\frac{1}{r} \tag{5.26}$$

M_I is calculated using Eq. (5.26) as

$$M_I = M_{cs} - N_{Ed}\left(\frac{L^2}{c}\right)\frac{1}{r} = (87.86 \times 10^6) - (500 \times 10^3)\left(\frac{3436^2}{8.53}\right)(4.1652 \times 10^{-5}) = 59.04 \text{ kNm} \tag{5.27}$$

But the required moment capacity is 75 kNm. Therefore, the $\omega = \omega' = 0.14$ is not sufficient for the required design moment at the design axial load level.

Iteration 2:

Satisfying the design requirement, the total design moment shall be $M_{tot,d} \leq M_{cs}$ would also make $M_I \geq M_{Ed}$. Further iterations are made by increasing the ω'so as to satisfy this requirement. In this example, for the next iteration, $\omega' = 0.4$ is considered. Using the universal interaction diagram and nominal curvature equations (Eq. 5.2 to 5.12) as shown previously in this example, the following is calculated as,

$$\frac{1}{r_0} = \frac{0.0035 + 0.01}{270} = 5 \times 10^{-5} \text{ mm}^{-1} \tag{5.28}$$

The value for n_{bal} is taken from the cross-section analysis with $n_{bal} = 0.019$ and $n_u = 1.08$

$$n_r = \frac{n - n_{bal}}{n_u - n_{bal}} = \frac{0.2 - 0.019}{1.08 - 0.019} = 0.1706 \tag{5.29}$$

and

$$C_k = 2.32 + 0.0064\,\lambda - 0.0051\frac{\omega}{\varepsilon_{tud}} = 2.32 + 0.256 - 0.204 = 2.372 \tag{5.30}$$

$$k_{\mathrm{r}} = e^{-(C_k \cdot n_r)} = e^{-(2.372 \times 0.1706)} = 0.6672 \tag{5.31}$$

and $k_{\varphi,\mathrm{FRP}} = 1$,

$$\frac{1}{r} = k_{\mathrm{r}} \cdot k_{\varphi,\mathrm{FRP}} \cdot \frac{1}{r_0} = 0.6672 \times 1 \times 5 \times 10^{-5} = 3.336 \times 10^{-5}\ \mathrm{mm}^{-1} \tag{5.32}$$

With $\mu_{Ed,cap} = 0.161$ from the universal interaction curve for $\omega' = 0.4$ and $n = |\nu_{Ed}| = 0.2$, M_{cs} is calculated as $M_{cs} = \mu_{Ed,cap}\, A_c\, f_{cd}\, h = 119.78$ kNm.

Further,

$$e_{cs} = \frac{M_{cs}}{|N_{\mathrm{Ed}}|} = \frac{119.78 \times 10^3}{500} = 239.6\ \mathrm{mm} \tag{5.33}$$

$$c = c_I + \frac{1}{r}\frac{l_0^2}{\pi^2}\frac{1}{e_{cs}}(\pi^2 - c_I) = 8 + (3.336 \times 10^{-5})\left(\frac{3436}{\pi}\right)^2\left(\frac{1}{239{,}6}\right)(\pi^2 - 8) = 8.3113 \tag{5.34}$$

$$M_{tot,d} = M_{Ed} + N_{Ed}\left(\frac{L^2}{c}\right)\frac{1}{r} = (75 \times 10^6) + (500 \times 10^3)\left(\frac{3436^2}{8.3113}\right)(3.336 \times 10^{-5}) = 98.6937\ \mathrm{kNm} \tag{5.35}$$

$$M_I = M_{cs} - N_{Ed}\left(\frac{L^2}{c}\right)\frac{1}{r} = (119.78 \times 10^6) - (500 \times 10^3)\left(\frac{3436^2}{8.3113}\right)(3.336 \times 10^{-5}) = 96.0863\ \mathrm{kNm} \tag{5.36}$$

As $M_{tot,d} \leq M_{cs}$ and also $M_I \geq M_{Ed}$, the $\omega' = 0.4$ is sufficient for the given design load and moment.

5.6.3.2 Application of universal interaction diagrams for slender FRP-RC column

The universal interaction diagram for a slender FRP-RC column with a slenderness ratio of $\lambda = 40$ in Fig. 5.4 is used to design the column of Example III. The cross-sectional area of the concrete, $A_c =$ 87523.1 mm² for $\omega' = 0.4$ ($\rho = 2{,}83\%$) from Example III is taken as a starting point. The normalized load calculates to $\nu_{Ed} =$ -0.2 and the required first order moment M_0=75 kNm is μ_{Ed}= 0.10. Fig. 5.4 shows that $\omega' = 0.25$ already provides a safe design. With $\varepsilon_{tud} = 10$ mm/m the reinforcement ratio becomes $\rho = \omega'\, f_{cd}\, /\, (E_{FRP}\, \varepsilon_{tud}) = 0.25 \cdot 28.33/(40000 \cdot 0.01) = 1.8$ %.

5.7 Conclusions

1. Universal interaction diagrams, independent of the modulus of elasticity E_{FRP} and ultimate tensile strain ε_{tud} of the FRP reinforcement, were introduced for designing FRP-RC cross-sections with compressive force and bending moment. The normalized mechanical reinforcement ratio ω' is introduced in place of the conventional mechanical reinforcement ratio ω.
2. A universal interaction diagram as Fig. 5.1 for rectangular cross-section design for effective concrete cover to the depth $(d_1/h) = 0.1$ with reinforcement distributed on two sides, was presented for practical application. This curve is a valuable addition to the design of short FRP-RC columns and of cross-sections with *N-M* interaction, as no such curves are available in the literature for all types of FRP reinforcement. Further, this diagram would facilitate to design slender FRP-RC columns using the equations of the nominal curvature method.
3. For cross-sections and design load-moment combinations in the region of tension failure in the universal interaction diagram, the universal interaction curve for the given ω' must be supplemented with the capacity curve for tension failure. This is achieved for a given value of ε_{FRP1} by drawing a curve parallel to the universal interaction curve for $\omega' = 0$ starting from the balance point on the universal interaction curve corresponding to the given value ε_{FRP1}. If the design point lies to the left of the capacity curve for tension failure, the bearing capacity is verified; however, this design point is not recommended as the failure tends to be a tensile failure of the FRP bar for accidental increase of loads or moments.
4. The concept of universal interaction diagrams was extended for column design for slender columns based on the nominal curvature method according to Syed and Goldack [2]. Fig. 5.4, 5.5 and 5.6 are presented for the design of slender columns with slenderness ratios of λ = 40, 60 and 80. These universal interaction diagrams simplify the design of slender FRP-RC columns and avoid the iteration of the cross-section design while using nominal curvature equations. These diagrams are an important and useful practical contribution, especially given that no such curves are currently available in the literature.

5.8 Data availability statement

All data that support the findings of this study are available from the corresponding author upon reasonable request.

5.9 Acknowledgements

The authors would like to gratefully acknowledge the funding support provided by the German Academic Exchange Service (DAAD) to pursue this research work.

5.10 Notation

The following symbols are used in this paper:

A = total area of cross-section;
A_c = net cross-section area of concrete without reinforcement;
A_{FRP} = total area of the longitudinal FRP;
b = cross-sectional breadth;
c = total curvature distribution factor;
c_I = first-order curvature distribution factor;
C_k = factor for the shape of the failure surface in the *N-M* interaction diagram;
d = effective depth of a cross-section;
d_1 = effective concrete cover;
e_0 = first order eccentricity;
e_{cs} = eccentricity for the moment capacity of the cross-section for a given design load;
E_{FRP} = modulus of elasticity of FRP bar;
f_c = peak compressive stress of concrete;
f_{ck} = characteristic concrete compressive strength;
f_{cd} = design concrete compressive strength;
h = height of the cross-section;
k_r = coefficient depending on the axial force;
$k_{\varphi,\mathrm{FRP}}$ = coefficient for creep;
L = effective length of the column;
M_{Ed} = first order design moment;
M_{cs} = cross-section moment capacity;
M_I = first-order moment capacity;

$M_{tot,d}$ = maximum total design moment;

n = non-dimensional axial force;

N_{bal} = value of the load at the balance point;

n_{bal} = balanced load ratio;

N_{Ed} = design value of applied axial load;

n_r = normalized load ratio;

n_u = normalized maximum load capacity of the column from cross-sectional analysis;

x_c = neutral axis depth of the cross-section for the moment equal to the moment capacity in pure bending;

ε_{c2} = compressive strain in the concrete at the peak stress f_c of concrete;

$\varepsilon_{c,2}$ = concrete compressive strain of the outermost concrete in the cross-section;

ε_{cu} = maximum compressive strain of concrete;

ε_{FRP1} = tensile strain in FRP reinforcement;

ε_{FRP2} = compressive strain in FRP reinforcement;

ε_{tud} = design ultimate tensile strain of the FRP reinforcement;

λ = slenderness ratio;

λ_{lim} = slenderness limit;

μ_{Ed} = normalized design moment;

$\mu_{Ed,cap}$ = normalized moment capacity from the universal interaction curve;

$\mu'_{Ed,cap}$ = normalized moment capacity from the capacity curve;

ν_{Ed} = normalized design load;

ρ = reinforcement ratio;

ω = mechanical reinforcement ratio;

ω' = normalized mechanical reinforcement ratio;

$\frac{1}{r_0}$ = curvature at maximum moment resistance;

$\frac{1}{r}$ = nominal curvature;

5.11 References

[1] Syed AU, Goldack A. Slenderness limit for GFRP reinforced concrete columns based on axial force ratio. Engineering Structures 2024;298:117026.

[2] Syed AU, Goldack A. Simplified Second-Order Analysis of Slender FRP-Reinforced Concrete Columns Using the Nominal Curvature Method. J. Compos. Constr. 2025;29(2).

[3] Syed AU, Goldack A. Analysis of slender FRP-reinforced concrete columns subjected to unequal end moments. Engineering Structures 2025;340:120768.

[4] Bujotzek L, Waldmann D. Innovative buckling safety verification method for the determination of second-order effects in slender FRP reinforced columns including effects of FRP creep. Engineering Structures 2025;322:119143.

[5] EN 1992-1-1:2004. Eurocode 2: Design of concrete structures - Part 1-1:General rules and rules for buildings(EN 1992-1-1:2004). Brussels: European Committee for Standardisation.

[6] Goldack A, Syed AU, Koehler R. Proposal for the Adjustment of the prEN 1992-1-1:2023 Annex O for the Design of Slender FRP-RC Columns with the Nominal Curvature Method; 2025.

[7] Korentz J, Czarnecki W. Prediction of Ultimate Capacity of Concrete Columns Reinforced with FRP Bars. Polymers 2023;15(5).

[8] Niyazuddin, Umesh B. Analytical load-moment (P-M) interaction diagram for GFRP-reinforced rectangular concrete column in uniaxial bending. Materials Today: Proceedings 2023.

[9] Hosseini AS, Sadeghian P. Evaluation of ACI CODE 440.11-22 design provisions for GFRP - RC columns: Constitutive models and practical interaction diagrams. Structural Concrete 2025.

[10] Hadhood A, Mohamed HM, Benmokrane B, Nanni A, Shield CK. Assessment of Design Guidelines of Concrete Columns Reinforced with Glass Fiber-Reinforced Polymer Bars. ACI Structural Journal 2019;116(4):193–207.

[11] Fib Bulletin 40. FRP reinforcement in RC structures. Stuttgart: The International Federation for Structural Concrete; 2007.

[12] Choo CC, Harik IE, Gesund H. Minimum Reinforcement Ratio for Fiber-Reinforced Polymer Reinforced Concrete Rectangular Columns. SJ 2006;103(3):460–6.

[13] Pfeiffer U. INCA2, Interactive cross-section analysis biaxial; 2002.

[14] Kordina K, Quast U. Bemessung von schlanken Bauteilen – Knicksicherheitsnachweise. In: Betonkalender 1990. Teil I. Berlin: Ernst & Sohn; 1990, p. 489–583.

[15] Kordina K, Quast U. Bemessung von schlanken Bauteilen für den durch Tragwerksverformungen beeinflussten Grenzzustand der Tragfähigkeit – Stabilitätsnachweis. In: Betonkalender 1996. Teil I. Berlin: Ernst & Sohn; 1996, p. 499–566.

[16] DAfStb-Heft 525 – Erläuterungen zu DIN 1045-1. 2nd ed. Berlin, Wien, Zürich: Beuth Verlag GmbH; 2010.

6. Summary and Outlook

6.1 Summary

This thesis comprehensively investigates the structural behavior of slender FRP-RC columns. Numerical methods for the second-order analysis of reinforced concrete columns were developed and successfully implemented. Through an extensive parametric study, design guidelines are developed for FRP-RC columns. By achieving all the objectives established in this research, a complete framework for simplified analysis and design of slender FRP-RC columns consistent with the Eurocode 2 philosophy has been developed. The outcomes of this study have been proposed for incorporation into future European design guidelines and codes. This chapter presents a general summary including the interlinkages between the chapters, conclusions, and outlook.

The interconnection among the chapters of this thesis is structured as follows:

For the design of reinforced concrete columns, it is of interest to determine whether a column behaves as short or slender. For short columns, second-order effects can be safely neglected, and the design is governed solely by material strength. For eccentrically loaded short columns, load–moment interaction is used for cross-sectional analysis. Therefore, **Chapter 2** develops a slenderness limit equation specifically for GFRP-RC columns. Moreover, it is found that the modulus of elasticity of FRP bar does not have a significant effect on slenderness limit of FRP-RC columns. GFRP bars have the lowest value of modulus of elasticity compared to other FRP bars types. Further, with increase in modulus of elasticity of FRP bar, minor increase in slenderness limit is observed at low values of axial force ratio and at higher values of axial force ratio, insignificant change in slenderness limit is seen. Hence, the developed slenderness equations for GFRP-RC columns can be safely and conservatively adopted for FRP-RC column with all kind of FRP bars. Once a column is identified as slender, second-order effects become significant and must be accounted for in the analysis and design. In line with the Eurocode 2 framework, **Chapter 3** develops a nominal curvature method for the simplified second-order analysis of FRP-RC columns. For columns subjected to unequal end moments, an equivalent moment factor is essential for simplified second-order analysis. Therefore, **Chapter 4** examines the applicability of

existing expressions developed for steel-RC columns to FRP-RC columns and proposes a modified expression suitable for FRP-reinforced members. Moreover, both short and slender column designs require load–moment interaction diagrams for analysis and design. To address this, **Chapter 5** introduces a novel concept of universal interaction diagrams, which are applicable to various types of FRP bars with differing ultimate strain capacities. This approach eliminates the need to generate separate interaction diagrams for different FRP materials, offering a unified and efficient design tool.

6.2 Major results and conclusions

Chapter 2 thoroughly examines the slenderness limit of GFRP-RC columns. It is found that the slenderness limit of GFRP-RC columns is not the same as that of steel-RC columns and the available equations for steel-RC columns are not appropriate for GFRP-RC columns. Moreover, it was also observed that the axial force ratio is the governing parameter to estimate the slenderness limit of GFRP-RC columns, other parameters such as concrete compressive strength, modulus of elasticity of FRP bars and reinforcement ratio do not have any significant effect. In general, it was found that the slenderness limit of GFRP-RC columns is lower than steel-RC columns. The value of slenderness limit and extent of variation of slenderness limit for GFRP-RC columns with axial force ratio is not the same as for steel-RC columns. Hence, two equations were proposed for slenderness limit of GFRP-RC columns based on the parametric study on 720 columns and considering two criteria of slenderness limit. Furthermore, the numerical method for second-order analysis based on the estimation of the curvature including the first-order end eccentricities was successfully developed and verified with experimental results.

In **Chapter 3**, the behaviour of the nominal curvature of FRP-RC columns was extensively investigated. It was observed that the nominal curvature of FRP-RC columns with respect to load capacity differs from that of steel-RC columns, owing to the low modulus of elasticity and linear stress-strain behaviour of FRP bars. Furthermore, using linear interpolation with load to estimate the nominal curvature at load levels other than balanced failure load is found to be unsuitable for FRP-RC columns. Moreover,

balance point may not appear in the load-moment interaction of FRP-RC column in compression for every combination of concrete compressive strength, reinforcement ratio, and modulus of elasticity of FRP-bar. Also, the effect of slenderness on the nominal curvature of FRP-RC columns is more pronounced than in steel-RC columns. Based on these findings, an equation to estimate the nominal curvature of FRP-RC columns was developed from a parametric study of 26,880 columns. Furthermore, an equation to calculate the total curvature distribution factor was proposed, an important factor for nominal curvature method, applicable to both FRP-RC and steel-RC columns. The performance of the proposed nominal curvature equation for FRP-RC columns was found to be safe and in good agreement with experimental results.

In **Chapter 4**, the equivalent moment factor for FRP-RC columns essential for the simplified analysis of the columns subjected to unequal end moments was studied in detail. The behaviour of equivalent moment factor for FRP-RC columns was examined for different eccentricity ratios, end moment ratios, material properties, slenderness ratio, and reinforcement ratio. A detailed parametric study on 12288 columns was performed. It was found that the behaviour of equivalent moment factor for FRP-RC columns is not the same as for steel-RC columns. The equivalent moment factor calculated for FRP-RC columns using the expression for steel-RC columns would lead to unconservative results for a large number of cases. The equation for equivalent moment factor of steel-RC columns was found not be appropriate and safe for FRP-RC columns based on the percentile analysis for the ratio of equivalent moment factor from the equation to the equivalent moment factor from second-order analysis ($C_{m(Eq)}/C_{m(num)}$). Hence, an equation for equivalent moment factor of FRP-RC columns was developed based on the detailed parametric study with an average, five percentile and one percentile values of 1.12, 1 and 0.96 for $C_{m(Eq)}/C_{m(num)}$. Moreover, the first-order end moment ratio was found to be the determining parameter for equivalent moment factor of FRP-RC columns similar to the steel-RC columns. Furthermore, the numerical analysis method, namely direct curvature method (DCM) based on the estimation of the curvature was successfully developed and implemented for columns subjected to unequal end moments. It was observed that DCM with an estimation of curvature can

perform analysis with comparable accuracy to other tedious methods without estimation of the curvature.

In **Chapter 5**, it is presented that the normalised mechanical reinforcement ratio can effectively be used to develop universal interaction diagrams for the design of short and slender FRP-RC columns for various kinds of FRP bars. Further, the concept of universal interaction diagrams can also be extended to slender FRP-RC columns, thus simplifying the design using nominal curvature method. The solved examples presented serve as fully worked-out illustrations intended to support practising engineers in applying the proposed design approach.

6.3 Outlook

The experimental research on the behaviour of slender FRP-RC columns is limited. This highlights the need to perform more experiments to build a database to support future probabilistic and reliability studies for FRP-RC columns. Investigating the performance of these columns under seismic and fire loading would be particularly valuable for the development of design guidelines within the Eurocode framework.

Moreover, the effects of creep and fatigue on the design of slender FRP-RC columns warrant further attention. It would also be beneficial to examine how different concrete types such as high-strength concrete, ultra-high-performance concrete (UHPC), fibre-reinforced concrete (FRC), and lightweight concrete influence the behaviour and design of FRP-RC columns.

7. Annexure

Effect of Slenderness on the Design of FRP reinforced Concrete Columns

Ahmed Usama Syed[1], Arndt Goldack[2]

[1 2] University of Wuppertal, Chair of Statics and Dynamics of Structures, Pauluskichstraße 7, 42285 Wuppertal, Germany.

Published in

Conference proceedings, IABSE Congress New Delhi 2023 (DOI: https://doi.org/10.2749/newdelhi.2023.0574)

ABSTRACT

Fibre-reinforced polymer (FRP) bars can be a promising sustainable alternative to steel due to their low life-cycle cost and potentially low environmental impact as a reinforcement. Also, due to their corrosion resistance and electromagnetic neutrality, they have attracted significant interest for use in reinforced concrete (RC) structures. This paper investigates the behaviour of FRP-reinforced concrete (FRP-RC) columns with varying slenderness ratios. The reduction in moment capacity, axial load capacity and load-moment interaction diagrams of FRP-RC columns with the increase in slenderness are studied in comparison to steel-reinforced concrete (steel-RC) columns. The study shows that guidelines and design standards such as Eurocode 2 for steel-RC pertaining to the simplified design of slender columns, slenderness limit and minimum reinforcement ratio need to be revised for FRP-RC columns.

Keywords: Fibre-reinforced polymer bars, FRP-reinforced concrete columns, slender columns, column curvature, second-order analysis, stability, slenderness limit, Eurocode 2, column stiffness.

7.1 Introduction

Owing to increasing global concerns about climate change and the need to reduce carbon emissions, sustainable and durable infrastructure is one of the most important factors in achieving sustainable development. Fibre Reinforced Polymer (FRP) reinforcement may be a promising solution for developing sustainable infrastructure due to its corrosion resistance, low life-cycle costs [1] and potentially low environmental impact [2] compared to traditional steel reinforcement. Despite having high tensile strength, they have low axial stiffness compared to steel, which makes their behaviour in reinforced concrete structures of concern when they replace steel bars. Considerable research work has been reported in the literature examining the flexural behaviour of FRP-reinforced concrete (FRP-RC) structures. However, limited work has been done on FRP-RC columns, especially slender FRP columns, and their design guidelines. In this study, the behaviour of FRP-RC columns is examined along with the consideration of geometric non-linearity arising out of slenderness. A comparison between the behaviour of FRP-RC columns and steel-reinforced concrete (steel-RC) columns is presented to determine the applicability of the available guidelines of steel-RC design standards such as Eurocode 2 [3] for FRP-RC columns.

7.2 Non-linear analysis of reinforced concrete columns

A numerical method based on the sinusoidal assumption of the column curvature is implemented in Matlab (R2022b) for the analysis of the reinforced concrete columns. The assumed curvature (φ) can be expressed as presented in Eq. (7.1)

$$\varphi = \frac{e_{max}}{L^2}\left(2cos^{-1}\frac{e_i}{e_{max}}\right)^2 \tag{7.1}$$

To account for the non-linear material properties of the cross-section, the area of reinforcement and concrete in the cross-section is transformed into an equivalent linearly elastic and homogenous material with a modulus of elasticity the same as concrete [4] as shown in Fig. 7.1. More details about the numerical method can be found in the literature [5].

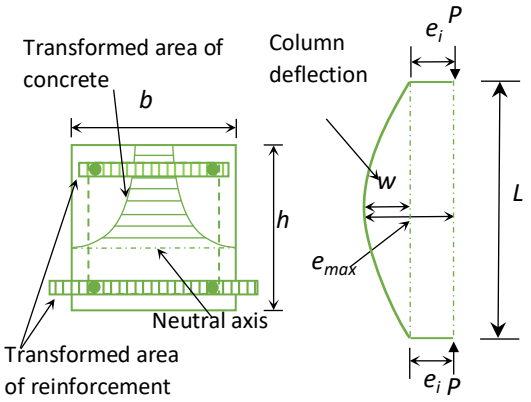


Fig. 7.1. Column cross-section for transformed area and deflection when bent in single curvature

Table 7.1. Properties of FRP bars reported in the literature

FRP Type	**Reference**	**Ultimate tensile strain (ε_{TFRP}) [%]**	**Tensile modulus of elasticity [GPa]**
Carbon-FRP (CFRP)	*fib* bulletin 40[6]	0.50-1.70	100-580
	Choo et al.[7]	1.60	147
	Hadhood et al.[8]	1.19-1.20	130-141
	Mohamed et al.[9]	1.20-1.33	120-140
	Othman et al.[10]	1.32-1.38	145-151
Aramid-FRP (AFRP)	*fib* bulletin 40[6]	1.90-4.40	40-125
	Choo et al.[7]	2.40	87
Glass-FRP (GFRP)	*fib* bulletin 40[6]	1.20-3.70	35-60
	Choo et al.[7]	1.40	45
	Abdelazim et al.[11]	2.35-2.51	51-62

	Afifi et al.[12]	1.56-1.90	53-55
	Almomani et al.[13]	2.40	64
	Alnajmi and Abed[14]	1.90	45
	Elchalakani et al.[15]	1.60	59
	Elmesalami et al.[16]	1.75	45
	Guérin et al.[17]	2.10-2.60	51.3-53.3
Basalt-FRP (BFRP)	Alnajmi et al.[14].	2.10	49.3
	Elmesalami et al.[16]	2.02-2.55	45.9-49.3
	Fan et al.[18]	2.76-2.79	42.5-50.3*

7.3 Material Properties

The compressive strength of the concrete (f_c) was modelled using the stress-strain model proposed by Popovics [19]. Concrete inside the lateral ties was considered as confined and it was modelled adopting the confinement model by Mander et al. [20]. The tensile strength of concrete, the effect of creep and shrinkage was not considered. Bond slip between reinforcement concrete was also neglected in this study. The compressive strain of concrete at failure was assumed to be 0.0035. Details of the implemented material model can be found in the literature [5].

FRP reinforcement is modelled as a linear-elastic material. The tensile properties of different FRP bars types as reported in the literature are presented in Table 6.1. It is observed that the ultimate tensile strain (ε_{TFRP}) of GFRP bars is normally higher than 0.012. AFRP and BFRP bars may have high ultimate tensile strain values around 0.020 and higher. However, considering high ultimate strain values may lead to high curvatures and practically undesirable deflections [21]. CFRP bars have low ultimate strain values while they have a high tensile modulus of elasticity compared to other types. The values reported in the literature for the commercially available CFRP bars used in the experiments are generally around

0.012 or higher. Hence in this study, the ultimate tensile strain of FRP bars is considered as 0.012 for all the values of tensile modulus of elasticity considered. However, for CFRP bars it can be as low as 0.005 [6]. The effect of low ultimate strain in such cases of CFRP bars shall be mentioned in further sections. The contribution of FRP reinforcement was also considered in compression. The modulus of elasticity of the FRP bar (E_{FRP}) was considered to be the same in tension and compression. An elastic-plastic stress-strain relationship was used to model the behaviour of steel with a modulus of elasticity of 200 GPa and yield strength (f_y) of 500 MPa.

7.4 Design of FRP-reinforced concrete column

The behaviour of the FRP-RC column was examined in terms of the characteristics of its load-moment interaction curves. The effect of slenderness on their load and moment capacity and increase in the second-order moment was also examined. A comparison with steel-RC columns is presented. A rectangular column cross-section of 300 x 300 mm with corner reinforcement is considered throughout this study. Steel stirrups of strength 500 MPa and spacing of 150 mm were considered for all the columns in this study including FRP-RC columns.

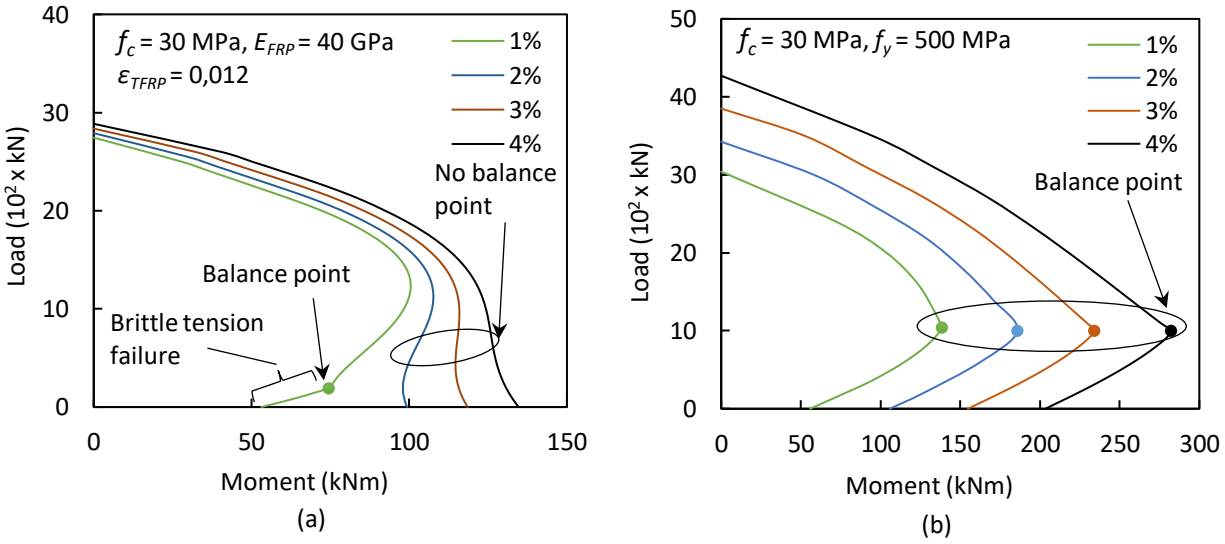


Fig. 7.2. Load-moment interaction curves for (a) FRP-RC and (b) steel-RC columns with $\lambda = 0$ (no second-order effects)

7.5 Load-moment interaction

The load-moment interaction of FRP-RC and steel-RC column for reinforcement ratio (ρ) varying from 1% to 4% is presented in Fig. 7.2 using cross-sectional analysis without considering the effect of slenderness that is with slenderness ratio ($\lambda = L/r$) of 0, where L is the effective length of the column and r is the radius of gyration of the column cross-section. The balance point in the load-moment interaction diagram of FRP-RC columns is observed only for low reinforcement ratios such as 1% and at low values of axial force as seen in Fig. 7.2(a). However, for steel-RC columns, a balance point is observed for all values of the reinforcement ratio which signifies that it is not affected by the reinforcement ratio as shown in Fig. 7.2(b).

The portion of the FRP-RC load-moment interaction diagram below the balance point will lead to a failure due to the sudden rupture of the FRP bar in tension owing to the linear elastic property of FRP bars. Hence, this region is termed a region of brittle-tension failure and it is undesirable to design a section in this region [6]. To avoid brittle-tension failure appearing in the design envelope of GFRP-reinforced concrete (GFRP-RC) columns a minimum reinforcement ratio of 1% is suggested in the literature [22–24]. However, in the case of a low ultimate tensile strain (ε_{TFRP}) such as 0.005 of FRP bar which may occur in the case of CFRP bars, the balance point would appear at a higher value of axial force in comparison to Fig. 7.2(a) as shown in Fig. 7.3 and it is also be seen for the reinforcement ratio of higher than 1%.

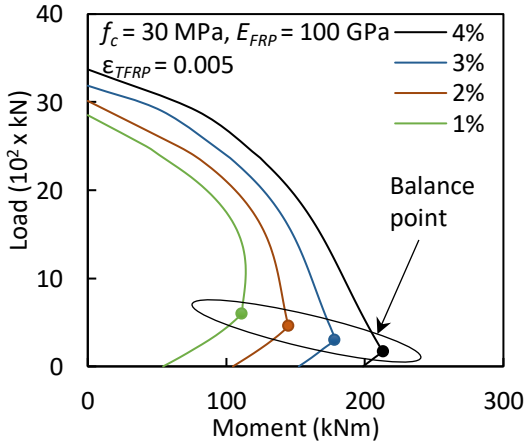


Fig. 7.3. Load-moment interaction curves of CFRP-RC columns for ε_{TFRP}= 0.005 with λ=0

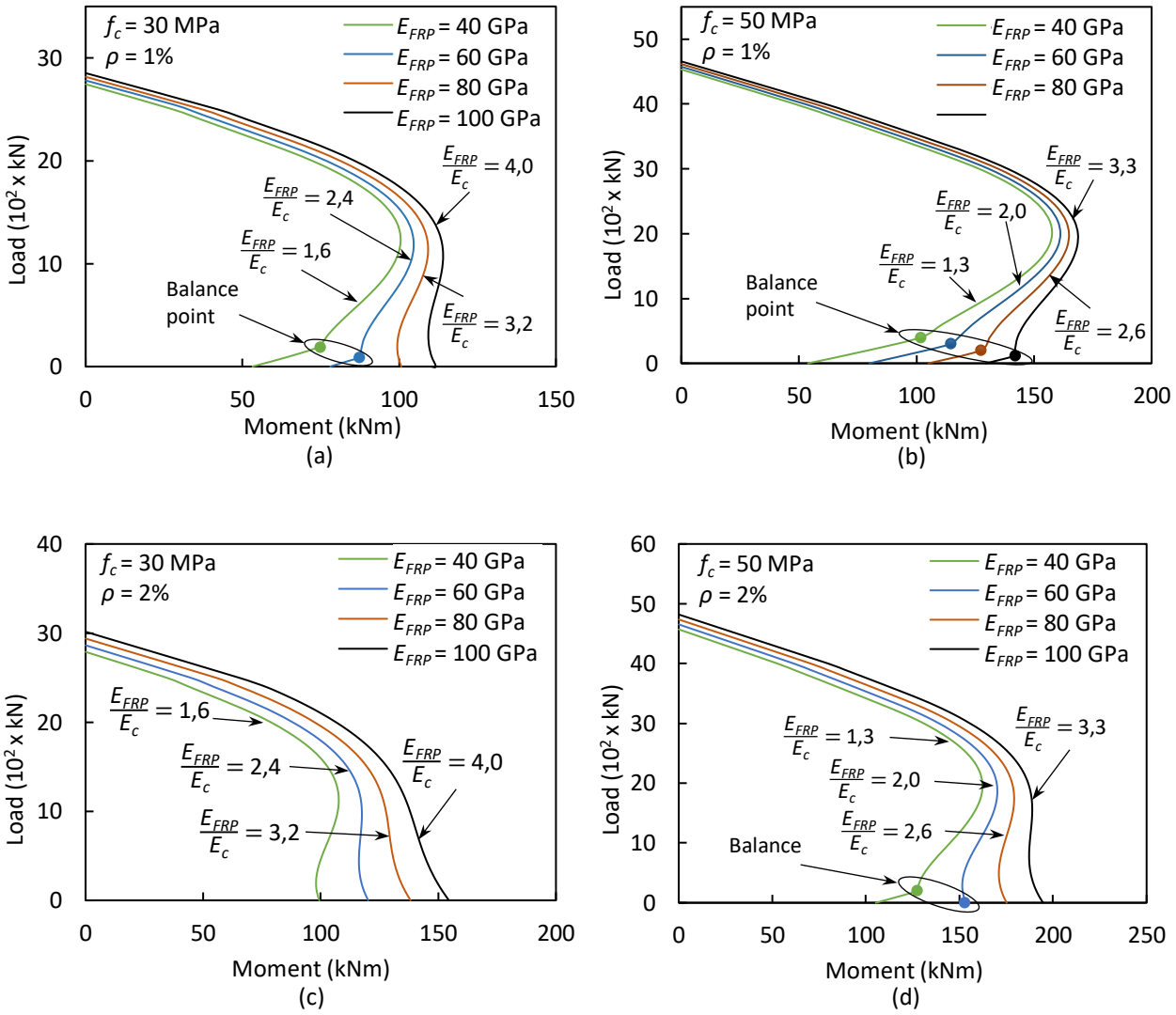


Fig. 7.4. Load-moment interaction curves of FRP-RC columns with a varying modulus of elasticity of FRP bar at λ=0

It can be observed from Fig. 7.2 and Fig. 7.4 that the effect of increasing the reinforcement ratio or modulus of elasticity of FRP bar on the load and moment capacity of FRP-RC columns is very less at the high value of load capacity compared to the low values of load capacity. While increasing the reinforcement ratio for steel-RC columns has a similar effect on load and moment capacity for both high and low values of load capacity as seen in Fig. 7.2(b). As the concrete compressive strength increases the balance point shifts upward and it can also be seen for a reinforcement ratio of 2% as shown in Fig. 7.4. However, the balance point shifts downwards with the increase in the modulus of elasticity of the FRP bar. With the increase in the ratio of the modulus of elasticity of FRP to the

modulus of elasticity of concrete (E_{FRP}/E_c), the balance point shifts downwards however, the location of the balance point is also affected by concrete strength and reinforcement ratio. Hence to avoid brittle-tension failure a minimum reinforcement ratio based on all the affecting parameters shall be ascertained such as concrete compressive strength, modulus of elasticity of FRP bar, ultimate strain of FRP bar and axial force in the column.

For steel-RC columns, the balance point occurs generally at the "knee" bend of the load-moment interaction curve and normally this is at the location of maximum moment capacity. However, for FRP-RC columns balance point does not occur at the "knee" bend of the load-moment interaction curve and the location of the balance point is not the location of maximum moment capacity. The position of the balance point would be of importance in estimating the curvature for the design of long columns using approximate design methods based on the column curvature such as the nominal curvature method in Eurocode 2 [3]. In such methods for steel-RC, the curvature of the column at the maximum moment capacity or at the balance point is used to estimate the column curvature at the level of design load [3,25]. Hence such methods need to be reworked when used for FRP-RC columns.

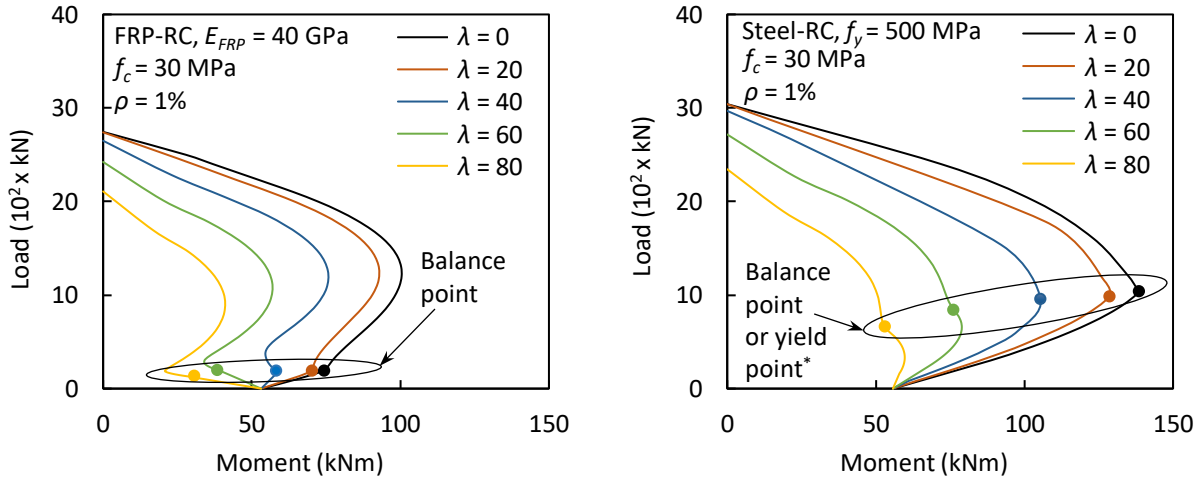


Fig. 7.5. Load-moment capacity interaction curves of FRP-RC and steel-RC columns with a varying λ at ρ = 1%

The effect of the increase in the slenderness ratio of FRP-RC and steel-RC columns is presented in Fig. 7.5. As the slenderness ratio increases a decrease in moment capacity is observed for both FRP-RC and steel-RC columns. However, for steel-RC columns the difference in moment capacity for slender columns with regards to cross-sectional moment capacity starts to decrease after the load value decreases below the balance point which occurs at the "knee" bend. However, for FRP-RC columns a significant difference in moment capacity is observed for slender columns compared to the moment capacity from cross-sectional analysis even at the load value below the "knee" and the moment capacity values start converging at a very low load value. Similar behaviour is also observed for FRP-RC columns at other reinforcement ratios where the balance point does not appear in the load-moment interaction curve as shown in Fig. 7.6.

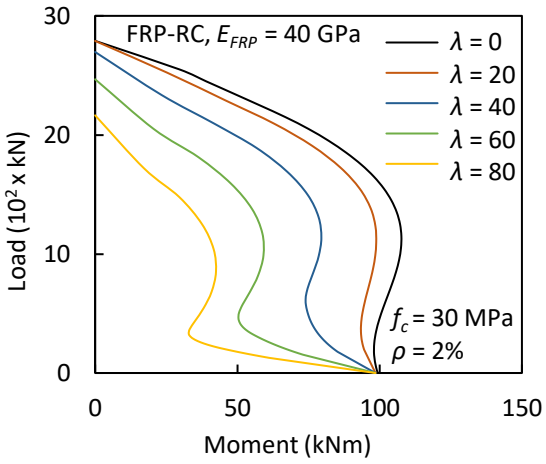


Fig. 7.6. Load-moment capacity interaction curves of FRP-RC column with a varying λ at ρ = 2%

7.6 Capacity reduction for slender columns

The effect of an increase in slenderness ratio on the load capacity (P_{long}) and moment capacity (M_{long}) of FRP-RC and steel-RC columns is presented in Fig. 7.7 with respect to the cross-sectional load capacity (P_{short}) and moment capacity (M_{short}). At a constant value of eccentricity ratio (e), the load capacity of FRP-RC columns falls faster than steel-RC columns as the slenderness ratio increases as shown in Fig. 7.7(a). Here, the eccentricity ratio (e) is considered as the ratio of load eccentricity (e_i) to the depth of the column cross-section (h) in the direction perpendicular to the axis of bending. Increasing

the eccentricity ratio from 0.2 to 0.6, the decrease in the load capacity reduces for steel-RC columns however for FRP-RC columns the decrease in load capacity is higher at $e = 0.4$ than at $e = 0.2$. Similarly, at a constant value of axial force ratio (n), the moment capacity of the FRP-RC column reduces faster than for steel-RC columns as shown in Fig. 7.7(b). Here, the axial force ratio is considered as shown in Eq. (7.2).

$$n = \frac{P}{A_c f_c} \tag{7.2}$$

Where P is the axial force in the columns and A_C cross-sectional area of concrete. The difference in the behaviour of FRP-RC compared to steel-RC columns in terms of capacity reduction due to slenderness may affect the nominal stiffness estimation of FRP-RC columns for simplified methods of design of long columns such as nominal stiffness method in Eurocode 2 [3].

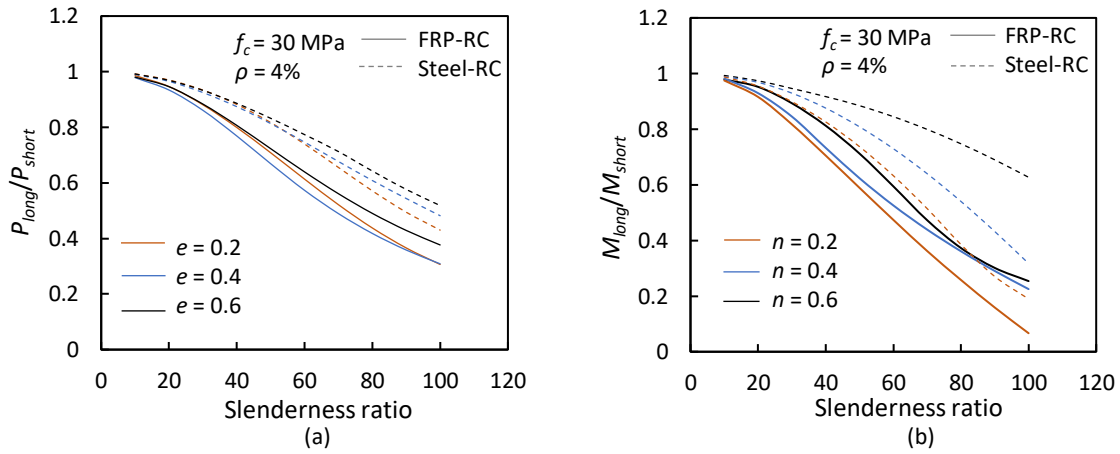


Fig. 7.7. Reduction in (a) load capacity and (b) moment capacity due to an increase in λ for FRP-RC and steel-RC columns

The ratio of the second-order moment or the moment induced due to column deflection (M_{II}) to the first-order moment or the moment due to initial load eccentricity (M_I) is presented in Fig. 7.8 for a comparison between FRP-RC and steel-RC columns. Here, M_I is also the moment capacity of the slender column. For steel-RC, Eurocode 2 classifies a column to be a short column if this ratio is not more than 10%, the corresponding slenderness ratio is termed as slenderness limit (λ_{lim}) and the second-order effects can be neglected in the design of such columns. However, as observed in Fig. 7.8 that the

ratio M_{II}/M_I rises faster for FRP-RC than for steel-RC as the slenderness ratio is increased. Therefore, at a constant ratio of M_{II}/M_I say 10% for λ_{lim}, FRP-RC columns may have a lower value of λ_{lim} compared to steel-RC columns.

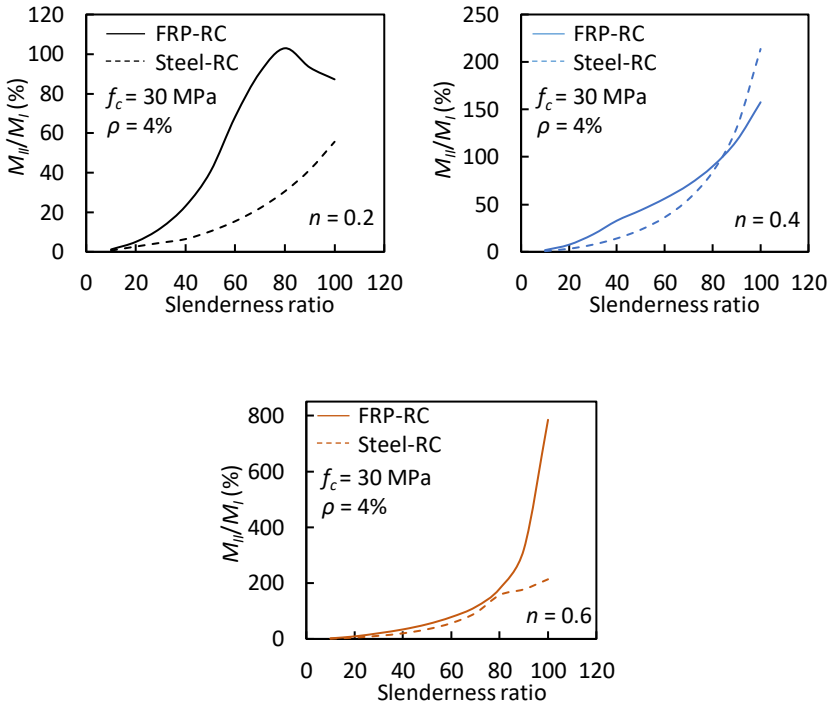


Fig. 7.8. Increase in second-order moment with the increase of λ for FRP-RC and steel-RC columns for n = 0.2, 0.4 and 0.6

The effect of the modulus of elasticity of the FRP reinforcement on the capacity reduction of FRP-RC columns is presented in Fig. 7.9. With the increase in slenderness ratio, it is observed that the reduction in load capacity at constant eccentricity ratio and moment capacity at constant axial force ratio decreases with the increase of E_{FRP}; however, the capacity reduction for FRP-RC is more than steel-RC for all the values of E_{FRP} considered in this study. The reduction in the ratio of M_{II}/M_I is also observed with the increase in E_{FRP} up to a slenderness ratio of around 50, indicating a higher value of λ_{lim} for the FRP bar with a higher value of E_{FRP}.

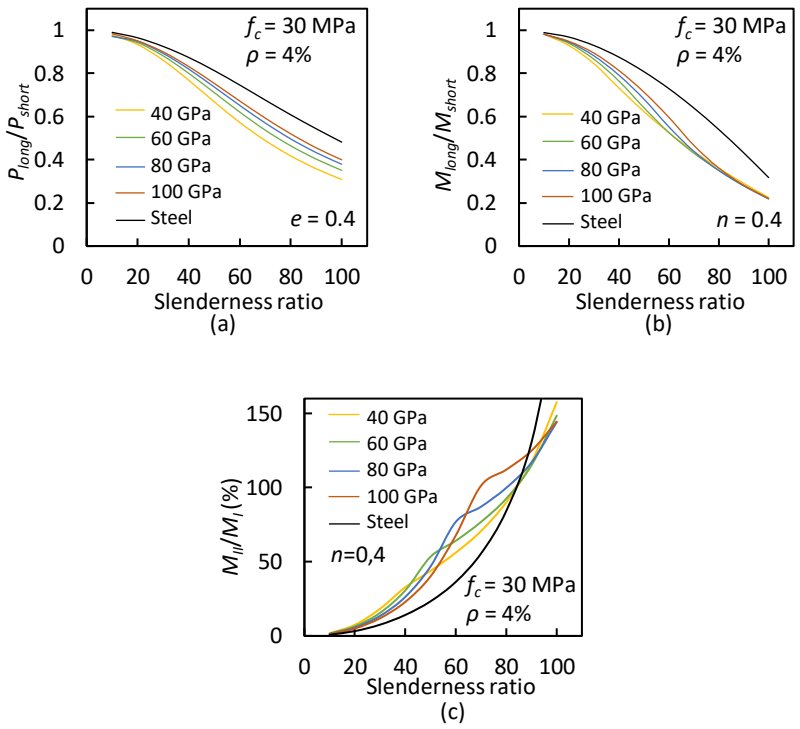


Fig. 7.9. (a) Load capacity reduction, (b) moment capacity reduction and (c) increase in M_{II}/M_I due to an increase in λ for varying modulus of elasticity of FRP bar

7.7 Conclusions

In this study, second-order analysis of FRP-RC columns was performed to assess the effect of slenderness on the design of FRP-RC columns in comparison with steel-RC columns. It is observed although FRP-RC columns exhibit the typical "knee" bend load-moment interaction curve but the characteristics of the load-moment interaction curve of FRP-RC column is different in comparison to steel-RC column such as the appearance and location of balance point for both short and slender columns. FRP-RC columns are more susceptible to capacity reduction in terms of load and moment capacity as the slenderness ratio increases. Also, the rise of second-order moments is faster in FRP-RC columns as compared to steel-RC columns. The estimation of nominal curvature and nominal stiffness for approximate design methods of long columns in Eurocode 2 need to be amended for FRP-RC columns. Also, the minimum reinforcement ratio and slenderness limit equation need to be revised for FRP-RC columns.

7.8 Acknowledgements

The authors would like to acknowledge the funding support provided by German Academic Exchange Service (DAAD) to pursue this research work.

7.9 References

[1] Cadenazzi T, Dotelli G, Rossini M, Nolan S, Nanni A. Life-Cycle Cost and Life-Cycle Assessment Analysis at the Design Stage of a Fiber-Reinforced Polymer-Reinforced Concrete Bridge in Florida. Adv. Civ. Eng. Matls. 2019;8(2):20180113.

[2] Pavlović A, Donchev T, Petkova D, Staletović N. Sustainability of alternative reinforcement for concrete structures: Life cycle assessment of basalt FRP bars. Construction and Building Materials 2022;334:127424.

[3] EN 1992-1-1. Eurocode 2: Design of concrete structures - Part 1-1:General rules and rules for buildings: EN 1992-1-1: Eurocode 2: Design of concrete structures - Part 1-1: General rules and rules for buildings(EN 1992-1-1:2004). Brussels: European Committee for Standardisation.

[4] Chuang P-H, Kong S-K. Strength of Slender Reinforced Concrete Columns. J. Struct. Eng. 1998;124(9):992–8.

[5] Syed AU, Goldack A. Slenderness Limit for GFRP Reinforced Concrete Columns based on axial force ratio. Manuscript submitted for publication 2023.

[6] Fib Bulletin 40. FRP reinforcement in RC structures. Stuttgart: The International Federation for Structural Concrete; 2007.

[7] Choo C.C., Harik I.E. and Gesund H. Strength of Rectangular Concrete Columns Reinforced with Fiber-Reinforced Polymer Bars. ACI Structural Journal 2006;103(3):452-459.

[8] Hadhood A, Mohamed HM, Benmokrane B. Flexural Stiffness of GFRP- and CFRP-RC Circular Members under Eccentric Loads Based on Experimental and Curvature Analysis. ACI Structural Journal 2018;115(4):1185–98.

[9] Mohamed HM, Afifi MZ, Benmokrane B. Performance Evaluation of Concrete Columns Reinforced Longitudinally with FRP Bars and Confined with FRP Hoops and Spirals under Axial Load. J. Bridge Eng. 2014;19(7).

[10] Othman ZS, Mohammad AH. Behaviour of Eccentric Concrete Columns Reinforced with Carbon Fibre-Reinforced Polymer Bars. Advances in Civil Engineering 2019;2019:1–13.

[11] Abdelazim W, Mohamed HM, Benmokrane B. Inelastic Second-Order Analysis for Slender GFRP-Reinforced Concrete Columns: Experimental Investigations and Theoretical Study. J Compos Constr 2020;24(3).

[12] Afifi MZ, Mohamed HM, Benmokrane B. Axial Capacity of Circular Concrete Columns Reinforced with GFRP Bars and Spirals. J Compos Constr 2014;18(1):4013017.

[13] Almomani M, Mahmoud K, El-Salakawy EF. Experimental Investigation of Large-Scale Eccentrically Loaded GFRP-Reinforced High-Strength Concrete Columns. J. Compos. Constr. 2022;26(2).

[14] AlNajmi L, Abed F. Evaluation of FRP Bars under Compression and Their Performance in RC Columns. Materials 2020;13(20).

[15] Elchalakani M, Dong M, Karrech A, Mohamed Ali MS, Huo J-S. Circular Concrete Columns and Beams Reinforced with GFRP Bars and Spirals under Axial, Eccentric, and Flexural Loading. J. Compos. Constr. 2020;24(3).

[16] Elmesalami N, Abed F, Refai AE. Concrete Columns Reinforced with GFRP and BFRP Bars under Concentric and Eccentric Loads: Experimental Testing and Analytical Investigation. J. Compos. Constr. 2021;25(2).

[17] Guérin M, Mohamed HM, Benmokrane B, Nanni A, Shield CK. Eccentric Behavior of Full-Scale Reinforced Concrete Columns with Glass Fiber-Reinforced Polymer Bars and Ties. ACI Structural Journal 2018;115(2):489–99.

[18] Fan X, Xu T, Zhou Z, Zhou X. Experimental Study on Basic Mechanical Properties of BFRP Bars. IOP Conf. Ser.: Mater. Sci. Eng; 2017.

[19] Popovics S. A numerical approach to the complete stress-strain curve of concrete. Cement and concrete research 1973;3:583–99.

[20] Mander JB, Priestly JN, Park, R. Theoretical Stress-Strain Model for Confined Concrete. J. Struct. Eng. 1988;114(8):1804–26.

[21] Zadeh HJ, Nanni A. Design of RC Columns Using Glass FRP Reinforcement. J Compos Constr 2013;17(3):294–304.

[22] Hadhood A, Mohamed HM, Benmokrane B, Nanni A, Shield CK. Assessment of Design Guidelines of Concrete Columns Reinforced with Glass Fiber-Reinforced Polymer Bars. ACI Structural Journal 2019;116(4):193–207.

[23] Hadhood A, Mohamed HM, Ghrib F, Benmokrane B. Efficiency of glass-fiber reinforced-polymer (GFRP) discrete hoops and bars in concrete columns under combined axial and flexural loads. Composites Part B: Engineering 2017;114(1):223–36.

[24] Guérin M, Mohamed HM, Benmokrane B, Shield CK, Nanni A. Effect of Glass Fiber-Reinforced Polymer Reinforcement Ratio on the Axial–Flexural Strength of Reinforced Concrete Columns. ACI Structural Journal 2018;115(4).

[25] Cranston WB. Analysis and design of reinforced concrete columns; 1972.

This page has been intentionally left blank in the electronic version

This page has been intentionally left blank in the electronic version

Berichte aus dem Konstruktiven Ingenieurbau
Bergische Universität Wuppertal

Heft 1 Andres, M.: Zum Stabilitätsnachweis von Schalentragwerken aus Hochleistungsbeton, 2004; ISBN 978-3-940795-00-7

Heft 2 Wörmann, R.: Zur Erfassung hygrothermischer Einflüsse auf das nichtlineare Trag- und Schädigungsverhalten von Stahlbetonflächentragwerken, 2004; ISBN 978-3-940795-01-4

Heft 3 Piel, W.: Zur Erhöhung der Durchstanztragfähigkeit von Flachdecken mit Stahlverbundsystemen, 2004; ISBN 978-3-940795-02-1

Heft 4 Mahran, E.: Finite-Infinite-Elemente-Modellierung zur Simulation der Boden-Bauwerk-Flüssigkeit-Interaktion unter dynamischer Anregung, 2004; ISBN 978-3-940795-03-8

Heft 5 Eusani, R.: Zur numerischen Zeitbereichssimulation der Aeroelastischen Instabilität bei Seilbrücken, 2005; ISBN 978-3-940795-04-5

Heft 6 Stracke, J.: Flachdecken aus Konstruktions - Leichtbeton, 2005; ISBN 978-3-940795-05-2

Heft 7 Hanswille, G., Porsch, M., Üstündağ, C.: Versuchsbericht SFB 398 -Projekt C8 -Teil 1, 2007; ISBN 978-3-940795-06-9

Heft 8 Schäfer, M.: Zum Tragverhalten von Flachdecken mit integrierten hohlkastenförmigen Stahlprofilen, 2007; ISBN 978-3-940795-07-6

Heft 9 Üstündağ, C.: Beitrag zur Bemessung von Verbundträgern unter ermüdungswirksamen Beanspruchungen, 2007; ISBN 978-3-940795-08-3

Heft 10 Hanswille, G., Porsch, M.: Versuchsbericht über die Durchführung von 36 Push-Out-Versuchen; ISBN 978-3-940795-09-0

Heft 11 Hanswille, G., Porsch, M.: Metallurgische Untersuchungen an Schweißnahtverbindungen, 2008; ISBN 978-3-940795-10-6

Heft 12 Jamali, N.: On the Numerical Simulation of Friction-Isolated Structures, 2008; ISBN 978-3-940795-11-3

Heft 13 Lippes, M.: Zur Bemessung von Hohlprofil – Verbundstützen aus hochfesten Stählen und Betonen, 2008; ISBN 978-3-940795-12-0

Heft 14 Mihajlov, Viktor: Numerical Model for Spatial Steel and Composite Frame-Structures Exposed to Fire and Elevated Temperatures, 2009; ISBN 978-3-940795-13-7

Heft 15 Neuhaus, Christian: Zur Identifikation selbsterregter aeroelastischer Kräfte im Zeitbereich, 2010; ISBN 978-3-940795-14-4

Berichte aus dem Konstruktiven Ingenieurbau
Bergische Universität Wuppertal

Heft 16 Stopp, Kirsten: Trag- und Verformungsverhalten großflächig gegründeter Stahlbetontragwerke unter Berücksichtigung der Boden-Bauwerk-Interaktion, 2010; ISBN 978-3-940795-15-1

Heft 17 Porsch, Markus: Modellierung von Schädigungsmechanismen zur Beurteilung der Lebensdauer von Verbundkonstruktionen aus Stahl und Beton, 2010; ISBN 978-3-940795-16-8

Heft 18 Mannsfeld, Thorsten Rolf: Tragverhalten von Stahlbetonflächentragwerken unter Berücksichtigung der temperaturbedingten Nichtlinearitäten im Brandfall, 2011; ISBN 978-3-940795-17-5

Heft 19 Gelien, Marion: Ein Beitrag zur Bemessung von Stahlbetonstützen im Brandfall, 2011; ISBN 978-3-940795-18-2

Heft 20 Festschrift Gerhard Hanswille, 2011; ISBN 978-3-940795-19-9

Heft 21 Bergmann, Marco: Zur Bemessung von Hohlprofilverbundstützen im Brandfall, 2013; ISBN 978-3-940795-20-5

Heft 22 Peter, Carsten: Tragverhalten von Verkehrstunneln im Brandfall mit einer Innenschale aus PP-Faserbeton 2017, ISBN 978-3-940795-21-2

Heft 23 Chanou, Mohamed: Zum Tragverhalten von Hohlprofil-Verbundstützen mit Mehrkernquerschnitten, 2018; ISBN 978-3-940795-22-9

Heft 24 Menkenhagen, Philipp: Beitrag zum Tragverhalten des Lasteinleitungsbereichs von Hohlprofil-Verbundstützen unter Berücksichtigung der Verformungseigenschaften von Schubringen, 2019; ISBN 978-3-940795-23-6

Heft 25 Zwolinski, Stefan: Ermittlung der Grünzugfestigkeit erdfeuchter Zementleimgemische als Grundlage für die Optimierung der Produktion von sofort entschalten Betonwaren, 2018; ISBN 978-3-940795-24-3

Heft 26 Dollase, André: Mikrowellenverfahren zur Untersuchung des Erhärtungs- und Trocknungsverhaltens von zementgebundenen Baustoffen, 2019; 978-3-940795-25-0

Heft 27 Loh, Lutz: Zum Torsionstragverhalten vorgespannter Segmenttürme -Ein Nachweismodell für überdrückte und klaffende Segmentfugen mit Kreisringquerschnitt, 2023; ISBN 978-3-940795-26-7

Heft 28 Blau, Nick: Untersuchungen zur Ermüdungssicherheit von Querrahmenanschlüssen bei Verbundbrücken, 2024, ISBN 978-3-940795-27-4

Berichte aus dem Konstruktiven Ingenieurbau
Bergische Universität Wuppertal

Heft 29 Schönfeld, Larissa: Einfluss von Imperfektionen auf die numerische Traglastbestimmung ausgesteifter Beulfelder; ISBN: 978-3-940795-28-1

Heft 30 Kischkewitz, Fabian: Ein Beitrag zur wirtschaftlichen Bemessung von Balkenbrücken in Verbundbauweise; ISBN: 978-3-94095-29-8

Heft 31 Ardelmann, Niklas: Ein Beitrag zu Tragverhalten von Sandwichelementen unter Punktlasten, 2025, ISBN: 978-3-940795-30-4

Heft 32 Schwenzer, Katharina: Ein Beitrag zur numerischen Untersuchung der Rissbildung zementgebundener Estrichplatten auf Dämmschichten, 2025, ISBN: 978-3-940795-31-1

Heft 33 Kämper, Dominik Matthias: Adaptive Multimodal Pushover Analysis of Bridges Considering Multidirectional Earthquake Excitations, 2025, ISBN: 978-3-940795-32-8

Heft 34 Iravani, Ahmad: Effect of concrete technological aspects on hot- and residual-strength of concrete subjected to cyclic high temperature, 2026, ISBN: 978-3-940795-33-5

Heft 35 Syed, Ahmed Usama: Numerical Investigation and Development of Design Guidelines for Slender FRP-RC Columns, 2026, ISBN: 978-3-940795-34-2